MATHEMATICAL AND PHYSICAL MODELING OF FLIP-CHIP SOLDERING PROCESSES

by

Scott E. Deering

Submitted to the Department of Materials Science and Engineering in
Partial Fulfillment of the Requirements for the degree of

DOCTOR OF PHILOSOPHY

In Materials Engineering
at the

Massachusetts Institute of Technology

June, 1995

Signature of Author ______________________________
Department of Materials Science and Engineering
May 5, 1995

Certified by ______________________________
Julian Szekely
Professor of Materials Engineering
Thesis Supervisor

Accepted by ______________________________
Carl V. Thompson II
Professor of Electronic Materials
Chair, Departmental Committee on Graduate Students

MATHEMATICAL AND PHYSICAL MODELING OF FLIP-CHIP SOLDERING PROCESSES

by

Scott E. Deering

Submitted to the Department of Materials Science and Engineering on
May 5, 1995 in Partial Fulfillment of the Requirements for the degree
of Doctor of Philosophy in Materials Engineering

Abstract

Flip chip solder reflow processing is a process of growing importance in the semiconductor packaging industry. With a major usefulness in opto-electronics applications requiring high precision placement and alignment, it is a growing focus for processing of high speed, high density devices. A great deal of research has been performed to study the behavior of the joints after fabrication. The majority of these studies have focused on reliability issues. Little research has been performed into the surface-tension driven effects that occur in the reflow process and control chip alignment. In order to develop the necessary predictive relationships relating certain joint parameters to process limits and behavior, a substantial research effort involving both mathematical models and physical experiments was performed. We developed a series of relationships to cover both individual parameter influences on alignment behavior and combined interactions as well. Presented in this work are a series of mathematical model results on the influence of in-process solder shapes and process parameters on restoring forces. These process parameters include solder volume, pad radius, joint height, surface tension and the influence of pad geometry. A number of experimental methods for measuring self-alignment restoring forces under process conditions were developed and used to confirm the mathematical results. These results will be presented in addition to a detailed discussion of important experimental issues to be addressed for accurate force measurement. The development of a series of solder alignment optimization rules will be discussed and solutions to current problems will be proposed.

Thesis supervisor: Professor Julian Szekely
Title: Professor of Materials Engineering

TABLE OF CONTENTS

LIST OF FIGURES

LIST OF TABLES

ACKNOWLEDGMENTS

I would like to thank my thesis advisor, Professor Julian Szekely, for providing me with his advice, support and resources for this research project and the opportunity to work with the Materials Process Modeling Group. I appreciate the numerous suggestions and excellent discussions that we have had throughout the years of my graduate study and for his seemingly endless network of contacts in a number of fields.

I would like to thank Professor Lionel C. Kimerling and Professor Christopher Scott for agreeing to serve on my thesis committee. Their input and insights have been both invaluable and encouraging.

I would like to thank AT&T Bell Laboratories and the Cooperative Research Fellowship Program for their financial support over the last several years. I would especially like to thank King Tai, Chee Wong, Dixon Dudderar and other members of the Interconnect Technology group in Murray Hill, N.J. for their help, the use of their facilities and input. I would also like to thank Dr. Tom Marinis for the use of lab facilities in the AT&T facility in Andover, MA and his commitment of precious hours of his busy schedule to help and advise.

I would like to thank Ken Brakke, the developer of the Surface Evolver for his comments, insights and willingness to answer questions about the code. I would also like to thank him for his help in changing aspects of the code in later revisions. I would like to thank Mr. John Prior for his help in developing the final dimensionless formulations.

I would like to thank former and present members of the Materials Process Modeling Group for their support and many useful discussions over the years, particularly my officemates and classmates, Dr. Elliot Schwartz and Dr. Livia Racz.

I would like to thank Pastors Gilbert and Yvonne Thompson and my friends and family at New Covenant Christian Center in Mattapan for their support, encouragement and prayers over the last several years. I would like to thank them for providing me with the opportunity to serve the community at large and for helping me to say connected to my cultural roots

I would like to thank Dr. Luis Martins for his help in developing discipline and for learning how to continually press for excellence.

I would like to thank the many residents at Next House, 500 Memorial Drive, especially housemasters Prof. Bora Mikic and Mrs. Liba Mikic, longtime house manager and friend, Mr. George Hosker and the residents of the Second West Wing who provided a great deal of fun, excitement and activity to my graduate student life.

I would like to thank my parents, Mr. and Mrs. Nathan and Niataja Deering and my siblings Eric and Cheryl for their love, patience and understanding throughout the last several years at M.I.T. Their support is very precious.

I would especially like to thank my wife, Michelle Deering, M.Ed., for her love, support, constant prayer, and companionship over the last several years. Her patience, understanding, long-suffering, and belief in me has made all the difference in the world and allowed me to complete a very difficult program in good fashion. I also thank her for her sacrifice of her educational goals for a season and her example as a part-time graduate student that was my inspiration.

Most importantly, I would like to thank Jesus Christ, without whom none of this would have been possible. I thank him for his encouragement, love, and the strength to see this program to its end. I also would like to thank him for his friendship and guidance into a bright and exciting future.

Chapter 1

INTRODUCTION

1.1 Background

This research program was undertaken with the goal of developing a characterization of the self-alignment reflow technique used in high density chip manufacturing. "Flip-Chip" solder processing (Fig. 1.1) involves the use of solidified solder droplets to form electrical and mechanical joints between chips and substrates. A standard solder joint is shown in Fig. 1.2, along with a cross-section of the metallization and deposited layers with which it is formed. These joints are very small relative to wire bonding and other joining methods (Fig. 1.3). This results in a much shorter interconnection length between devices. This reduction in joint length allows for a denser placement of devices and a higher density of I/0s when compared to traditional packaging methods. Another useful feature of this process is the self-alignment capability (Fig. 1.4) of the solder joints in their liquid state that results in precision alignment of devices to 1-5 micron tolerances. This level of positioning accuracy is useful in optoelectronics applications (Fig. 1.5) where precise alignment of components is normally performed only with expensive placement equipment. Using flip-chip solder bumping, alignment tolerances of 1-5 microns are possible without the use of costly placement equipment and increases in chip production volume.

Flip-chip processes are growing in importance due to the need for new packaging and interconnection technologies to produce high speed, high density and high reliability devices at low manufacturing costs. The ultimate limits of this joining method as well as the impact of process variables have become a growing field of study. The complex nature of standard semiconductor devices and the need to study these systems efficiently, have led to the development of new methods of evaluation. Mathematical models are being used more and more to predict process behavior and determine those factors that need to be controlled to optimize the process. There has been a great deal of research on the behavior of post-reflow flip-chip solder joints for a number of applications. Little research has been performed on the alignment process itself and the impact of process variables on alignment forces. There is a great need for reliable relationships between process parameters -- such as joint height, pad size, and surgace tension, and alignment forces. In order to optmize the alignment process, an understanding of the influences of these variables must be developed. A detailed understanding of these factors is also needed to define design rules for solder bumps used in precision alignment applications. A set of guidelines that aids in the optimization of the amount of alignment force generated by solder joints would be very useful for future applications of this technology. One application of this would be in the proper design of smaller or larger bumps to handle different chip and fiber optic sizes.

The main focus of this study was to design techniques, using a combination of mathematical models and physical experiments, to measure alignment restoring forces and those factors that have the greatest influence on them. Several mathematical models were developed to aid in the study of the alignment process and to calculate the restoring forces as a function of individual and combinations of process parameters. The physical experiments allowed us to directly measure the level of restoring force for a series of initial misalignments. Since there are no methods available for measuring self-alignment effects for the standard joint system, a major goal of this study was to examine the direct influence of process variables on chip positioning. A number of direct measurement techniques were developed to examine these variables. As a result of this research, major issues in developing these techniques were addressed, and solutions and ideas for addressing them were proposed.

This research project was also undertaken to construct methods for studying and addressing capillary problems. Capillary problems involve those materials systems where the combination of small scale and surface tension driven effects produce a new scale of processing problems. These pertinent issues include systems involving soldering, brazing and other joining methods using liquid metal.

The next few sections in this chapter will discuss in more detail some of the technological issues, industrial needs and process problems that motivated this work. Project goals will be outlined and the organization of this project will be presented.

1.2 Interconnect Technology Issues

Current chip interconnection trends in the semiconductor industry include the move toward higher density VLSI and ULSI type [1], [2], [3] , [4] architectures and the resultant need for a large number of devices connected within a device package. One of the driving requirements for packaging and interconnection technology is the need to meet the evolving requirements of portable electronic and other small scale devices [5], [6]. Some of the needs of these devices include the ability to manufacture high performance, high density devices at high volumes, but with low cost [7], [8], [9], and [10]. To meet these device requirements, chip manufacturers and designers are moving toward packaging systems that are able to handle a large increase in terminal counts and number of I/Os [11].

One of the main considerations in chip design currently revolves around the areas of packaging and interconnection development [6], areas that hold the greatest potential for producing breakthroughs in device speed, miniaturization and manufacturing cost. Some of the technologies examined are those that depart from the industry-standard plastic encapsulated device (which is based on the use of metal leads) and use other methods for connecting chips to each other and the main printed wiring board. These include TAB Bonding, C4, and flip-chip bonding -- technologies based on the use of solder rather than wire for connections. Details of these technologies will be presented in Chapter 2 along with a comparison of their advantages and disadvantages.

1.3 Industrial Needs

Current trends in chip manufacturing are based on the need for high performance devices the cost less to manufacture and allow for more miniaturization [12], [13]. As a result some of the major needs in the semiconductor industry include a need for higher circuit densities, i.e. more devices and circuits placed in a closer assembly on more expensive substrates and device surfaces [14]. The need exists for a greater number of I/O terminals for more functionality and for shorter electrical interconnection lengths between devices that would facilitate higher overall device speeds [13], [15]. The long gold wire bonds used in current joining methods have the problem of high self-inductance and put an upper limit on ultimate device speed. Another major need is greater reliability in high density soldering methods like flip-chip processing [12]; a problem that is caused by a lack of full understanding about the process. The current growth in the use of optoelectronicronic devices and connectors has also produced a need for high precision alignment with tolerances on the micron scale.

Each of these industry-related needs points to the central necessity for a full characterization of the reflow soldering process in general and the self-alignment mechanism specifically. This will involve acquiring a detailed understanding of the limitations of the process and the influence of process parameters. To optimize the solder reflow process for the several applications that require it, predictive relationships between parameters like joint radius, height, solder volume, and surface tension have to be developed.

1.4 Project Motivations

One of the main problems with flip-chip processing is that the use of surface tension for self-alignment is not well understood. Previous research into self-alignment has included a variety of modeling studies to characterize the process and relate the final joint morphology to process parameters. Goldmann [16] studied self-alignment using models that assumed predetermined shapes to describe the mechanics of droplet coalescence. Process parameters were studied and process specifications were developed by Miller [8] and Bache [17] to describe the characteristics of properly formed joints. Patra and Lee [18] developed a 2D modeling scheme to describe the initial, intermediate, and final solder profiles and their associated restoring forces during solder reflow.

Each of the above-mentioned studies provided us with useful information on the soldering process, but was limited to specific cases. These earlier studies focused on two-dimensional, axisymmetric models; even the most recent study was confined only to standard circular pad geometries. While these provide predictive relationships to determine the solder profiles and restoring forces for solder bumps currently in use, a more in-depth study of the relationships between these factors and the solder profile throughout the process needs to be undertaken for four reasons:

1) First, models which can be used to fully explore the interplay between solder volume, joint height, pad area and diameter, and pad size need to be developed in order to determine how these parameters affect the final shape of the joint. Final joint shape information is especially useful for process optimization as it can form the basis of further investigations aimed at joint reliability and fatigue life. An understanding of the physics of the small scale soldering processes which develop these final profiles and an understanding of the influence of process parameters will allow the process to be optimized effectively.

2) Second, models that are flexible, yet reliable representations can be used to study the influence of the use of different materials for chips and substrates. There is also a need for models to address the impact of different fluxing compounds used to clean off the bonding surfaces. Systems that are designed to accommodate several different solid surface and liquid surface properties are very useful in studying capillary issues.

3) Third, information on other types of solder joint shapes and their usefulness in producing other levels of restoring aligning forces is key for future process enhancements. The limitations of flip-chip processing methods given a range of process conditions, chip sizes and solder volumes are not well understood. There are currently no models available that can be used to study alternative bond shapes. Developing an understanding about and reliable models for other types of joints would be useful in designing joints capable of generating different levels of restoring forces. Calculating the final free surface configuration of non-standard joints is difficult using classical analytical methods and cannot be used to rigorously study the influence of process parameters on final joint shape. In order to characterize the full range of the process' usefulness, reliable and predictive relationships need to be developed between process parameters, joint geometry, and self-alignment. In addition the final solder profiles and information about final three dimensional surface morphologies need to be developed as well.

4) Fourth, a new order of three dimensional mathematical models for surface tension-driven shape changes would provide useful tools for studying not only systems involving coalescing solder droplet, but also similar systems on the micron scale. An understanding of the physics of small scale free surface motion and the influence of process parameters can be used to both characterize and optimize processes involving spray-forming, screen printing, thin coatings, etc. The advantage of this modeling scheme is that it is not geometry-limited and would allow for full analyses to be performed on various systems involving droplets, surface pools and flowing liquids controlled by capillary action.

In order to address these needs and properly characterize reflow soldering (particularly those joints using alternative geometries), a series of three dimensional mathematical models was developed to characterize the minimization of surface free energy that drives self-alignment. The goal of this portion of the project was to develop a database containing information linking major process parameters to the evolution of liquid bond morphology and final joint structure. Using standard pad sizes, the liquid-vapor surface tension coefficient, solder volume and vertical and horizontal misalignments, the free surface shapes, energies and restoring forces of three different pad geometries were calculated. These data were compared and contrasted to develop an understanding of the limits and ranges of the reflow soldering process.

The main motivations for this research project's focus were to gather information and gain a better understanding of the details of the flip-chip based self-alignment process. As mentioned earlier, flip-chip processing is not well understood beyond the empirical data employed by most companies that use the process in terms of joint shape, size, etc. While these companies utilize a standard set of process parameters developed in-house for joint connections, there are few or no industry standards or sources of data on the influence of a broad range of process parameters on self-alignment during reflow. The growing use of flip-chip manufacturing for alignment and other applications warrants a better knowledge of:

a) the process in terms of process limits and factors that affect its efficiency.

b) the actual restoring forces during the process and how these forces are influenced by process parameters. [Currently, very little physical data or measurements of restoring forces exists.]

c) solder joint morphology for addressing reliability issues.

In addition there is a need for predictive relationships for process optimization and an understanding of how various joint parameters, like pad geometry affect the reflow process. Finally, there is a need for the development of methods of measuring final chip alignments and related forces accurately.

The use of mathematical models provides a fast and low cost method both for studying the process without the need for expensive prototypes and for providing a flexible way of examining varying process parameters and their interactions. Because there are currently no methods available for studying alternative geometries and their effect on restoring force levels, developing new models is critical. These types of radical joint designs need to be evaluated for their possible usefulness as substitutes for traditional pads. In addition, they are a possible means for process enhancement by improving the ease of the initial rough tacking step.

1.5 Project Goals

In light of the reasons for investigating this system (as mentioned above), we sought to accomplish developing:

- a characterization of self-alignment phenomena in terms of process parameters;
- mathematical models of small-scale joining systems, systems involving capillary effects and the influences of surface tension;
- experimental methods to measure self-alignment effects during reflow soldering operations (methods which, prior to this study, did not exist).

In order to develop a full characterization of the process, this project focused on an approach that included a combination of mathematical models and parallel physical experiments. The mathematical models are designed to relate joint parameters to self-alignment restoring forces through a series of predictive relationships. This is accomplished by:

- calculations of restoring force
- calculations of the effects of solder pad geometry, solder joint height, surface tension, and solder volume

This project, the result of a joint effort between the M.I.T. Materials Process Modeling Group and AT&T Bell Laboratories, has as its goal the development of a better fundamental understanding of self-alignment phenomena and related process variables. It should be noted that the approach to be described in the following sections could be applicable to the modeling of a broad range of processing operations, where surface tension phenomena and free surface behavior play an important role.

1.6 Organization

All of the topics mentioned above will be discussed in detail in the chapters that follow. Their precise organization is as follows:

<u>Chapter 2</u> contains a literature survey of the research work done on both self alignment phenomena as well as the state of the art in the field of packaging and interconnects. Some publications which have resulted from the work presently being discussed are also included in the survey.

<u>Chapter 3</u> contains the principles governing the formulation of a series of mathematical models of the self-alignment behavior of a standard bump system as well as a brief survey of mathematical model schemes used to study the flip-chip alignment process.

<u>Chapter 4</u> contains the methodology, structure and results of the studies undertaken by this project focusing on calculating restoring forces as a function of individual and combined joint parameters. In addition, results for the restoring force calculations are presented and discussed.

<u>Chapter 5</u> contains the study of a number of alternative pad geometries and insights developed by studying these types of joint designs.

Chapter 6 contains a description of a static measurement scheme for studying horizontal restoring forces.

Chapter 7 presents a dynamic method for the measurement of horizontal alignment forces, along with a discussion of issues in dealing with this system.

Chapter 8 presents concluding remarks and recommendations for continuing the work presented in Chapters 1-7 as well as discuss their significance in developing design rules for self-aligning devices.

It should also be noted that Chapter 5 (with minor additions) has been published, with co-author J. Szekely, in the Journal of Electronic Materials, December 1994. Chapters 6 and 7 were presented at the 1995 TMS Annual Meeting with co-author J. Szekely as well. Chapter 4 will be submitted to a refereed journal.

1.7 References

[1] Satoh, R., Oshima, M, Komura, Ishi, I., Serizawa, K., "Development of a New Micro-Solder Bonding Method for VLSI's", IEPS, 1983, pp. 455.

[2] Misunas, D., "Advanced Packaging and Interconnection Technology", IEEE Micro, April 1993, pp. 7-9.

[3] Seraphim, D.P., Barr, D.E., "Interconnect and Packaging Technology in the 90's", SPIE vol. 1390, International Conference on Advances in Interconnection and Packaging, 1990, pp. 39-55.

[4] Hannermann, R.J., Kraus, A.D., Pecht, M., "Physical Architecture of VLSI Systems", Wiley-Interscience, N.Y., 1994, pp. 2-427.

[5] Kang, S.K., Woychik, C.G., "Mechanisms for Interconnection Formation in VLSI Packaging", The Metal Science of Joining, The Minerals, Metals, and Materials Society, 1992, pp. 319-324.

[6] Herell, D.J., "Addressing the Challenges of Advanced Packaging and Interconnection", IEEE Micro, April 1993, pp. 10-18.

[7] Wong, C.C., "Comparison of Chip Attachment Technologies", AT&T Bell Laboratories Technical Memorandum #11553-920526-22TM, May 1992, pp. 1-22.

[8] Miller, L.F., "A Survey of Chip Joining Techniques", IBM Technical Memo, pp. 60-76.

[9] Koopman, N.G., Reiley, T.C., Totta, P.A., "High Density Chip Interconnections", ISHM 1988 Proceedings, pp. 295301.

[10] Harper, C.A., "Electronic Packaging and Interconnection Handbook", McGraw-Hill, Inc., N.Y., 1991, pp. 10.48-10.57, pp. 6.70-6.79.

[11] Selvaduray, G., Singh, A., "Modeling of Flip-Chip-Bonded and Wired-Bonded MCM Interconnects for Electrical Performance Comparison", The International Journal of Microcircuits and Electronic Packaging, vol. 17, no. 1, 1994, pp. 28-35.

[12] Tobias, P.A., "The Reliability of Controlled-Collapse Solder LSI Connections, ISHM Proceedings, 1976, pp. 360.

[13] Maliniak, D., "Future Packaging Depends Heavily on Materials", Electronic Design, January 9, 1992, pp. 83-97.

[14] Dehkordi, P.H., Bouldin, D.W., "Design for Packagability; The impact of bonding technology on the size and layout of VLSI dies", Proceedings of the IEEE Multichip Module Conference, 1993, pp. 153-159.

[15] Ohsaki, T., "Electronic Packaging in the 1990's-A Perspective From Asia", IEEE Transactions on Components, Hybrids, and Manufacturing Technology, vol. 14, no. 2, June 1991, pp. 254-261.

[16] Goldmann, L.S. "Self-alignment Capability of Controlled Collapse Chip Joining", Proc. 22nd Electronic Components Conference. 1972, pp. 332-339.

[17] Bache, R.A.C., Burdett. P.A., Pickering, K.L., Parson, A.D., Pedder, D.J., "Bind Design and Alignment in Flip-Chip Solder Bonding", IEPS, 1988, pp. 830.

[18] Patra, S.K., Lee, Y.C., "Quasi-static Modeling of the Self-Alignment Mechanism in Flip-Chip Soldering-Part I; Simple Solder Joint", Journal of Electronic Packaging, vol. 113, 1991, pp. 337-342.

[19] Imler, W.R., Scholz, K.D., Cobarruviaz, M., Nagesh, V.K., Chao, C.C., Haitz, R., "Precision Flip-Chip Solder Bump Interconnects for Optical Packaging", IEEE Transactions on Components, Hybrids, and

manufacturing Technology, vol. 15, no. 6, December 1992, pp. 977-982.

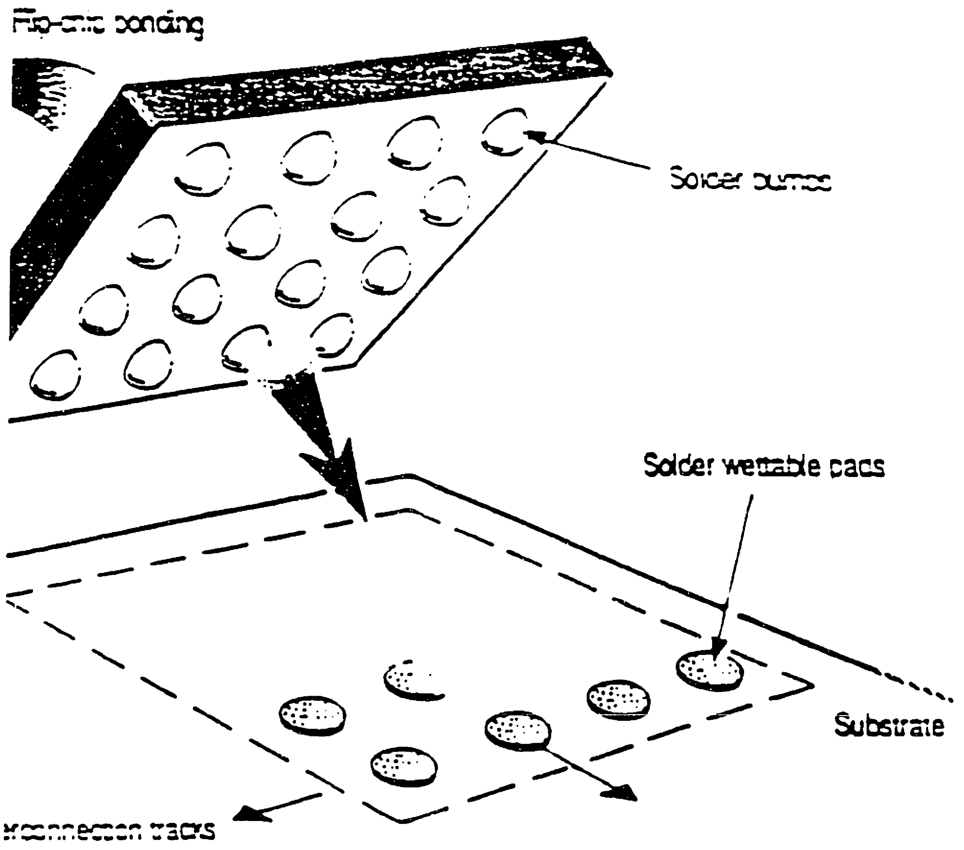

Fig. 1.1 Flip-Chip Processing

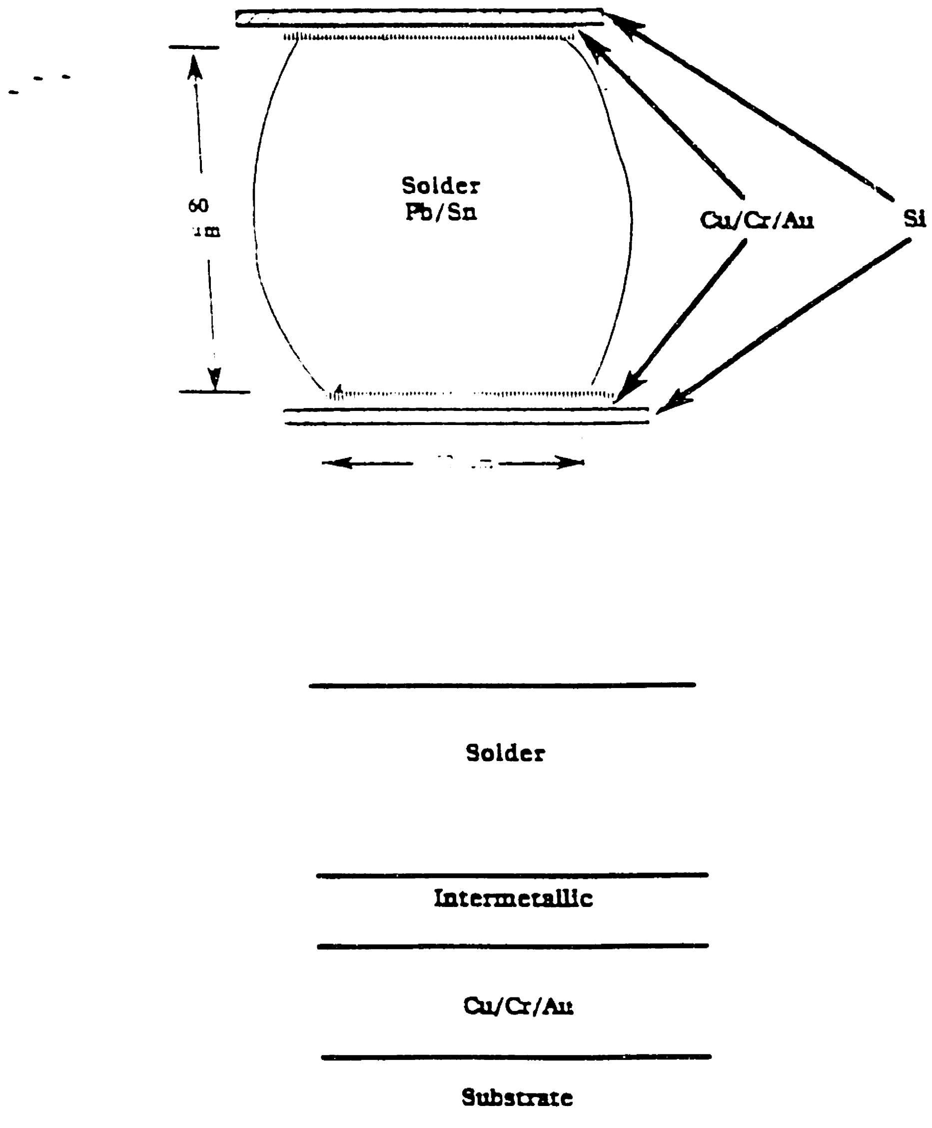

Fig. 1.2: A standard solder joint

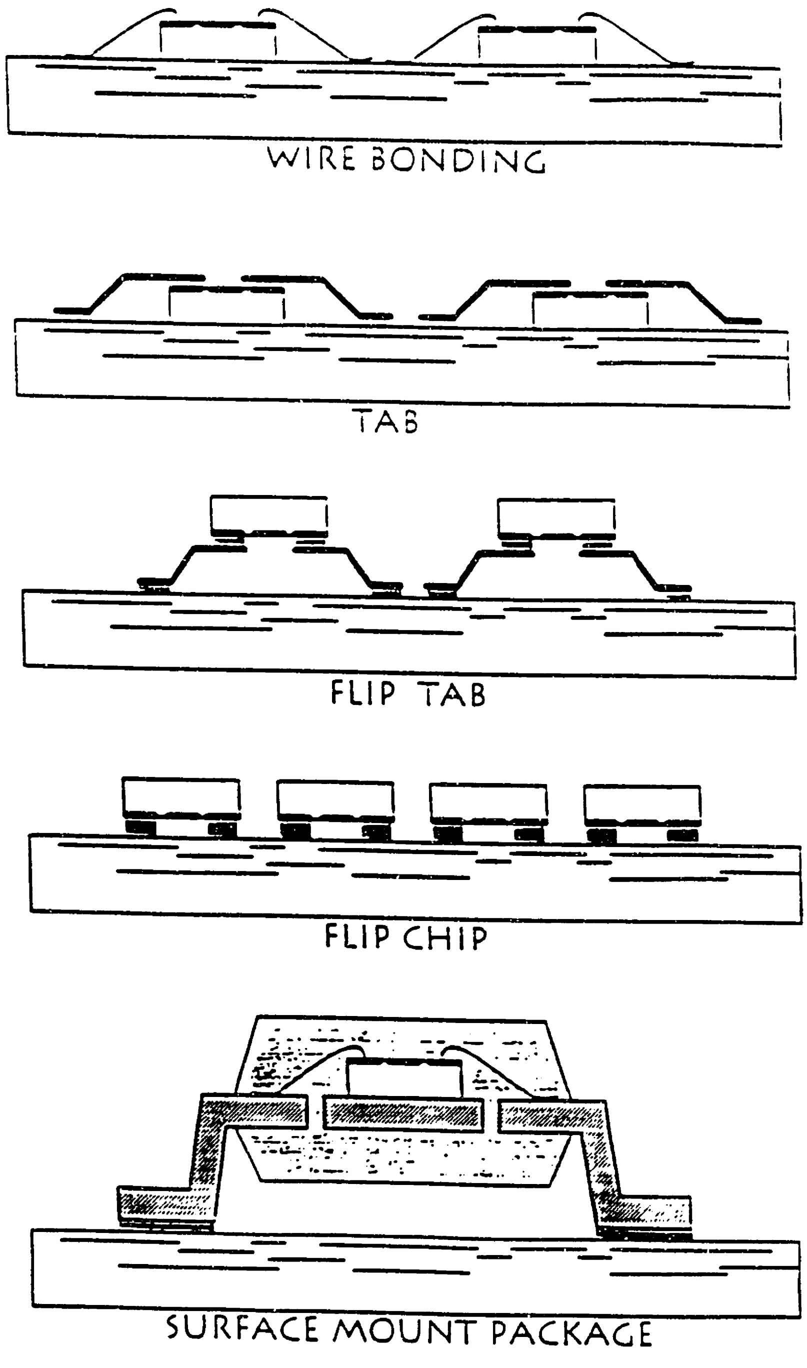

Fig. 1.3 **Comparison of bonding methods**

REFLOW REALIGNMENT

1. Misaligned "Tack"

2. Reflow

3. Surface Tension Driven Realignment

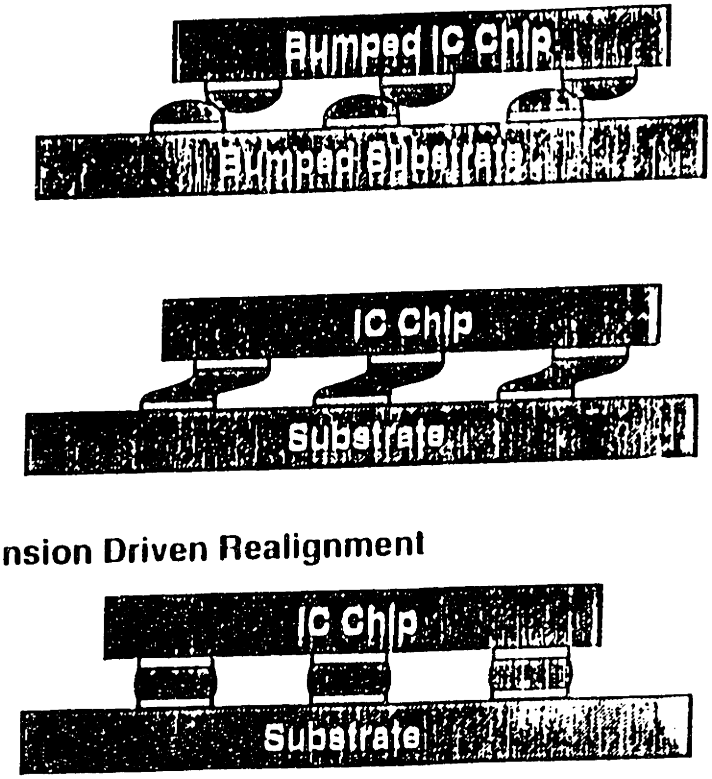

Fig. 1.4 **Self-alignment process**

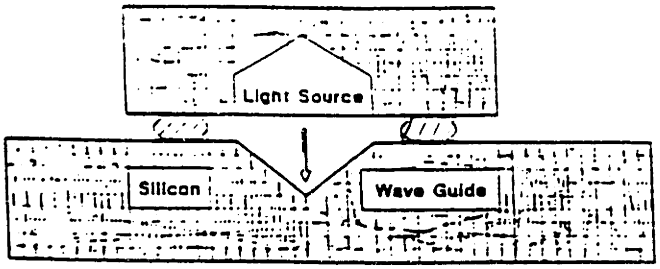

Fig. 1.5 Use of flip-chip for high precision alignment applications.

Chapter 2

LITERATURE SURVEY

2.1 Introduction

As it is discussed in Chapter 1, this work is based on the study of self-alignment restoring forces used in optoelectronic device alignment. In this Chapter, a brief survey of current research work in the field of interconnection technology, flip-chip manufacturing methods and their applications in opto-electronic applications will be outlined. Important issues will summarized and details of the flip chip process will be presented.

2.2 Interconnects and Packaging

In this section we will discuss a number of packaging and interconnection issues that are driving the semiconductor industry to use alternative bonding technologies, like flip-chip, over traditional technologies like wire bonding. A brief overview of current interconnect technologies will be presented in addition to a survey comparison of advantages and disadvantages of each type.

2.2.1 Industrial Issues

The electronic packaging technology area is undergoing a number of major changes as more attention is focused on the development of technologies to protect, carry, connect and organize higher performance electronic devices [1].

The need for high density and high performance at low cost for future portable equipment demands sophisticated developments in interconnect and joining technology. These two areas -- cost and performance -- are the main driving factors in the need for better interconnection technologies. These technologies include tape-automated bonding and flip-chip assembly.

2.2.2 Flip-Chip Applications and Advantages

Flip-chip technology provides several process and device advantages to a number of current semiconductor manufacturing applications. Some of the driving forces of these applications are a need for higher amount of I/Os, particularly for future logic function type modules which will require exceptionally high pin counts of greater than 2000 per chip [2], [3]. These high performance assemblies will require smaller interconnection pitches and sizes arranged in larger array dimensions than ever before. At the same time, cost factors will push for the development of approaches using radically different metallurgies, processes, packages, and designs.

There are three major types of chip interconnection schemes available for packaging operations: wire bonding, tape-automated bonding, and flip-chip bonding. Fig. 1.3 showed the different types of bonding methods available and Fig 2.1 shows the rough distribution of the usage of these joining technologies.

Wire Bonding: In wire bonding, interconnects between chip and substrate are formed by gold and aluminum wires bonded at the matching I/Os of each system. For each set of I/O's, two bonding operations must be carried out at the periphery of the chip. Wire bonding has been used primarily for integrated circuit applications with IC chips bonded to a package base and electrically connected using gold or aluminum wires 1 mil in diameter [4]. Wire bonding technologies include ultrasonic bonding, thermo-compression bonding and thermosonic bonding, each forming bonds with either ball joints or wedge joints. Many of the current applications of wire bonding systems include uses in chip on board systems [5].

Tape-Automated Bonding: Tape-automated bonding methods [6] use a metallization interconnection pattern and inner- and outer-lead bonding processes. Inner-lead bonding is done first using a hot thermode to gang bond to the tape and then outer-lead bonding to the package connections. TAB bonding offers several advantages over wire-bonding some of which include the ability to test electrically prior to assembly, and the ability to do gang bonding simultaneously instead of individual interconnections.

Some of the problems of wire bonding, in terms of device performance, are based the geometry of the wire joint and the related limitations associated with manufacturing them. These geometry factors include the use of long wires, the bonding around the periphery, and the large area of these wires. Wire bonding use of long wires to form interconnections is a major problem in that this generates self-inductance effects that interfere with transmission. In terms of manufacturing limitations, it is a relatively slow technique in terms of processing due to the need to form each bond individually instead of simultaneously. Other limitations include: the minimum separation dictated by the bonding tool; the intermetallics formed by the aluminum (Al) and gold wires; and the stress cracks at the interconnect locations caused by the bonders.

One example [7] of a common application of flip-chip technology as a replacement for wire bonding is in the fabrication of Multichip modules (MCM) [8]. MCM is a semiconductor packaging technology designed to support several chips on a single package. It is an architecture which uses flip-chip bonding to bond chips and substrates directly together in a single package, improving device density and overall system performance [6]. Given the closer proximity of the individual components, a significant increase in signal speeds is possible due to the decreased travel distances relative to other bonding schemes. The advantages of flip-chip manufacturing over other joining methods for high density applications have been studied by several researchers. Jeannotte [9] and Goldmann [10] studied different aspects of the usage of solder as a structural support material. Mones [11], Tummala [12], and Ginsberg [13] performed studies on solder in terms of packaging and interconnection issues.

Flip-Chip Bonding: In addition to these design and performance advantages, flip-chip provides a far less expensive means of manufacturing unique functions. These include combinations of substrates (GaAs and Silicon), plus the mixture of analog, digital control, and digital signal processing technologies. The use of flip-chip bonding makes it possible to avoid the increased time and difficulty needed to process a large number of wire interconnections on modules which are growing in complexity and highly limited in space. By eliminating a large number of wire connections, it is much easier to reduce assembly costs, increase connection and device volume, and improve reliability [4]. Additionally, replacing wire bonds with solder bumps provides the means for a chip attachment which allows testing, precise alignment of the chip, and simultaneous joint formation which is valuable for high volume interconnection needs.

Flip-chip bonding also provides several advantages over these other types of joining technologies in terms of packaging and electrical performance. Flip chip offers the packaging advantages of high I/O density, smaller bond pitches, shorter interconnections and higher device density. In terms of electrical performance, there is a factor of four difference in lead cross-sectional area of leads among the three joint types. Another major comparative characteristic is the level of die connection parasitics, associated with each type of interconnect, which affect operating frequencies. Flip-chip interconnects produce the lowest values in terms of joint resistance, inductance and capacitance, mainly due to their small size. Table 2.1 shows a summary comparison of other aspects of flip-chip when compared to TAB and wire bonding for chips on board applications.

The next section of this chapter we shall focus on the state of interconnection research as it pertains to joining technology in general and flip-chip joining specifically. Following that section a survey of some of the current applications of flip-chip processing for standard joining operations for logic circuits as well as its special uses in the production of optical devices, will be discussed.

2.2.3 Interconnect Technology Research

Research into interconnects in electronics and electronic packaging is a well-established field. The field contains a large number of research projects studying many different aspects of joint metallurgy, process effects, and reliability issues. General interconnect technology research falls into two main categories: study of joint integrity during the testing and service stages; the study of joint formation characteristics during the manufacturing stage. The majority of research efforts have focused on testing and service problems like joint mechanical stress determination, joint deformation, fatigue life, thermal cycling behavior and reliability/quality control issues. In terms of joint geometry studies, past works include those of Charles and Clatterbaugh [14], Engelmaier [14], Shah [16], and Sherry and Erich [17], who focused on various aspect of thermochemical effects, fatigue effects and process variable research. Hwang and Lee [18], focused on soldering issues and solder paste while Lau, Rice and Avery [19] performed an electroplastic analysis surface mount solder joints and Reimer and Russel [20] discussed methods for optimizing solder bonds for ceramic applications. Almost all of these studies centered on surface mount technology assembly with regard to a combination of reliability and process control issues.

Some of the manufacturing issues driving the development of better electronic packaging techniques include: reliability, fatigue properties, joint optimization, ease of manufacture, and high chip joining yields. Reliability issues for solder joints have been addressed by Nir [21], Norris [22], Tobias [23], and Lodge [24] in terms of mechanical fatigue properties, reliability models, thermal fatigue and creep experiments. Goldmann [10] and Singh [25] addressed joint and process optimization with the development of methods to predict optimal chip dimensions and placement schemes.

2.3 Flip-Chip Process History

There is a strong relationship between integrated circuits and electronic packaging, particularly as device speeds and circuit densities increase. In order to lower manufacturing costs and improve device performance and reliability, packaging has received increased attention in the development of new technologies. It is discussed, in Chapter 1, that this work is based on the study of solder joint formation in flip-chip solder interconnects. The flip-chip technique was originally developed by IBM in 1964 as part of their development work on interconnection techniques that would provide improvements in manufacturability, economy and reliability over the Solid Logic Technology connection [23]. The original SLT, show in Fig. 2.2, was formed by reflow soldered connections using three or more non-melting 5 mil Cu balls to produce a strong copper ball connection capable of a low failure rate over the life of the joint [26], [27]. This joining system was a departure from the traditional chip-to-substrate attachment method in the use of area arrays of terminals with advantages in increased terminal density and exceptionally high reliability. One major disadvantage of the process was its need for more cooling due to poor thermal dissipation. SLT was replaced by C4 (Controlled Collapse Chip Connection) technology which eliminated the use of copper ball standoffs between the module and chip, and using solder alone as the mechanical and electrical joining medium. C4 interconnects are formed through the coalecsence of two separate solder bumps which forms a "collapsed" final joint. Fig. 2.3 shows a standard C4 joint with solder connecting a chip to a substrate via matching metallization pads.

The next section will provide a detailed description of the flip-chip bonding process and discuss each of the process steps used to form a complete bump.

2.4 Flip-Chip Process Details

The basic flip-chip package consists of an IC chip that has been processed through photolithography, metallization, and dicing, atop a series of metal pedestals or columns, commonly called "bumps". The bumps are placed on a substrate with a film interconnection pattern and external leads. A typical solder bump structure is composed of several elements. The first of these is a via defined [Fig. 2.4] through a passivation layer, usually a polyimide on the chip surface down to the aluminum metallization employed on the I/O pads. The via is usually cleaned using an in situ sputter or ion beam process to remove alumina film from the aluminum alloy to insure an ohmic connection. The via is then covered and sealed by the application of a solderable metallization area, usually Cr-Cu-Au. The Cr layer provides adhesion and a diffusion barrier between solder and the aluminum layer. The alloyed Cr-Cu layer provides solderability combined with resistance to solder dissolution to allow for multiple soldering operations. A pure copper layer is added for solderability, followed by a gold layer to prevent oxidation of the underlying layers after the completion of deposition. Solder is laid down for each solder bump by an electrodeposition process using photolithography and a resist mask. The solder used in most bumping operations for silicon ICs requiring a high-temperature alloy is 95%Pb, 5% Sn with a liquidus temperature of 312 degrees C. After solder deposition, the joints are generally reflowed in non-oxidizing conditions to allow for formation of a fully formed joint. Since the flipped chip and substrate are aligned face-to-face and bump-to-bump, the solder bump coalesces through surface tension to form complete, aligned joints at each site (Fig. 2.5). The aligned joints translate into an aligned component with an extremely accurate registration [28], [29].

The IC chip is bonded face down (Fig. 1.1), using the bumps as electrical connections and physical attachment to the substrate [4]. The basic structure of a controlled collapse terminal used in flip-chip processing relies on a solder alloy droplet, which forms a mechanical and electrical bond between an IC chip and a substrate. Fig. 2.6 shows some of the details of a solder interconnect while Fig. 1.2 depicts a cut-away view of the relevant materials, including a metallization pad which the solder wets (Cu/Cr/Au in our studies) and an intermetallic layer which forms later in the joints life-cycle. The actual joint formation process involves the joining of an area array of matching solder bumps which are deposited onto the surface of both the substrate and chip during the wafer-scale processing stage. The initial solid solder mounds used by different in-house processes vary in both diameter and height usually, but tend to be in the range of 75-150 µm in diameter and approximately 60-85 µm in height.

After the individual solder bumps are deposited, the wafers are diced to form separate chips which are placed and tacked to specific contact sites on Si substrates to insure a primitive bond. Using a specialized IR belt oven the system is heated and individual solder bumps at each contact site liquefy, coalesce, and form complete bonds providing electrical contact and a permanent mechanical bond between chip and substrate after the joints solidify [23]. As the joints form, the tendency of the system to minimize its surface energy causes the solder bead to assume a new surface shape; in effect, the solder bonds will move along their surfaces to form perfect truncated spheres. The force generated by this phenomenon across an area array of joints causes the chips to align themselves atop the substrate terminals, a phenomena known as self-alignment (Fig. 1.4). The usefulness of this aspect of the process is that it allows for precise alignment and corrective realignment of misaligned chips onto substrates. Previous research [30] has shown that a chip that is misaligned up to 24 degrees rotationally can be fully realigned by the process during the heating stage and in terms of horizontal displacements, as long as the bumps are in contact, full realignment will also occur. This study set out to determine the restoring forces which are generated by self-alignment and the surface morphologies of the joints which are formed as a result. Our objective here is twofold: first, provide a fundamental, quantitative explanation of the observed phenomena; second, use this fundamental understanding as a rational basis for new technology development.

2.5 Flip-Chip Research

The growing interest in flip-chip bonding for a wide variety of electrical, mechanical and optical device applications has lead to a great deal of research in these areas. In terms of mathematical modeling, the most recent research projects have examined the morphology of standard bumps and the calculation of joint geometry factors. The main focus of physical research has been on determining mechanical reliability and joint fatigue life characteristics. Another area of research has concentrated on the electrical properties and signal characteristics of these connections. These studies have examined the material, process, and structure influences that determine the overall performance of flip-chip soldered interconnects.

In one of the earliest mathematical studies of flip-chip joints, Goldmann [10] developed an analytical study which demonstrated the importance of joint geometry on thermal fatigue behavior and the optimal joint developed for controlled collapse chip connection systems. Other models of solder geometry in fillet-type joints include those of Alexander and Bello [31], Klein Wassink [32], and Chu [33], and that of Ellis and Masada [34] which focused on pin-in-hole devices and surface mounted chip capacitors.

Research on packaging issues for devices using flip-chip includes the work of Dehkordi [35], Malinak [36], Lodge [24], Mones [11], Singh [25], and Ohsaki [37]. Mechanical behavior in post-reflow flip-chip assemblies has been undertaken by Chiou [38], Subrhmanyan [39], Nir [21], Norris [22], Goldmann [10], and Tobias [23]. Studies of thermal behavior in solder interconnects has been performed by Oktay [40], who examined temperature profiles of chips and solder during heating. Analysis of the influence of inert atmosphere and fluxing compounds includes the work of Pickering and Southworth [28], who studied hydrogen plasma fluxing processes, and the work of Shipley [41] who studied changes in solder composition during joining. Testing and quality control issues were examined by Putltitz [42], who surveyed a number of flip-chip replacement technologies for flip-chip bonded multilayer ceramic multichip modules.

2.6 Self-Alignment Applications

The successful implementation of opto-electronic integrated circuits is a growing area of research for the realization of economically efficient optical systems [43]. The main challenge of developing these systems as an evolution of current semiconductors is the development of packages and interfaces that provide sturdy couplings and electrical connections between chips and fiber. Optical devices (Fig. 2.7) have extremely high physical alignment tolerances that must be met for them to operate properly. In order to achieve a high level of optical power for an integrated optical waveguide (switch matrix or high speed modulator), optimum positioning in terms of lateral and vertical displacements must be kept under 1 micron.

For example, a semiconductor laser with a near spot field size of approximately 2 microns requires positioning tolerances of 0.2 microns. The high tolerances required result in a relatively high cost for producing high performance opto-electronic parts. A large part of this cost stems from the need for a substantial amount of expensive manual alignment and adjustment during final assembly. In addition, the need for many devices to be operational during final assembly for testing requires even more expensive machine vision equipment and robotics. Flip-chip solder bonding provides an assembly method capable of achieving < 1 micron tolerances without manual adjustments or placement equipment. In addition, flip-chip reflow alignment methods avoid the disadvantages of other processes using visual placement which are tedious, time consuming and expensive. Some of the applications for this level of tolerance include silicon ICs, GaAs chips on microwave circuits, infrared detector arrays, and hybrid spatial light modulator structures. Each of the applications has demonstrated alignment tolerances better that 2 microns with a 30 micron initial placement tolerance [44], [45].

One of the main applications of flip-chip bonding is for fiber interfacing of integrated optical chips. These assemblies usually have several waveguides to be coupled at each end of the chip, requiring alignment tolerances of 0.5-1 micron. In addition, a number of electrical contacts need to be made to the chip. In order to fabricate these devices, a series of fiber-carrying V-grooves are etched into silicon, and then aligned with respect to waveguides using an array of solder-wettable pads in precisely determined positions. These individual process steps can be seen in [Fig. 2.8]. In order for this alignment to take place it is necessary only for the pads to overlap by one-half of their diameter for self-alignment action to take place.

In order to develop more cost-effective methods of aligning precisely, these passive alignment methods using surface tension forces generated by an area array of solder joints have been investigated by several researchers [44], [46], High precision alignment research has been carried out for a number of applications in the field of laser and fiber optic research. The work of Jackson, Flint and Cina [47], focused on the use of joints spaced by waveguide material for alignment in order to demonstrate the feasibility of laser alignment to parallel waveguides. Cohen [48] focused on the development of the ability to align four optic fibers in silicon V-grooves to laser devices using a set of fiduciary marks and a glass alignment plate.

2.7 Area Array vs. Peripheral Array

One of the important considerations in the use of flip-chip bonding in a number of applications is the bonding format by which the solder bumps on chip and substrate are organized. Module design decisions generally fall into two different areas: an area array format and a peripheral (or perimeter) array format. In an area array format, bumps are spread across the entire area of the die surface. In a perimeter array format the bumps are arranged around the periphery of the chip and substrate in single or double row. Fig. 2.9 shows the layout of a standard area array layout, while Fig. 2.10 shows the arrangement of a peripheral array format [49].

The key determining factors governing the use of area arrays vs. perimeter arrays of solder bumps are generally cost or performance considerations, depending on the requirements of the planned module. For applications requiring high potential I/O pin counts, an area array format is better than perimeter formats due to the far higher density of I/Os that can be laid out. One example of this type of application would be in the interconnection scheme for a VLSI Bipolar logic chip [53] which require I/O densities of at least 120 connections. Another application of area array flip-chip bonding would be in the manufacture of Multichip Modules (MCM) which require large numbers of I/Os, high density packaging potential combined with low production costs [49], [50]. Area array formats allow for high density arrays with a much larger pitch spacing than a peripheral array with a comparable I/O density -- an advantage particularly for applications where pitch and the danger of shorting or leakage are important [51]. Another benefit of high density is that smaller systems can be developed, systems that have the die placed closer together and have a higher level of performance (due to a reduction in effective bond inductance, line drivers can potentially be smaller). Some of the disadvantages of area array bonding include the extensive requirements for die preparation and the lack of an infrastructure to support this technology. An additional disadvantage is a limited understanding of the details of area array bonding.

In general, assessing the need for area array vs. peripheral bonding is a function mainly of the needs that are to be addressed. Rent's Rule [49], [48], a quasi-empirical topological law developed to relate the number of signal and control I/O counts to the number of logic partitions is seen below, where:

$$\text{\# of signal I/Os} = a\ (\text{\# of circuits/partition})^{b}$$

where a and b denote prefactor and exponent which are related
to the type of chip and device architecture (MCM, etc.)
and a number of constants

Using Rent's rule, the need for a large number of I/Os provided by area array formats can be addressed [52].

Research into Rent's rule and area array vs. perimeter array decisions have been performed by a number of researchers including Sandborn [49], Krusis [50], Fried [53], Donath [54], and Koons [2] who each addressed different design implications of these two bonding methods.

2.8 References

[1] Herell, D.J., "Addressing the Challenges of Advanced Packaging and Interconnection", IEEE Micro, April 1993, pp. 10-18.

[2] Koons, J.P., "Design Factors With Realistic I/O Distributions", Journal of Electronic Packaging-Transactions of the ASME, March 1991, vol. 113., pp. 76-80.

[3] Borgesen, P., Li, C.Y., Conway, H.D., "Mechanical Design Considerations for Area Array Solder Joints", IEEE Transactions on Components, Hybrids, and Manufacturing Technology, vol. 16, no. 3, May 1993, pp. 272-283.

[4] Myers, T.R., "Flip-chip Microcircuit Bonding Systems", IIT Research Institute Paper, pp. 131-144.

[5] Kang, S.K., Woychik, C.G., "Mechanisms of Interconnection Formation in VLSI Packaging", The Metal Science of Joining. TMS, 1992, pp. 319-324.

[6] Selvaduray, G., Singh, A., "Modeling of Flip-Chip-Bonded and Wired-Bonded MCM Interconnects for Electrical Performance Comparison", The International Journal of Microcircuits and Electronic Packaging, vol. 17, no. 1, 1994, pp. 28-35.

[7] Jin, H., Vahldieck, R., Minkus, H., Huang, J., "Rigorous Field Theory Analysis of Flip-Chip Interconnections in MMICs using the FDTLM Method", IEEE MTT-S Digest, 1994, pp. 1711-1714.

[8] Barlett, C.J., Segelken, J.M., "Multichip Packaging for VLSI-based systems", IEEE Electronic Components Conference, May 1987, pp. 518-525.

[9] Jeannotte, D.A., "Solder as a Structural Member for Chip Joining", Proceedings 1969 Electronic Components Conference, pp. 334.

[10] Goldmann, L.S., "Geometric Optimization of Controlled Collapse Interconnections", Journal of IBM Research and Development, vol. 113, 1969, pp. 251-265.

[11] Mones, A.H., Speilberger, R.K., "Interconnecting and Packaging VLSI Chips", Solid State Technology, January 1984, pp. 119-122.

[12] Tummala, R.,"Microelectronics Packaging Handbook", N.Y., Van Nostrand Reinhold, 1989.

[13] Ginsberg, G., "Surface Mount and Related Technologies", N.Y., M. Dekker, pp. 1-5, 220-258., 1989.

[14] Clatterburgh, G.V., Charles, H.K., 'Thermochemical Behavior of Soldered Interconnects for Surface Mounting: A Comparison of Theory and Experiment", Proc. 35th Electronic Components Conference, Washington, D.C., 1985a, pp. 60-72.

[15] Englermaier, W., "Fatigue Life of Leadless Chip Carrier Solder Joint During Power Cycling", IEEE Transactions on Components, Hybrids, and Manufacturing Technology, vol, CHMT-6, no. 3. pp. 232-237

[16] Shah, M.K., "Analysis of Parameters Influencing Stresses in the Solder Joints of Leadless Chip Capacitors", ASME Winter Annual Meeting, San Francisco, CA, Paper No. 89-WA/EEP-31, 1989.

[17] Sherry, W.M., Erich, J.S., "Analytical and Experimental Analysis of LCCC Solder Joint Fatigue Life", Proc. 35th Electronic Components Conference, Washington, D.C., 1985, pp. 81-90.

[18] Hwang, J.S,, Lee, N.C., "A New Development in Solder Paste with Unique Rheology for Surface Mounting", Proc. of the 1985 International Symposium on Microelectronics, Anaheim, CA, 1985, pp. 23-30.

[19] Lau, J.H., Rice, D.W., Avery, P.A., "Elastoplastic Analysis of Surface Mount Solder Joints", IEEE Transactions on Components, Hybrids, and Manufacturing Technology, vol. CHMT-10, no. 3, 1987, pp. 346-357.

[20] Remimer, D.E., Russell, J.D., "The Optimized Solder Bond for Ceramic Chip Carriers on Ceramic Boards", Proc. 1983 International Microelectronics Symposium, International Society for Hybrid Microelectronics, 1983, pp. 217-222.

[21] Nir, N., Dudderar, T.D., Wong, C.C., Storm, A.R., "Fatigue Properties of Microelectronics Solder Joints", Transactions of the ASME, vol. 113, June 1991, pp. 92-101.

[22] Norris, K.C., Landzberg, A.H., "Reliability of Controlled Collapse Interconnections", IBM Journal of Research and Development, May 1969, pp. 266-271.

[23] Tobias, P.A., "The Reliability of Controlled-Collapse Solder LSI Connections, ISHM Proceedings, 1976, pp. 360.

[24] Lodge, K.J., Pedder, D.J., "The Impact of Packaging on the Reliability of Flip-Chip Solder Bonded Devices", IEEE Transactions on Components, Hybrids and Manufacturing Technology, vol. 13, no. 4, December 1990, pp. 847-855.

[25] Singh, P., Landis, D.L., "Optimal Chip Sizing for Hybrid-WSI", 1994 IEEE International Conference on Wafer Scale Integration Proc. 6th Annual IEEE International Conference Wafer Scale Integration, 1994, pp. 374-386.

[26] Totta, P.A., "Flip Chip Solder Terminals", 21st Electronics Components Conference, Washington, D.C., pp. 275-284.

[27] Berry, B.S, Ames, I., "Studies of the SLT Chip Terminal Metallurgy", IBM Journal of Research and Development, May 1969, pp. 286-296.

[28] Pickering, K., Southworth P., Wort, C., Parsons, A., Pedder, D.J., "Hydrogen Plasmas for Flux Free Flip-Chip Solder Bonding", Journal of Vacuum Science Technology, vol. 8, No. 3, May/June 1990, pp. 1503-1508.

[29] Powell, D.O., Triverdi, A.K., "Flip-Chip on FR-4 Integrated Circuit Packaging", Circuits and Devices, 1993, p. 182-186.

[30] Dudderar, D., Personal Communication on unpublished research, AT&T Bell Laboratories, 1992.

[31] Alexander, P.T., Bello, D.C., "The Single Key Process Variable in SMT Solder Joint Reliability", Proc. Expo SMT 1987, Las Vegas, NV, 1987, pp. 85-89.

[32] Klein Wassink, R.J., Soldering In Electronics, Second Edition, Electrochemical Publications Ltd., Ayr, Scotland, 1989, pp. 46-51.

[33] Chu, T., "A Hydrostatic Model of Solder Fillets", Western Electric Engineer, vol. 19, no.2, 1975,

[34] Ellis, J.R., Masada, G.Y., "Dynamic Behavior of SMT Chip Capacitors During Solder Reflow", Proc. 5th IEEE/CHMT International Electronics Manufacturing Technology Symposium, San Francisco, CA, 1989,

[35] Dehkordi, P.H., Bouldin, D.W., "Design for Packagability; The impact of bonding technology on the size and layout of VLSI dies", Proceedings of the IEEE Multichip Module Conference, 1993, pp. 153-159.

[36] Maliniak, D., "Future Packaging Depends Heavily on Materials", Electronic Design, January 9, 1992, pp. 83-97.

[37] Ohsaki, T., "Electronic Packaging in the 1990's-A Perspective From Asia", IEEE Transactions on Components, Hybrids, and Manufacturing Technology, vol. 14, no. 2, June 1991, pp. 254-261.

[38] Chiou, B., Cheng J-C, "Effect of Cooling Rate on the Mechanical and Electrical Behavior of a 63 Sn/37 Pb Solder Bump on a Metallized Si Substrate", Journal of Materials Science; Materials in Electronics, vol. 5, No. #4, Aug. 1994, pp. 229-234.

[39] Subrhmanyan, Ravi, "Mechanical and Accelerated Testing of Flip-Chip Interconnect Systems", Electronic Packaging Materials Science VII Materials Research Society Symposium Proceedings, vol. 323, 1994, pp. 395-406.

[40] Oktay, S., "Parametric Study of Temperature Profiles in Chips Joined by Controlled Collapse Techniques", 1969 Electronic Components Conference, IEEE, May 1969, pp. 272-285.

[41] Shipley, J.F., "Influence of Flux, Substrate and Solder Composition on Solder Wetting", Welding Journal, 1975, 54, (10), 357s

[42] Puttlitz, K.J., Shutler, W.F., "C-4/BGA comparison with other MLC single chip package alternatives", Proceedings-Electronic Components and Technology Conference, 1994, pp. 16-21.

[43] Weber, R., Fidorra, F., Hamacher, M., Heldrich, H., Jacumeit. G., "Multi fiber/chip Coupling and Opto-electronic Integrated Circuit Packaging Based on Flip Chip Bonding Techniques", SPIE Vol. 1849 Opto-electronic Interconnects, 1993, pp. 149-152.

[44] Wale, M.J., Edge, C., "Self-Aligned Flip-Chip Assembly of Photonic Devices with Electrical and Optical Connections", IEEE Trans. on CHMT, vol. 13, no. 4, Dec. 1990, pp. 780-786.

[45] Deshmukh, R.D., Brady, M.F., Roll, R.A., Shmulovich, J., Zolnowski, D.R., King, L.A., "Active Atmosphere solder self-alignment and bonding of optical components", International Journal of Microcircuits and Electronic Packaging, vol. 16, No. 2, 1993, pp. 97-108.

[46] McGroarty, J., Borgesen, P., Yost, B., Li, C., "Statistics of Solder Joint Alignment for Opto-electronics Components", IEEE Transactions on Components, Hybrids, and Manufacturing Technology, vol. 16, no. 5, August 1993, pp. 527-529.

[47] Jackson, K.P., Flint, E.B., Cina, M.F., Moll, A.J., Ewen, J.F., Flagello, D., Rand, R., Purushotaman, S., "Packaging of 1 Gb/s OEIC Fiber-Optic Data Link", Proceedings of the Electronic Component Conference, Houston, 1989, pp. 374-377.

[48] Cohen, M.S., Cina, M.F., Bassous, E., Oprysko, M., Speidell, J.L., "Passive Laser-Fiber Alignment by Index Method", IEEE Transactions Photonics Technology Letters, vol. 3, no. 11, Nov. 1991, pp. 985-987.

[49] Sandborn, P.A., Abadir, M.S., Murphy, C.F.,"Tradeoff Between Peripheral and Area Array Bonding of Components in Multichip Modules." IEEE Transactions on Components, Packaging, and Manufacturing Technology Part A, vol. 17, no. 2, 1994, pp. 249-256.

[50] Krusius, J.P., "System Interconnection of High Density Multichip Modules", SPIE vol. 1390 International Conference on Advances in Interconnection and Packaging, 1990, pp. 261-270.

[51] Koopman, N.G., "High Density Chip Interconnections", ISHM 1988 Proceedings, 1988, pp. 295-300.

[52] Hannemann, R.J., Kraus, A.D., Pecht, M., "Physical Architecture of VLSI Systems", Wiley-Interscience, N.Y., 1994, pp. 2-427.

[53] Fried, L.J., Havas, J., Lechaton, J.S., Logan, J.S., Paal, G., Totta, P.A., "A VLSI Bipolar Metallization Design with Three-Level Wiring and Area Array Solder Connections", IBM Journal of Research and Development, vol. 26, no. 3, May 1982, pp. 362-371.

[54] Donath, W.E., "Placement and Average Interconnection Lengths of Computer Logic", Microelectronics System Interconnections, IEEE Press, 1979, pp. 147-151.

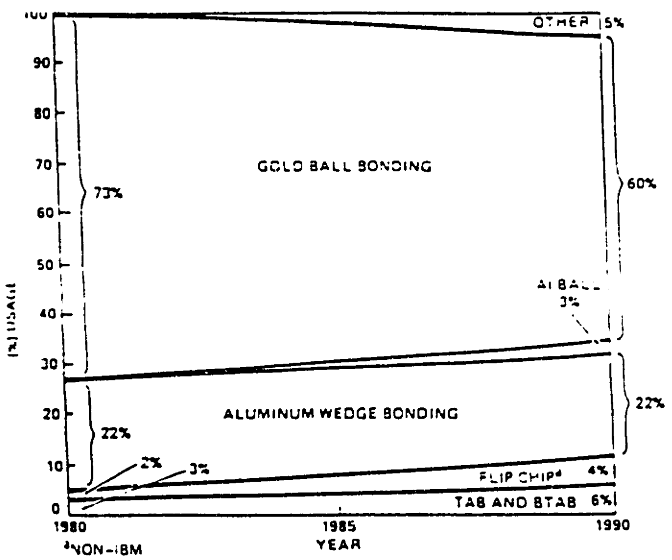

Fig. 2.1 Usage of joining technologies

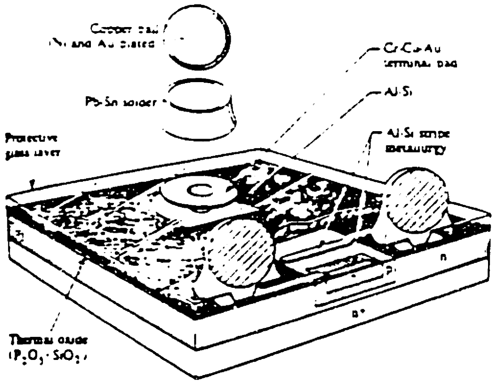

Fig. 2.2 Original SLT joint

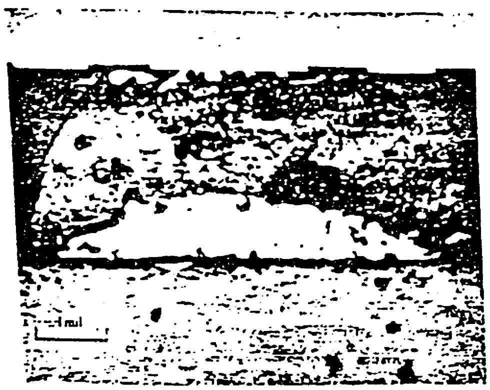

Fig. 2.3 Controlled collapse chip joint

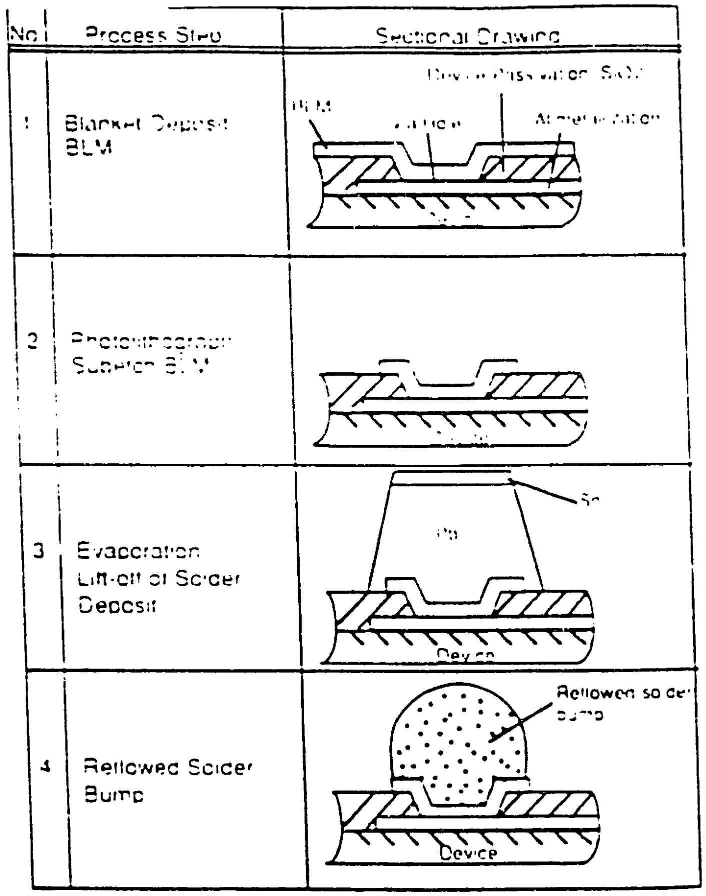

Fig. 2.4 Flip-Chip processing steps

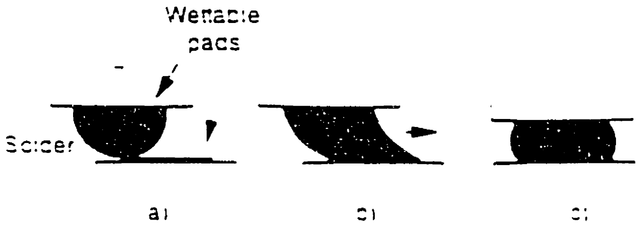

Fig. 2.5 Formation of a bond

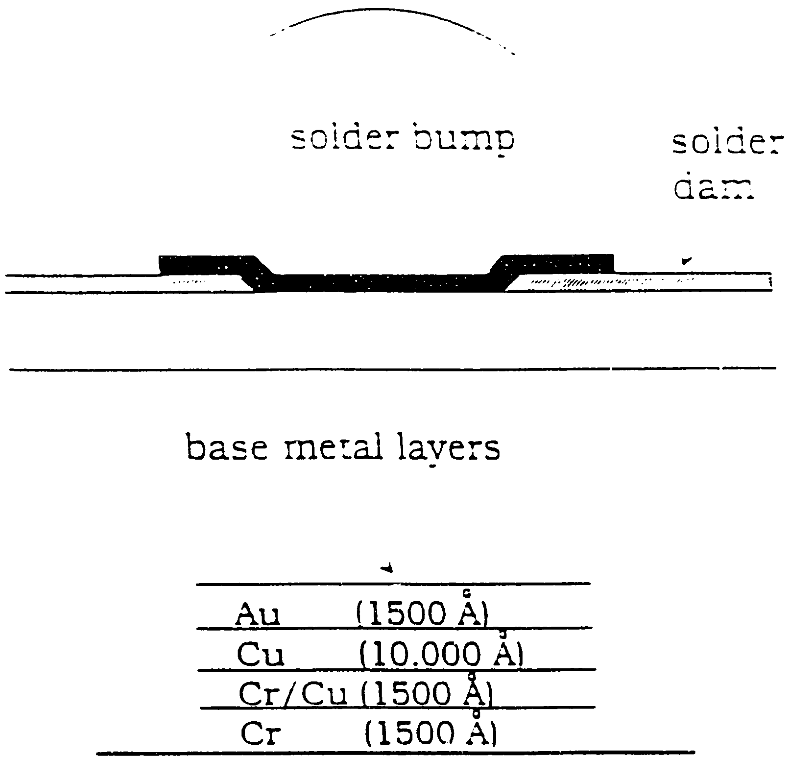

Fig. 2.6 Details of a solder bump

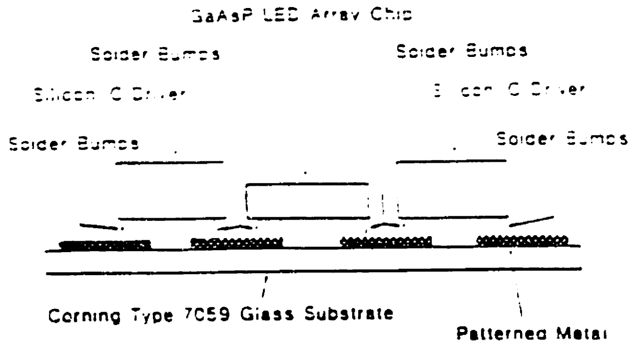

Fig. 2.7 Optical device applications

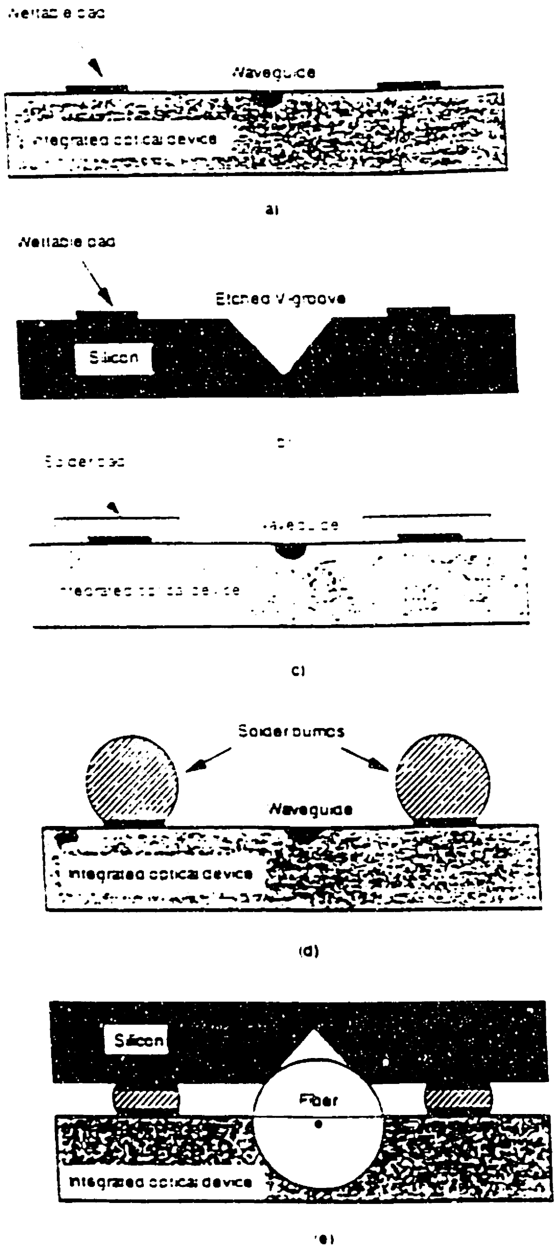

Fig. 2.8 Fabrication for flip-chip alignment

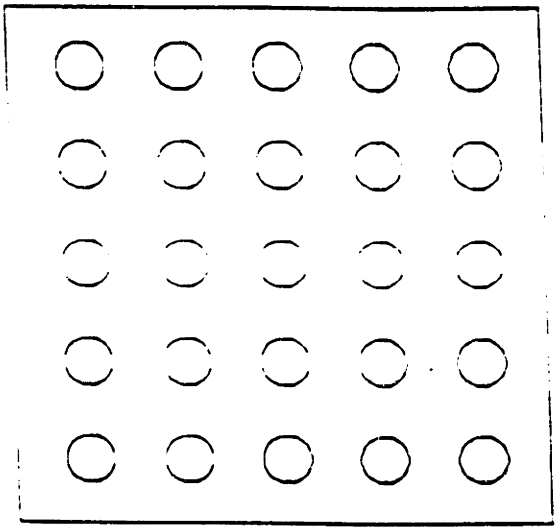

Fig. 2.9: Area Area Format

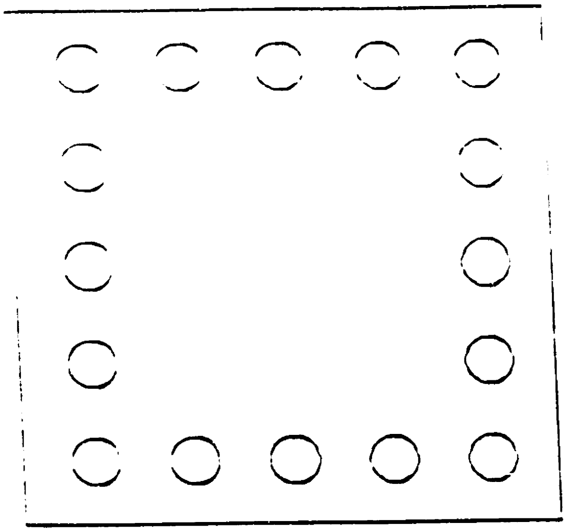

Fig. 2.10: Perimeter Array Format

Property/requirement	Wire bond	TAB	Flip-chip[a]
Circuit density	Medium	High	High
Special circuit process	No	Yes	No
Circuit cost	Low	High	Medium
Bonding process	Simple	Complex	Moderate
Profile	High	Low	Low-medium
Easy pretest	No	No	No
Special chips	No	Yes/no[b]	Yes
Development status	Mature	Emerging	Mature
Density capability	Med. high	Very high	Medium
High speed	No	Yes	Yes
Reliability	High	High	High
Aluminum pads OK	Yes	No	No
Gang bonding	No	Yes	Yes
TCE stress	No	Sometimes	Yes
Thermal characteristics	Good	Good	Poor
Substrate choices	Wide	Limited	Limited

Table 2.1 Comparison of Chip-on-Board Process

Chapter 3

THEORY

3.1 Introduction

Mathematical process modeling is a growing field of study in the semiconductor design and manufacturing industry. With numerous constraints, requirements and design specifications that must be met on an ever-shortening design timeline, models present a low cost option for examining processes that would otherwise receive limited study.

A number of models of the reflow solder joint have been developed, with a large majority focused on the post-reflow aspect of solder behavior; i.e. mechanical behavior, creep response, etc. These include the work of Oktay [1] and Sarihan [2], who studied temperature dependencies and thermal cycling effects. Selvaduray [3] has modeled the electrical performance of flip-chip and wire-bonded interconnects for MCM, while Sandborn [4] and Sarihan have modeled this system in terms of electronic packaging design limits and partitioning. In terms of mechanical behavior, Jin [5], Nir [6] and Dudderar [7] have studied the reliability of solder joints under a variety of mechanical cycling.

In-process models include those of Patra [8], Martino [9], and Heinrich [10], who studied solder joint formation for two-dimensional cases for a limted number of process parameters. In terms of general formulations, the work of Racz [11] can be applied to a number of capillary systems and other joint systems inciuding gull and J-lead surface mount connections.

The mathematical models used to study the self-alignment mechanism occurring during reflow solder are based on an examination of the free surface shape changes between the solder bumps in their molten state. As the molten bumps coalesce, their morphology is dominated by the effects of surface tension as gravity forces tend to be negligible because of the small scale of the system. Thermodynamic driving forces will force the liquid surface to reduce the total area thus reducing the surface energy, and move toward a more stable equilibrium shape. The classical solution for the problem of the minimal energy surface of a free floating droplet is obviously a sphere, since it has the highest surface area to volume ratio of any kind of morphology. In our system where a liquid is trapped between two plates, the equilibrium shape is a truncated sphere and corresponds to the "zero" position of self-alignment, where the restoring force is zero. As self-alignment proceeds those joints which are misaligned will have higher surface free energy, and thus higher restoring forces driving the surface change toward the zero position. As a result, the solder in these joints will move towards the equilibrium shape, dragging the attached chip until it is aligned.

The mathematical models that we used to study self-alignment behavior addressed the following issues:

1) calculation of the horizontal restoring forces generated in self-alignment from first principles.
2) calculation of the free surface shapes developed for circular pad geometries during reflow when an external displacement is applied.
3) calculation of the dependency of restoring forces on joint parameters including pad radius, solder height, solder volume, and surface tension.

The following sections will deal with the details of the principles governing self-alignment such as capillary effects and wetting effects. In addition, the computer methodology and tools developed to model self-alignment will de described in detail. As the subsequent chapters will show, these methods and tools are readily applicable to other small scale electronic soldering operations.

3.2 Theory

3.2.1 Capillary Effects

An important set of fluid problems involves the influence of capillary forces and surfaces. This set of phenomena includes a number of small scale systems with liquids governed primarily by the influence of surface tension. The classic example of a capillary system would be a liquid interface rising and falling in a thin circular tube. Capillary effects have been studied for several years, from the early work of Young and Laplace [12], to the current work of Cliff [13], Hiram [14], and Finn [15] in calculating equilibrium capillary surfaces in droplets, bubbles and particles. Vogel [16], Boucher [17] and Fortes [18] have extended this work to liquids trapped between parallel plates and Racz [19] studied a number of capillary effects when applied to standard joint designs.

There is a broad range of applicability of capillary problem solutions to a variety of modern processes, particularly in the area of soldering, due the interaction of a number of free surface energy and surface area driven effects. Wetting and spreading of liquids in standard brazing and soldering operations is a well-studied and understood area in terms of process details [20], [21], [22], [23].

The main driving force of soldering actions is capillary action. The study of these small scale effects is a well research field due to its importance in many processing operations involving small scale liquids. Many governing relationships of capillary systems have been studied previously, including the Young Equation for the wetting of surfaces [12] and liquid droplet shapes for various surface energy interactions. Another major equation is the Euler-Lagrange equation and the Laplace Equation for calculating the equilibrium droplet shape of simple meniscus systems by relating surface shape to density and pressure differences [24], [23], [19]. A major application of capillary principles is in describing soldering effects. In the next section we will define a subset of capillary effects, namely wetting behavior.

3.2.2 Wetting Effects

A major subset of capillary effects-type problems are those which involve the influence of wetting effects. One of the major areas of current research in soldering is in studies of basic wetting effects, both measuring their magnitude and developing a better understanding of those process related factors that govern their behavior. With a large variety of materials used in electronics soldering and higher solder wetting requirements, solderability test techniques have become not only a crucical quality control tool but also a means for developing a better understanding of the process factors influencing wetting behavior. Standard experiments and measurements include: the use of wetting balances [27] to measure surface tension; studies of solder spread over surfaces usings the sessile drop method over varying surface chemistry, roughness and shape [26]; and wetting in binary and ternary metallic systems [27]. Other research has focused on the soldering of gold-coated substrates due to the problems associated with the reaction of tin in PbSn solder and the gold, which result in lower strength joints.

An important aspect of wetting behavior is the influence of flux. Fluxes are highly reactive organic resins and solvents applied to the solder during processing. This is used to remove surface films, such as various oxides, to provide surfaces on the basis metals and on the liquid solder which are free to interact. These chemicals interact with the metal oxides and exclude oxygen from the surrounding atmosphere. [21], [22]. Some of the problems associated with flux use include developing efficient ways to introduce it into the joint and ensure full cleaning of the joint area for its removal. Alternative methods being utilized currently to protect the solder surface from oxidation involve the use of an inert nitrogen atmosphere for soldering to remove the need for a fluxing step [28]

3.2.3 The Young Equation

Soldering is accomplished through the use of a filler metal and flux, which form a liquid link between two joined surfaces, as the joint is heated above the melting temperature of the solder. One of the main requirements for a good soldered joint is the full wetting of the base materials by the filler metal. This characteristic is strongly dependent on existing surface conditions, chemical reactions at the interfaces, and the geometry of the joint [23]. All these factors affect the final properties of the joint. One of the main equations describing wetting effects is the Young Equation, which is applied normally to pendant or sessile drops for conditions of chemical equilibrium. The equation as seen below :

$$\gamma_{sv} = \gamma_{sl} + \gamma_{lv} \cos\theta \tag{3.1}$$

where the surface tensions are: γ_{SV} at the solid/vapor interface, γ_{Sl} at the solid/liquid interface, and γ_{lV} at the liquid/vapor interface. The wetting angle, θ is measured through the liquid phase with wetting occuring for theta < 90 deg. and non-wetting for theta > 90 deg (Fig. 3.1).

3.2.4 Surface Tension vs. Gravity Issues

There are two competing influences on the shape and motion of a liquid free surface in systems, of this scale, that need to be considered in any study of soldering effects. The first is the influence of gravity on the bulk mass of the liquid; the second is the influence of surface tension on the free surface. Depending on the scale of the system, these factors will play a role of varying magnitude in determining how the liquid will behave. In general, for liquids with a large length scale like standing pools of liquid, gravity effects tend to dominate over the effects of gravity, while for liquids on the small scale (like tiny droplets) surface tension effects are more dominant than gravity in determing fluid behavior. The key dimensionless group [29] used to discriminate between these competing influences is known as the Bond # and provides information on what effects will determining free surface shape as a function of size of the system in question.

$$Bond\# = \frac{g(\rho - \rho_f)d_p^{\,2}}{\sigma^t} \tag{3.2}$$

where ρ is the drop density
dp is the drop diameter
ρ_f is the fluid density
g is gravitational acceleration
and σ^t is the surface tension

For large values of the Bond number (heavily dependent on dominant length scale), gravity effects dominate. Smaller values indicate that surface tension is the governing morphology factor. For the flip-chip solder system, where the characteristic dimension (the pad diameter) is very small, the value of the Bond number is 6.6×10^{-6}. Thus the free surface shape will be determined by the influence of surface tension while gravity effects may be neglected.

3.2.5 Heat Transfer Effects

Another major effect that should be considered in the study of soldered joints is the presence or absence of internal fluid flow generated by temperature gradients. Given the nature of the solder in its molten state, internal flows can have a large effect on the behavior of the liquid surface. The main determinant of this is the Biot number which, by its magnitude, determines the presence or absence of temperature gradients in a body of liiquid and their prodution of internal temperature gradient driven flows of the liquid.

The dimensionless Biot number (shown below) is used as a measure of the presence or absence of [33] large temperature gradients that would produce internal flows. The Biot number relates the relative effects of heat transfer away from the surface by convection to internal heat transfer away from the internal body of material by conduction. When heat transfer away from the surface is large, there are low or no internal gradients; and when internal conduction is greater, large internal temperature gradients exist in the body. The main parameter in determining the presence of these gradients is the length scale of the system. For values of the Biot # greater than unity, large temperature gradients will exist in the body of the liquid (large pools, etc.). For values less than unity, no large temperature gradients will exist and the system is at constant temperature (small droplets, etc.).

$$Biot\# = \frac{hl}{k} \tag{3.3}$$

where l is the characteristic length of the system

k is the thermal conductivity
h is the heat transfer coefficient

For the systems considered in this study, the Biot number is 2.23 x 10^{-3} due to the small linear scale involved, thus internal temperature gradients are unlikely to be of importance. While some internal fluid flow will no doubt occur during the realignment process, this will be neglected in our calculations. On the basis of experience with somewhat related systems this assumption is thought to be reasonable.

3.3 Young-Laplace Equation and Solution

Research into the shape of droplets began in 1805 with the work of Laplace [12]. Bashforth and Adams [30] developed a table using numerically obtained values describing the shapes of axially symmetric pendant drops. A solution to the exact shape of an axially symmetric drop was developed by Padday [31] in 1950, and a number of investigators followed this work with studies of the symmertic droplet shape and stability [32], [33], [34], [17], [19].

Numerical studies of surface shapes which deviate from symmetry are a recent development [35], and a number of similar numerical solutions have been applied to study restoring force generation of liquid droplets in C4 arrays [37], [38], [8], [10]. Numerical solutions for self-alignment restoring force are based upon a differential equation which describes the shape of a liquid gas interface in cylindrical coordinates using a derivation of the Euler-Lagrange Equation. This is solved using variational calculus and the method of finite differences [14].

The Young-Laplace equation for the equilibrium shape of a liquid-gas interface is shown below:

$$\frac{\Delta P}{\gamma}=\left(\frac{1}{R_1}+\frac{1}{R_2}\right) \tag{3.4}$$

where ΔP is the pressure difference across the interface,

is the surface tension of the interface and R_1 and R_2 are the two radii of curvature of the surface in the orthogonal directions. By writing an integral expression for the surface free energy of the drop and applying the Euler Lagrange equation to find a condition for minimizing the surface energy, a differential equation describing the equilibrium shape of the liquid surface can be developed. The equation for a small element of surface area in cylindrical coordinates is shown below:

$$dA=\left(1+r_z^2+\frac{r_\theta^2}{r^2}+\frac{r_z^2 r_\theta^2}{r^2}\right)^{\frac{1}{2}} r\,dz\,d\theta \tag{3.5}$$

where r is the radius in cylindrical coordinates, z is the height and

is the angle. The total surface energy, U, of the drop is equal to the differential surface area element times the surface tension, integrated over the area of the drop:

$$U=\gamma\int_0^{2\pi}\int_0^{h}\left(1+r_z^2+\frac{r_\theta^2}{r^2}\right)^{\frac{1}{2}} r\,dz\,d\theta \tag{3.6}$$

When the Euler-Langrange method is used to minimize U, the result is a differential equation describing the minimal surface, which would have no pressure difference across the surface. Pressure differential effects can be absorbed into the potenial function, resulting in an effective potential energy, V shown below:

$$V = \int_0^{2\pi}\int_0^{h}\left[\gamma\left(1 + r_z^2 + \frac{r_\theta^2}{r^2}\right)^{\frac{1}{2}} - r\Delta P\right] r\,dz\,d\theta \tag{3.7}$$

When V is minimized, the result will be a general differential equation for a surface with constant radius of curvature in cylindrical coordinates. This minimization is accomplished through an application of the Euler-Lagrange method, defining a functional, f which for a cylindrical system is:

$$f = r\left[\gamma\left(1 + r_z^2 + \frac{r_\theta^2}{r^2}\right)^{\frac{1}{2}} - r\Delta P\right] \tag{3.8}$$

By substituting f into a Euler-Lagrange equation, the dfferential equation which minimizes the integral is developed:

$$f_r - \frac{\partial}{\partial z} f_{r_z} - \frac{\partial}{\partial \theta} f_{r\theta} = 0 \tag{3.9}$$

where r, r_z, r_θ, and, are independent variables and f_{rz} is the devivative of f with respect to r_z. Solder joint shapes can be calculated from the resulting differential equation using the method of finite differences or a numerical method [20]

3.4 Restoring Force Calculation

The main principles guiding the formation of self-aligned bonds rests in the surface tension driven surface motion which occurs in the liquid state of the solder. To relate this to the previous derivation and calculate restoring forces, the following assumptions should be made. They include assuming constant volume and constant displacement in the perpendicular dimension, in addition to a series of displacements from equilibrium. The restoring force in the z direction is related to the surface area by:

$$f_z = \gamma \frac{\Delta A}{\Delta z} \tag{3.10}$$

where ΔA is the area difference resulting from a displacement of Δz in the vertical or horizontal dimension. This equation can be recast in terms of three general formulations seen below:

$$E_{solder} = \gamma A_{solder} \tag{3.11}$$

where E_{solder} is the surface energy of the solder
A_{solder} is the total surface area of the solder
and γ is the surface tension coefficient

By using this relation to calculate the surface energy of the solder joint, the restoring forces associated with vertical or horizontal displacements can be determined. The normal restoring force, acting along the vertical axis of the joint is given by the equation:

$$F_{normal} = \frac{\partial E}{\partial H} \tag{3.12}$$

where for constant horizontal displacement, P,
E is surface energy and H is the distance
between chip and substrate

while the shear restoring force, operating in the horizontal direction is given by:

$$F_{shear} = \frac{\partial E}{\partial P} \tag{3.13}$$

for a constant vertical separation, H
where E is the surface energy and
P is the horizontal displacement of chip to substrate

Therefore, with data on the surface area and surface tension of a particular solder surface, the restoring forces generated by an initial misalignment in the horizontal and vertical directions can be calculated as a function of a displacement from the final, equilibrium position. For the standard circular pad used commonly in industry currently, the energy equation to be solved is:

where:

$$E_s = \gamma \int_0^H \int_0^{2\pi} r \left[1 + \left(\frac{\partial r}{\partial z} \right)^2 + \left(\frac{\partial p}{\partial z} \right)^2 + 2 \frac{\partial r}{\partial z} \frac{\partial p}{\partial z} \cos\theta \right]^{\frac{1}{2}} d\theta dz \tag{3.14}$$

It should be noted that for more complex surfaces or for a study of standard solder surfaces, which require a variation in a number of joint parameters, the classical solution based on an indirect solution to the energy minimization has limited usefulness [19]. In order to solve for special cases, a numerical solution for the surface energy of the solder is superior. As a result, in the following section we shall discuss the Surface Evolver code, a software tool which models the evolution of minimal energy surfaces through a series of finite-difference calculations of surface area and energy. This program is used for all of the mathematical models discussed in this thesis.

3.5 Description of the Surface Evolver

3.5.1 Introduction

Given the need for a numerical solution for the surface energy for a number of complex combinations of surfaces and joint parameters, a number of numerical packages were examined. One public domain package, known as the Surface Evolver is a software tool which is designed to calculate and display the evolution of minimal energy surfaces in a variety of systems from droplet and bubble formation and interaction to crystal growth. These are each systems were surface tension, gravity and other user-defined energies can play a major role in determining surface motion. It was developed by Ken Brakke at the University of Minnesota as part of the Supercomputing Project to solve multidimensional theoretical math problems involving surface minimization.

The Surface Evolver [36], [19], uses user-defined boundary conditions, constraints, and surface conditions to form an initial surface which is evolved toward minimum energy by a gradient decscent method. The evolution is meant to be a computer model of the process of evolution by mean curvature, which is studied for surface tension energy in the context of varifolds and geometric measure theory. It is an interactive program designed to study surfaces shaped by surface tension and other energies. The energy in the Surface Evolver can be a combination of surface tension, gravitational energy, squared mean curvature, user-defined surface integrals or knot energies. Motion is simulated by mean curvature and the user is able to interactively modify a surface in order to change properties or keep the surface evolution well-behaved. The result is a graphical output of the mininmal area surface, along with the area and energy as produced by user constraints and boundary conditions.

The Surface Evolver is especially designed to minimize complex surface morpohlogies affected by a number of variables for a number of different systems. It can handle any number of volume constraints, boundary constraints, boundary contact angles, prescribed mean curvature, crystalline intergrands, and gravity constraints. For details on other features and capabilites of the code, the reader is referred to the Surface Evolver Manual, Surface Evolver source code, or papers by Ken Brakke on the code in the journal *Experimental Mathematics.*

The following sections discuss relevant portions of the Surface Evolver capabilites and features including the represention of surfaces, role of constraints and energies and how surface motion is handled by the code.

3.5.2 Surface Representation

The Surface Evolver defines a series of basic elements that it used to calculate and represent a free surface and its motion. These basic elements forming surfaces include: *vertices*, which are Euclidean 3-space points; *edges*, which are straight line segments joining pairs of vertices; and *faces* (or facets) which are planar or equiangular triangles made up of three or four edges. Bodies are defined as a complete sum of the bounded space of all the facets or mini-surfaces. Surfaces are defined as the sum of all the facets linked together. Orientation is extended to edges and facets for bookkeeping purposes, but not to bodies or vertices in the definition of a surface, the topology of which may be arbitrary. The representation of all the parameters and pertinent information about a surface is defined in C-programming syntax in a file known to the Surface Evolver as a *datafile*. A simple example of a datafile shown below is cat.fe [36], which is used to define a catenoid surface. Units and length scale are defined by the user so careful consideration must be used to maintain units throughout a datafile that make physical sense. The datafile for this surface is shown in Fig. 3.2.

The resultant final surface of cat.fe will be that of a stable or unstable catenoid formed between two rings after a few iterations. Stability will depend on on the separation and radius defined by the user initially and during the iteration runs. A diagram of the basic structure of the vertex, edge, and facet elements is shown in Fig. 3.3, while Fig. 3.4 shows the initial surface generated by the Surface Evolver for the cat.fe datafile settings. The output surface can be defined with any number of facets through a refinement command, providing the cabaility to study complex surfaces composed of several curvatures. Fig. 3.5 shows the final minimal surface for cat.fe after 50 iterations and three levels of refinement.

3.5.3 Energy, Constraints and Boundary Conditions

Energy is one of the main quantities modeled by the Surface Evolver and can vary from surface tension to gravitational energy, depending on the user defined conditions for energy within the [36]. A surface is defined as having a total energy surface tension is the default energy condition and will act upon the surface unless otherwise defined in the datafile. Surface tension is defined in the Surface Evolver as an energy density quanity in generic units of energy per unit area. This energy density is applied on a facet-by-facet basis as defined by the user in the facet definition component of the datafile. So, it is possible to have several different energies defined across a entire surface. The total energy of the system is then calculated as the sum of all the contributions fo surface tension on each individual facets times their respective surface tensions.

Another type of energy recognized by the Surface Evolver is that of gravitational potential energy, which is represented by a volumetric density applied to a specified body. G, the gravitional constant can be defined by the user to any value with gravitaional potential energy written as:

$$E = \iiint_{\text{body}} G\rho z\,dV \tag{3.11}$$

Gravity is calculated by the divergence theorem shown below:

$$E = \iint_{\text{surface of body}} G\rho \frac{z^2}{2} \hat{k} \cdot d\bar{S} \tag{3.12}$$

and this integral is then applied to each facets for the body of interest.

Energy has another use in the Surface Evolver scheme which involves the definition of *Constraint Integrals* to represent other types of energies applied to the surfaces. These formulations are useful in controlling the motion of the surface and are made up of constraint edge type integrals for energies applied to surface edges, and constraint surface energy integrals which control the application of a vector field over the facets of a defined body. A sample constraint edge integral is shown below:

$$E = \int_{\text{edge}} \bar{F} \cdot d\bar{l} \tag{3.13}$$

where $\bar{F}$ is the vector field being integrated over the specified edge.

One example of a common constraint edge integral is that used to define a contact angle between a liquid and a solid surface [19]. The formulation in terms of Surface Evolver code would look this:

$$E = \iint_{facets} \vec{F} \cdot \hat{n} d\vec{S} \tag{3.14}$$

where n is the specified contact angle.

3.5.4 Motion

Motion in the Surface Evolver is handled by moving individual vertices of a surface as a function of defined energies, constraints, and boundary conditions. Magnitude and direction of forces on each vertex are equal to the magnitude and direction of the velocity of the surface. Due to the nature of the Surface Evolver representation, there is no relationship between this defined velocity and the time step of the iteration, though the work of [19] points toward a possible formulation for addressing this in future versions of the Surface Evolver.

Force calculations are performed at each vertex with the velocity equal to the negative gradient of the total energy as a function of vertex position. Vertices can be declared FIXED as in the case of solids with zero forces, or FREE with forces acting on them for each iteration toward the minimal surface. After forces are calculate the next step in the formulation is the application of all constraints, which are obeyed as closely as possible. One example of a major type of constraint is the inequality constraint which is defined as a boundary that the fluid may not cross. This is useful for confining a liquid to wetting or non-wetting regions, or preventing surface interpenetration. Another example of a major constraint is the volume constraint, which can be set in the initial surface or defined during the iteration stage. This allows the user to directly control the volume of all defined bodies and avoid runaway calculations for bodies stretched beyond their realistic limits.

The next chapter will give discuss the application of the surface evolver to the problem of calculating restoring forces for a number of joint parameters. Details of the approached used, model types designed and computational methodology will be outlined and results presented for a number of cases

3.6 References

[1] Oktay, S., "Parametric Study of Temperature Profiles in Chips Joined by Controlled Collapse Techniques", 1969 Electronic Components Conference, IEEE, May 1969, pp. 272-285.

[2] Sarihan, V., "Temperature Dependent Viscoplastic Simulation of Controlled Collapse Solder Joint Under Thermal Cycling", Transactions of the ASME, vol. 115, March 1993, pp. 16-21.

[3] Selvaduray, G., Singh, A., "Modeling of Flip-Chip-Bonded and Wired-Bonded MCM Interconnects for Electrical Performance Comparison", The International Journal of Microcircuits and Electronic Packaging, vol. 17, no. 1, 1994, pp. 28-35.

[4] Sandborn, P.A., Abadir, M., Murphy, C.F., "A Partitioning Advisor for Studying the Tradeoff Between Peripheral and Area Array Bonding of Components in Multichip Modules", 1993 IEEE/CHMT International Electronics Manufacturing Technology Symposium, 1993, pp 271-276.

[5] Jin, H., Vahldieck, R., Minkus, H., Huang, J., "Rigorous Field Theory Analysis of Flip-Chip Interconnections in MMICs using the FDTLM Method", IEEE MTT-S Digest, 1994, pp. 1711-1714.

[6] Nir, N., Dudderar, T.D., Wong, C.C., Storm, A.R., "Fatigue Properties of Microelectronics Solder Joints", Transactions of the ASME, vol. 113, June 1991, pp. 92-101.

[7] Dudderar, D., Personal Communication, AT&T Bell Laboratories, 1992.

[8] Patra, S.K., Lee, Y.C., "Modeling of self-alignment mechanism in flip-chip soldering--Part II: Multichip solder joints." Proceedings-Electronic Components Conference, 1991, pp. 783-788.

[9] Martino, P.M., Freedman, G.M., Racz, L. Szekley, J., "Predicting solder joint shape by computer modeling", Proceedings-Electronic Components and Technology Conference, 1994, pp. 1071-1078.

[10[Heinrich, S.M., Elkouh, A.F., Nigro, N.J., Lee, P.S., "Solder Joint Formation in Surface Mount Technology-Part I: Analysis", Transactions of the ASME, vol. 112, September 1990, pp. 210-222.

[11] Racz, L., Szekely, J. ,"Analysis of the Applicability of Wetting balance measurements of components with dissimilar surfaces", Advances in Electronic Packaging-American Society Mechanical Engineers, EEP, vol. 4-2, 1993, pp. 1103-1111.

[12] Young, T., "On the Cohesion of Fluids", Phil. Trans. R. Soc. London A, vol. 95, pp. 68, 1805.

[13] Cliff, R., "Bubbles, Drops, and Particles", Academic Press, N.Y. 1978.

[14] Hiram, Y, Nir. A, "A Simulation of Surface Tension Driven Coalesence", Journal of Colloid and Interface Science, vol. 95, no. 2, pp. 462-470.

[15] Finn, R., "Equilibrium Capillary Surfaces",Springer-Verlag, N.Y. 1986.

[16] Vogel. T.I., "Stability of a Drop Trapped Between Two Parallel Planes: Preliminary Report", Variational Methods for Free Surface Interfaces", 1987, pp. 139-144.

[17] Boucher, E.A.. McGarry, S., "Capillary Phenomena; Fluid bridges Between Horizontal Solid Plates in a Gravitational Field", Journal of Colloid and Interface Science. vol. 89, no. 1, September 1982, pp. 154-165.

[18] Fortes, M. A., "Axisymmetric Liquid Bridges Between Parallel Plates", Journal of Colloid and Interface Science, vol. 88, no. 2, August 1982, pp. 338-352.

[19] Racz, L. "Mathematical Modeling of Meniscus Problems in Materials Processing", Doctoral Thesis, 1993.

[20] Yost, B., McGroarty J., Borgesen, P., Li, C.Y., "Shape of a Nonaxisymmetric Liquid Solder Drop Constrained by Parallel Plates", IEEE Transactions on Components, Hybrids and Manufacturing Technology, vol. 16, no. 5, August 1993, pp. 523-527.

[21] Manko, H., "Soldering Handbook for Printed Circuits and Surface Mounting", Van Nostrand Reinhold Publishing, N.Y. 1986.

[22] Wassink, K, "Brazing and Soldering", No. 8, pp. 57. 1985.

[23] Santella, M., "Fundamental Metallurgical Considerations in Brazing and Soldering", The Metal Science of Joining, TMS, 1992, pp. 61-65.

[24] Weinstock, R., Calculus of Variations, New York, N.Y., McGraw-Hill, 1952.

[25] Okamoto, I, Omori, A., Den, K., and Tamaki, K., Trans. JWRI, 1980, 9, (1), pp.19.

[26] Thwaites, C.J., " Soldering Technology-A Decade of Developments", International Metals Review, vol. 29, no. 2, 1984, pp. 45-74.

[27] Shipley, J.F., "Influence of Flux, Substrate and Solder Composition on Solder wetting", Welding Reserach Supplement, October 1975, pp. 357a-359.

[28] McManus, J. J., Welding Journal, 1975, 54, (10), pp. 734.
Laplace, P.S., Theory of Capillary Attraction, 1805.

[29] Zong, J., Li, B., Szekeley, J., "The Electrodynamic and Hydrodynamic Phenomena in Magnetically-Levitated Molten Droplets-II. Transient Behavior and Heat Transfer Considerations", Acta Astronautica, Vol. 29, No. 4, (1993), pp 305.

[30] Bashforth, F. and Adams, J.C., An Attempt to Test the Theories of Capillary Attraction, Cambridge University Press, 1883.

[31] Padday, J.F., "Profiles of Axially Symmetric Menisci", Phil. Trans. R. Soc. London, A, vol. 269, pp. 265-293, 1971.

[32] Michael, D.H., Williams, P.G., "The Equilibrium and Stability of Axisymmetric Pendent Drops", Proc. R. Soc. London, A, vol. 351, pp. 177-127, 1976.

[33] Concus, P, Finn, R., "Shape of a Pendant Liquid Drop", Phil. Trans. R. Soc. London, A, vol. 292, pp. 307-340, 1979.

[34] Gillette, R.D., Dyson, D.C., "Stability of Axisymmetric Liquid-Fluid Interfaces Towards General Disturbances", Chem Eng J, 3, pp. 196-199, 1972.

[35] Orr, F.M., Scriven, L.E., "Menisci in Arrays of Cylinders: Numerical Simulation by Finite Elements" Journal of Colloid and Interface Science", vol. 113, no. 1, Sept 1986, pp. 154-163.

[36] Brakke, K.A., "The Surface Evolver", Experimental Mathematics, 1993.

[37] Miller, L.F., "A Survey of Chip Joining Techniques", IBM Technical Memo, pp. 60-76.

[38] Goldmann, L.S., "Geometric Optimization of Controlled Collapse Interconnections", Journal of IBM Research and Development, vol. 113, 1969, pp. 251-265.

[39] Brakke, K., Surface Evolver Manual, University of Minnesota, ver. 1.4,1994.

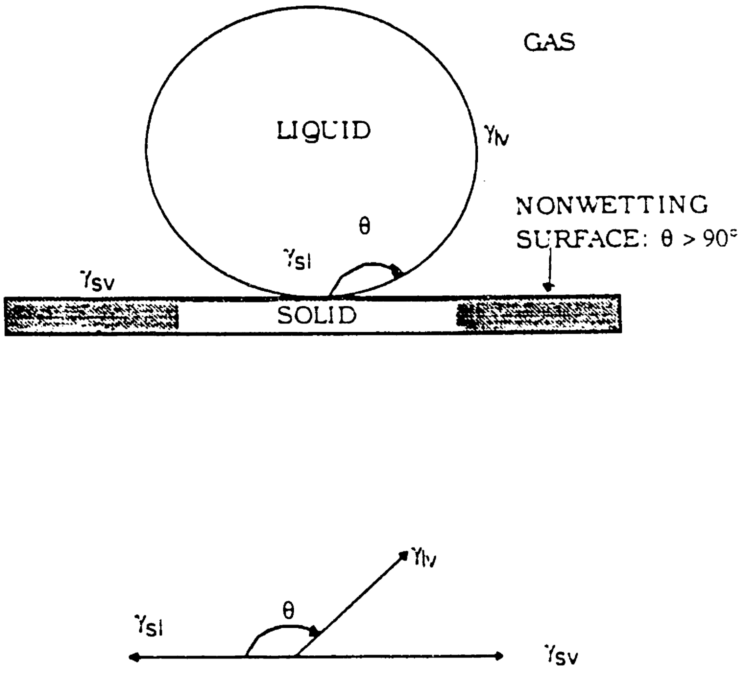

Fig. 3.1: Young Equation

```
   cat.fe

 // Evolver data for catenoid.

PARAMETER  RMAX = 1.5088795     // minimum radius for height
PARAMETER  ZMAX = 1.0

boundary 1 parameters 1       //  upper ring
x1:  RMAX * cos(p1)
x2:  RMAX * sin(p1)
x3:  ZMAX


boundary 2 parameters 1    //   lower ring
x1:  RMAX * cos(p1)
x2:  RMAX * sin(p1)
x3:  -ZMAX


vertices    // given in terms of boundary parameter
1     0.00  boundary 1   fixed
2     pi/3  boundary 1   fixed
3   2*pi/3  boundary 1   fixed
4     pi    boundary 1   fixed
5   4*pi/3  boundary 1   fixed
6   5*pi/3  boundary 1   fixed
7     0.00  boundary 2   fixed
8     pi/3  boundary 2   fixed
9   2*pi/3  boundary 2   fixed
10    pi    boundary 2   fixed
11  4*pi/3  boundary 2   fixed
12  5*pi/3  boundary 2   fixed

 edges
1     1  2  boundary 1   fixed
2     2  3  boundary 1   fixed
3     3  4  boundary 1   fixed
4     4  5  boundary 1   fixed
5     5  6  boundary 1   fixed
6     6  1  boundary 1   fixed
7     7  8  boundary 2   fixed
8     8  9  boundary 2   fixed
9     9  10 boundary 2   fixed
10    10 11 boundary 2   fixed
11    11 12 boundary 2   fixed
12    12 7  boundary 2   fixed
13    1  7
14    2  8
15    3  9
16    4  10
17    5  11
18    6  12

 faces
1    1 14 -7 -13
2    2 15 -8 -14
3    3 16 -9 -15
4    4 17 -10 -16
5    5 18 -11 -17
6    6 13 -12 -18
```

Fig. 3.2 Evolver datafile for catenoid surface.

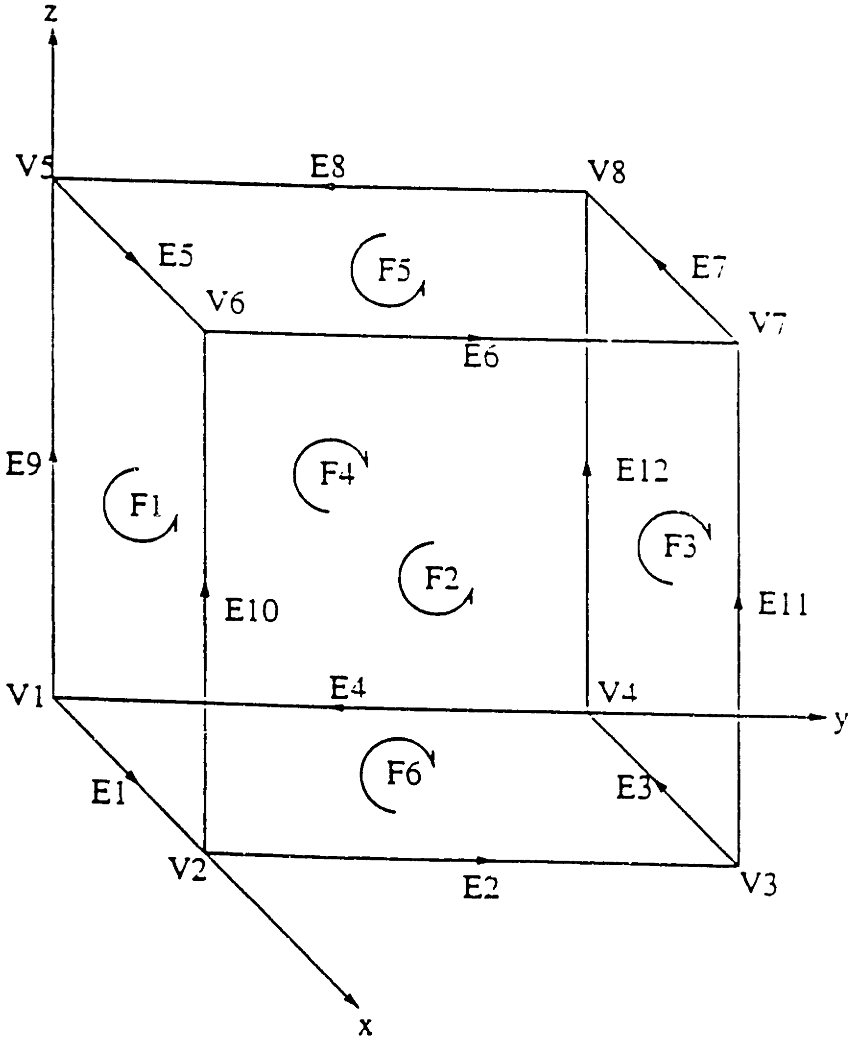

Fig. 3.3 A diagram of the basic structure of the vertex, edge, and facet elements.

Fig. 3.4 Initial Evolver surface for cat.fe.

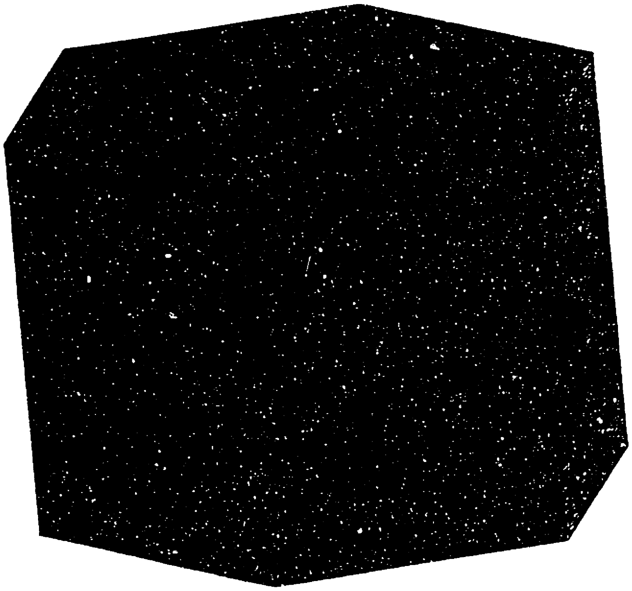

Fig. 3.5 The final minimal surface for cat.fe after 50 iterations and three levels of refinement.

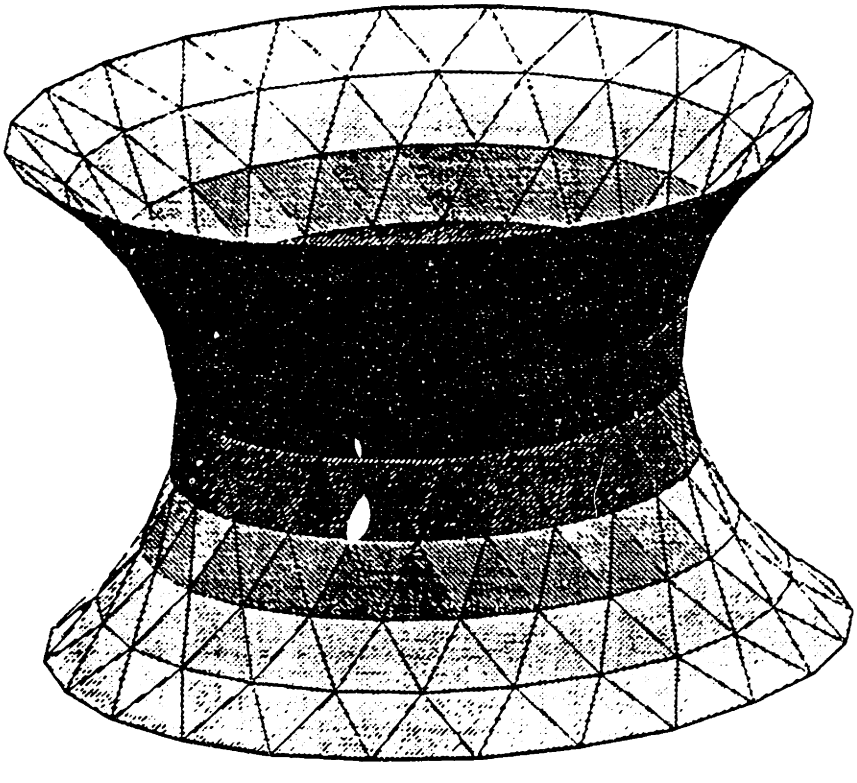

Chapter 4

MATHEMATICAL MODELING OF STANDARD CASE

4.1 Introduction

A direct application of the modeling code described in Chapter 2 for determining restoring forces will be described in this chapter. We will also present the details of the joint parameters studied, an outline of the major assumptions made, and a presentation of the results. These results will be discussed in the context of individual and combined interactions, and recommendations for optimum solder joint design will be presented.

4.2 Mathematical Model

4.2.1 Constraints

Fig. 4.1 shows a sample output surface produced by the Surface Evolver for the minimized surface of a liquid solder droplet and Fig. 4.2 shows a sample datafile. For the flip-chip solder system, important boundary conditions included in the model focused on the interaction between the solder and the metallization pads. In the solder reflow system, the liquid solder is generally confined to the surface area of the metallization pad to prevent shorting of the electrical contacts. As a result, a major boundary condition was that the solder was fixed directly to the edges of the pad. This removed a dependence on contact angle for the solder since the shape of the solder was mainly produced by an interaction of joint geometry factors of solder volume, height and pad radius for a non-moving solder confined to a pad. Volumes of the liquid solder and the surface tension coefficient for the surface energy to be applied to the facets were set as other major boundary constraints in the system. The negligible gravity effects on the surface were represented by G being set to zero. This removed force as a consideration in the development of the minimal energy surface.

4.2.2 Model Parameters

The initial surface of a series of solder joints examined -- including relevant dimensions, materials properties and constraints -- were obtained through a collaborative effort with AT&T Bell Laboratories. The information gained there was used to form a series of datafiles to study the minimal surfaces developed for both individual joint parameters and for combinations of joint parameters. A sample datafile representing a basic combination of parameters is shown in Fig. 4.2 and called cir.v60.r60. Using the traditional Evolver syntax, constraints on solder density, volume and liquid-vapor interfacial energy were defined as RHO, VOLUME, GAMMLV, respectively. Motion constraints were defined to limit the solder to the edges of the metallization pad, as per our assumptions, using a FIXED vertices constraint for vertices as the pad edges. Units were defined in the cgs system for convenience and kept consistent throughout the datafile through the use of a constant conversion factor for ease of surface definition. Energies were defined in terms of both surfaces. Contact angles, through the fixed constraints on the edges, were applied preferentially before the angle constraint.

4.2.3 Model Setup

Circular pads were analyzed for a number of joint parameters including volume, surface tension, diameters, and vertical height for a number of vertical and horizontal separations. Joint parameters in industrial applications can vary greatly given the large number of different joint types being used. In order to cover the broad range of possible values, a number of models were built. Pad radii studied varied from 60 microns to 80 microns, which covers the range of standard pad diameters from 120 to 160 microns. Solder volumes ranged from 1.28e^5 micron^3 to 9e^5 micron^3 to cover the range of standard solder volumes currently being used. Solder joint heights for joints formed in industry vary from low values of 40-50 microns to 110 micron separations for large joints. Joint height values in the model system were designed to cover each of these possible values. Surface tension values in industry can vary greatly, depending on the type of solder and fluxes used; average values for PbSn solder range from 500 to 900 ergs/cm^2. Surface tension values used in the mathematical models ranged from 100 ergs/cm^2 up to 1000 ergs/cm^2 to cover all PbSn values in addition to those of other types of fluxes. Each model was studied for horizontal displacements from 0 to 35 microns.

4.2.4 Computational Methodology

The methodology used to determine the surface area, energy, and shape of a defined flip-chip solder joint will be defined in this section. Initial surfaces were defined for each joint and the surface was established through the use of a two levels of refinement to increase the number of facets. The surface was then averaged over the vertices twice and facets were changed from triangular geometries to equiangular facets to improve accuracy. The constraints and parameter values were then checked and the surface allowed to move toward its equilibrium surface for 1000 iterations. This was the number of iterations determined to provide the highest level of accuracy, while maximizing computer time. At the end of the iterations, surface energy and area were recorded for each combination of joint parameter. Fig. 4.3 shows an example of Evolver output after 1000 iterations for an average circular pad.

4.2.5 Assumptions

There were four major areas where assumptions were made in the development of models of the solder joint system. The first assumption was made in terms of gravity-surface tension effects on the surface. Due to the small Bond number for this system (6.6×10^{-6}), surface tension effects tend to dominate over gravity and the models reflect this influence. The second assumption addressed the issue of the presence and influence of internal temperature-gradient driven flow within the solder. A calculation of the Biot number for this system produced a result of 2.23×10^{-3} a number which is less than unity. This indicates that there are no large temperature gradients present in the system and no gradient driven flow. On the basis of somewhat related systems, this assumption is thought to be reasonable [1].

The third assumption made in the models was that the liquid is fully wetting the metallization pads; i.e. that the solder is not forming surface voids or non-wetting spots either internally or on the edge of the pads. This is a reasonable assumption given the extensive efforts in industry devoted to insuring full wetting using various fluxes, surface preparation steps, and metallization layers. The fourth assumption made concerned the internal composition of the solder. For the models, the solder composition was assumed to be constant, though in real life, this is unlikely. There is research that shows that the solder composition is changing during the reflow process as Sn reacts with the Au contact layer to form an intermetallic [2], [5]; but there is currently no detailed information of the exact composition of the liquid solder throughout the heating and cooling cycle to be included in a model of the liquid surface.

The body of the solder is assumed to be homogeneous to simplify the problem, since calculating the exact composition of the alloy during and after reflow with a number of chemical interactions occurring with the base metals is extremely difficult.

4.3 Model Results for Standard Case

Restoring forces were calculated for circular pads displaced horizontally as a function of important design factors of solder volume, pad radius, joint height and surface tension. These results are summarized in the next several sections. We address the effects of each of these factors individually and then compare the generated restoring forces as a result of their combined interactions during reflow. The implications of these results will be discussed in the Discussion section, and their impact on design rules will be outlined in the Conclusion section.

4.3.1 Restoring Force as a Function of Volume

The horizontal alignment forces and free surface shapes generated for a pad with variable solder volume with constant joint height, pad radius, surface tension values were calculated and compared for a number of different pad types. Restoring force values are shown in Fig. 4.4 for a average sized solder joint with a 55 micron radius pad, 60 micron joint height and surface tension of 100 ergs/cm^2. Plots of the different types of free surface morphologies produced by solder volumes of 4, 6, and 7e5 micron^3 are shown in Fig. 4.5 - 4.7. The calculated positioning forces generated were small for volumes of $4e^5$ and $5e^5$ micron^3 and rose smoothly to a maximum for a volume of $6e^5$ micron^3. As solder volume increased to $9e^5$ micron^3, the restoring force dropped off quickly toward its local minimum value. This type of behavior was observed for a number of solder volume variation studies using different pad heights, radii, and surface tensions. A more detailed discussion of volume influences will be undertaken in the next section on parameter interactions due to the heavy correlation between a number of joint factors and the influence of solder volume.

Force values had an order of magnitude of 0.1 of dynes per bump, a quantity which makes physical sense given the small size of the system and the nature of a force which is generated by surface tension. These numbers are in good agreement with those produced by other modeling codes used to solve 2-D formulations for the restoring force [3], [4]. The surface morphologies were spherical and matched classical solutions for systems of this type. Also, restoring force is linear with regard to horizontal displacement for individual volumes, as expected, given the similarity of self-alignment forces to springs in their displacement dependence. In a classic spring system, restoring force is linear for small displacements away from the equilibrium position of the system.

4.3.2 Restoring Force as a function of Solder Height

The joint height dependence of horizontal alignment forces was studied using a series of pads with fixed pad radius, solder volume and surface tension. Fig. 4.8 shows the restoring force for 50 micron radius pads with constant solder volume and surface tension and a vertical gap separation of 60 to 80 microns. In another comparison, forces generated for solder heights of 40 microns to 70 microns were compared for a pad radius of 75 microns in Fig. 4.9. In both sets of studies, for fixed volume and surface tension, the smallest bump heights generate the highest level of horizontal restoring force, while the taller bumps generated the lowest forces. Surface morphologies for a set of vertical separations are shown in Fig. 4.10-4.12.

4.3.3 Restoring Force as a function of Pad Radius

Horizontal restoring force results and free surface shapes were calculated using the parameters described above. Surface Evolver output for solder pads with 55 - 75 micron radii are shown in Fig. 4.13-4.15 for the joint described earlier. Plots of restoring force for this range are shown in Fig. 4.16. The highest level of restoring force was generated by a solder joint radius of 75 microns. The lowest level of restoring force was generated by the 55 micron radius bump. The behavior is linear, as expected, for a series of small horizontal displacements from equilibrium.

4.3.4 Restoring Force as a function of Surface Tension

Surface tension dependency study results of horizontal alignment forces were performed for a number of pad radii, fixed volumes, and vertical separations. Fig. 4.17 shows the surface tension variations for average pad radii from 70 microns, solder volume of $4e^5$ micron^3 and vertical separations of 60 microns. Restoring force values ranged in a linear manner from approximately 0.18 dynes for a surface tension of 100 ergs/cm^2 to 1.8 dynes per bump for a 35 micron displacement (for a surface tension of 1000 ergs/cm^2).

4.4 Restoring Force as a result of Parameter Interactions

A number of studies were performed to assess the influence of pairings of joint parameters to determine design rules to maximize alignment forces as a function of joint geometry. Due to the large number of variables which impact restoring forces, optimizing the process depended on understanding the possible interactions for a basic set of normal joint parameters. These studies included interactions between joint height variations, surface tension variations, pad radius variations and variable volume.

4.4.1 Joint Height and Surface Tension

Joint height and surface tension influences on horizontal restoring forces were studied together for joint heights between 60 and 80 microns and surface tension values from 100-1000 ergs/cm^2. Results are summarized in Fig. 4.18-4.20 for a 60 micron radius bump and with a solder volume of 4e^5 micron^3. Restoring force values reach a maximum for higher values of surface tension and reach their highest levels overall for the smallest vertical separation.

4.4.2 Pad Radius and Joint Height

Solder restoring force as a function of radius and joint height is shown in Fig. 4.21-4.36 with a comparison of joint heights from 60 microns to 80 microns and solder pad radii from 50 microns to 80 microns for a range of volumes and constant surface tension. A number of solder volumes where investigated in order to cover a broad range of radii and height interactions. Each of these figures represents a surface of restoring force as defined by a combination of solder volume, pad radius and solder height. Fig. 4.21-4.26 shows a series of surfaces

4.4 Restoring Force as a result of Parameter Interactions

A number of studies were performed to assess the influence of pairings of joint parameters to determine design rules to maximize alignment forces as a function of joint geometry. Due to the large number of variables which impact restoring forces, optimizing the process depended on understanding the possible interactions for a basic set of normal joint parameters. These studies included interactions between joint height variations, surface tension variations, pad radius variations and variable volume.

4.4.1 Joint Height and Surface Tension

Joint height and surface tension influences on horizontal restoring forces were studied together for joint heights between 60 and 80 microns and surface tension values from 100-1000 ergs/cm^2. Results are summarized in Fig. 4.18-4.20 for a 60 micron radius bump and with a solder volume of 4e^5 micron^3. Restoring force values reach a maximum for higher values of surface tension and reach their highest levels overall for the smallest vertical separation.

4.4.2 Pad Radius and Joint Height

Solder restoring force as a function of radius and joint height is shown in Fig. 4.21-4.36 with a comparison of joint heights from 60 microns to 80 microns and solder pad radii from 50 microns to 80 microns for a range of volumes and constant surface tension. A number of solder volumes where investigated in order to cover a broad range of radii and height interactions. Each of these figures represents a surface of restoring force as defined by a combination of solder volume, pad radius and solder height. Fig. 4.21-4.26 shows a series of surfaces representing the types of forces generated for radius and volume variations for increasing pad radii with a vertical separation of 60 microns. Fig. 4.27-4.32 show similar data for a 70 micron separation while Fig. 4.33-4.36 displays the restoring forces generated at a 80 micron separation. Over all the variations of radius and height, the highest level of alignment force generated for all of the joint types resulted from a combination of a 60 micron vertical bump height and a pad radius of 70 microns (Fig. 4.24). This joint geometry is capable of producing a restoring force of up to 1.1 dynes for a solder volume of $9e^5$ cubic microns and a surface tension of 100 ergs/cm^2.

4.4.3 Pad Radius and Volume

A comparison of pad radius and solder volume influences was performed for a series of pads varying in radius from 55 - 80 microns and volume variations from 4.0 to $9.0e^5$ $micron^3$. Comparisons were made based on a constant surface tension (100 ergs/sq. cm) and for three different vertical separations to cover overall trends due to geometry factor interactions. Horizontal restoring forces for 60, 70, and 80 micron joint heights are shown in Fig. 4.37-4.41, Fig. 4.42-4.46, and Fig. 4.47-4.50. For this combination, the highest level of force was produced for a joint with a joint height of 60 microns, pad radius of 70 (Fig. 4.40) microns and a solder volume of $9e^5$ cubic microns.

4.4.4 Solder Height and Solder Volume

Solder pad height and solder volume relationships were investigated for a fixed range of surface tensions and pad radii. Fig. 4.51-4.53 contain the result of studies for a fixed pad radius of 55 microns for a series of height and volume variations. Fig 4.54-4.56, Fig. 4.57-4.59,

Fig. 4.60-4.62, Fig. 4.63-4.64, and Fig. 4.65 contain the results for fixed pad radii of 60. 65, 70, 75 and 80 microns respectively.

4.4.5 Solder Volume and Surface Tension

Restoring force values as a function of a combination of solder volume and surface tension are shown in Fig 4.66-4.71. for a solder joint separation of 60 microns and a pad size of 60 microns. The pairing that produced the highest levels of restoring force in this series was for a volume of $6e^5$ $micron^3$ and a surface tension value of 1000 $ergs/cm^2$ (Fig. 4.69). In this joint system, as noted before, increased surface tension produces increased restoring force, and solder volume is optimized around one maximum peak value with minimums at either variational extreme.

4.4.6 Surface Tension and Pad Radius

The influence of surface tension and pad radius was studied for surface tension values between 100 and 1000 $ergs/cm^2$ and pad sizes between 55 microns and 80 microns for fixed separations and volumes (Fig. 4.72-4.90). A number of trials were performed to also determine the influence of solder volume for this particular parameter combination. Several different trends were observed due to the influence of solder volume throughout the comparison. For small solder volumes (4-$5e^5$ $micron^3$), restoring force levels decreased as pad radius was increased. For a solder volume of $6e^5$ $micron^3$, the positioning force generated by the joint increased to a peak for a radius of 65 microns and then decreased sharply. A similar trend was observed in Fig. 4.85-4.87 as pad radius continued to increase with one main difference; there was a local maximum in restoring force, followed by very gradual drop-off. As solder volume was increased for more trials, repeated for volumes of $8e^5$ and $9e^5$ $micron^3$. The highest restoring force generated to correct for a 35 micron misalignment, was observed in the combination of the largest pad radius, surface tension and volume (Fig. 4.90 and Fig. 4.91).

4.5 Discussion

In this section, trends produced by the influence of individual process parameters (with other variables held constant) on restoring forces will be discussed. A dimensionless correlation between all process factor variations will be presented and it's impact on optimum joint design guidelines will be explained.

4.5.1 Volume Dependence

Solder volume influences on restoring forces as depicted in Fig. 4.4, show that there is an optimum volume of solder to produce restoring forces. This optimum volume is dependent on the other solder interconnect variables. As volume is increased for a fixed set of joint parameters, a local maximum is reached for which the highest amount of force for that particular configuration is generated. This has an impact on joint design rules in two areas: it emphasizes the need for determining the optimum volume for a joint configuration; it alludes to the importance of maintaining consistent volumes across an area array. For the joint type mentioned above, small variations in volume produced variations in restoring force for large initial misalignments of up to 10 %.

4.5.2 Height Dependence

For a fixed pad radius, solder volume and surface tension, the bumps with smaller heights produced the highest level of restoring force when compared to larger bumps in the 70 micron to 80 micron height range. Force levels for a solder bump with a joint height of 60 micron and 50 micron pad radius range from zero (for a zero displacement) up to approximately 0.6 dynes. This represents an increase of a factor of 1.5 over the other two solder joint heights.

All of the data showed a strong trend toward increased alignment force with decreasing pad joint height. This is explained by the functional dependence of restoring force on surface area gradients as surfaces are deformed away from a minimal area solution. The shorter solder bumps which produce the largest deviation away from the equilibrium shape have free surfaces which are convex (Fig. 4.6), for which area gradients are much larger for horizontal displacements. The taller bumps have been forced into a concave shape (Fig. 4.5) due to the fixed volume, and as a result have smaller surface area gradients for small horizontal displacements.

4.5.3 Radius Dependence

Solder joints have a strong dependence on pad radius, as shown by the previous results. Larger pad radii produce, in some cases, significantly larger restoring forces than small pad sizes, particularly when combined with small joint heights and certain geometries. This type of joint geometry is most likely to produce a convex free surface, given a fixed volume and surface tension. As discussed in the previous section, convex surfaces near the minimal surface solution have the highest area gradients for horizontal displacements.

4.5.4 Surface Tension Dependence

Surface tension effects on restoring force were found to be linear. This matches the theoretical formula mentioned in the Chapter 3 for the relationship between surface tension, surface energy gradients and restoring force. As expected, a maximum surface tension value produces the largest restoring forces for all types of joints.

4.5.5 Interactions Among Several Factors

In order to study the interaction of all joint parameters and their effects on restoring force, a series of dimensionless formulations were developed. These numbers were then used to develop insights into the influence of process variations of all the relevant process parameters. The analysis began with the use of the Buckingham Pi theorem, by which the main variables affecting restoring force were organized and evaluated. A number of possible dimensionless relationships were formed as a result of this analysis. The next step involved a multiple log linear regression using all of data points representing the calculated restoring forces and related process variables (total = 7451). The results of this study yielded the relationship seen below and coefficients for each of the process variables:

$$R.F. = \frac{kP^{0.996}\gamma^{1.0041}V^{1.43}}{r^{2.75}h^{1.48}} \tag{4.1}$$

where R.F. = Restoring Force

k = constant = $e^{-3.8473}$

P = horizontal displacement

γ = the surface tension

r = pad radius

h = solder joint height

Using the coefficients for each parameter and the previously calculated dimensionless group, two independent dimensionless groups were formed. The groups are shown below:

$$\Pi_1 = \frac{R.F.}{\gamma^{1.0041} P^{0.9961}} \tag{4.2}$$

$$\Pi_2 = k\left(\frac{V^{1.43}}{r^{2.75} h^{1.5}}\right) \tag{4.3}$$

A plot of the first dimensionless group vs. the second produces the plot shown in Fig. 4.94., relating dimensionless restoring force to other dimensionless process parameters. To interpret this plot it is useful to convert the dimensionless groups into a more recognizable format:

$$\Pi_1 = \frac{R.F.}{\gamma P} \tag{4.4}$$

and

$$\Pi_2 = k_1\left(\frac{V^{1.43}}{r^{2.75} h^{1,5}}\right) \approx \frac{k_1}{r^3}\left(\frac{v}{h}\right)^{\frac{3}{2}} \tag{4.5}$$

concave, alignment force is reduced. In these cases the surface area is already far removed from the equilibrium shape and surface energy gradients for displacements away from this are relatively small. This includes cases where solder volume, pad radius, and joint height are significantly different from the optimum value calculated above. In order to maximize alignment forces, these extreme cases should be avoided.

The data represented by the dimensionless groups matches with our calculated results very well. Common trends observed among each pad radius and volume variation showed an overall gradual increase to a local maximum of restoring force followed by a sharp decrease for higher volumes. The global maximum in positioning force for this range of volumes was produced by a 70 micron radius pad with a solder volume of $9e^5$ micron^3, the maximum values studied for this series of comparisons. Trends among each set of the other radii and volume pairings showed a definite dependence of restoring force on both pad size and quantity of solder relative to the vertical separation. For the 55 micron pads, a maximum restoring force was reached for a solder volume of $6e^5$ micron^3, with a sharp decrease in force as volume continued to increase. The 60 micron and 65 micron pads rose smoothly to a peak for a solder volume of $6e^5$ micron^3 and showed no sharp decreases for higher volumes. As solder volume increased for the 70 micron pads, it continued steadily toward the maximum volume studied for this set to produce the global set maximum of approximately 11.5 dynes per bump.

Some of the trends observed confirmed earlier observations on individual effect of pad radii -- that there is general increase in alignment force for higher pad radii with this effect reaching a maximum for $\Pi_2 = 1$. In comparing the restoring forces for pads of constant volume, vertical separation, and surface tension, the larger pads produced the highest level of restoring forces until the pad radius increased to a value which caused the surface to assume a convex shape. In addition, this series shows that there is a similar relationship with solder volume, for which there appears to be an optimum range for a fixed set of joint parameters which will produce the highest level of positioning force. In terms of free surface morphology this is the volume which produces a shape closest to the equilibrium shape of the solder, a slightly convex surface. The surfaces shown in Fig. 4.90-4.93 for this series with the maximum force for the 55 and 70 micron pads show a common surface which is nearly straight and very close to the equilibrium shape. The overall joint combination for optimizing alignment forces, in terms of solder volume and radius would appear to be one which favors this type of surface morphology. In terms of joint design, large broad pads with an optimum quantity of solder to form this type of surface produce the highest level of positioning capability, due to the influence of a fixed volume and pad radius on generated forces. This optimum solder volume is one that is determined by a combination of vertical joint height in process (which is also governed by chip weight and vertical load per bump) and the radius of the pad.

There is a definite correlation between radius and joint height for optimizing restoring force. The trends of the data indicated that increased pad size and decreased pad height produce the highest levels of restoring force. The individual influence of each parameter has been noted. However, one of the best methods of maximizing the force levels results from a combination for optimized pad radius and joint height. For each joint, for small pad sizes, the curving of the restoring force surfaces indicates that the restoring force is a strong function of solder volumes (normally in the midrange of all values). As pad radius increases, the curves flatten to form straight continuums from lowest to highest level across all the volumes. For large pads as all separations, forces increase continually with increased solder volume. For smaller pads, alignment forces increase and decrease across a positive volume variation. This behavior seems to indicate that there is an optimum volume for each set of height/pad values. This optimum volume enables the joint to generate the highest alignment force. As joint size increases this optimum volume increases to match it, as seen in this data starting from the midrange and moving to the upper volume extreme.

For a pad radius of 55 microns, restoring force is largest for a configuration of a 70 micron separation and a solder volume of $8e^5$ $micron^3$ (Fig. 4.53). For a 60 micron pad, the best configuration is that for a 60 micron separation and a solder volume of $7e^5$ $micron^3$ (Fig. 55). A 65 micron pad is optimized for a volume of $9e^5$ $micron^3$ and a joint height of 70 microns, while a 70 micron pad produces the strongest restoring forces for a configuration a height of 60 microns. 75 and 80 micron pads are optimized in a similar way for high volumes and low separations of 60 microns (Fig. 64 and 66). Interactions among each of the parameters with surface tension were each positive; for higher values of surface tension restoring force is increased. This was independent of joint geometry in all cases and was a common feature of all the geometries that optimized generated alignment forces.

It is useful to compare the process parameters studied in this project to real industrial numbers to establish a context in which to view them. Fig. 4.95 shows the range of industrial practice on the plotted curve, a range whose upper limits are currently just below the optimum levels possible for the solder joint. This range consists of solder joints with joint parameters determined by the application of the flip-chip method. Solder pad sizes range from low values of 50 microns in diameter to large pads of 160 microns or more. Solder joint heights in many flip-chip systems can vary between 15 and 90 microns, depending on solder volume and pad size used. Solder volume varies between $1e^5$ and$1e^6$ micron^3. Each of these parameters is set based on the specific application of this technology and the limits of the manufacturing processes used to form the joints. Current etching process and wet chemical process tolerances are limited to the 1-10 micron range for most interconnect forming operations. Future trends for solder joint geometry will be highly dependent on the application of the interconnect. For flip-chip interconnects used in high-density applications where they are used to provide the needed number of I/O connections, joints will most likely have smaller pad radii as more and more are placed in tighter pitch area arrays. This would place them toward the top and more on the right hand side of the curve in Fig. 4.95. Mechanical joining using flip chip solder bumps will tend toward larger bumps to maximize mechanical fatigue strength through an increase in cross-sectional area. This will cause a general decrease in restoring force (a drop along the left hand side of the curve) unless other process parameters are changed to optimize restoring force. Self-alignment applications will most likely use more optimized joints and result in process parameters combinations closer to the top of the dimensionless curve. This will result in solder bumps that have more optimized heights, volumes and radii in an array scheme that provides the highest level of alignment for a given number of bumps.

4.6 Conclusions

Design rules for the optimization of flip-chip solder bumps used in alignment applications can be formulated by the following guidelines. Restoring forces are maximized by the combination of a number of joint parameters. An optimum joint geometry would consist of a balance of competing parameters, parameters that result in a specific solder surface. An optimum solder joint would generally have very broad based metallization pads, small joint heights, high surface tension, and a volume optimized to form a resultant surface that is close to the equilibrium surface. This surface can be determined through a comparison of the cross-sectional area of the joint and the base pad area. For a ratio of approximately unity, restoring force is optimized. Using the model data, specific joint geometries can be evaluated for their potential in precision alignment applications. One sample configuration would consist of a 70 micron radius pad, an in-process joint height of 60 microns, a surface tension of 900 ergs/cm^2 and a solder volume of approximately 9e^5 micron^3. In terms of general joint design recommendations, optimizing the restoring force is strongly a function of solder joint shape and the proximity of this surface morphology to that of the equilibrium shape. In order to maximize restoring force, solder volume, radius and height should be controlled to form their optimum values for this system. Surface tension should be maximized as well as displacement distance away from the equilibrium position. If these quantities are maintained through the use of tight process controls, optimum levels of self-alignment forces can be produced.

In the next chapter, research into a number of alternative pad configurations and the influence of joint geometries will be outlined. Mathematical models of these types of systems will be discussed and results presented. In the two chapters following this, experimental methods which physically measure restoring force levels will be outlined and compared to model results for the circular pad system.

4.7 References

[1] Zong, J., Li, B., Szekely, "The Electrodynamic and Hydrodynamic Phenomena in Magnetically-Levitated Molten Droplets-II. Transient Behavior and Heat Transfer Considerations", Acta Astronautica, Vol. 29, No. 4, (1993), pp. 305.

[2] Shipley, J.F., Welding Journal, 1975, 54, (10), pp. 357s.

[3] Patra, S.K., Lee, Y.C., "Modeling of self-alignment mechanism in flip-chip soldering--Part II: Multichip solder joints." Proceedings-Electronic Components Conference, 1991, pp. 783-788.

[4] Yost, F.G., "Fundamentals of Wetting and Spreading with emphasis on soldering". The Metal Science of Joining, TMS, 1992, pp. 49-59.

[5] Kato Reference: Kato, H., Ikuzaki, K., Tsujita, M., Nakata, K., Kobayashi, Sano, Y., "A New Method for Measuring the Tin Content of Flip-Chip Solder Bumps, "1993 IEEE-CHMT International Electronics Manufacturing Technology Symposium, 1993, pp. 115-118.

Fig. 4.1 Sample Evolver Output

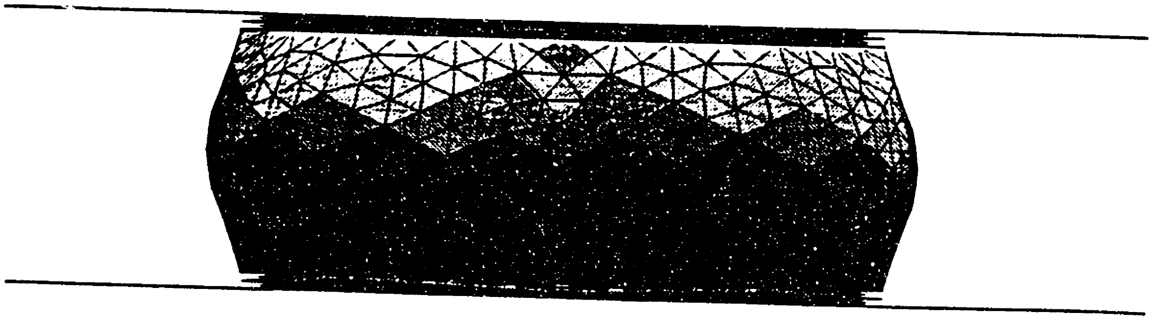

Fig. 4.2 Sample Surface Evolver Datafile

```
//cir.v60 -fixed cgs units in edge files

GRAVITY_CONSTANT 0.0

//Physical parameters
PARAMETER THETAL = 175 //angle between fluid and chip
PARAMETER THETAU = 175 //angle on top plate ?
PARAMETER GAMMALV = 325.00 //l-v surface energy  [ergs/cm^2]
PARAMETER VS = 0.00000128  //volume of solder in [cm^3]
PARAMETER RHOS = 9.00  //density of solder [g/cm^3]
PARAMETER F = .0001

//Geometric parameters
PARAMETER RMETA = .0075 //radius of lower met. pad constraints
PARAMETER RMETB = .0075 //radius of upper met. pad constraints
PARAMETER RSOLA = .0075 //radius of lower solder column constraints
PARAMETER RSOLB = .0075 //radius of upper solder column constraints
PARAMETER DISP  = 0.00*F //displacement in x direction

#define DIFFL (GAMMALV*cos(THETAL*pi/180))  //substrate energy on bottom
#define DIFFU (GAMMALV*cos(THETAU*pi/180))  //substrate energy up top

constraint 1
function: z = .0004
energy  //contact angle on lower metallization pad
e1:  -DIFFL*y
e2: 0
e3: 0
// need content for volume
content
c1: 0
c2: -z*x
c3: 0

constraint 2
function: z = .0064
energy  //contact angle on top met. pad
e1: -DIFFU*y
e2: 0
e3: 0
// need content for volume
content
c1: 0
c2: -z*x
c3: 0

constraint 3 // constraint for lower met pad
function:  x^2 + y^2 = RMETA^2

constraint 4 // constraint for lower solder column
function:  x^2 + y^2 = RSOLA^2

constraint 5 // constraints for upper solder column
function:  x^2 + (y - DISP)^2 = RSOLB^2

constraint 6 // constraints for upper met pad
function:  x^2 + (y - DISP)^2 = RMETB^2

//Initial shape of solder column and vertices of subs. and metal. pad
vertices
1  -200.0*F -200.0*F  0.0*F  fixed  /*vertices on ceramic substrate*/
2   200.0*F -200.0*F  0.0*F  fixed
3   200.0*F  200.0*F  0.0*F  fixed
4  -200.0*F  200.0*F  0.0*F  fixed

5  -200.0*F -200.0*F  68.0*F  fixed  /*vertices on silicon chip*/
```

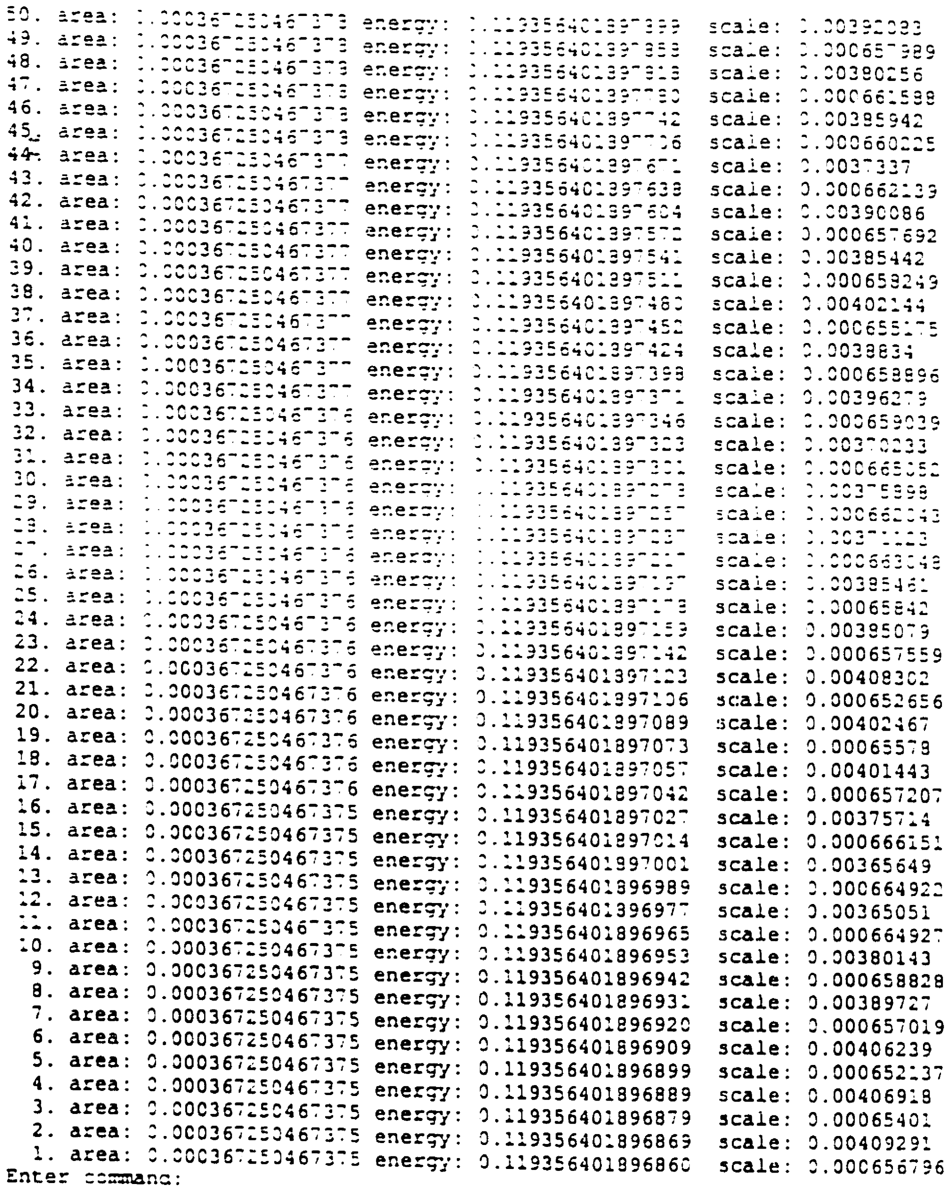

```
50. area: 0.000367250467378 energy: 0.119356401897899  scale: 0.00392093
49. area: 0.000367250467378 energy: 0.119356401897853  scale: 0.000657989
48. area: 0.000367250467378 energy: 0.119356401897818  scale: 0.00380256
47. area: 0.000367250467378 energy: 0.119356401897780  scale: 0.000661598
46. area: 0.000367250467378 energy: 0.119356401897742  scale: 0.00385942
45. area: 0.000367250467378 energy: 0.119356401897706  scale: 0.000660225
44. area: 0.000367250467377 energy: 0.119356401897671  scale: 0.0037337
43. area: 0.000367250467377 energy: 0.119356401897638  scale: 0.000662139
42. area: 0.000367250467377 energy: 0.119356401897604  scale: 0.00390086
41. area: 0.000367250467377 energy: 0.119356401897572  scale: 0.000657692
40. area: 0.000367250467377 energy: 0.119356401897541  scale: 0.00385442
39. area: 0.000367250467377 energy: 0.119356401897511  scale: 0.000659249
38. area: 0.000367250467377 energy: 0.119356401897480  scale: 0.00402144
37. area: 0.000367250467377 energy: 0.119356401897452  scale: 0.000655175
36. area: 0.000367250467377 energy: 0.119356401897424  scale: 0.0038834
35. area: 0.000367250467377 energy: 0.119356401897398  scale: 0.000658896
34. area: 0.000367250467377 energy: 0.119356401897371  scale: 0.00396279
33. area: 0.000367250467376 energy: 0.119356401897346  scale: 0.000659039
32. area: 0.000367250467376 energy: 0.119356401897323  scale: 0.00370233
31. area: 0.000367250467376 energy: 0.119356401897301  scale: 0.000665052
30. area: 0.000367250467376 energy: 0.119356401897278  scale: 0.00375898
29. area: 0.000367250467376 energy: 0.119356401897257  scale: 0.000662043
28. area: 0.000367250467376 energy: 0.119356401897237  scale: 0.00371123
27. area: 0.000367250467376 energy: 0.119356401897217  scale: 0.000663048
26. area: 0.000367250467376 energy: 0.119356401897197  scale: 0.00385461
25. area: 0.000367250467376 energy: 0.119356401897178  scale: 0.00065842
24. area: 0.000367250467376 energy: 0.119356401897159  scale: 0.00395079
23. area: 0.000367250467376 energy: 0.119356401897142  scale: 0.000657559
22. area: 0.000367250467376 energy: 0.119356401897123  scale: 0.00408302
21. area: 0.000367250467376 energy: 0.119356401897106  scale: 0.000652656
20. area: 0.000367250467376 energy: 0.119356401897089  scale: 0.00402467
19. area: 0.000367250467376 energy: 0.119356401897073  scale: 0.00065578
18. area: 0.000367250467376 energy: 0.119356401897057  scale: 0.00401443
17. area: 0.000367250467376 energy: 0.119356401897042  scale: 0.000657207
16. area: 0.000367250467375 energy: 0.119356401897027  scale: 0.00375714
15. area: 0.000367250467375 energy: 0.119356401897014  scale: 0.000666151
14. area: 0.000367250467375 energy: 0.119356401897001  scale: 0.00365649
13. area: 0.000367250467375 energy: 0.119356401896989  scale: 0.000664922
12. area: 0.000367250467375 energy: 0.119356401896977  scale: 0.00365051
11. area: 0.000367250467375 energy: 0.119356401896965  scale: 0.000664927
10. area: 0.000367250467375 energy: 0.119356401896953  scale: 0.00380143
 9. area: 0.000367250467375 energy: 0.119356401896942  scale: 0.000658828
 8. area: 0.000367250467375 energy: 0.119356401896931  scale: 0.00389727
 7. area: 0.000367250467375 energy: 0.119356401896920  scale: 0.000657019
 6. area: 0.000367250467375 energy: 0.119356401896909  scale: 0.00406239
 5. area: 0.000367250467375 energy: 0.119356401896899  scale: 0.000652137
 4. area: 0.000367250467375 energy: 0.119356401896889  scale: 0.00406918
 3. area: 0.000367250467375 energy: 0.119356401896879  scale: 0.00065401
 2. area: 0.000367250467375 energy: 0.119356401896869  scale: 0.00409291
 1. area: 0.000367250467375 energy: 0.119356401896860  scale: 0.000656796
Enter command:
```

Fig. 4.3 **A example of Evolver output after 1000 iterations for an average circular pad.**

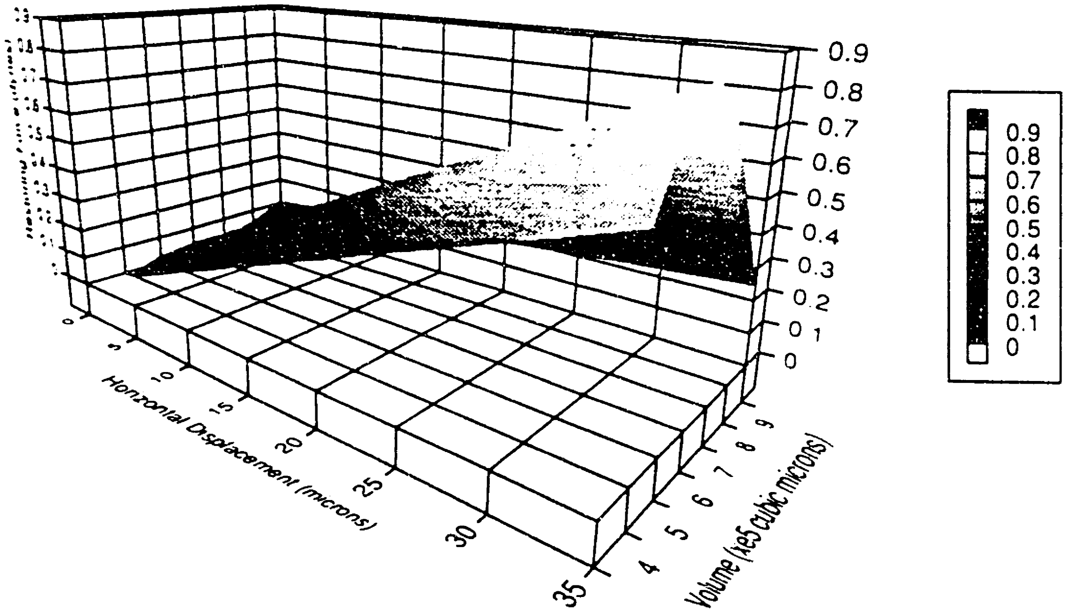

Fig. 4.4: Restoring Force as a function of Horizontal Displacement and Volume for a 55 micron radius circular pad with a 60 micron separation.

Fig. 4.5 Surface Morphology for volume = 4 e^5 cubic microns

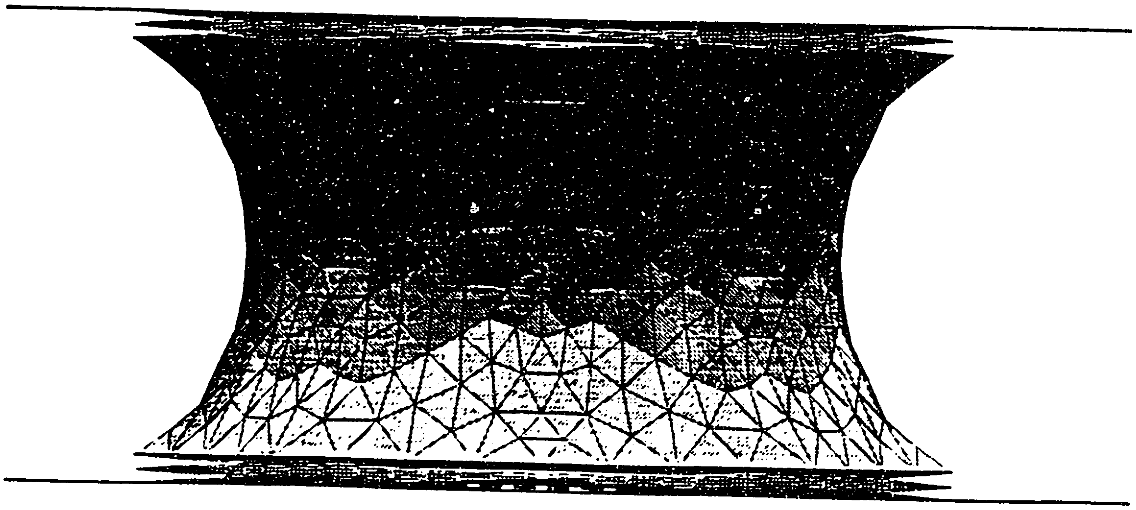

Fig. 4.6 Surface Morphology for volume = 6 e^5 cubic microns

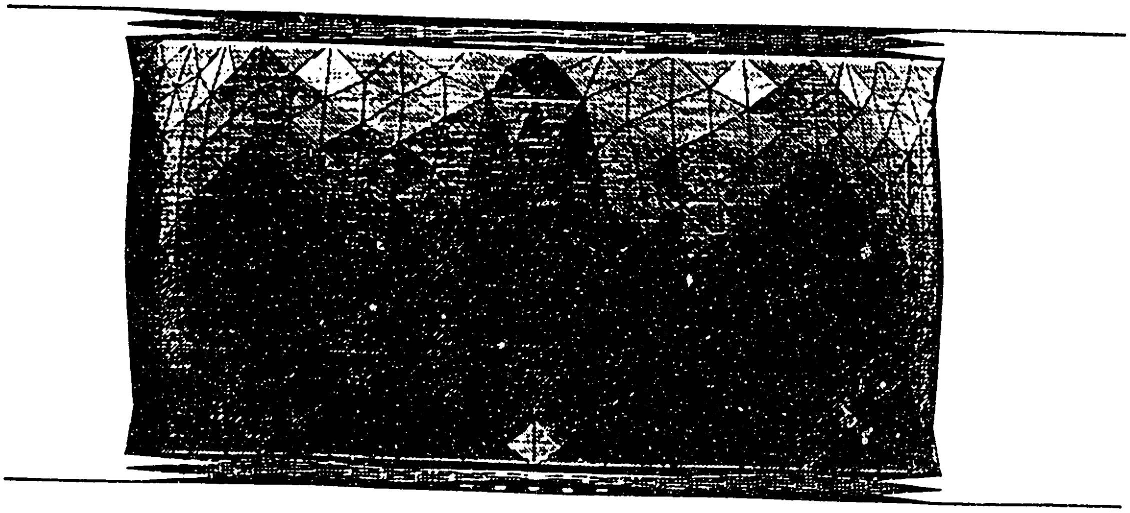

Fig. 4.7 Surface Morphology for volume = 7 e^5 cubic microns

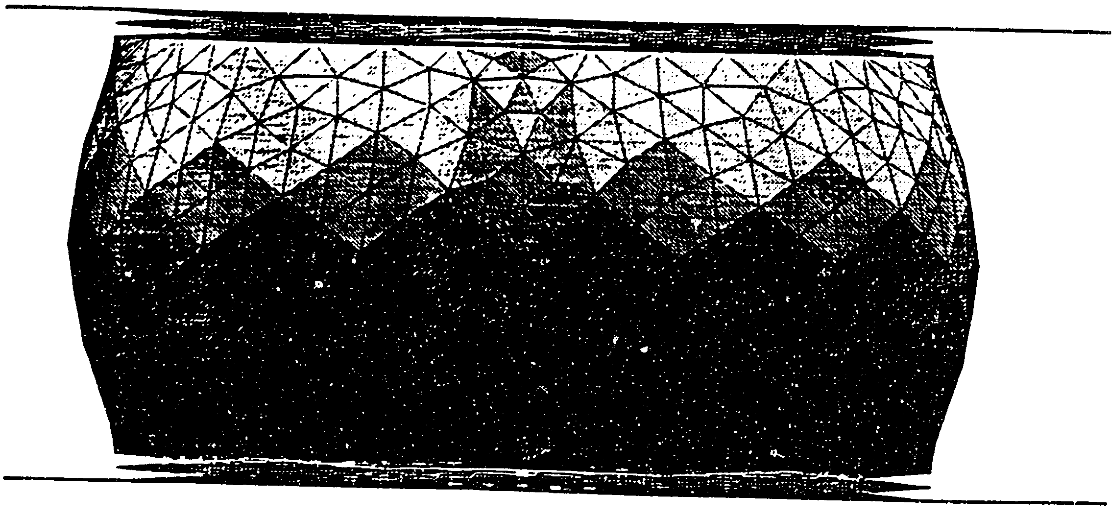

Fig. 4.8: Restoring force for 50 micron radius pads with joint heights of 60 to 80 microns.

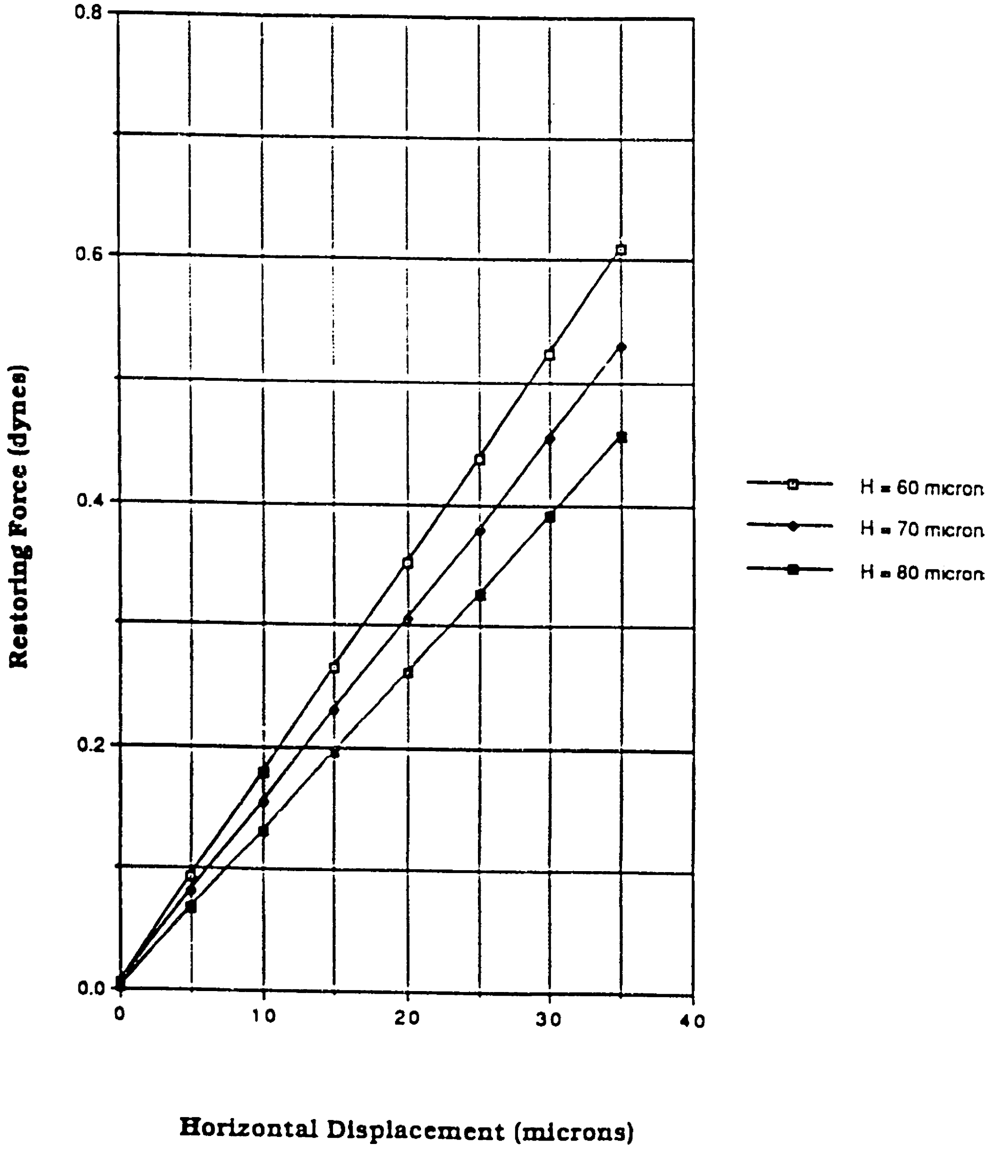

Fig. 4.9: Restoring forces generated for solder heights of 40 to 70 microns with a pad radius of 75 microns.

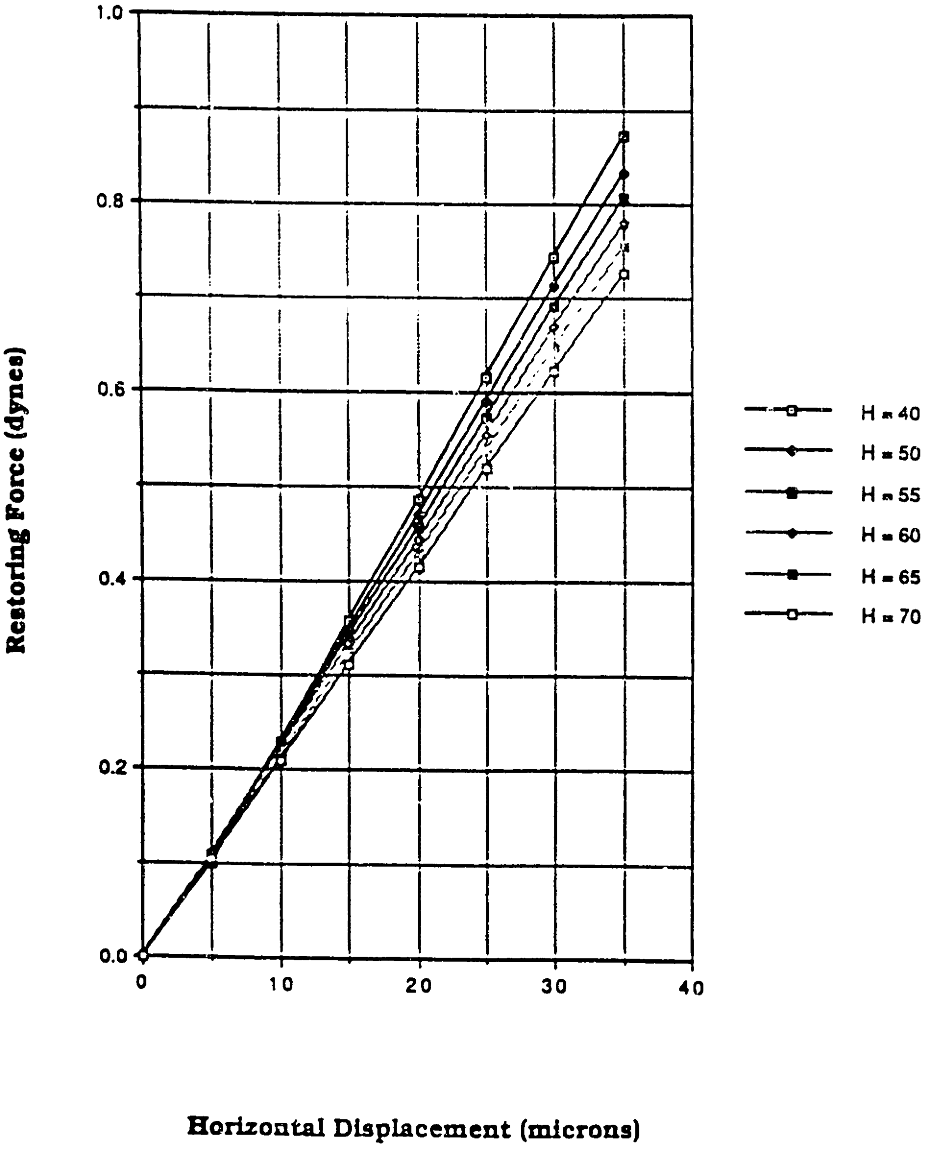

Fig. 4.10 Surface morphologies for a 50 micron vertical separation.

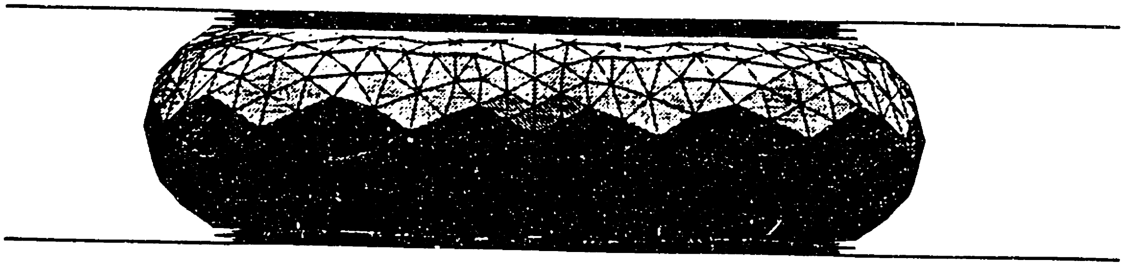

Fig. 4.11 Surface morphologies for a 60 micron vertical separation.

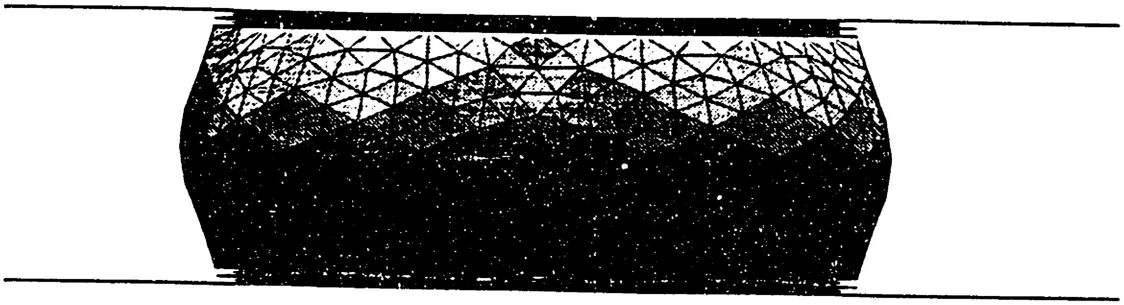

Fig. 4.12 Surface morphologies for a 70 micron vertical separation.

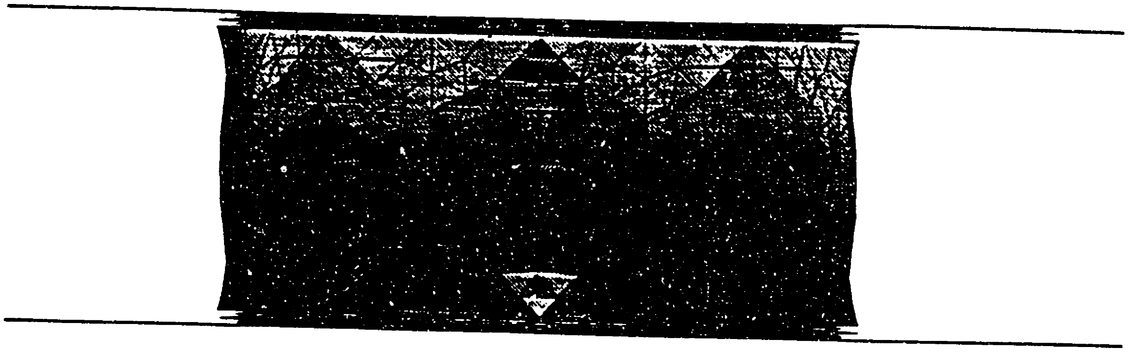

Fig. 4.13 Surface Evolver output for solder pad with 60 micron radii and 60 micron joint height (constant volume).

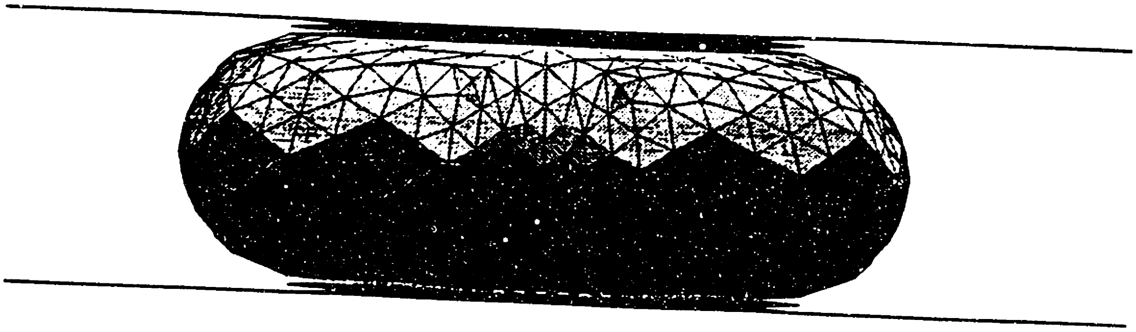

Fig. 4.14 Surface Evolver output for solder pad with 70 micron radii and 60 micron joint height (constant volume).

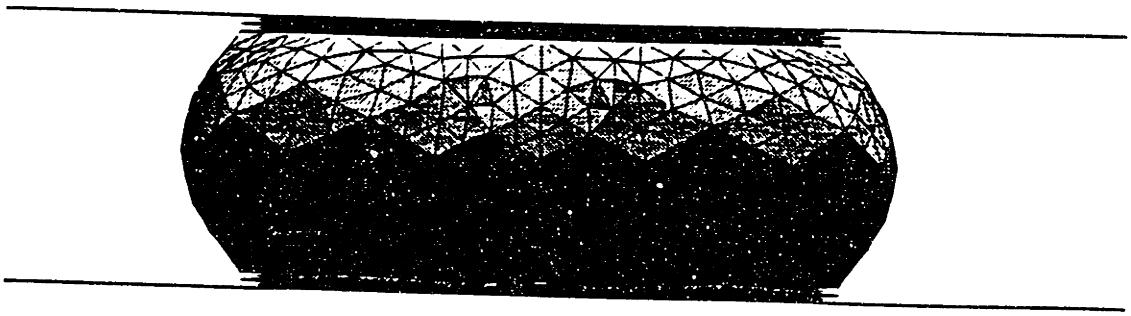

Fig. 4.15 Surface Evolver output for solder pad with 80 micron radii and 60 micron joint height (constant volume).

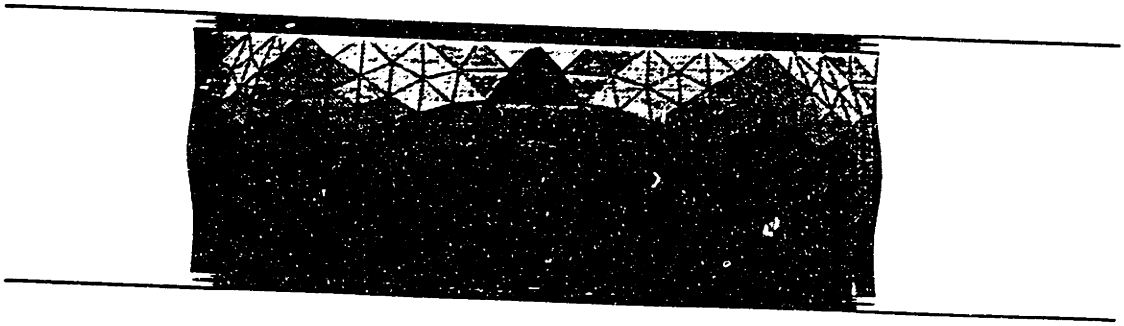

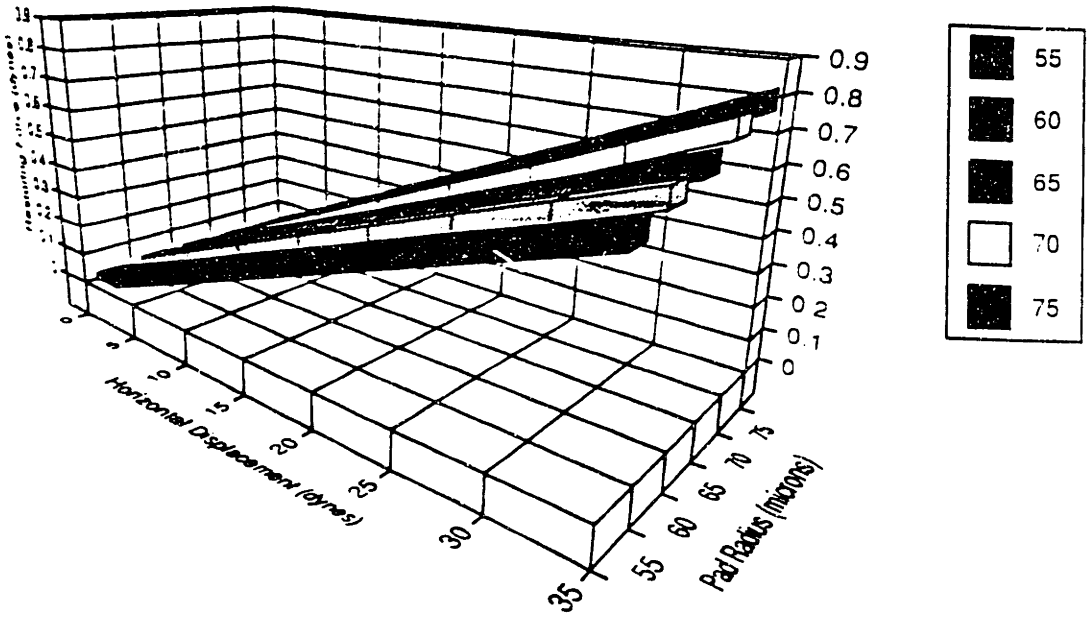

Fig. 4.16: Restoring Force as a function of Horizontal Displacement and Pad Radius for a solder joint height of 60 microns, constant surface tension, and constant volume.

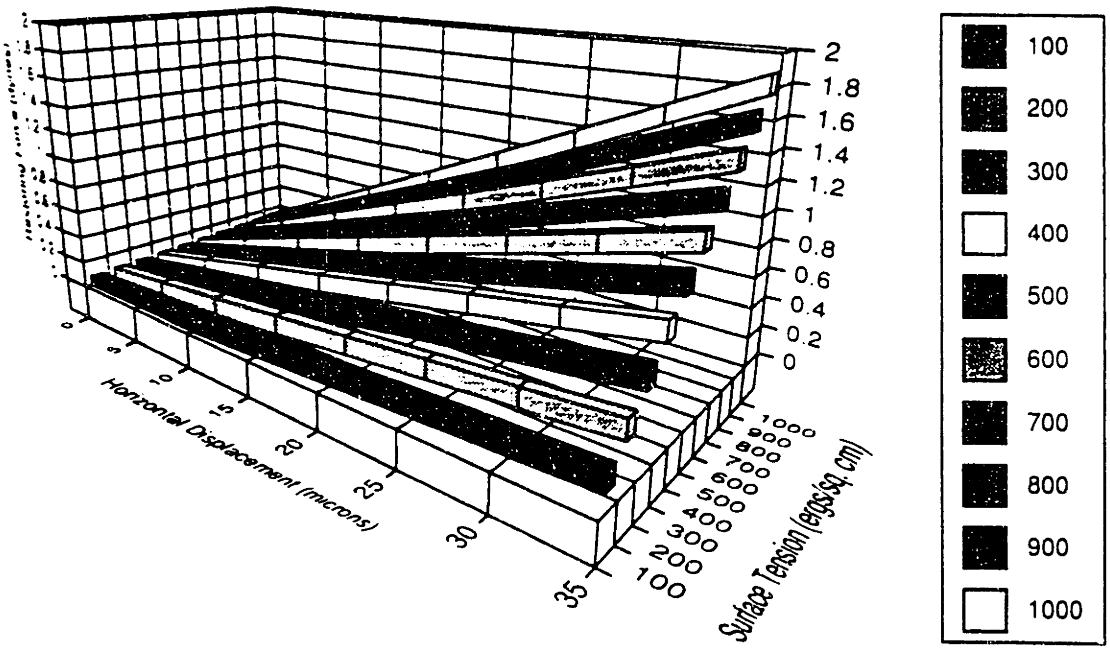

Fig. 4.17 :Restoring Force as a function of Horizontal Displacement and Surface Tension for a 70 micron radius circular pad (60 micron separation, Volume = 4e5 cubic microns).

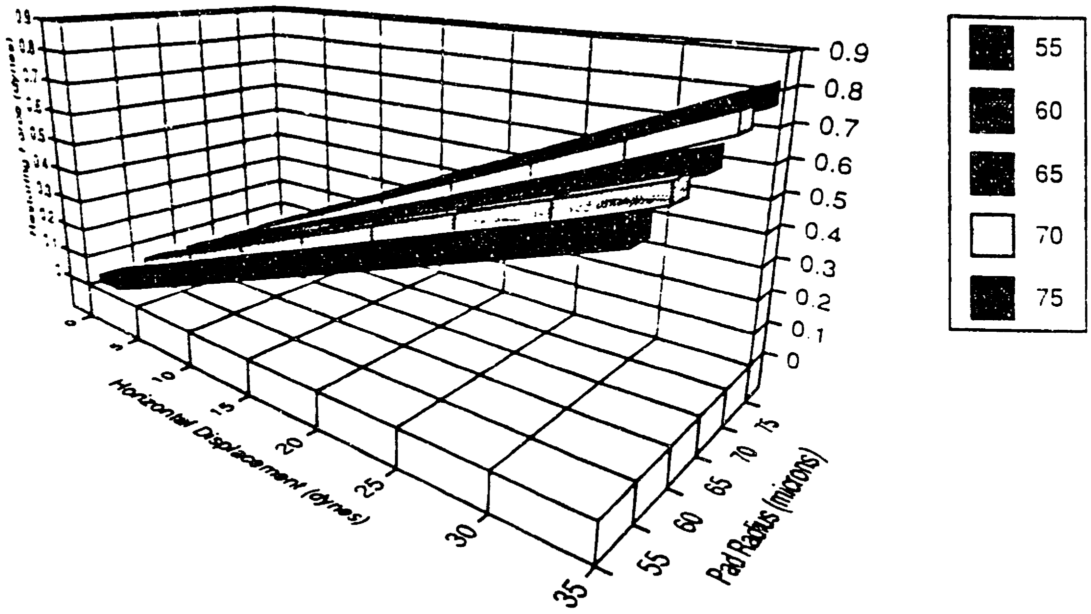

Fig. 4.18: Restoring Force as a function of Horizontal Displacement and Pad Radius for a solder joint height of 60 microns, constant surface tension, and constant volume.

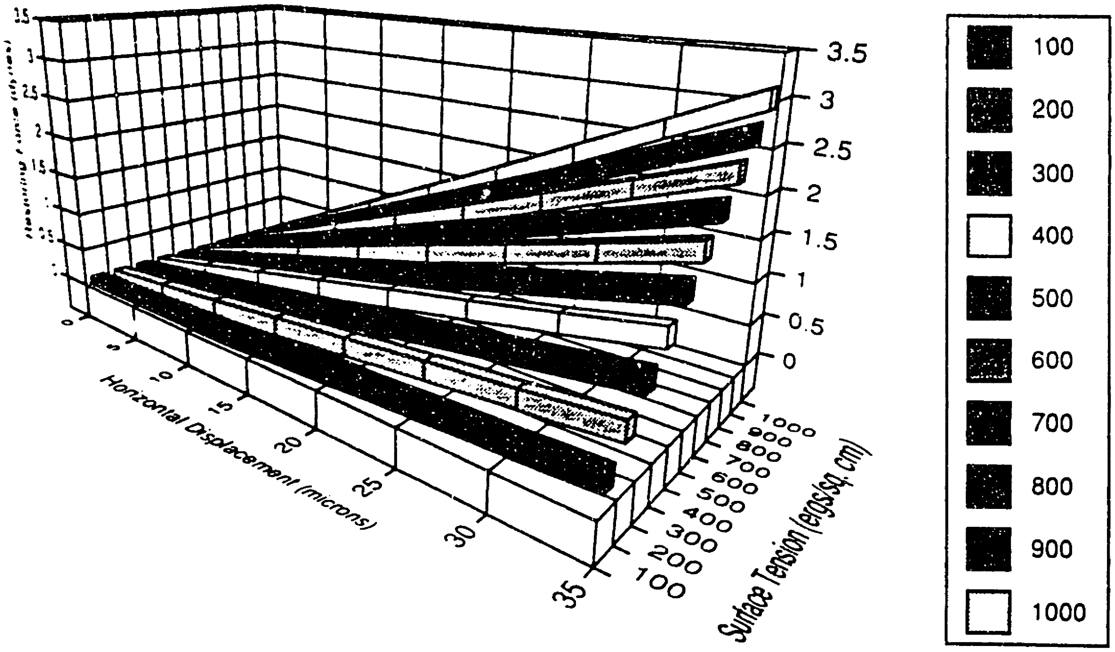

Fig. 4.19: Restoring Force as a function of Horizontal Displacement and Surface Tension for a 60 micron radius circular pad (70 micron separation, Volume = 4e5 cubic microns).

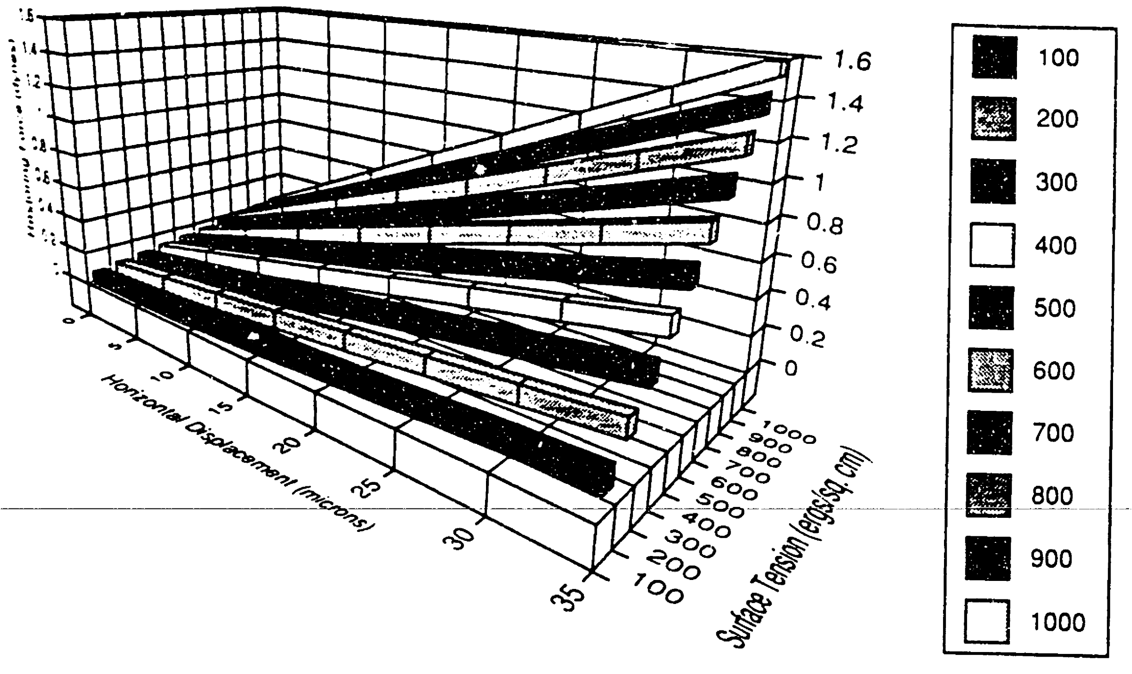

Fig. 4.20: Restoring Force as a function of Horizontal Displacement and Surface Tension for a 60 micron radius circular pad (80 micron separation, Volume = 4e5 cubic microns).

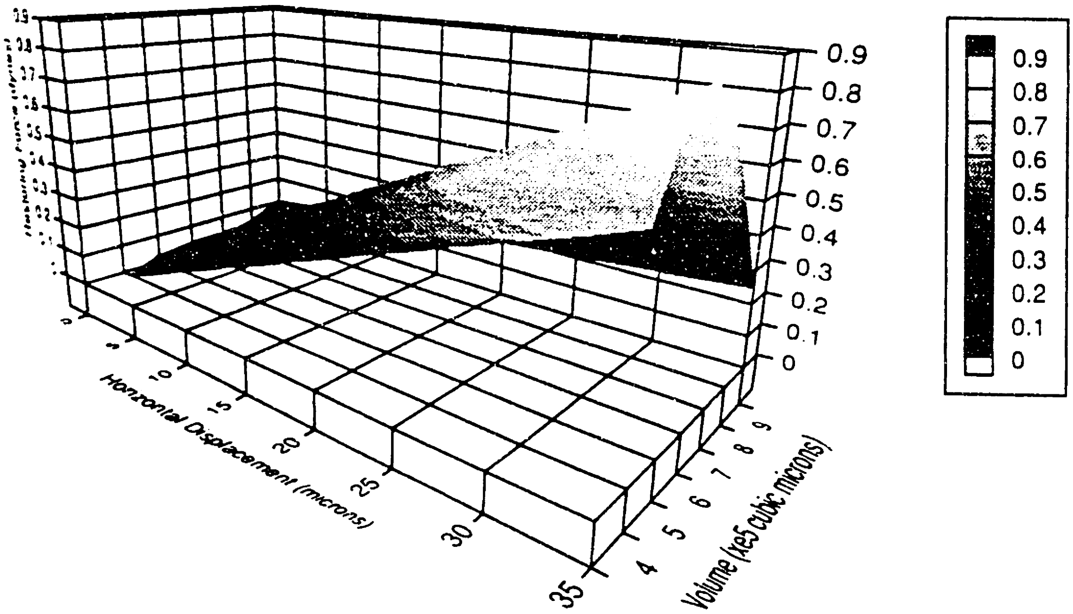

Fig. 4.21: Restoring Force as a function of Horizontal Displacement and Volume for a 55 micron radius circular pad with a 60 micron separation.

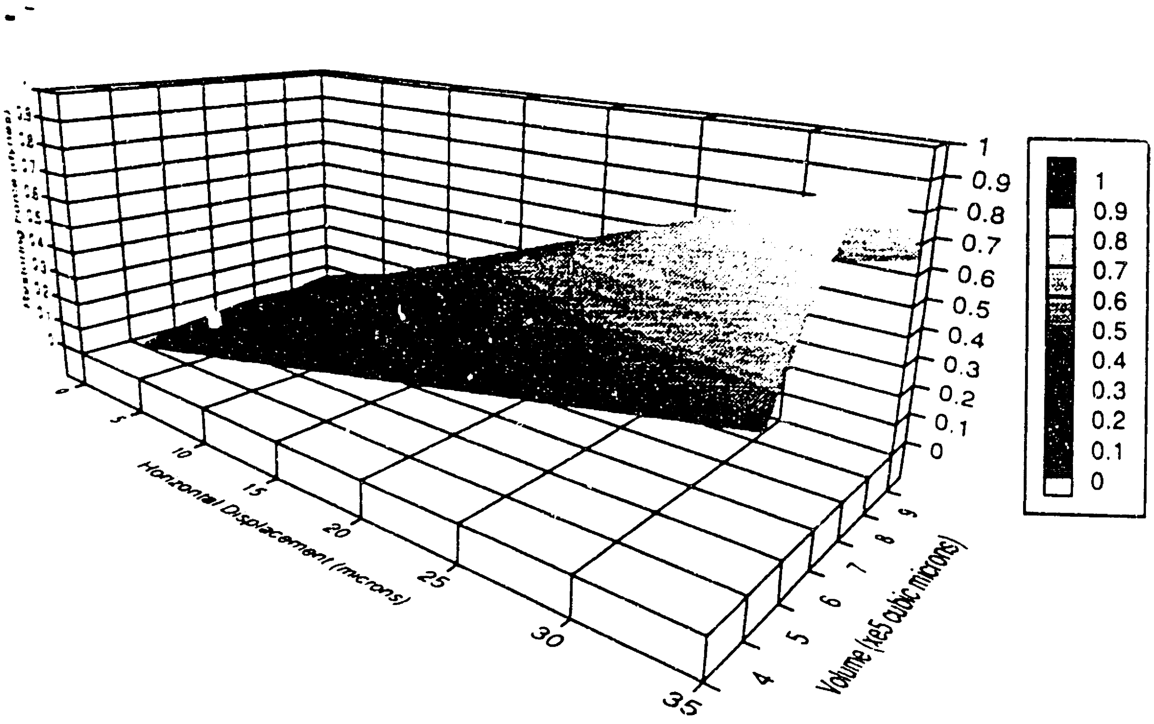

Fig. 4.22: Restoring Force as a function of Horizontal Displacement and Volume for a 60 micron radius circular pad with a 60 micron vertical separation.

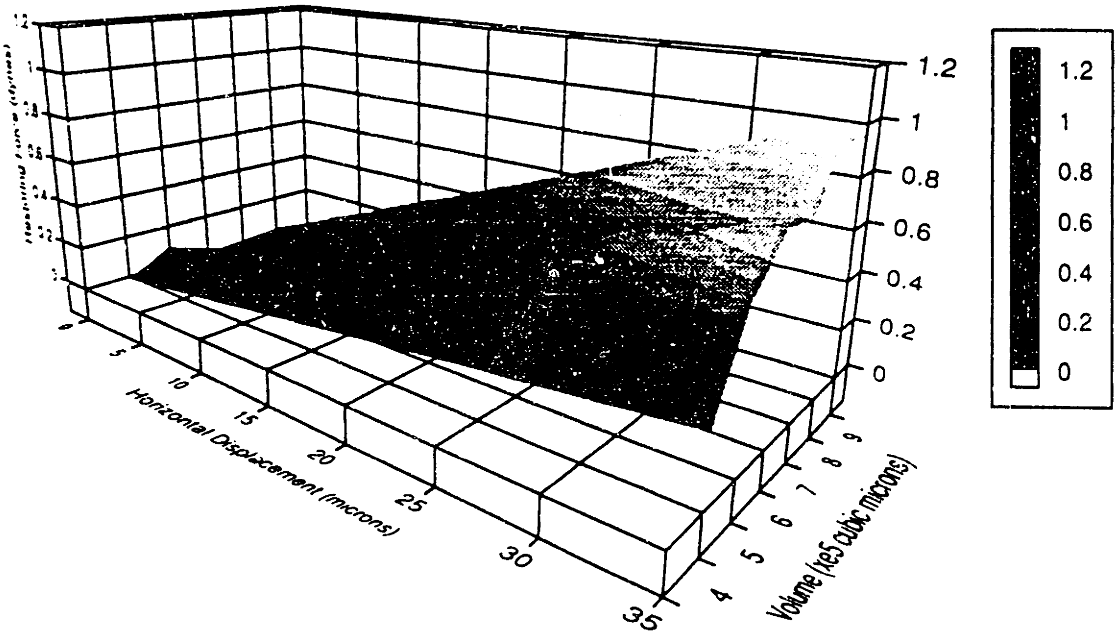

Fig. 4.23: Restoring Force as a function of Horizontal Displacement and Volume for a 65 micron radius circular pad with a 60 micron separation.

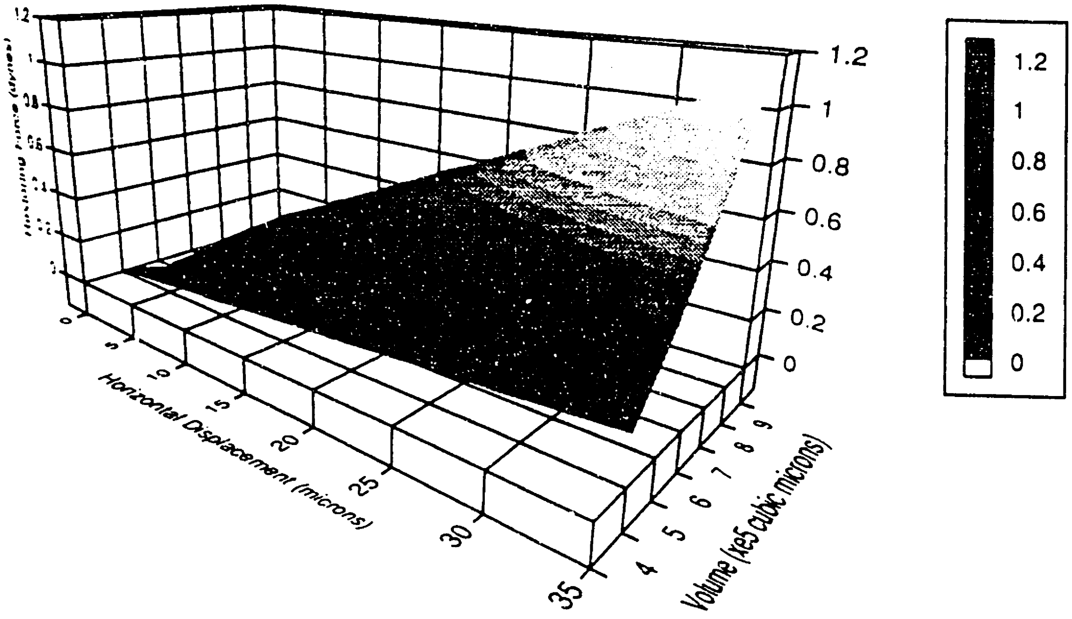

Fig. 4.24: Restoring Force as a function of Horizontal Displacement and Volume for a 70 micron radius circular pad with a 60 micron separation.

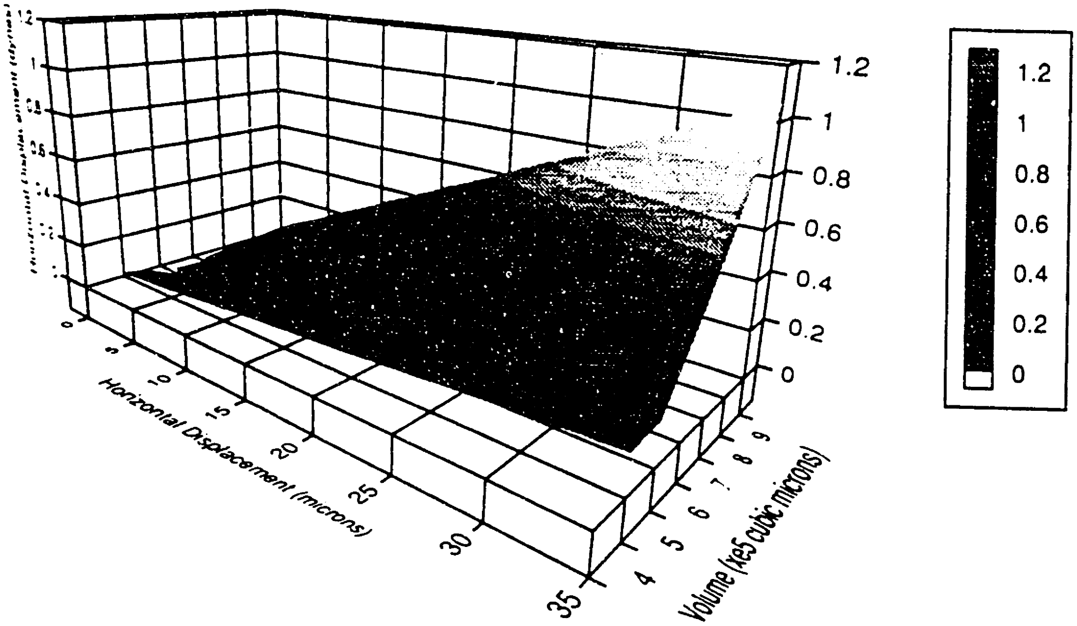

Fig. 4.25: Restoring Force as a function of Horizontal Displacement and Volume for a 75 micron radius circular pad with a 60 micron seperation.

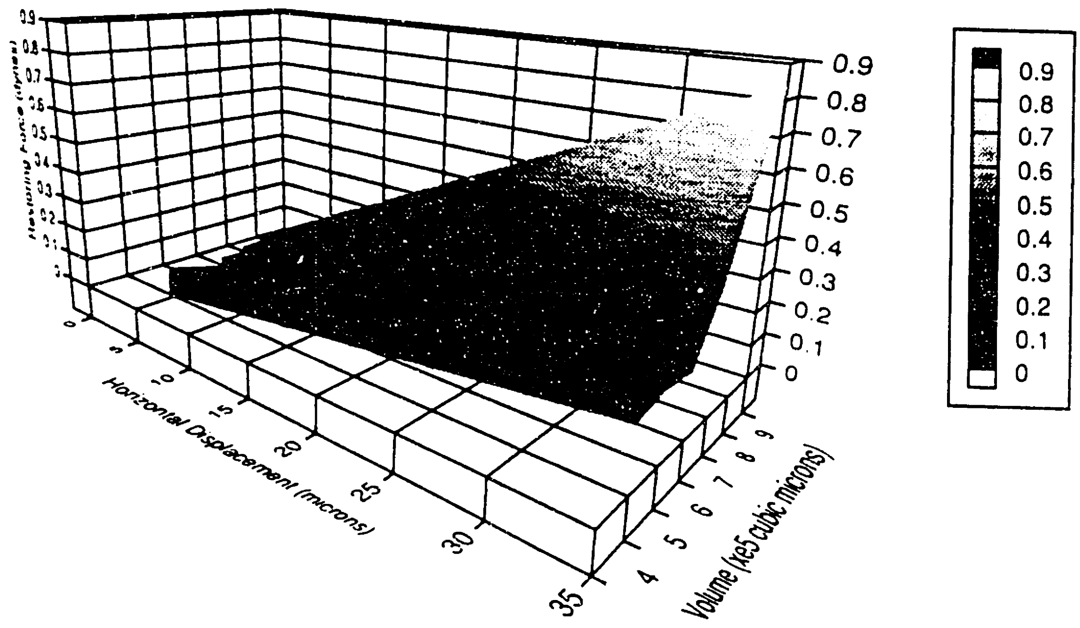

Fig. 4.26: Restoring Force as a function of Horizontal Displacement and Volume for a 80 micron radius circular pad with a 60 micron separation.

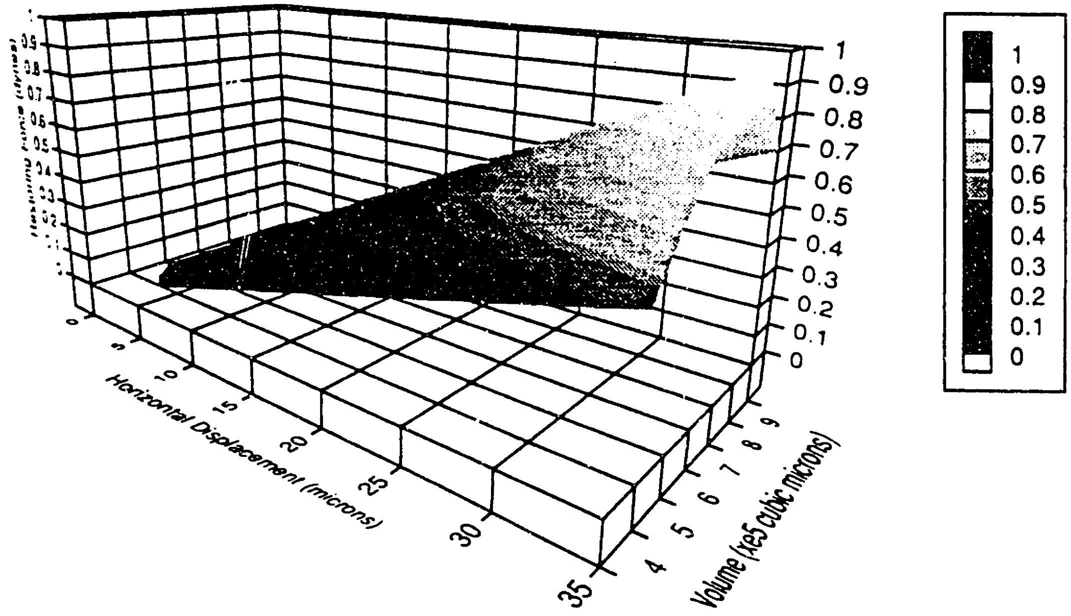

Fig. 4.27: Restoring Force as a function of Horizontal Displacement and Volume for a 55 micron radius circular pad with a 70 micron separation.

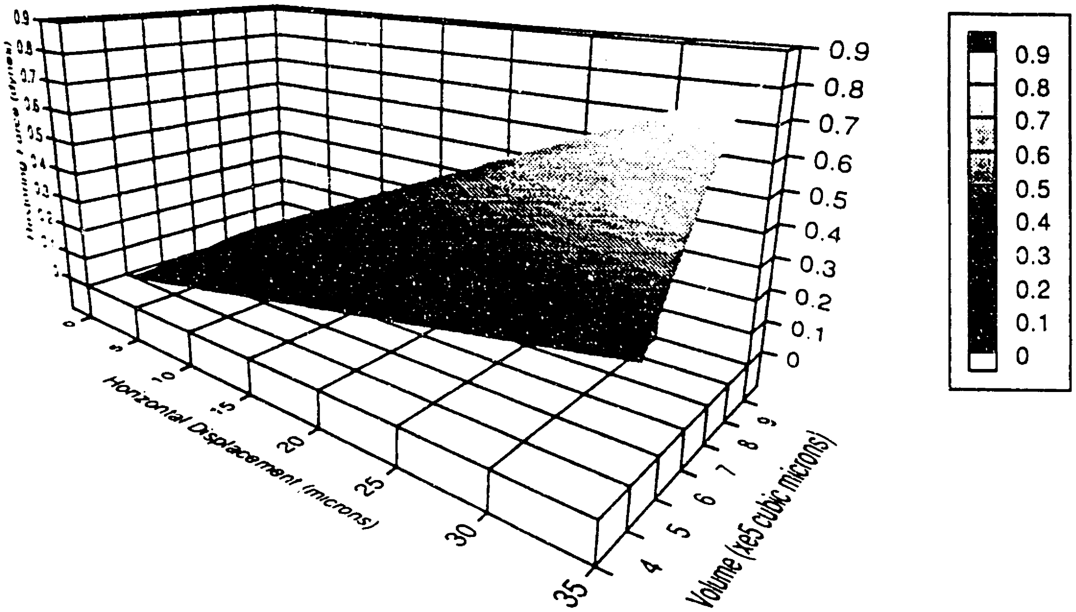

Fig. 4.28: Restoring Force as a function of Horizontal Displacement and Volume for a 60 micron radius circular pad with a 70 micron separation.

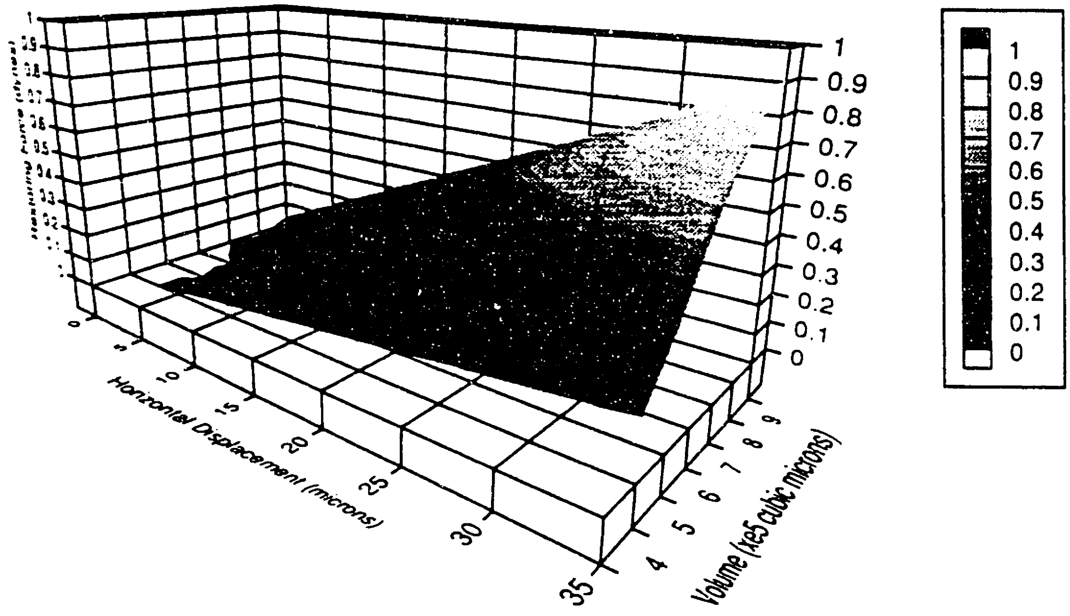

Fig. 4.29: Restoring Force as a function of Horizontal Displacement and Volume for a 65 micron radius circular pad with a 70 micron seperation.

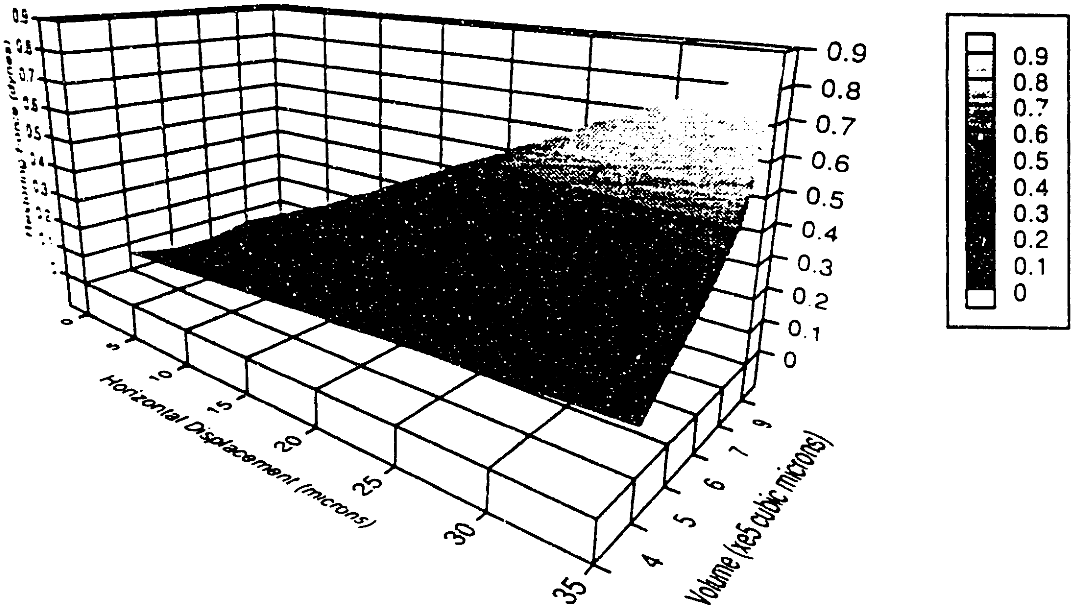

Fig.4.30: Restoring Force as a function of Horizontal Displacement and Volume for a 70 micron radius circular pad with a 70 micron separation.

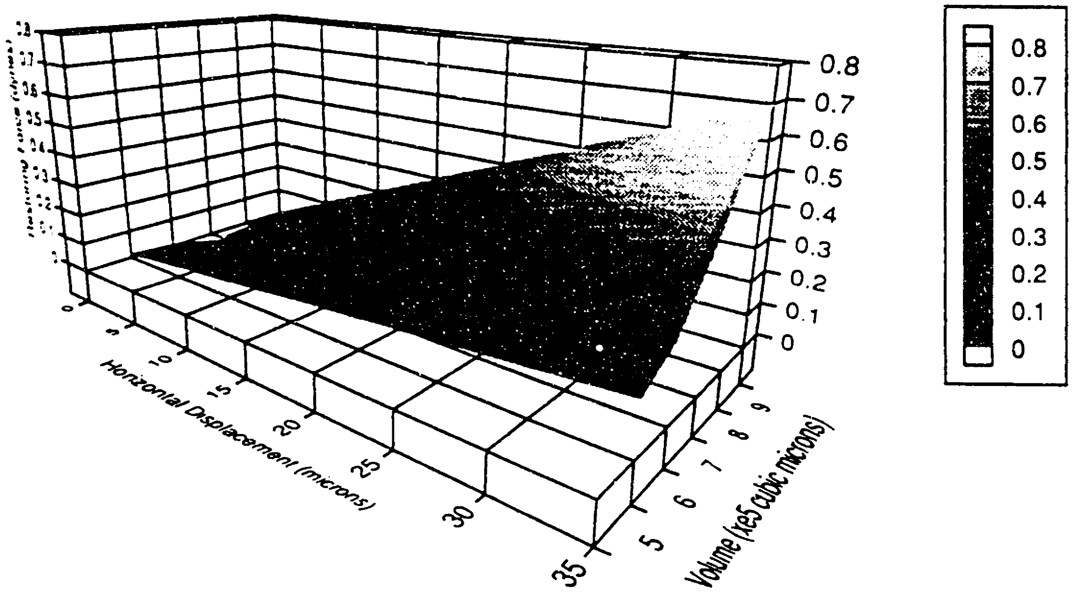

Fig. 4.31: Restoring Force as a function of Horizontal Displacement and Volume for a 75 micron radius circular pad with a 70 micron separation.

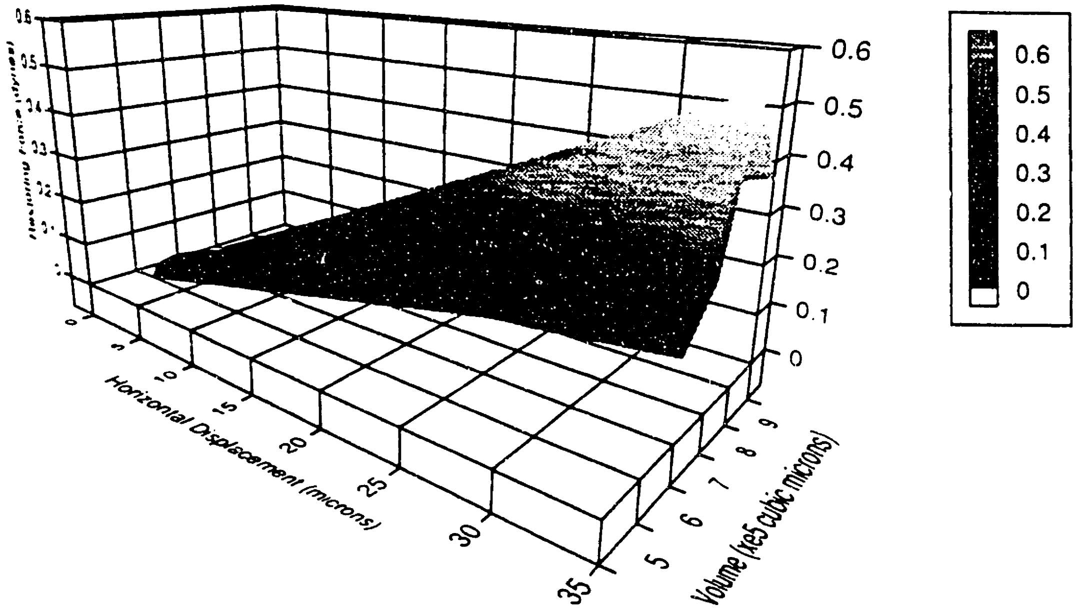

Fig. 4.32: Restoring Force as a function of Horizontal Displacement and Volume for a 80 micron radius circular pad with a 70 micron separation.

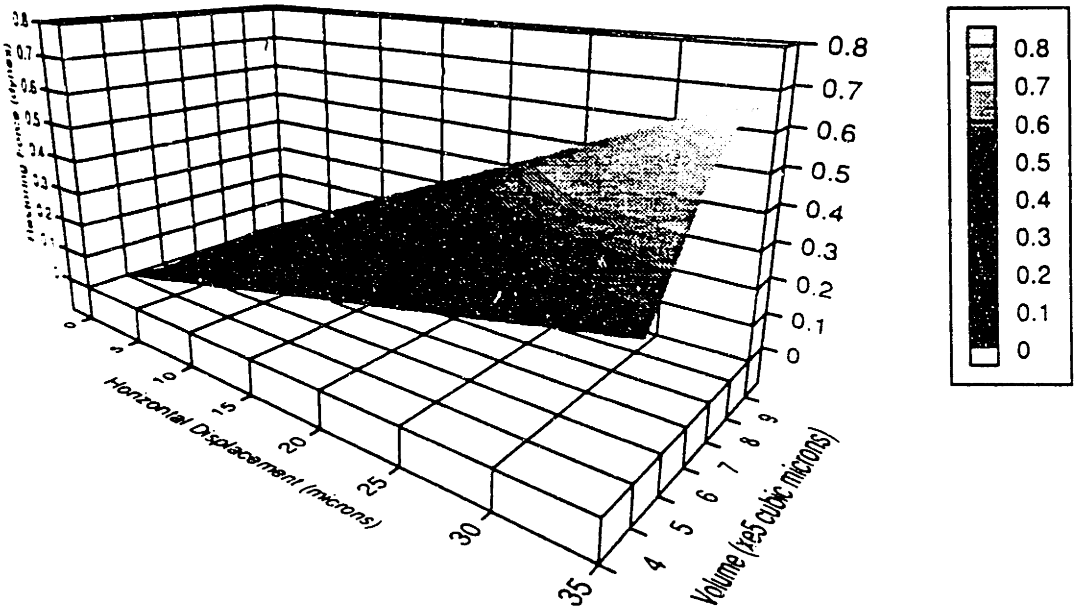

Fig. 4.33: Restoring Force as a function of Horizontal Displacement and Volume for a 55 micron radius circular pad with a 80 micron separation.

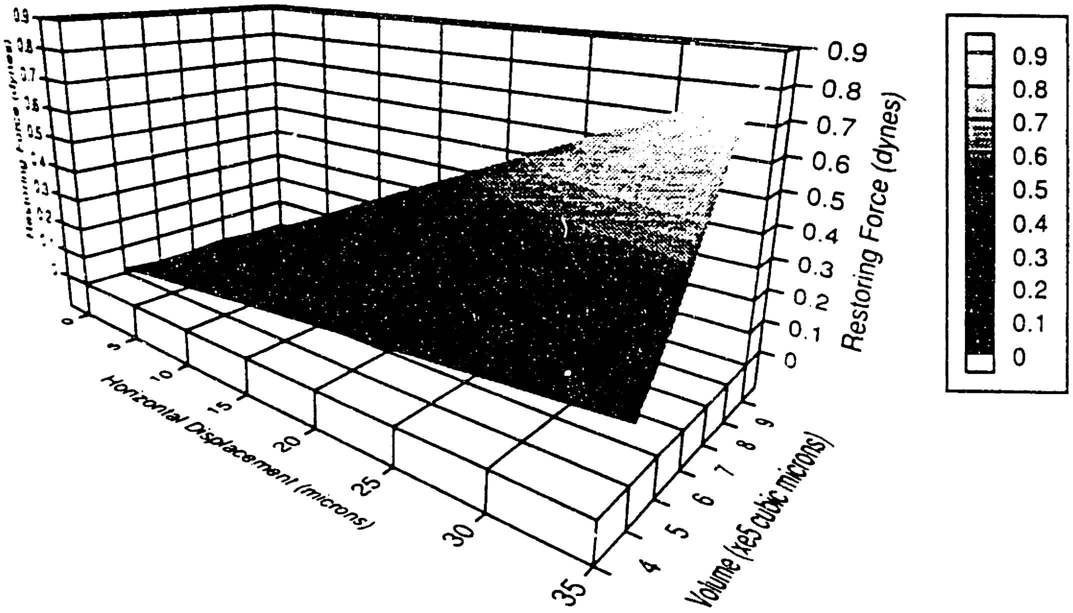

Fig. 4.34: Restoring Force as a function of Horizontal Displacement and Volume for a 60 micron radius circular pad with a 80 micron separation.

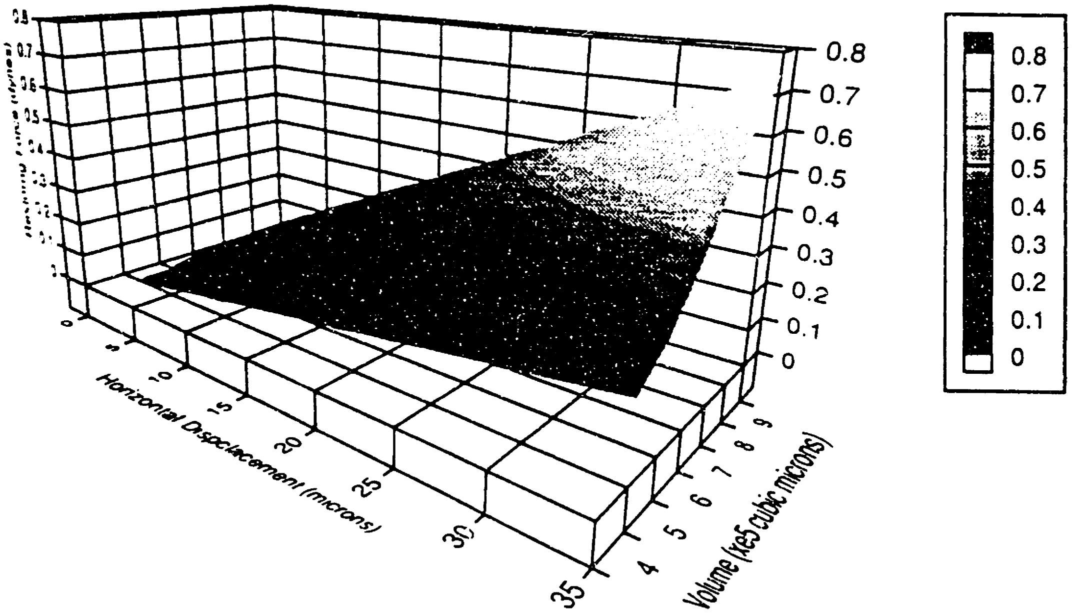

Fig. 4.35: Restoring Force as a function of Horizontal Displacement and Volume for a 65 micron radius circular pad with a 80 micron separation.

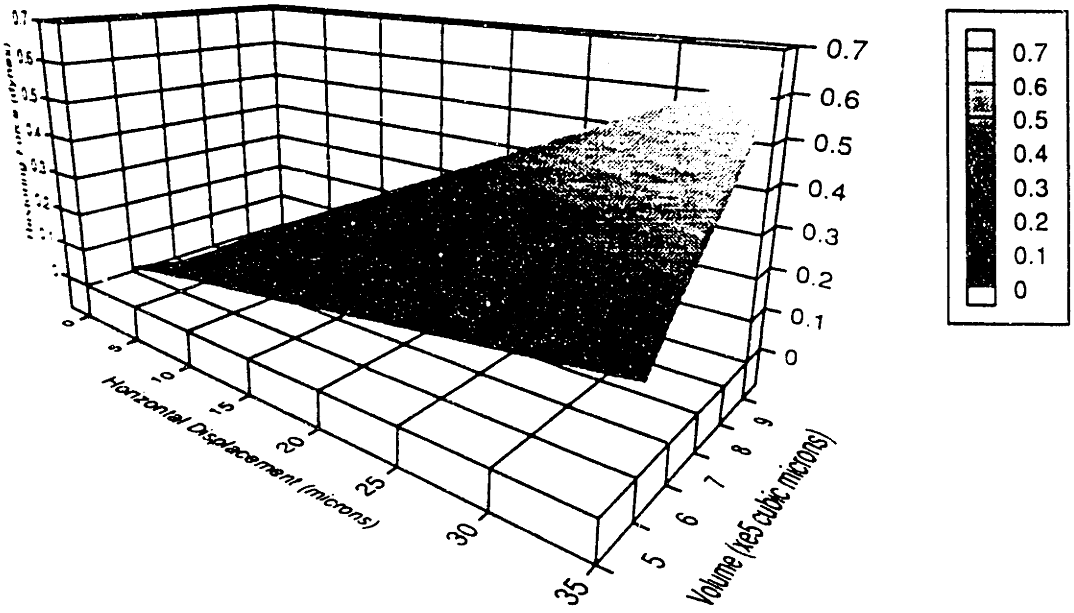

Fig. 4.36: Restoring Force as a function of Horizontal Displacement and Volume for a 70 micron radius circular pad with a 80 micron separation.

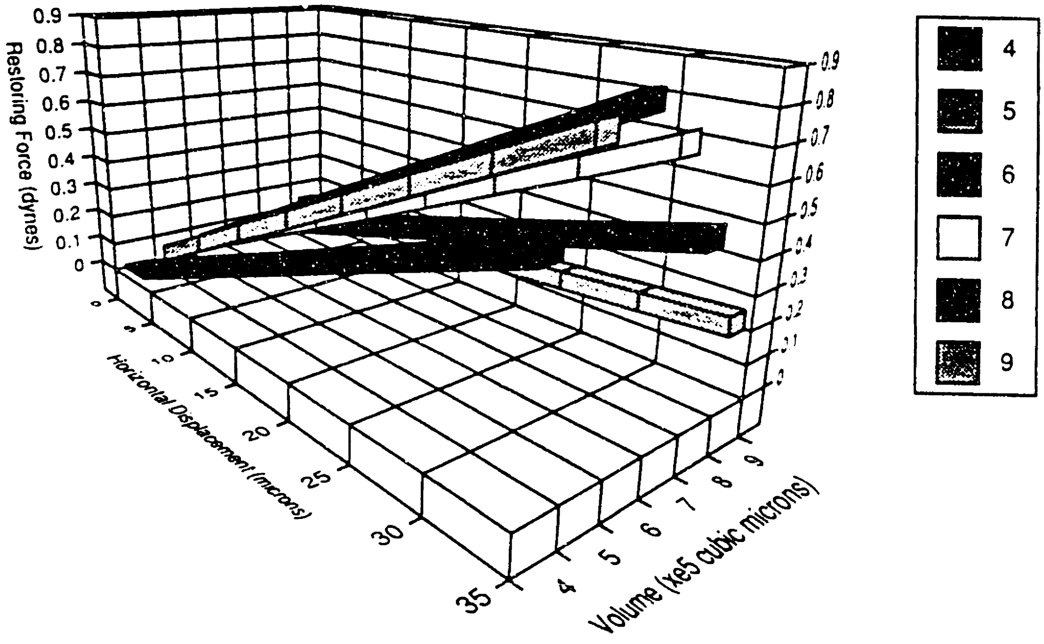

Fig. 4.37: Restoring Force as a function of Horizontal Displacement and Volume for a 55 micron radius circular pad with a 60 micron separation.

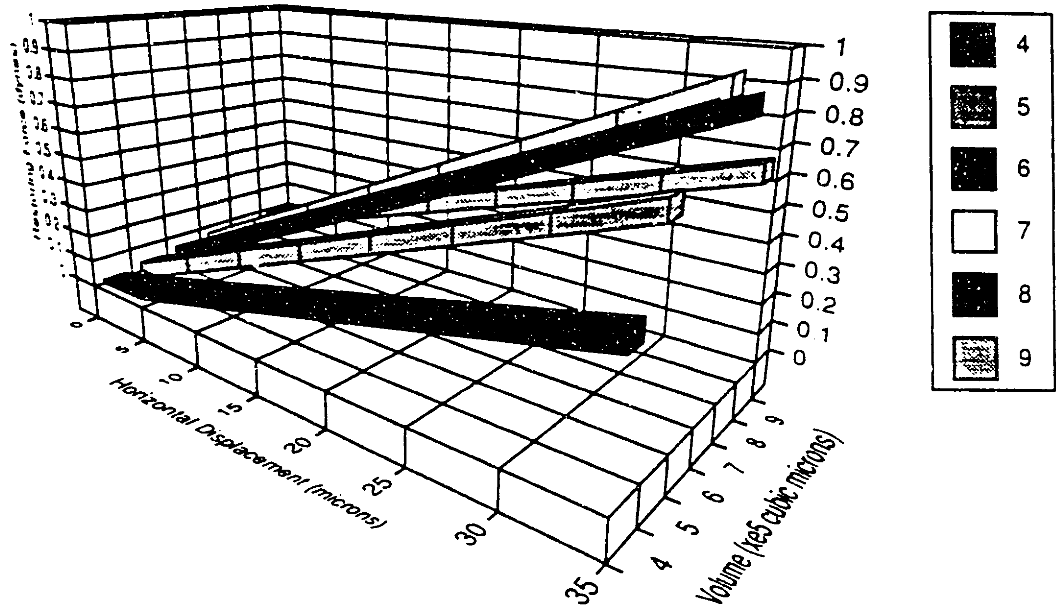

Fig. 4.38: Restoring Force as a function of Horizontal Displacement and Volume for a 60 micron radius circular pad with a 60 micron vertical separation.

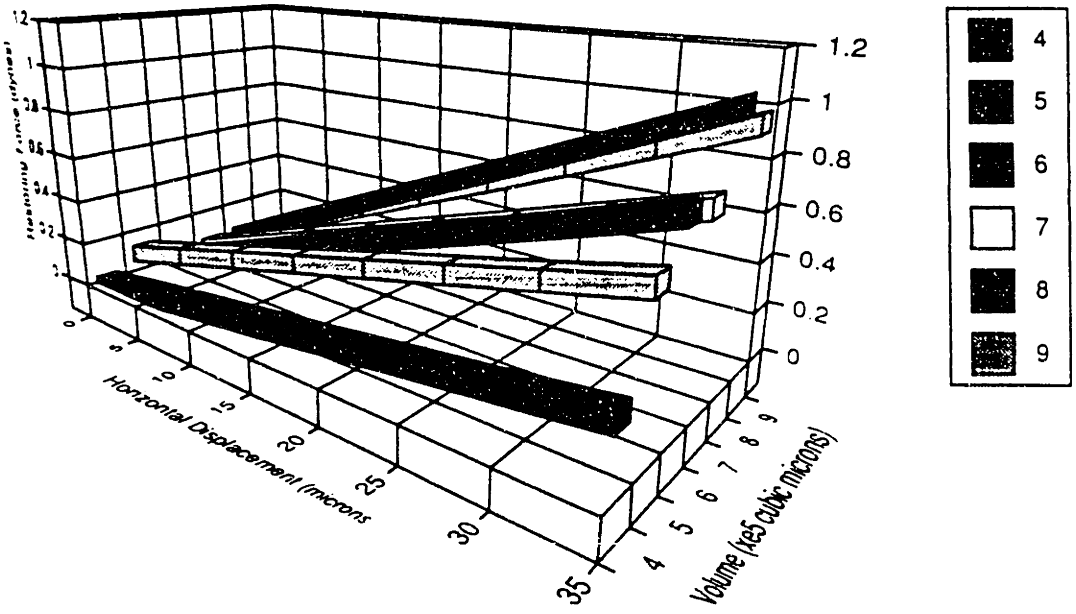

Fig.4.39: Restoring Force as a function of Horizontal Displacement and Volume for a 65 micron radius circular pad with a 60 micron separation.

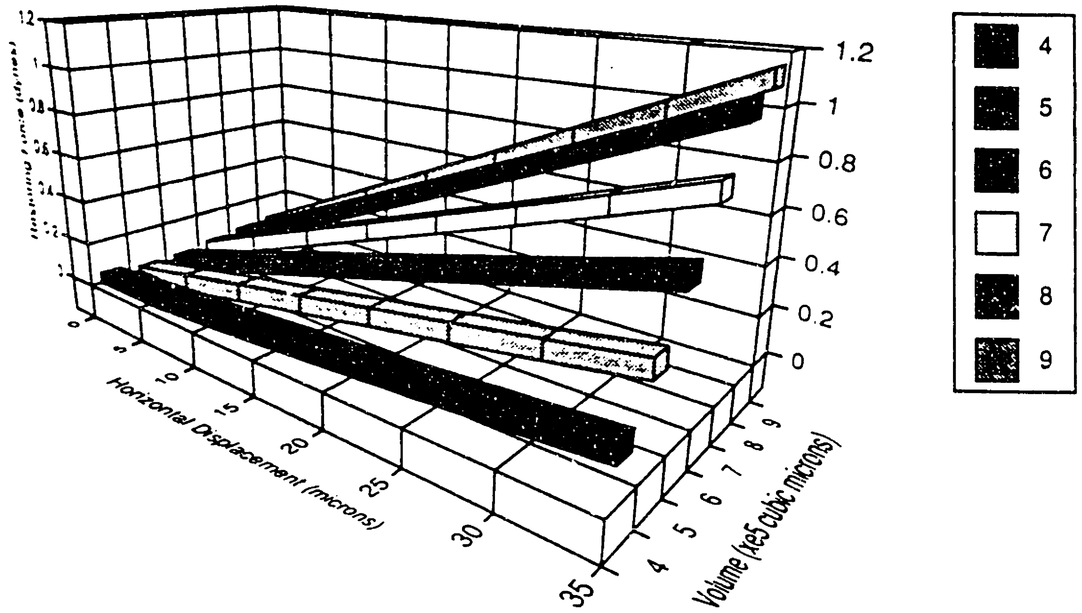

Fig. 4.40: Restoring Force as a function of Horizontal Displacement and Volume for a 70 micron radius circular pad with a 60 micron separation.

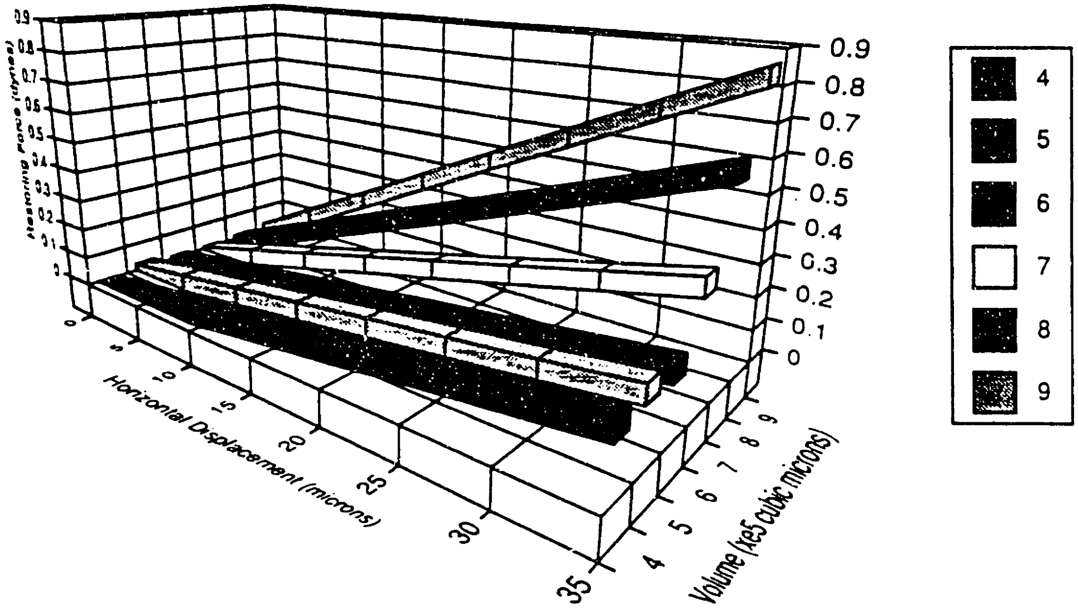

Fig. 4.41: Restoring Force as a function of Horizontal Displacement and Volume for an 80 micron radius circular pad with a 60 micron separation.

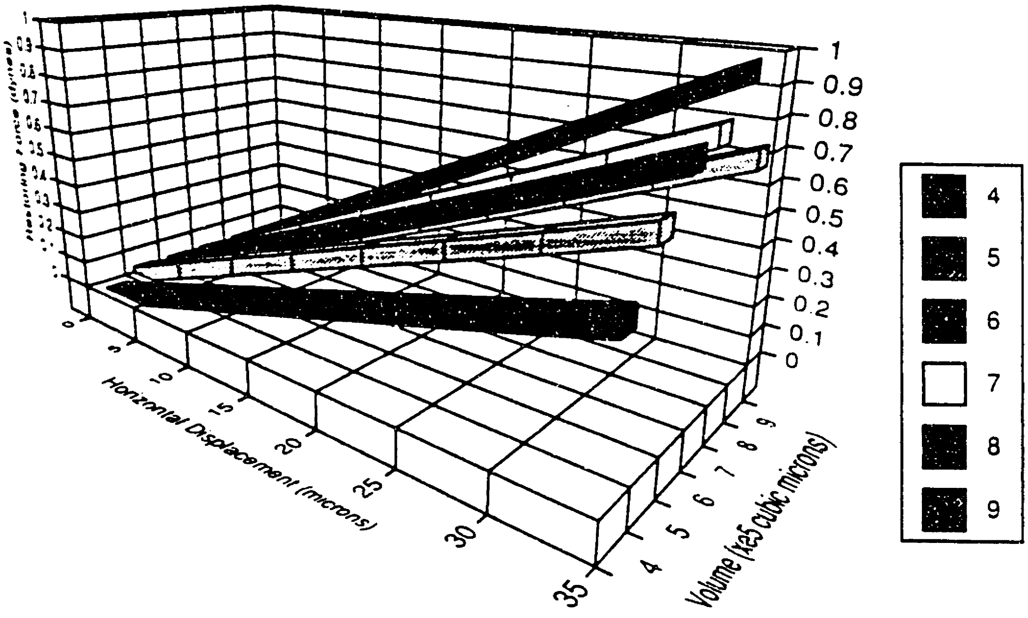

Fig. 4.42: Restoring Force as a function of Horizontal Displacement and Volume for a 55 micron radius circular pad with a 70 micron separation.

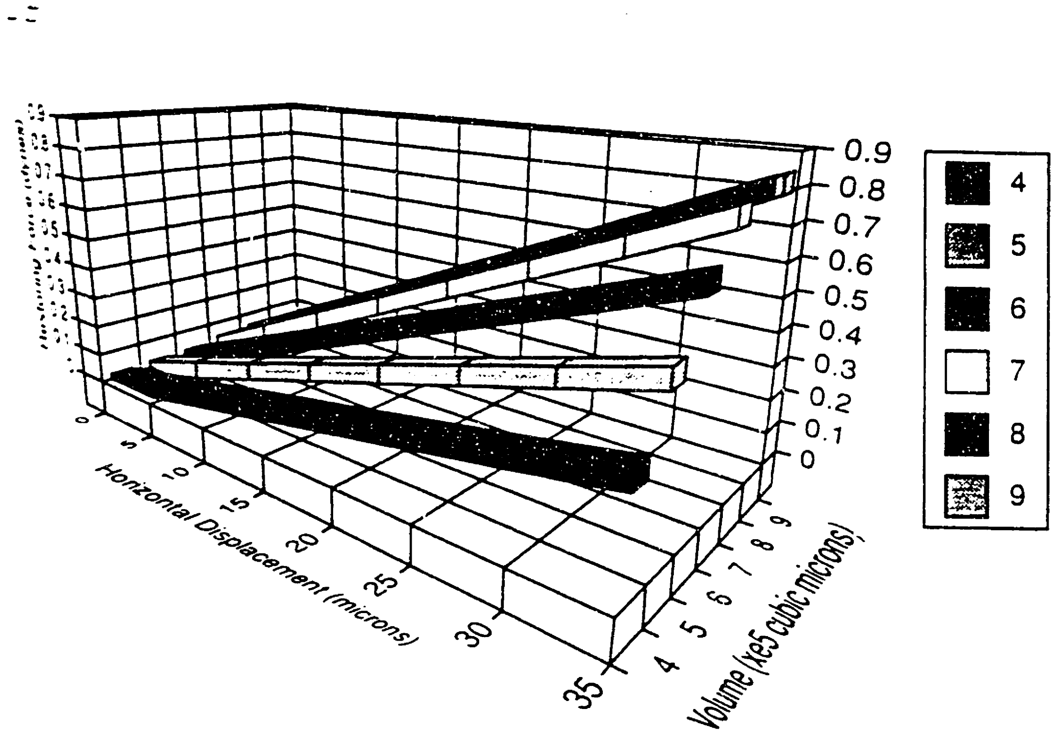

Fig. 4.43: Restoring Force as a function of Horizontal Displacement and Volume for a 60 micron radius circular pad with a 70 micron separation.

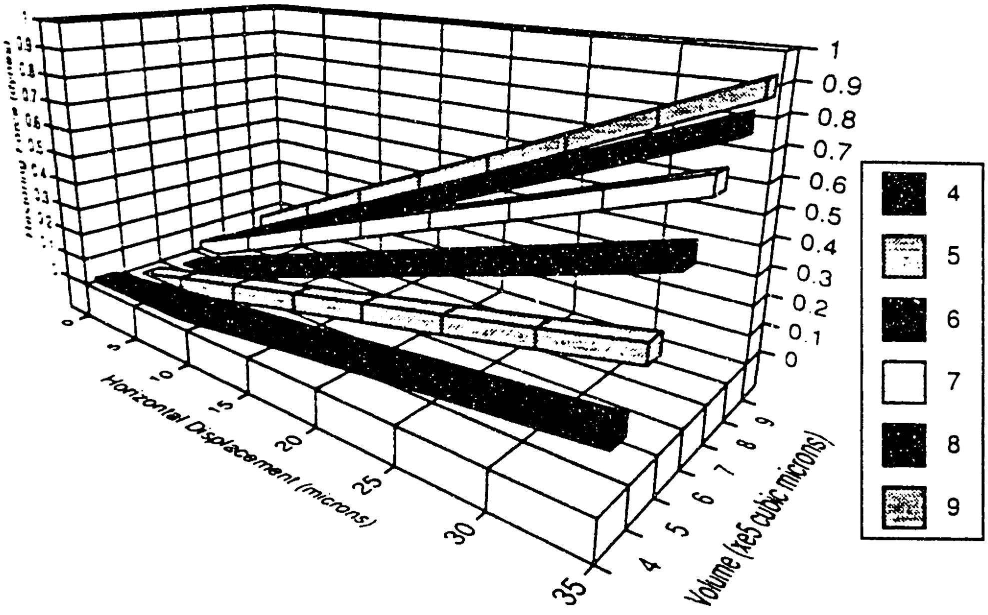

Fig. 4.44: Restoring Force as a function of Horizontal Displacement and Volume for a 65 micron radius circular pad with a 70 micron separation.

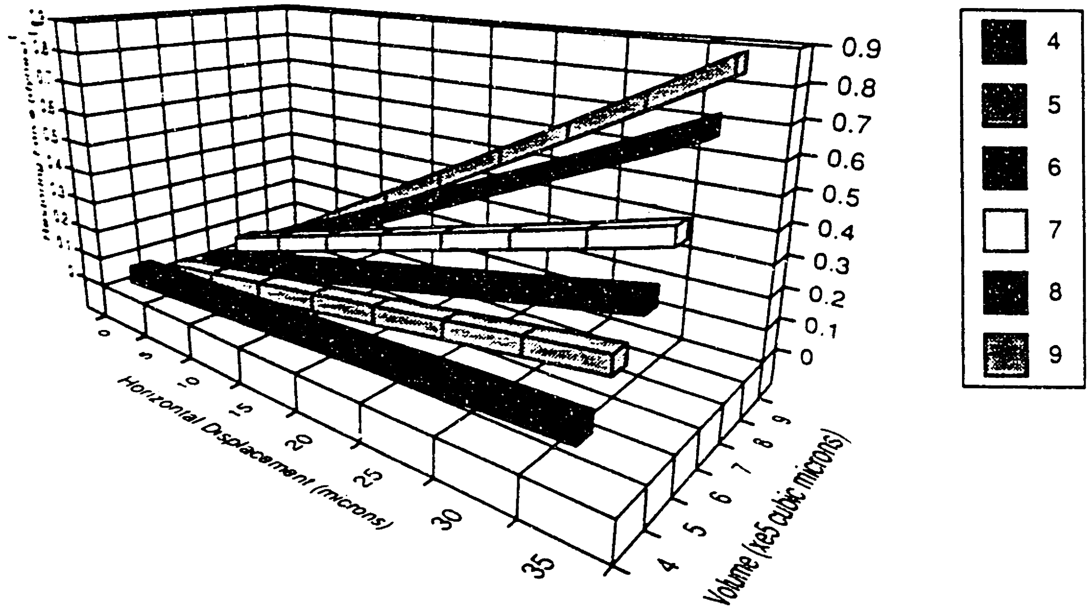

Fig. 4.45: Restoring Force as a function of Horizontal Displacement and Volume for a 70 micron radius circular pad with a 70 micron separation.

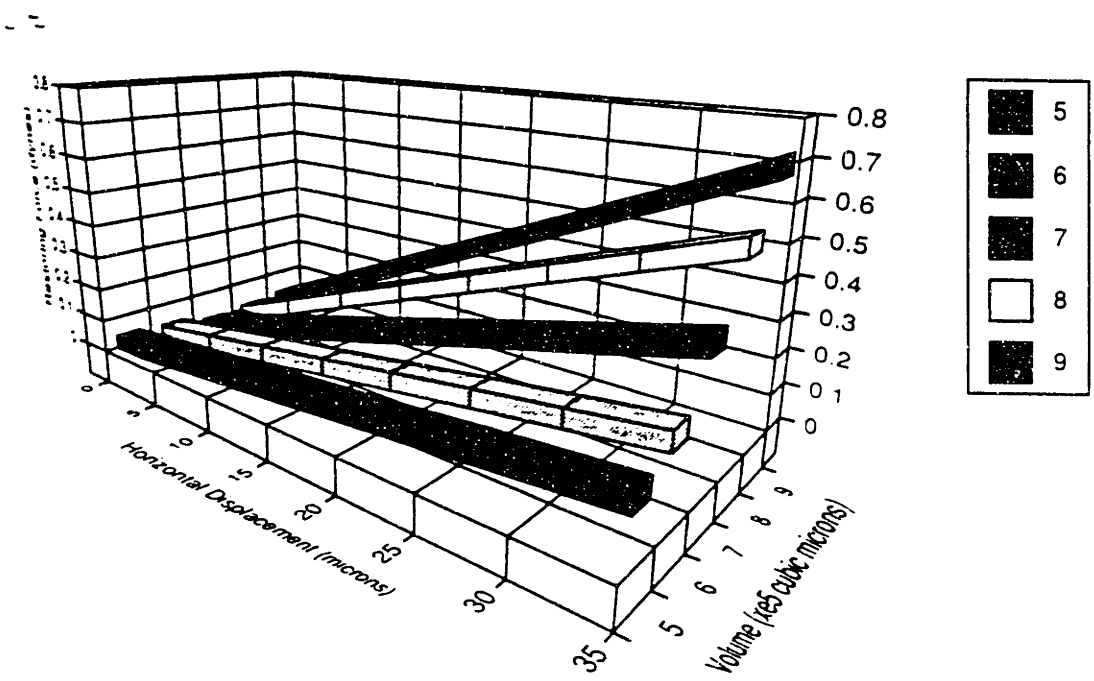

Fig. 4.46: Restoring Force as a function of Horizontal Displacement and Volume for a 75 micron radius circular pad with a 70 micron separation.

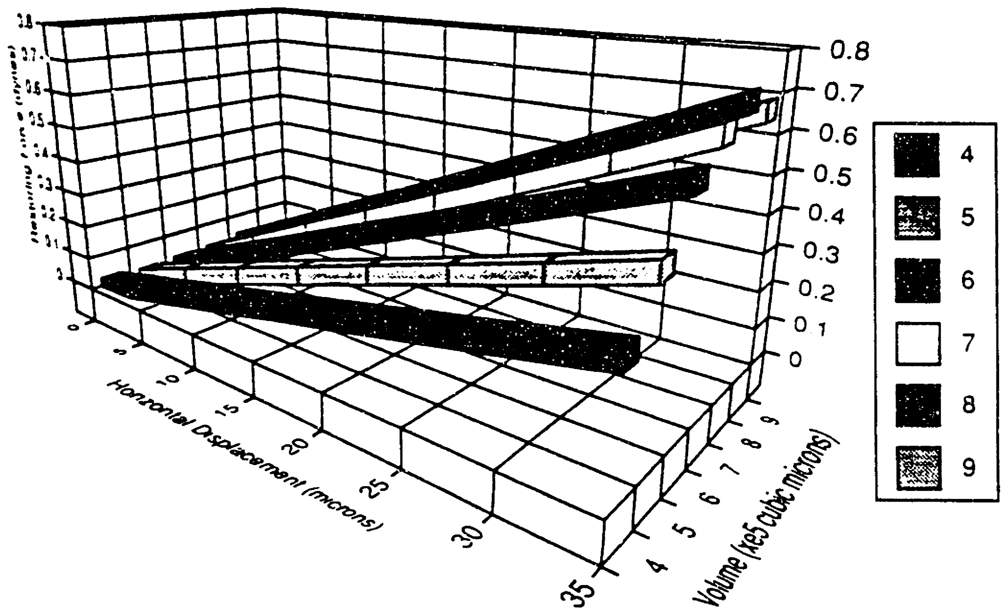

Fig. 4.47: Restoring Force as a function of Horizontal Displacement and Volume for a 55 micron radius circular pad with a 80 micron separation.

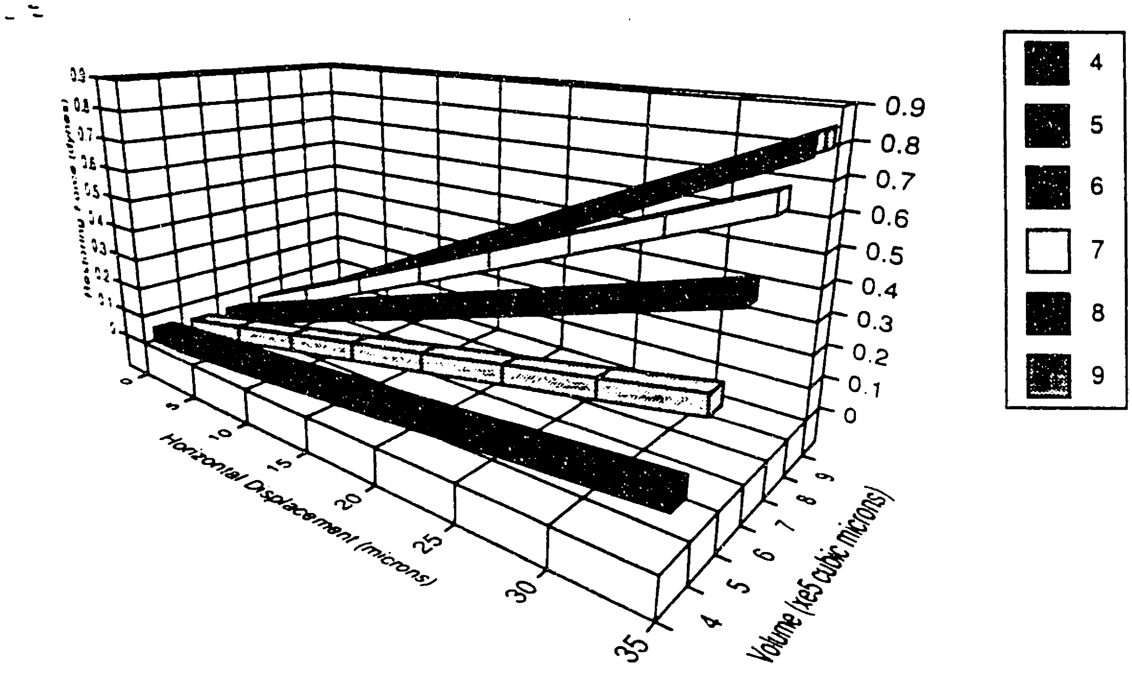

Fig. 4.48: Restoring Force as a function of Horizontal Displacement and Volume for a 60 micron radius circular pad with an 80 micron separation.

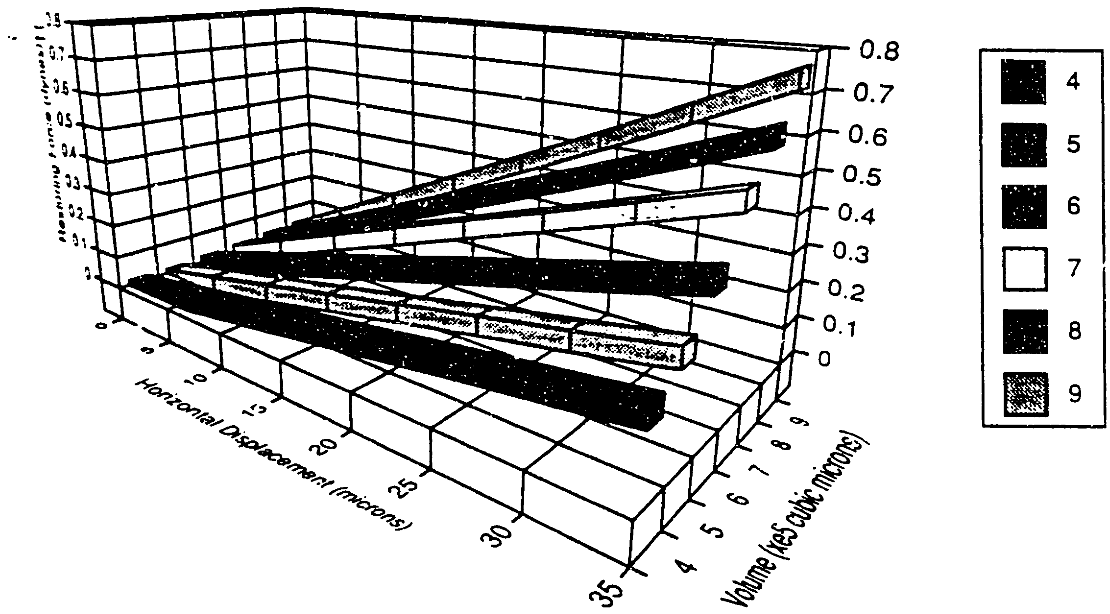

Fig. 4.49: Restoring Force as a function of Horizontal Displacement and Volume for a 65 micron radius circular pad with an 80 micron separation.

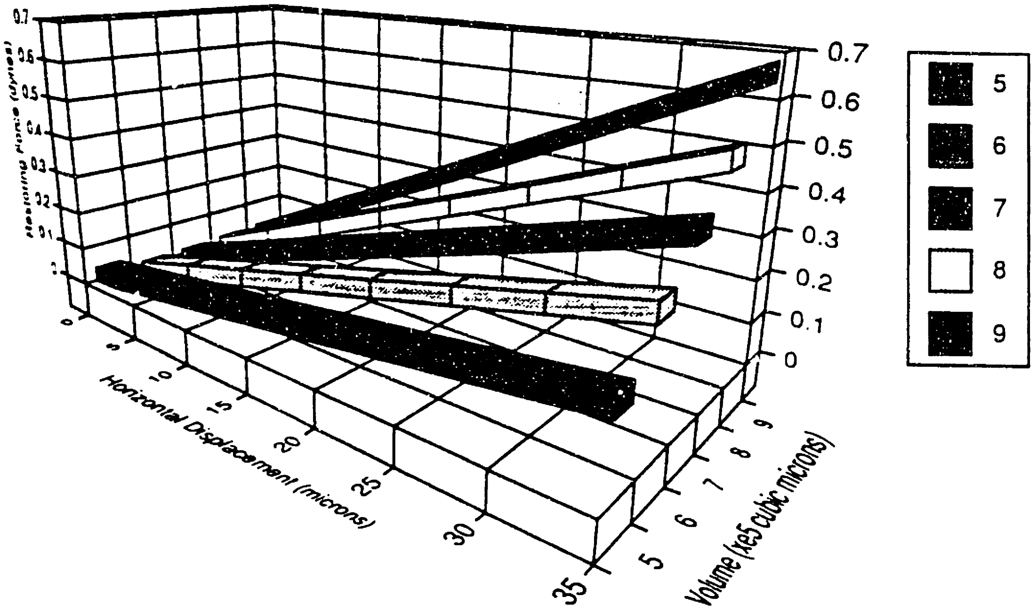

Fig. 4.50: Restoring Force as a function of Horizontal Displacement and Volume for a 70 micron radius circular pad with an 80 micron separation.

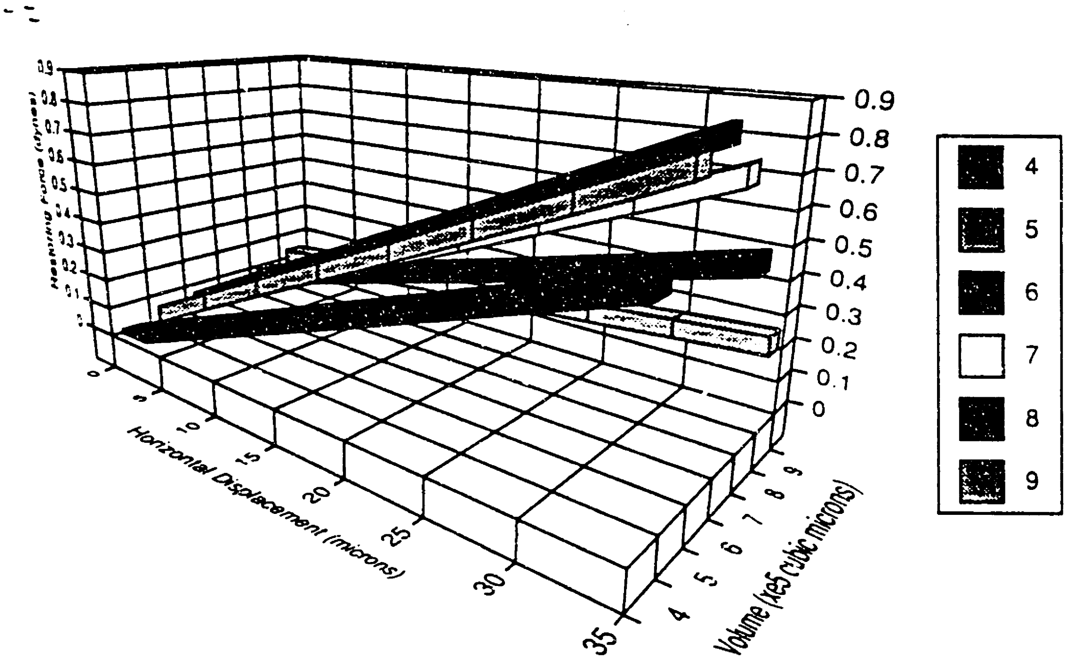

Fig. 4.51: Restoring Force as a function of Horizontal Displacement and Volume for a 55 micron radius circular pad with an 60 micron separation.

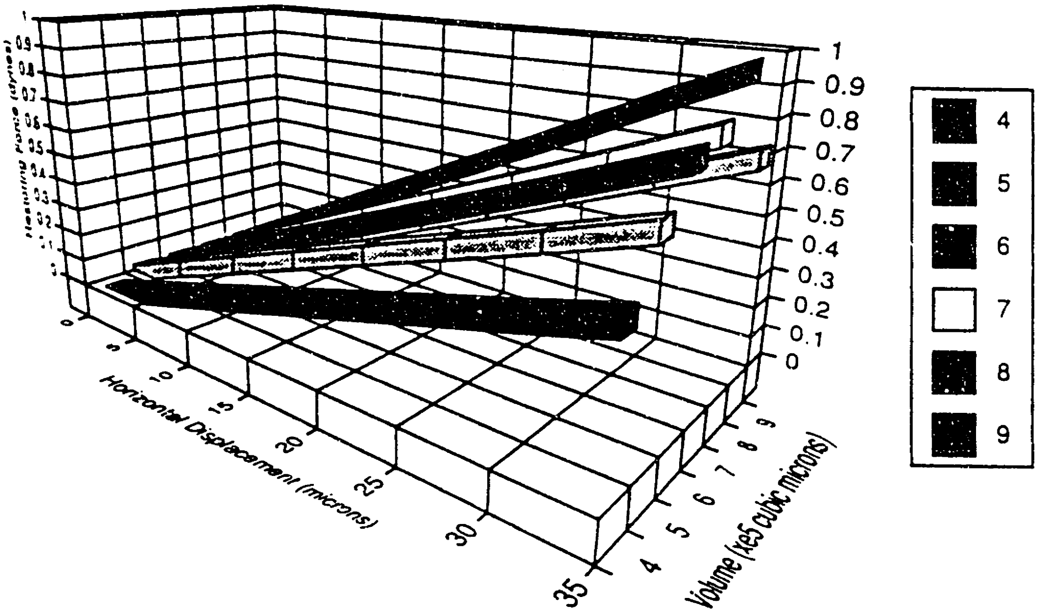

Fig. 4.52: Restoring Force as a function of Horizontal Displacement and Volume for a 55 micron radius circular pad with a 70 micron separation.

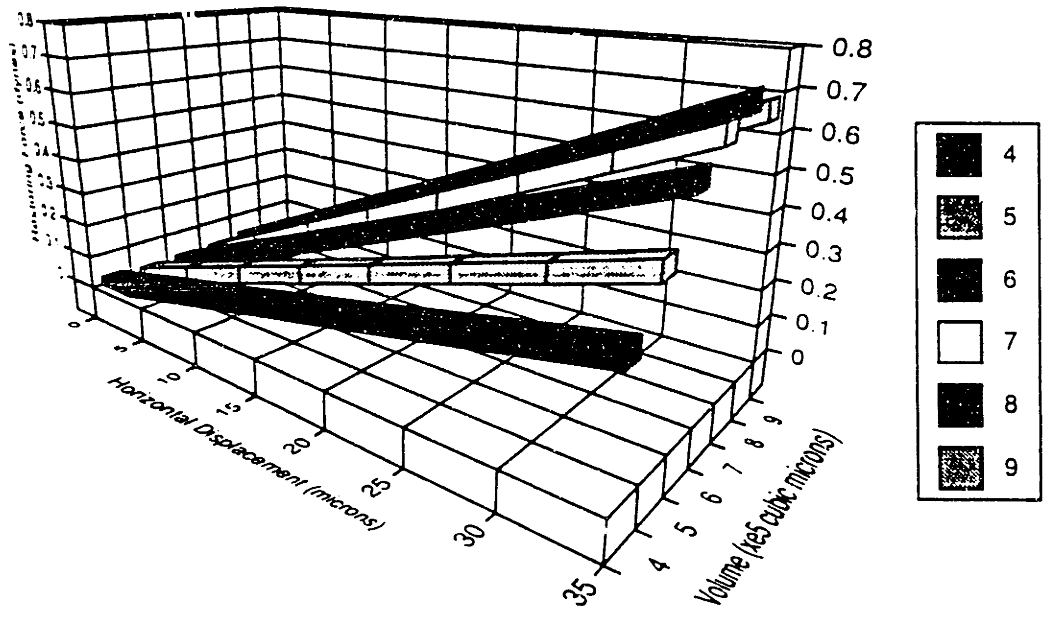

Fig. 4.53: Restoring Force as a function of Horizontal Displacement and Volume for a 55 micron radius circular pad with an 80 micron separation.

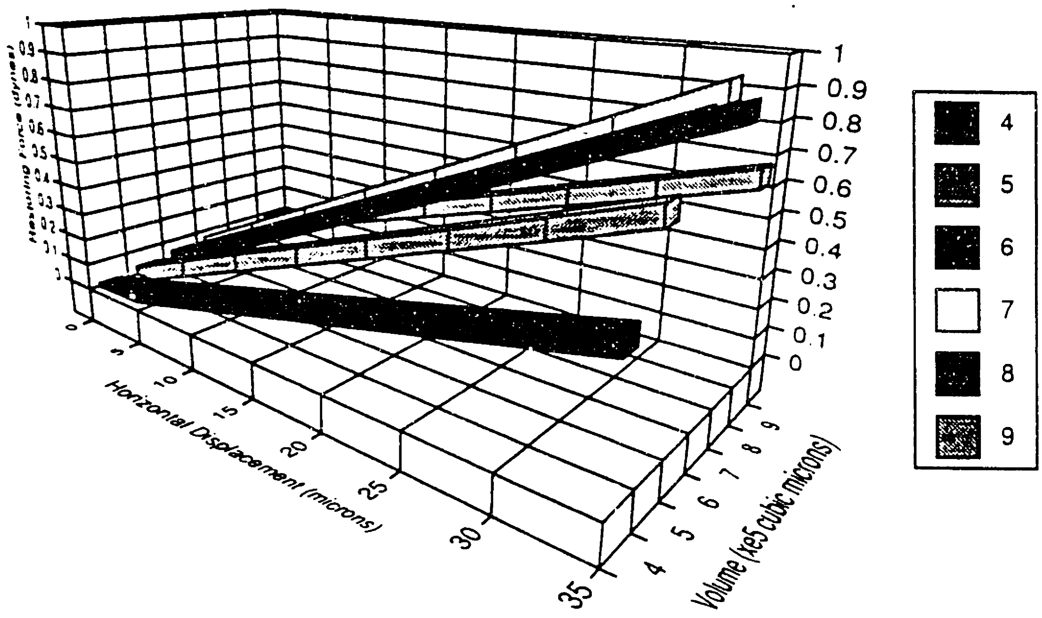

Fig. 4.54: Restoring Force as a function of Horizontal Displacement and Volume for a 60 micron radius circular pad with an 60 micron separation.

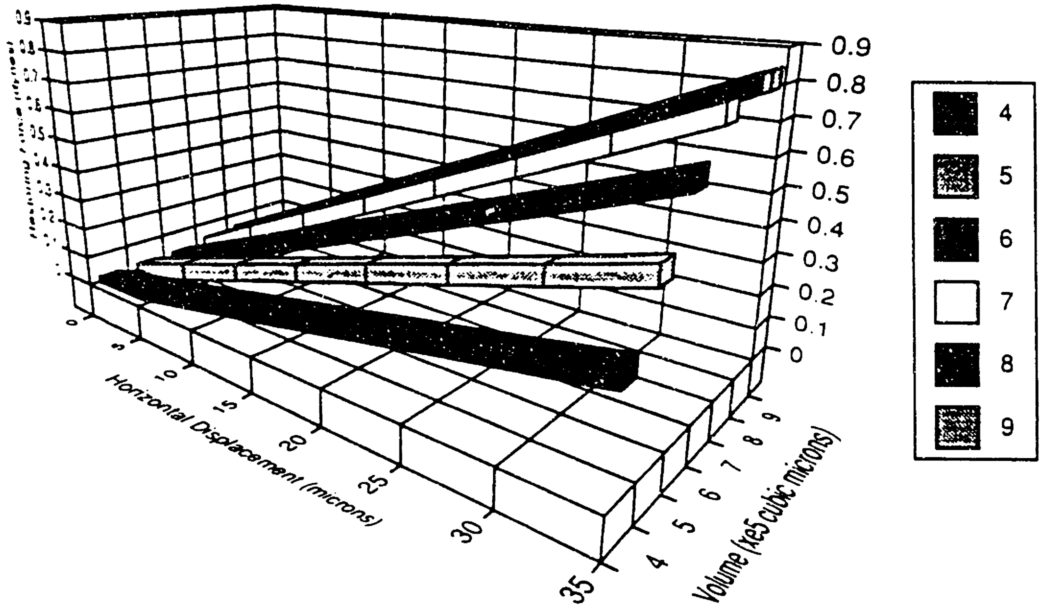

Fig. 4.55: Restoring Force as a function of Horizontal Displacement and Volume for a 60 micron radius circular pad with an 70 micron separation.

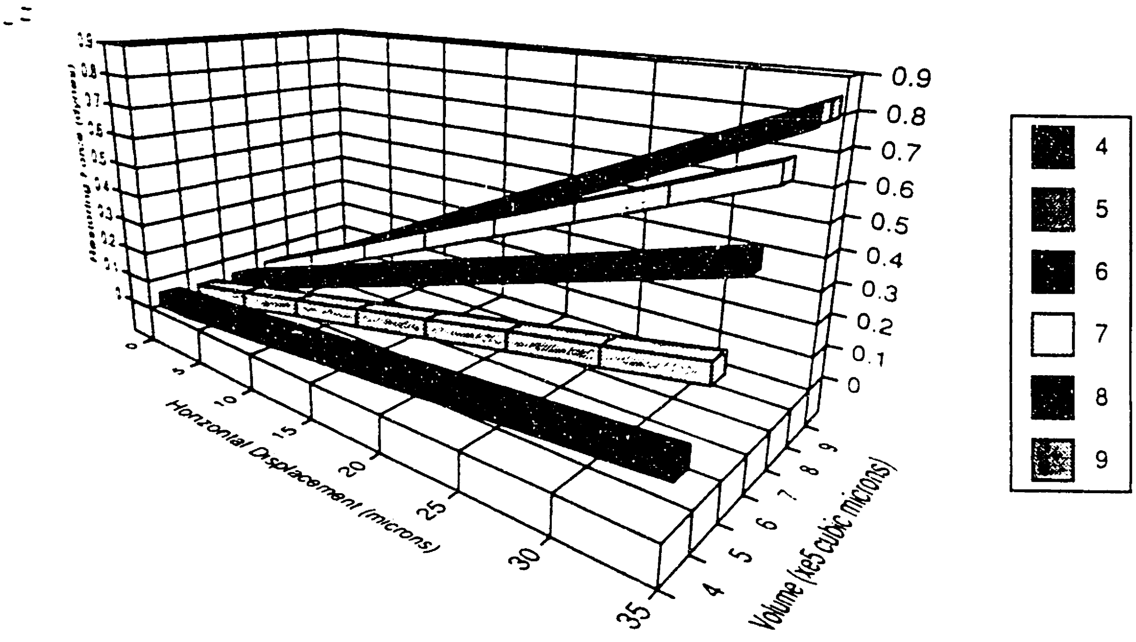

Fig. 4.56: Restoring Force as a function of Horizontal Displacement and Volume for a 60 micron radius circular pad with an 80 micron separation.

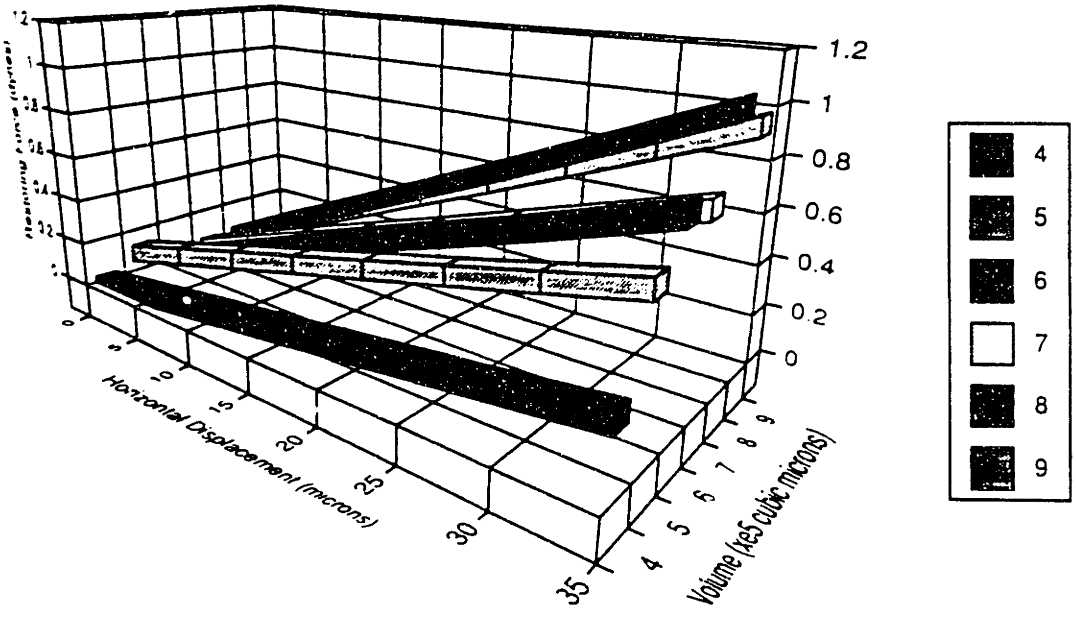

Fig. 4.57: Restoring Force as a function of Horizontal Displacement and Volume for a 65 micron radius circular pad with a 60 micron separation.

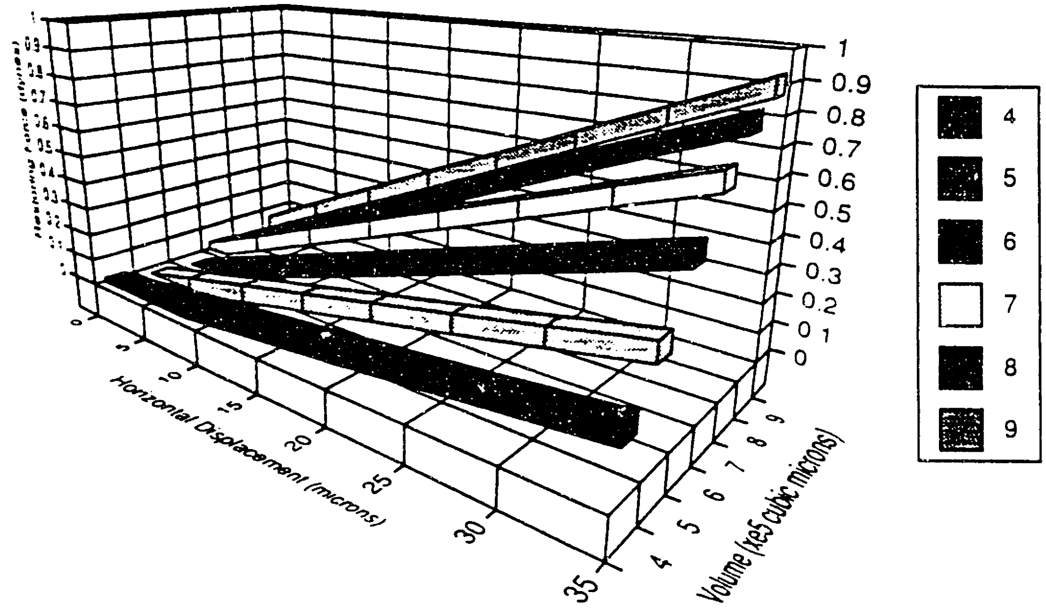

Fig. 4.58: Restoring Force as a function of Horizontal Displacement and Volume for a 65 micron radius circular pad with a 70 micron separation.

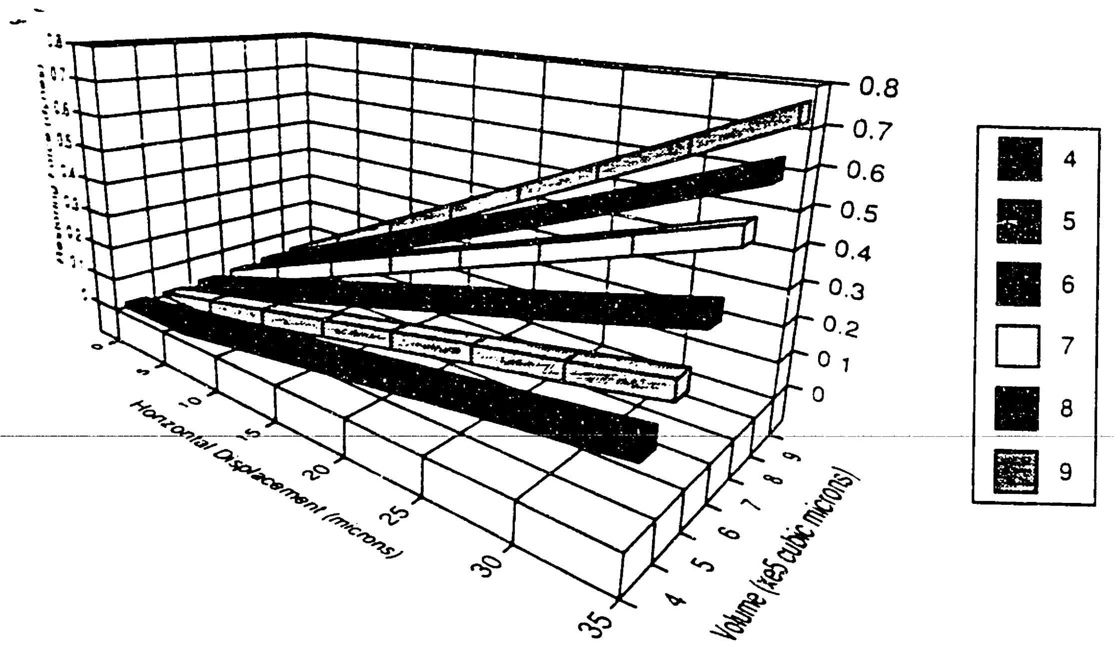

Fig. 4.59: Restoring Force as a function of Horizontal Displacement and Volume for a 65 micron radius circular pad with an 80 micron separation.

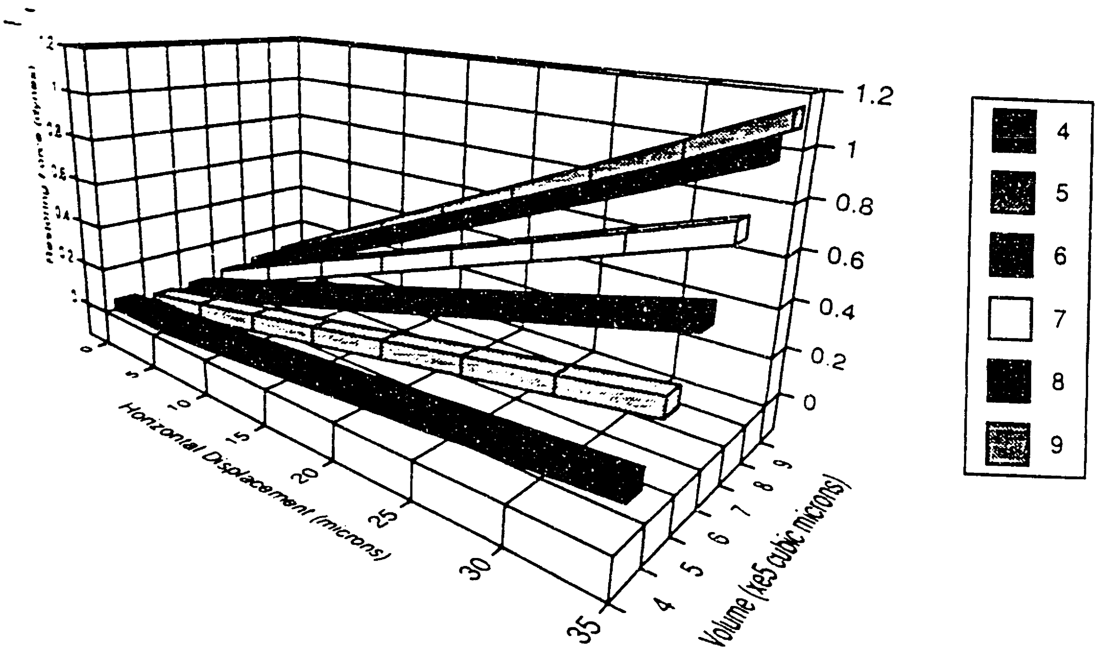

Fig. 4.60: Restoring Force as a function of Horizontal Displacement and Volume for a 70 micron radius circular pad with a 60 micron separation.

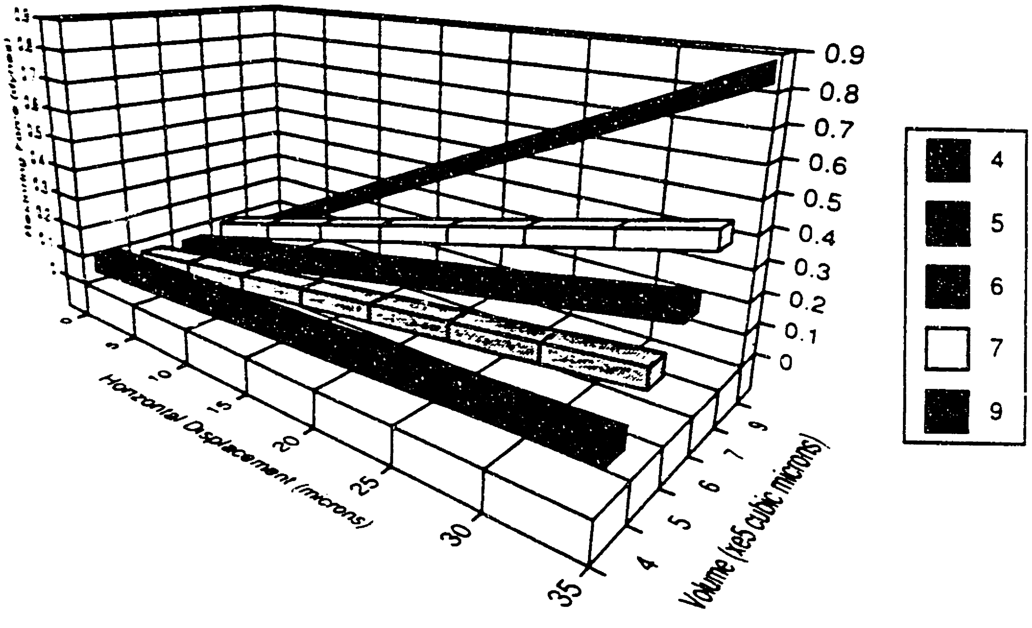

Fig. 4.61: Restoring Force as a function of Horizontal Displacement and Volume for a 70 micron radius circular pad with a 70 micron separation.

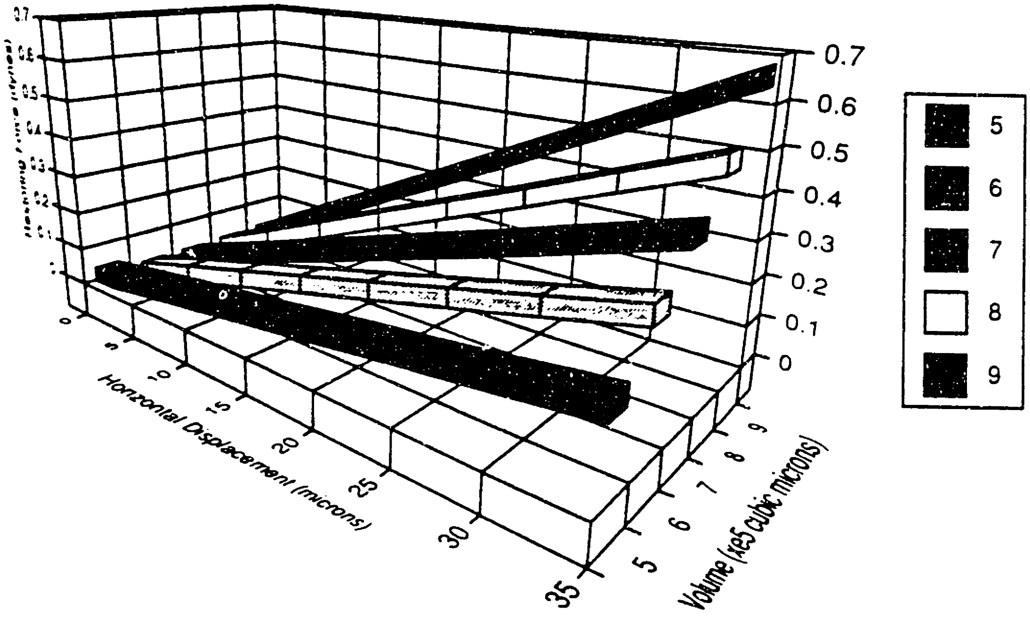

Fig. 4.62: Restoring Force as a function of Horizontal Displacement and Volume for a 70 micron radius circular pad with an 80 micron separation.

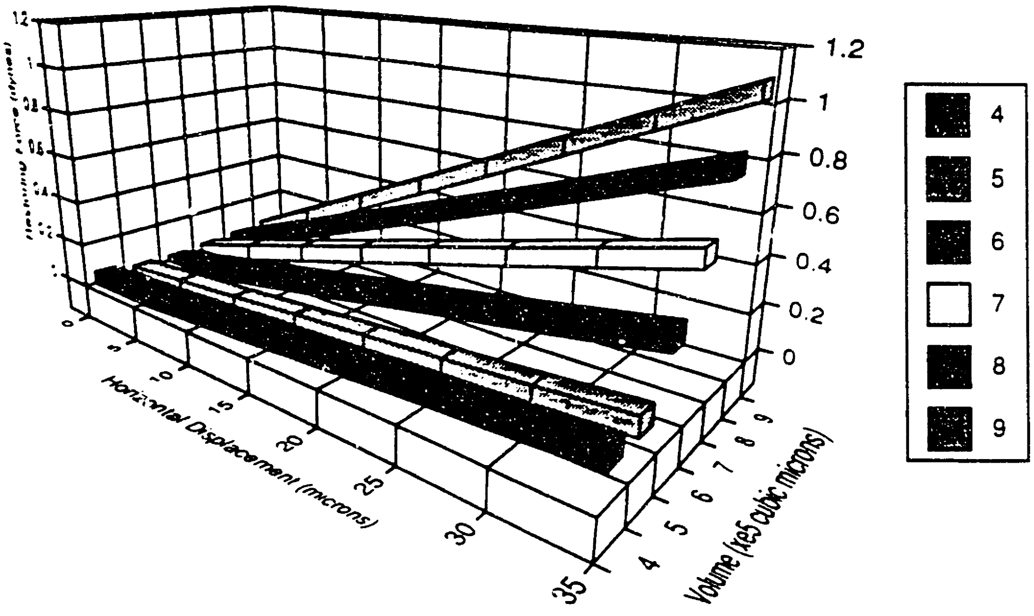

Fig. 4.63: Restoring Force as a function of Horizontal Displacement and Volume for a 75 micron radius circular pad with a 60 micron separation.

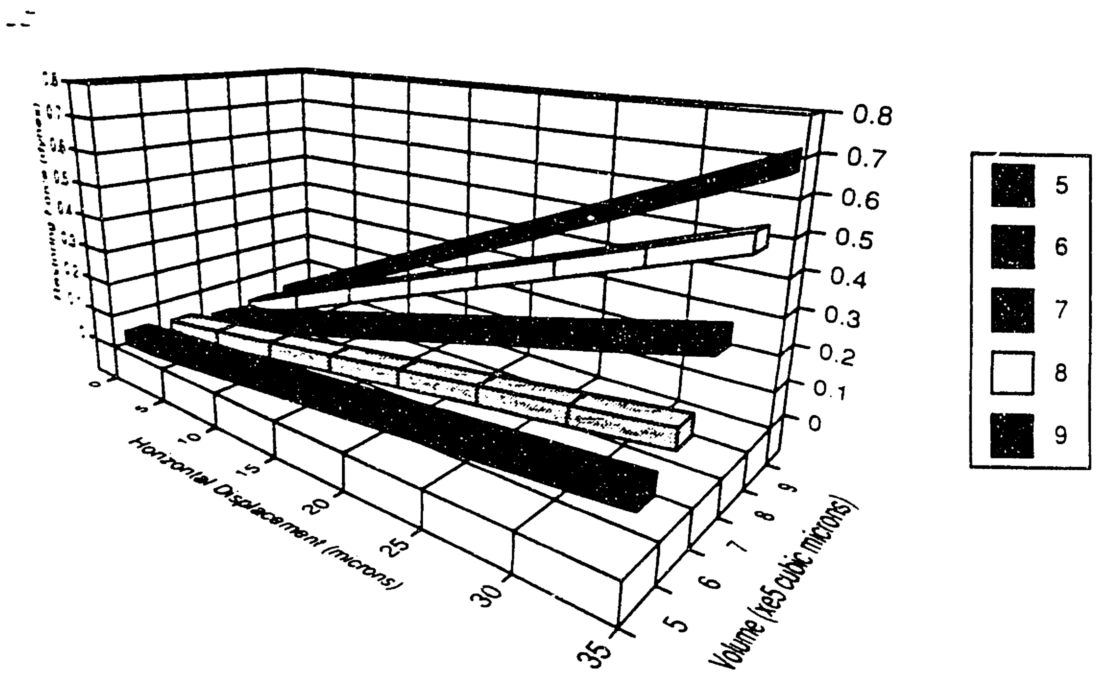

Fig. 4.64: Restoring Force as a function of Horizontal Displacement and Volume for a 75 micron radius circular pad with a 70 micron separation.

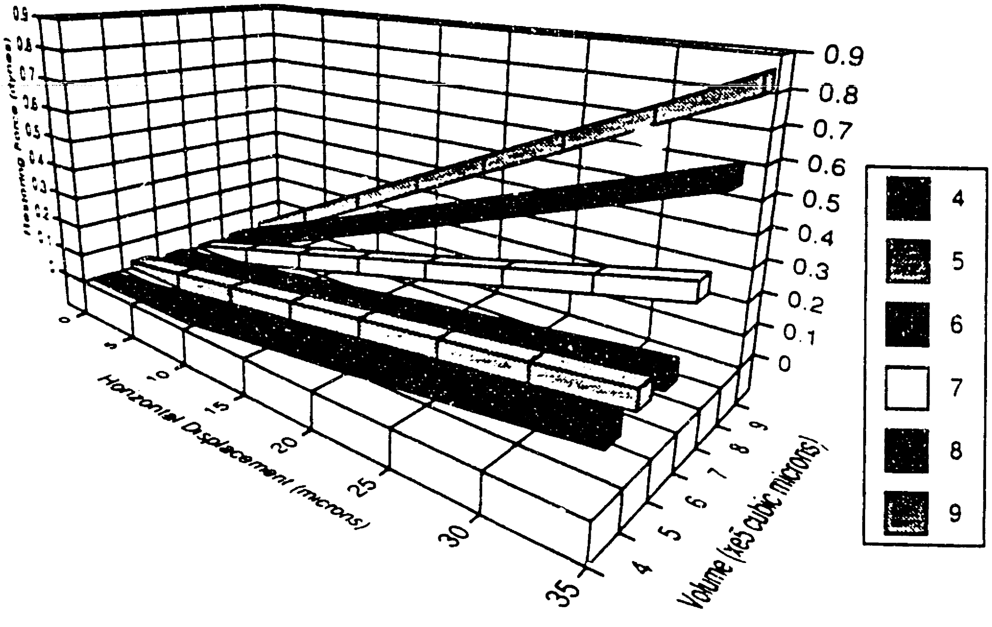

Fig. 4.65: Restoring Force as a function of Horizontal Displacement and Volume for an 80 micron radius circular pad with a 60 micron separation.

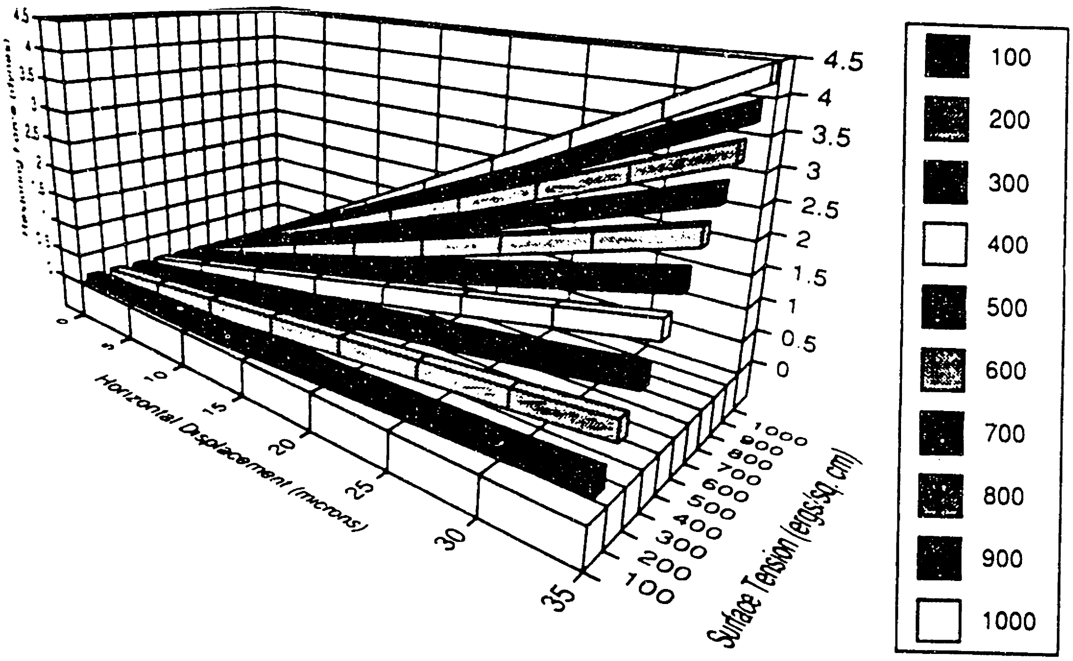

Fig. 4.66: Restoring Force as a function of Horizontal Displacement and Surface Tension for a 60 micron radius circular pad (60 micron separation, Volume = 4e5 cubic microns).

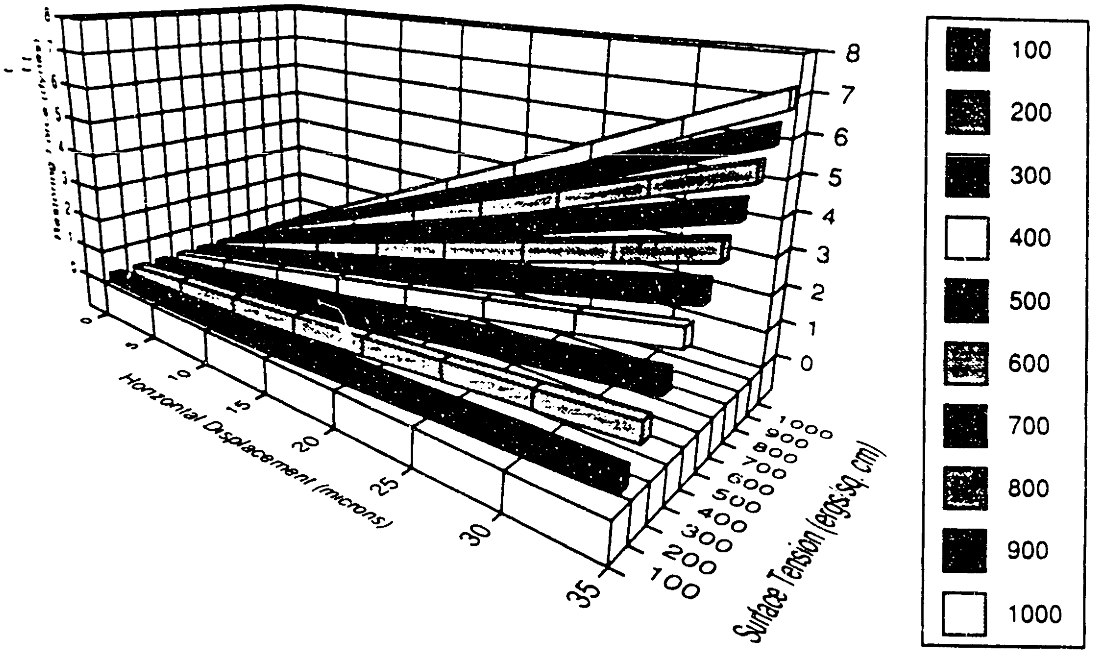

Fig. 4.67: Restoring Force as a function of Horizontal Displacement and Surface Tension for a 60 micron radius circular pad (60 micron separation, Volume = 5e5 cubic microns).

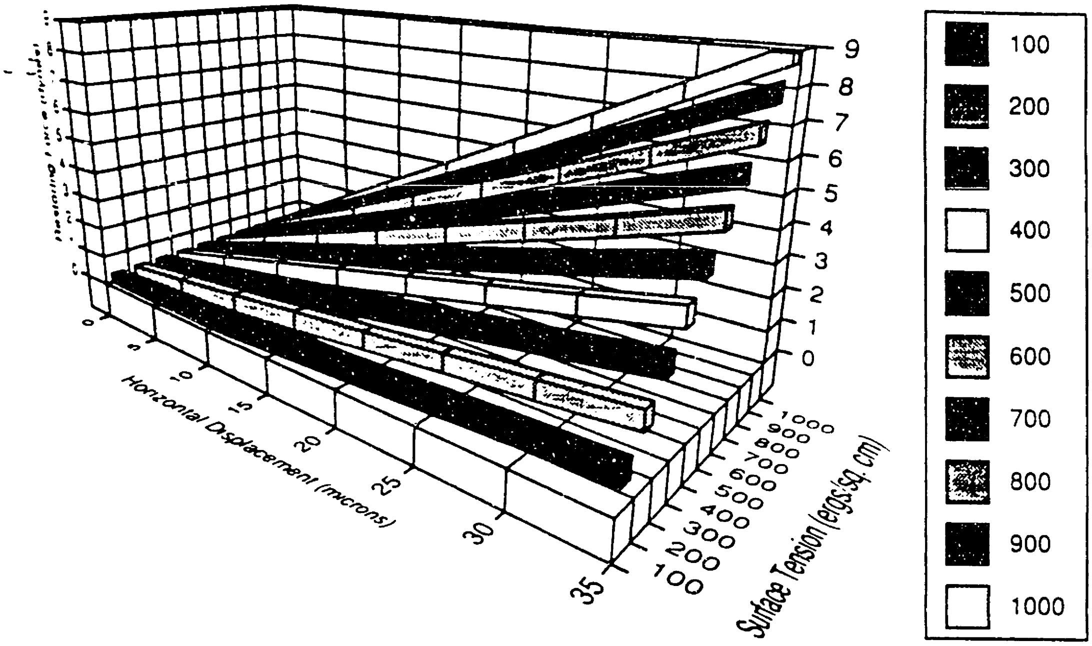

Fig. 4.68: Restoring Force as a function of Horizontal Displacement and Surface Tension for a 60 micron radius circular pad (60 micron separation, Volume = 6e5 cubic microns).

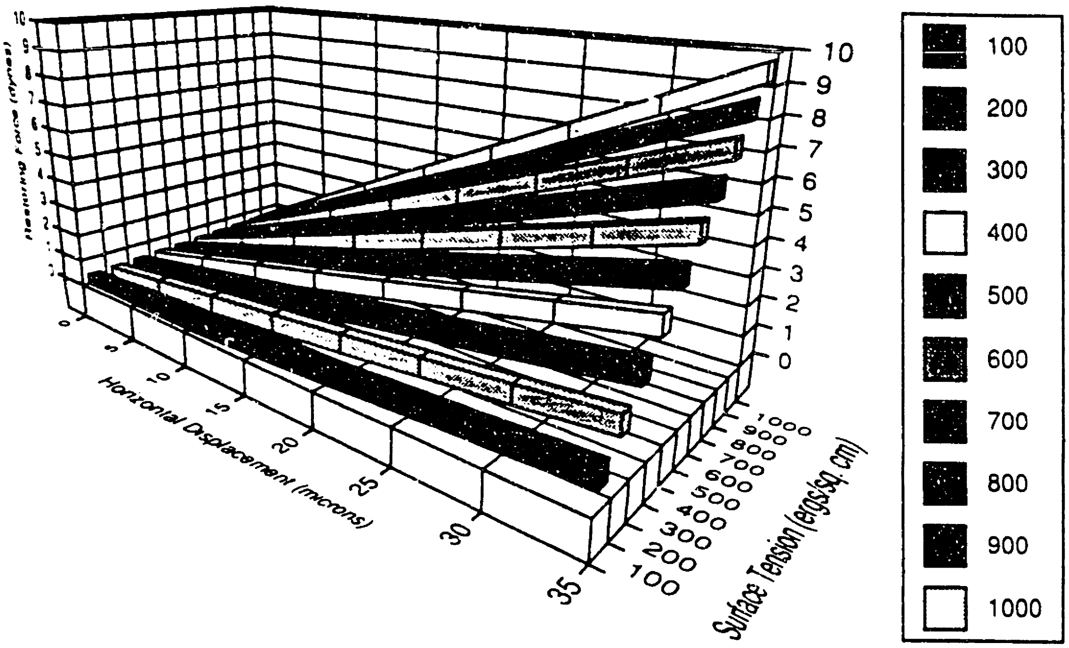

Fig. 4.69: Restoring Force as a function of Horizontal Displacement and Surface Tension for a 60 micron radius circular pad (60 micron separation, Volume = 7e5 cubic microns).

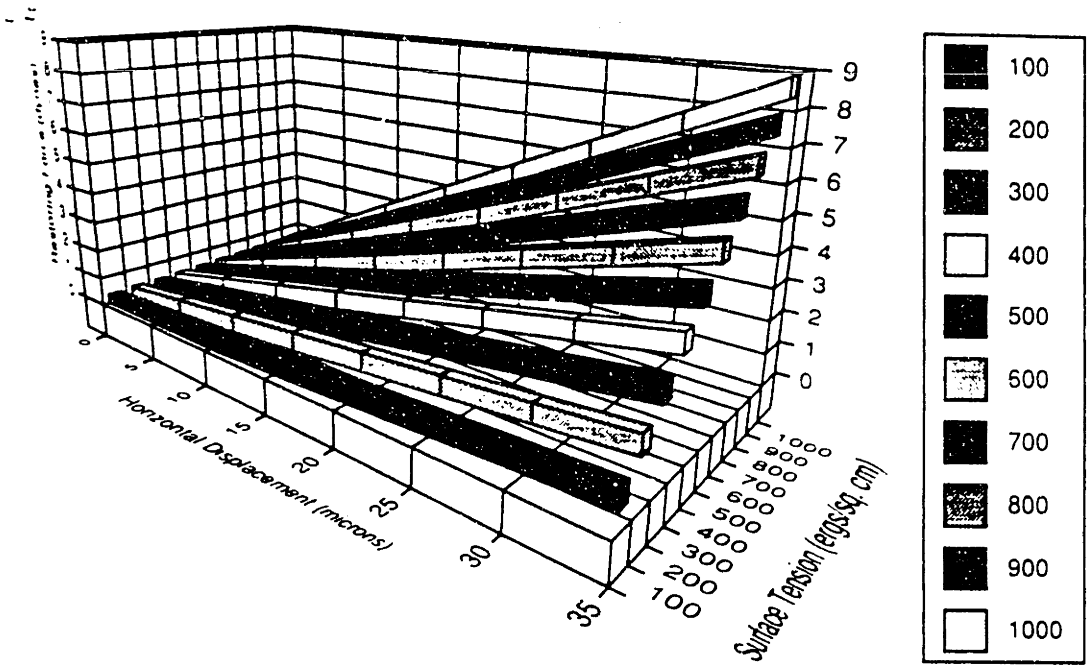

Fig. 4.70: Restoring Force as a function of Horizontal Displacement and Surface Tension for a 60 micron radius circular pad (60 micron separation, Volume = 8e5 cubic microns).

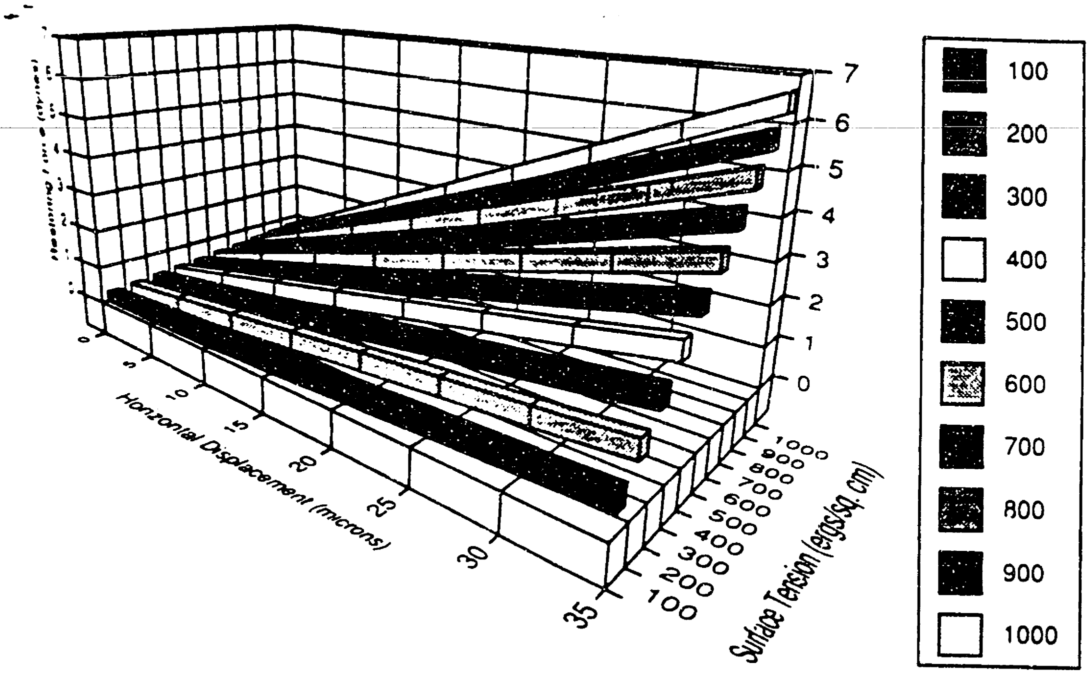

Fig. 4.71: Restoring Force as a function of Horizontal Displacement and Surface Tension for a 60 micron radius circular pad (60 micron separation, Volume = 9e5 cubic microns).

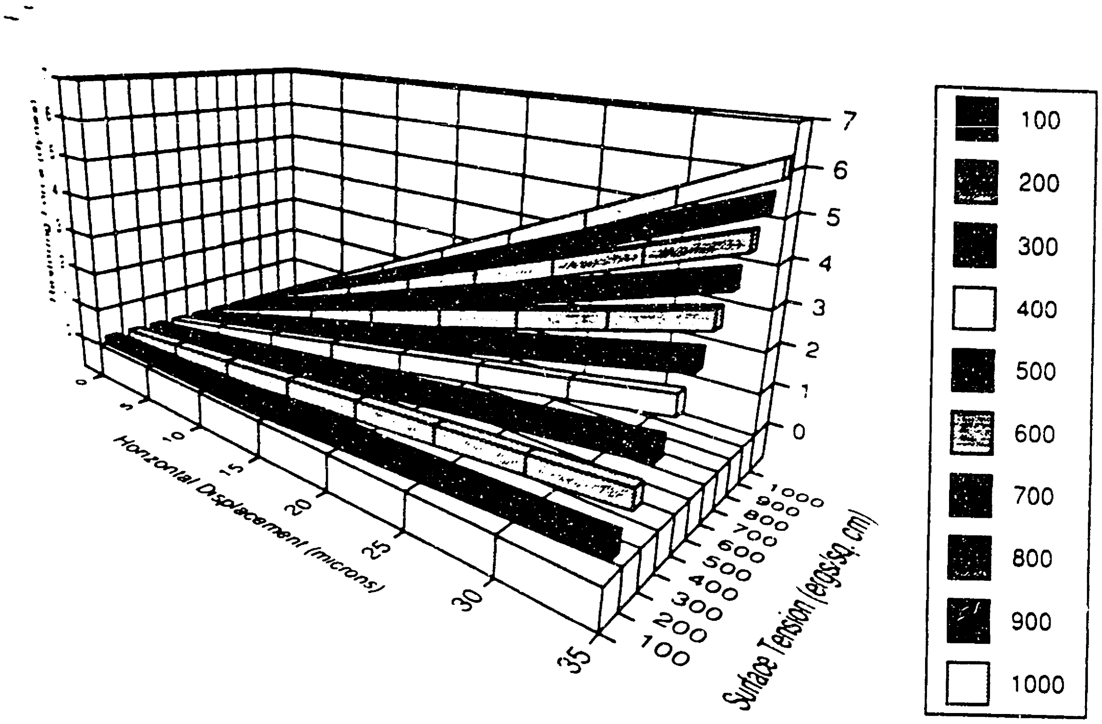

Fig. 4.72: Restoring Force as a function of Horizontal Displacement and Surface Tension for a 55 micron radius circular pad (60 micron separation, Volume = 4e5 cubic microns).

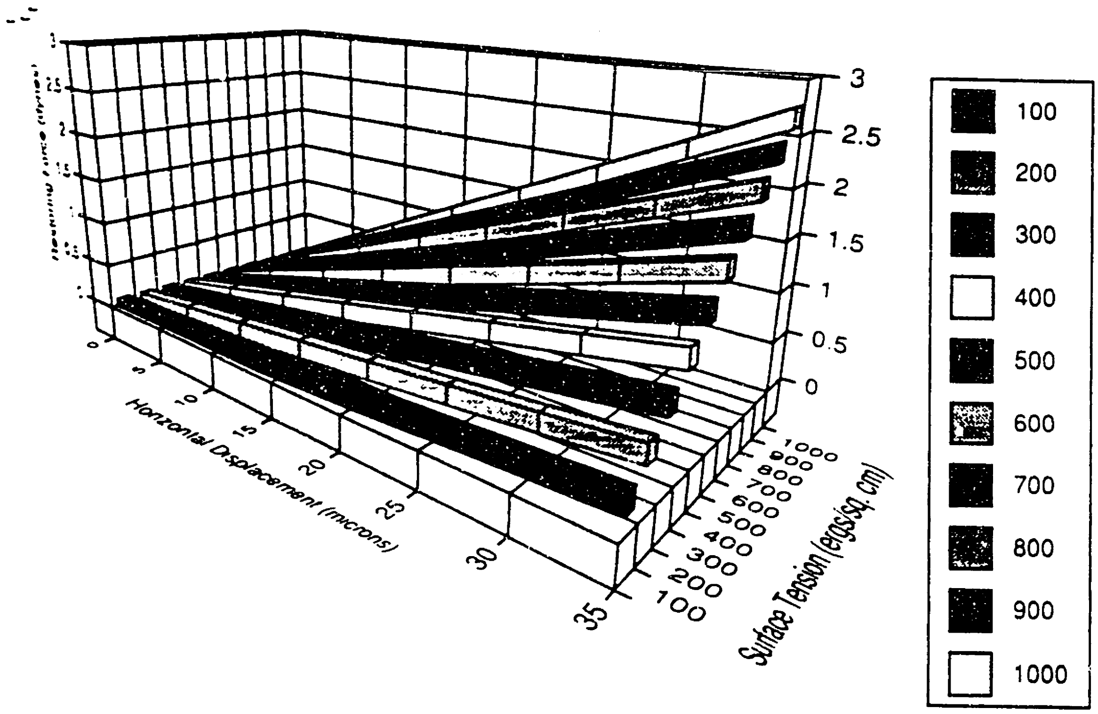

Fig. 4.73: Restoring Force as a function of Horizontal Displacement and Surface Tension for a 65 micron radius circular pad (60 micron separation, Volume = 4e5 cubic microns).

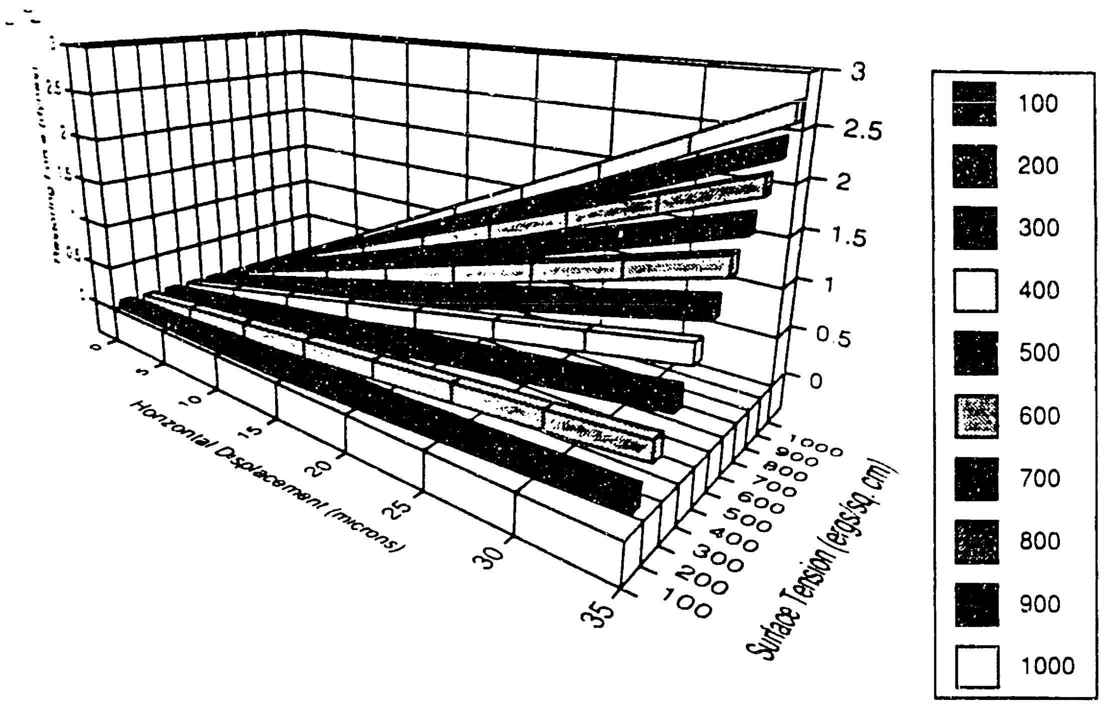

Fig. 4.73: Restoring Force as a function of Horizontal Displacement and Surface Tension for a 65 micron radius circular pad (60 micron separation, Volume = 4e5 cubic microns).

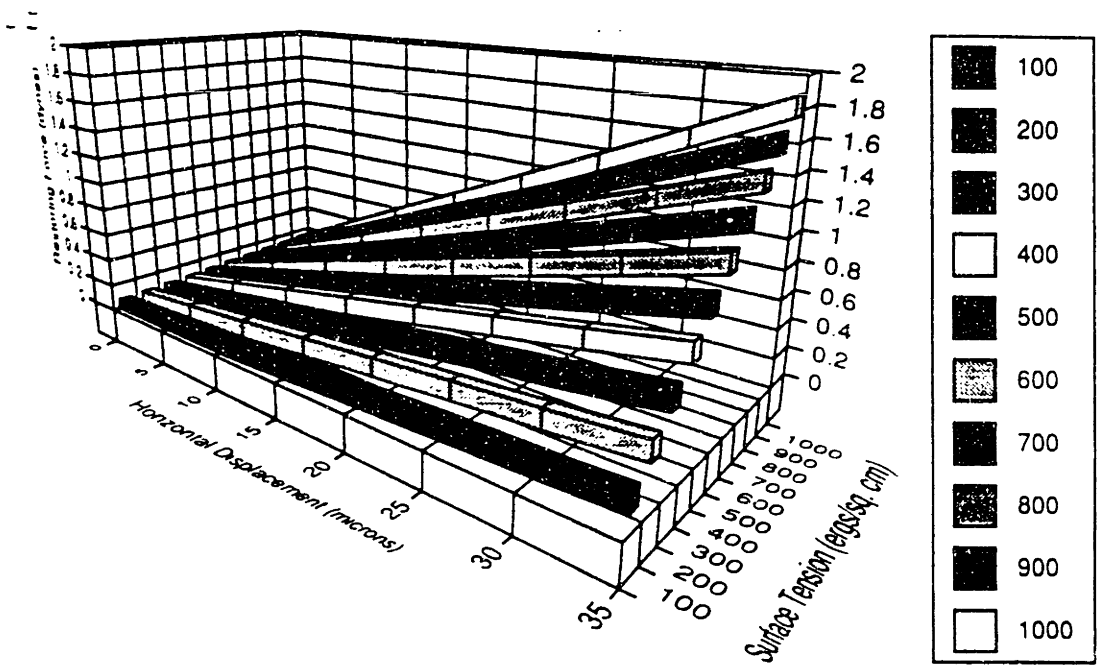

Fig. 4.74: Restoring Force as a function of Horizontal Displacement and Surface Tension for a 70 micron radius circular pad (60 micron separation, Volume = 4e5 cubic microns).

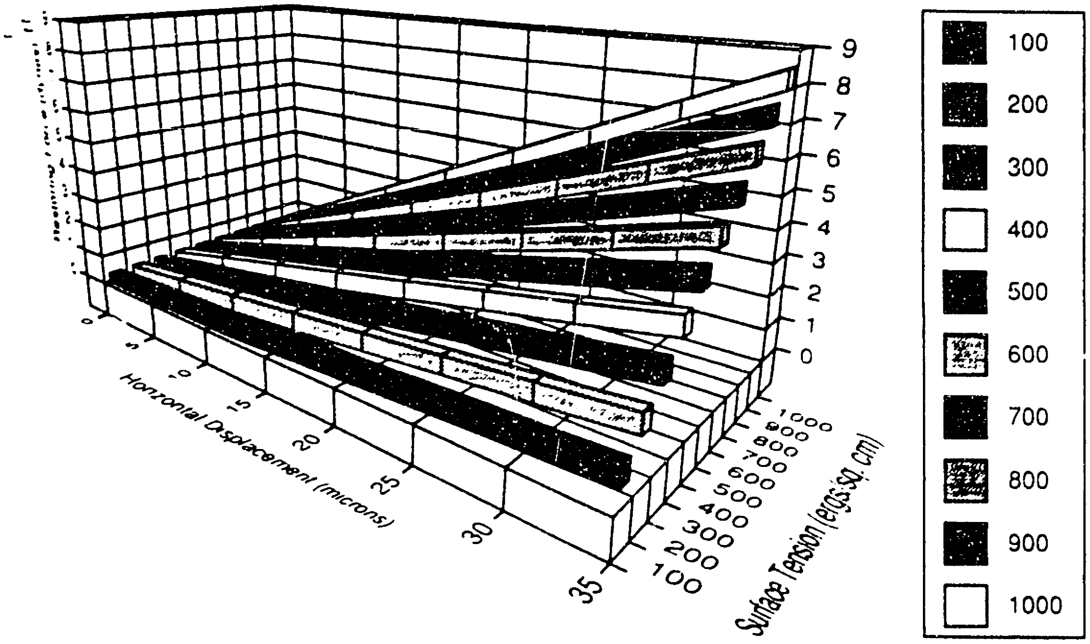

Fig. 4.75: Restoring Force as a function of Horizontal Displacement and Surface Tension for a 55 micron radius circular pad (60 micron separation, Volume = 5e5 cubic microns).

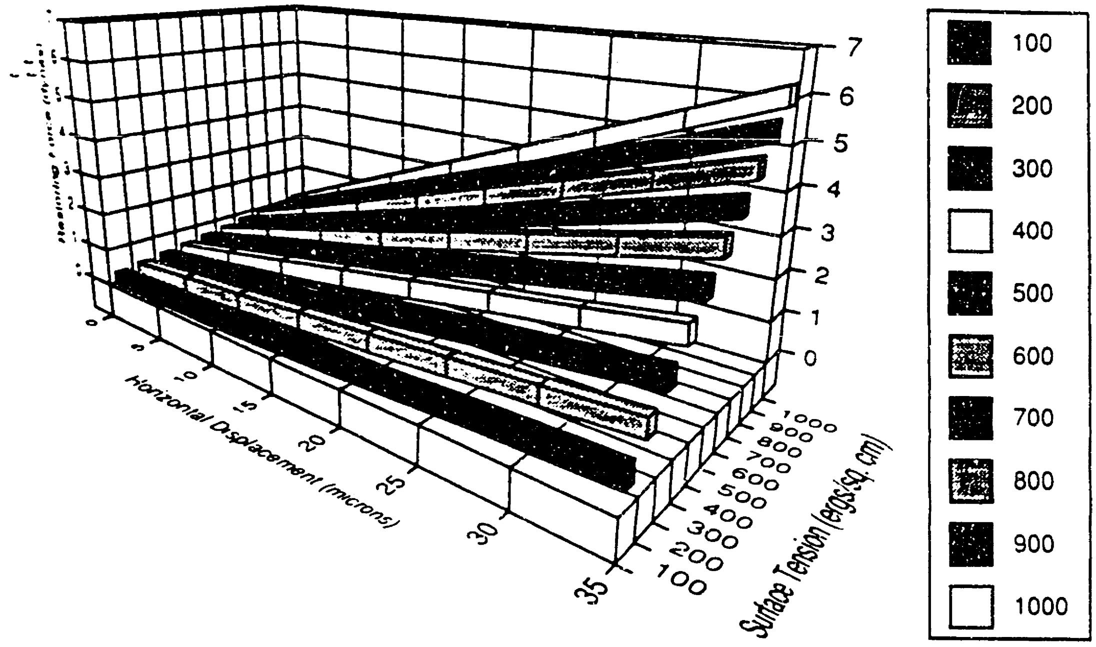

Fig. 4.76: Restoring Force as a function of Horizontal Displacement and Surface Tension for a 65 micron radius circular pad (60 micron separation, Volume = 5e5 cubic microns).

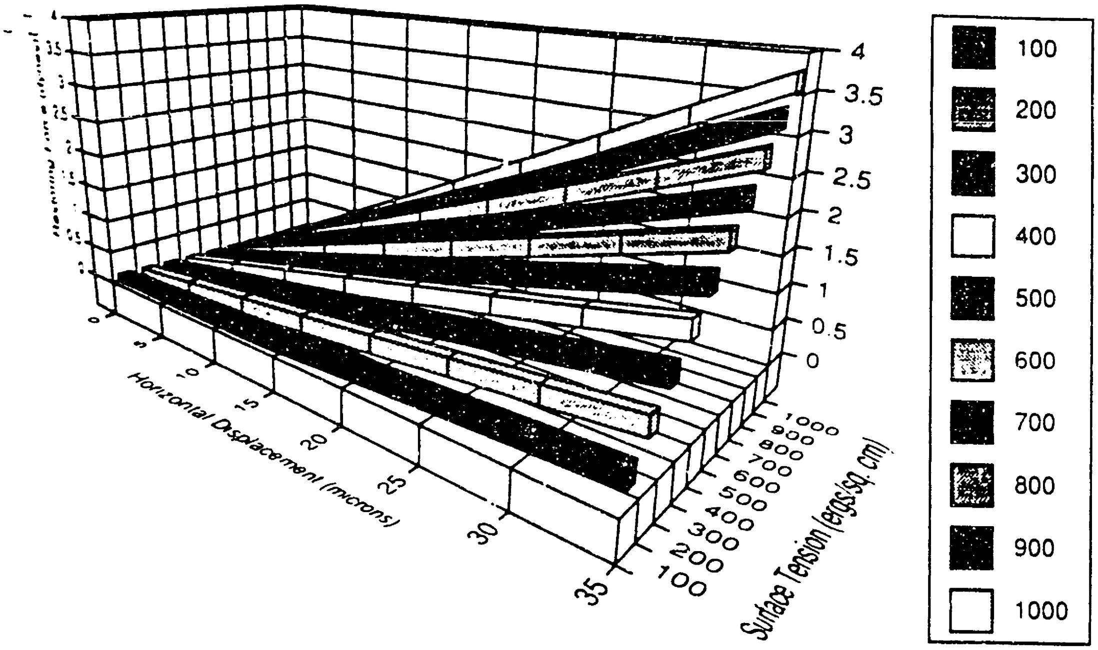

Fig. 4.77: Restoring Force as a function of Horizontal Displacement and Surface Tension for a 70 micron radius circular pad (60 micron separation, Volume = 5e5 cubic microns).

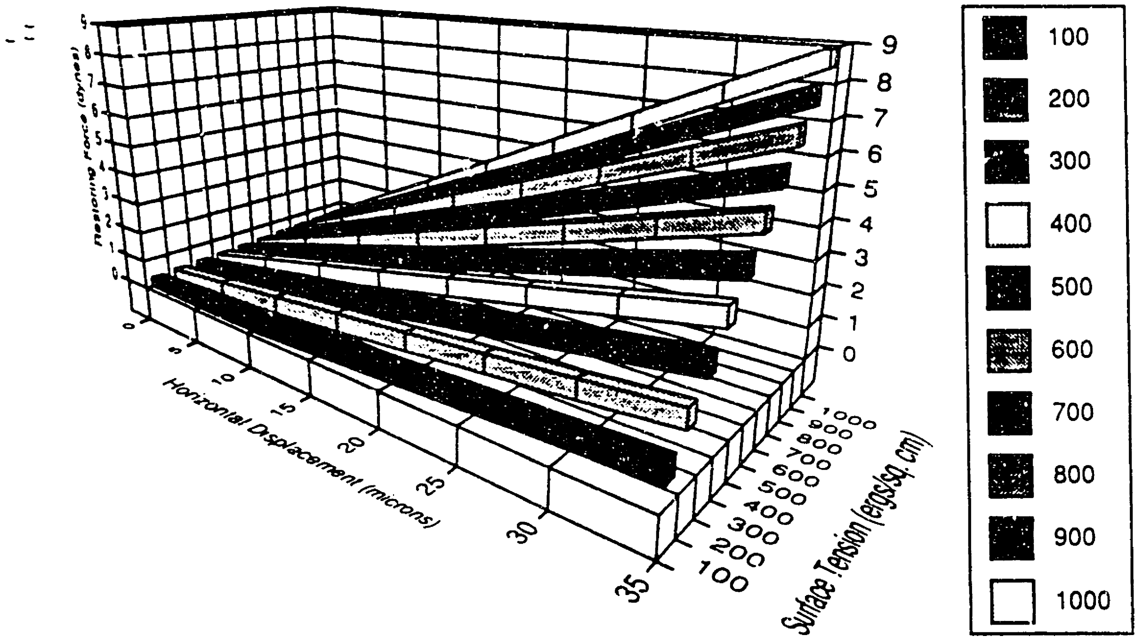

Fig. 4.78: Restoring Force as a function of Horizontal Displacement and Surface Tension for a 55 micron radius circular pad (60 micron separation, Volume = 6e5 cubic microns).

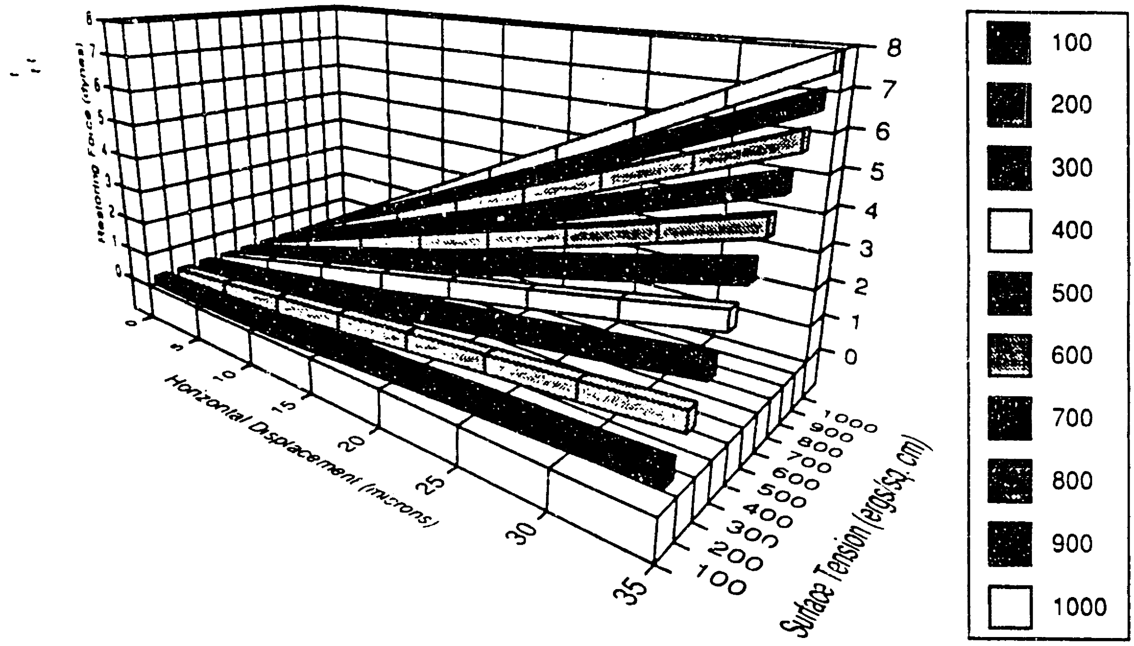

Fig. 4.79: Restoring Force as a function of Horizontal Displacement and Surface Tension for a 65 micron radius circular pad (60 micron separation, Volume = 6e5 cubic microns).

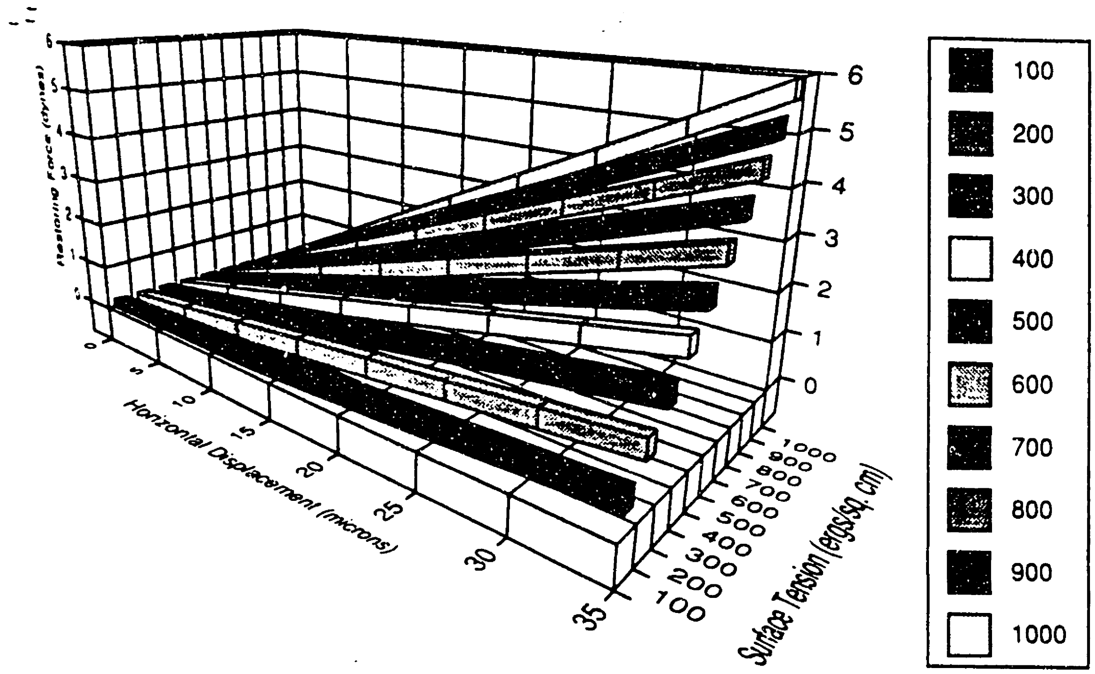

Fig. 4.80: Restoring Force as a function of Horizontal Displacement and Surface Tension for a 70 micron radius circular pad (60 micron separation, Volume = 6e5 cubic microns).

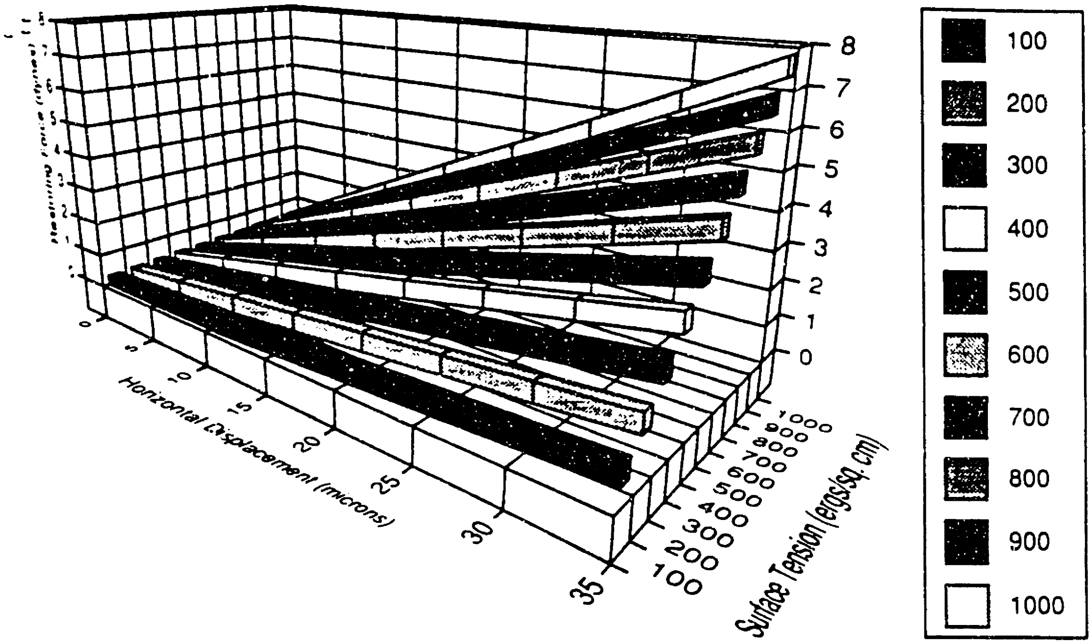

Fig. 4.81: Restoring Force as a function of Horizontal Displacement and Surface Tension for a 55 micron radius circular pad (60 micron separation, Volume = 7e5 cubic microns).

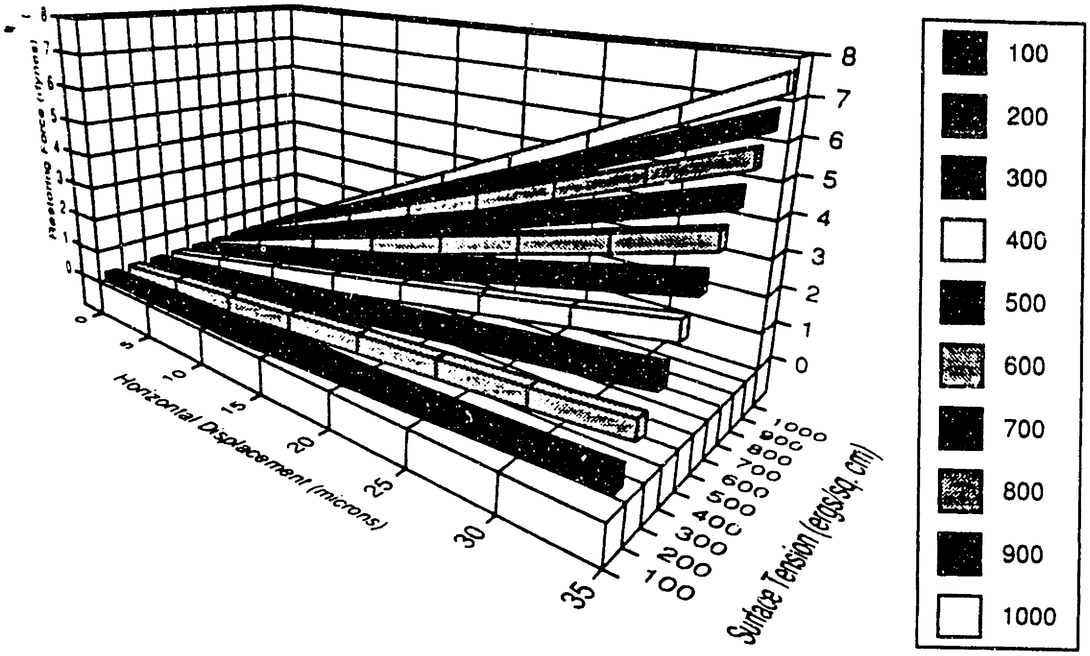

Fig. 4.82: Restoring Force as a function of Horizontal Displacement and Surface Tension for a 65 micron radius circular pad (60 micron separation, Volume = 7e5 cubic microns).

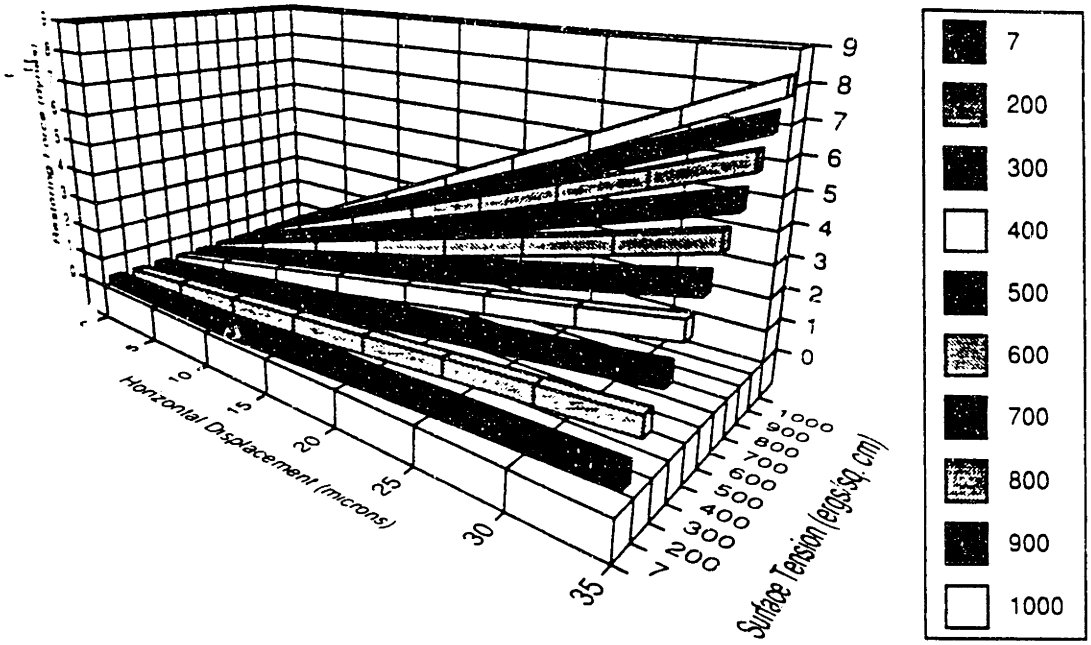

Fig. 4.83: Restoring Force as a function of Horizontal Displacement and Surface Tension for a 70 micron radius circular pad (60 micron separation, Volume = 7e5 cubic microns).

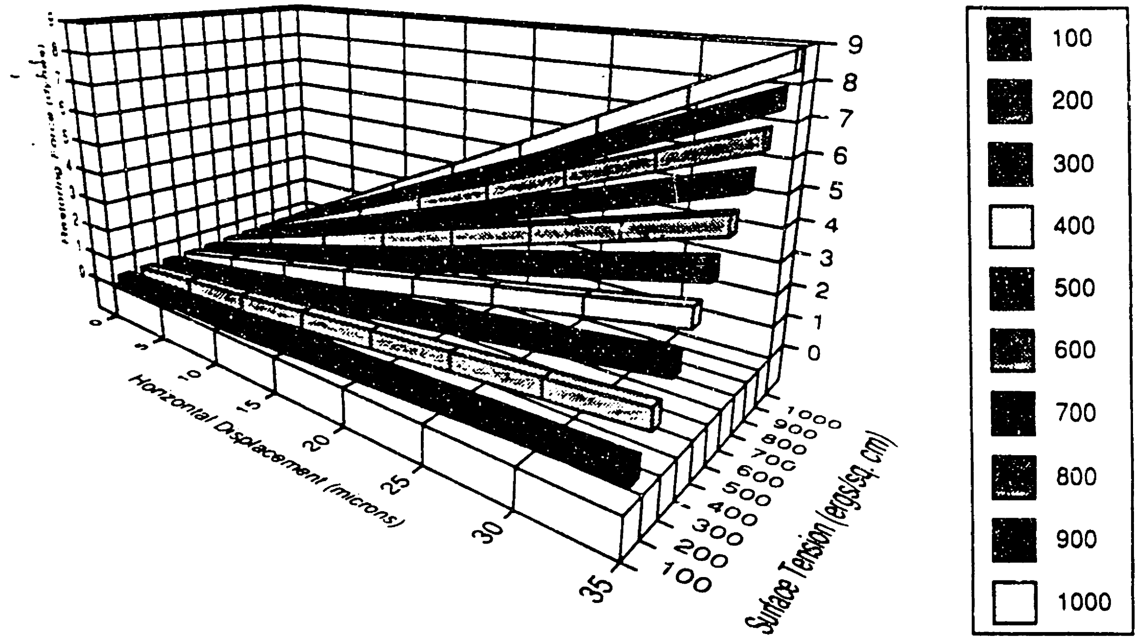

Fig. 4.84: Restoring Force as a function of Horizontal Displacement and Surface Tension for a 60 micron radius circular pad (60 micron separation, Volume = 8e5 cubic microns).

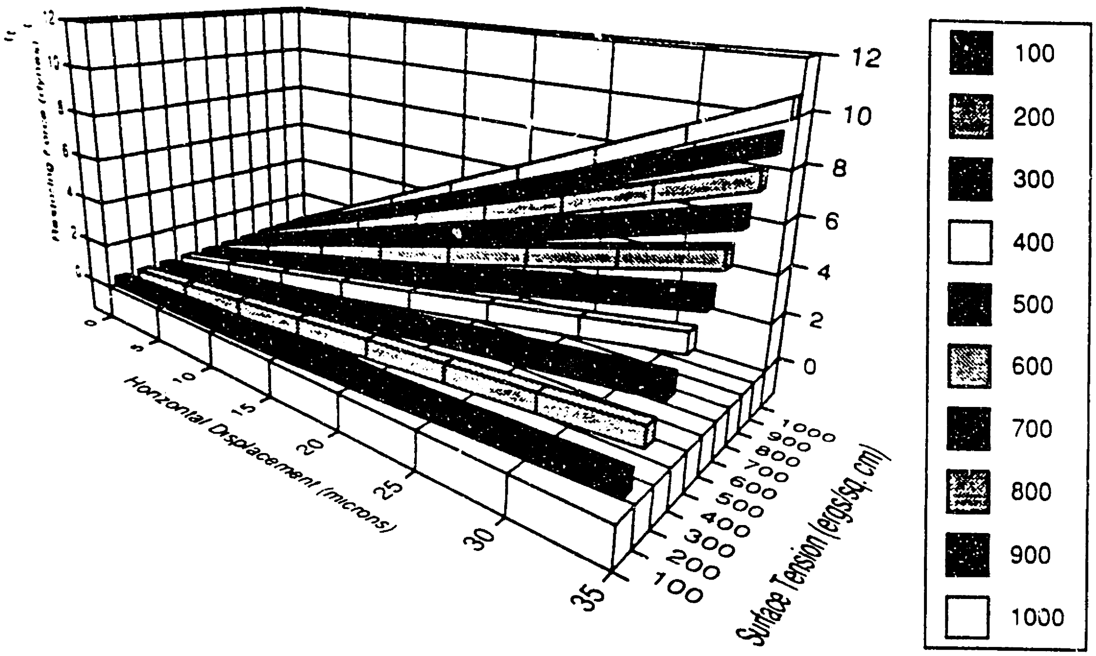

Fig. 4.85: Restoring Force as a function of Horizontal Displacement and Surface Tension for a 65 micron radius circular pad (60 micron separation, Volume = 8e5 cubic microns).

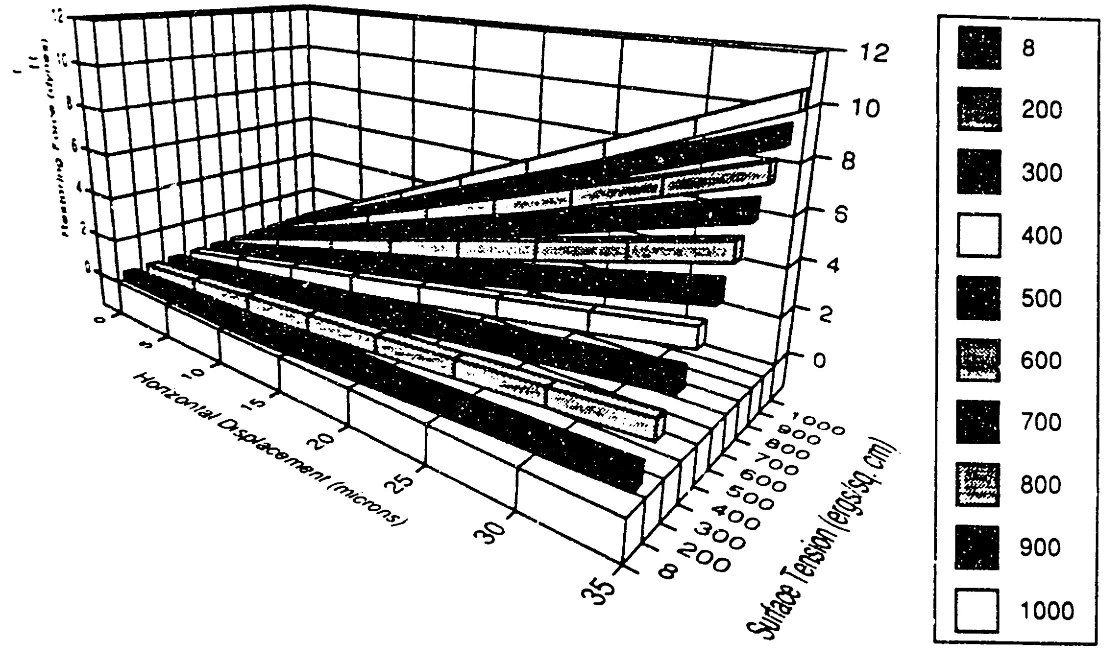

Fig. 4.86: Restoring Force as a function of Horizontal Displacement and Surface Tension for a 70 micron radius circular pad (60 micron separation, Volume = 8e5 cubic microns).

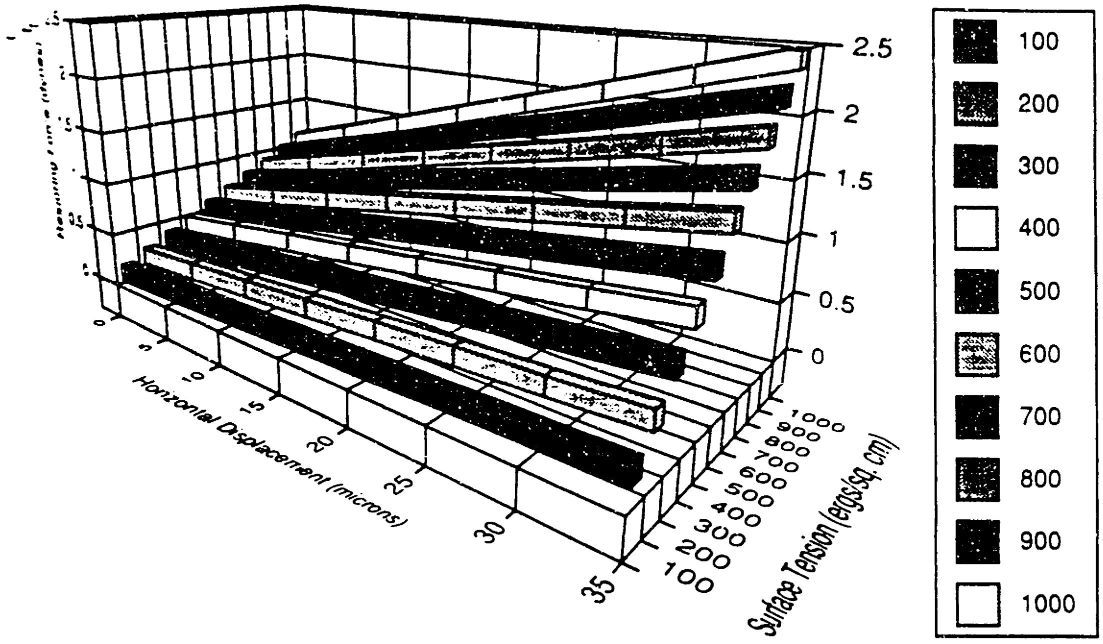

Fig. 4.87: Restoring Force as a function of Horizontal Displacement and Surface Tension for a 55 micron radius circular pad (60 micron separation, Volume = 9e5 cubic microns).

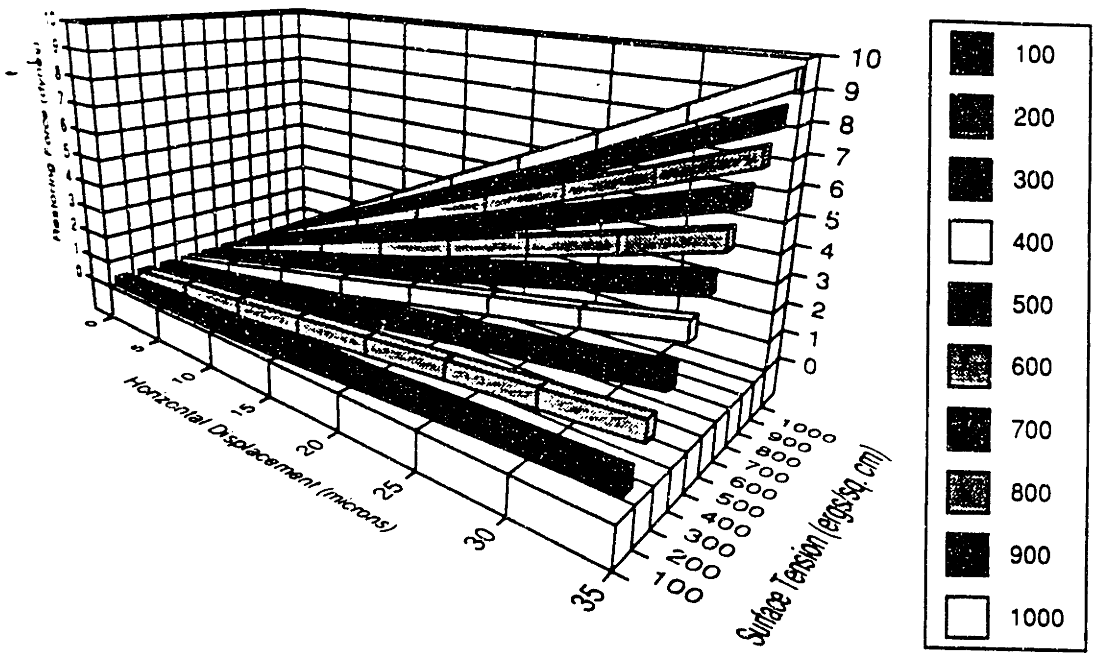

Fig. 4.88: Restoring Force as a function of Horizontal Displacement and Surface Tension for a 65 micron radius circular pad (60 micron separation, Volume = 9e5 cubic microns).

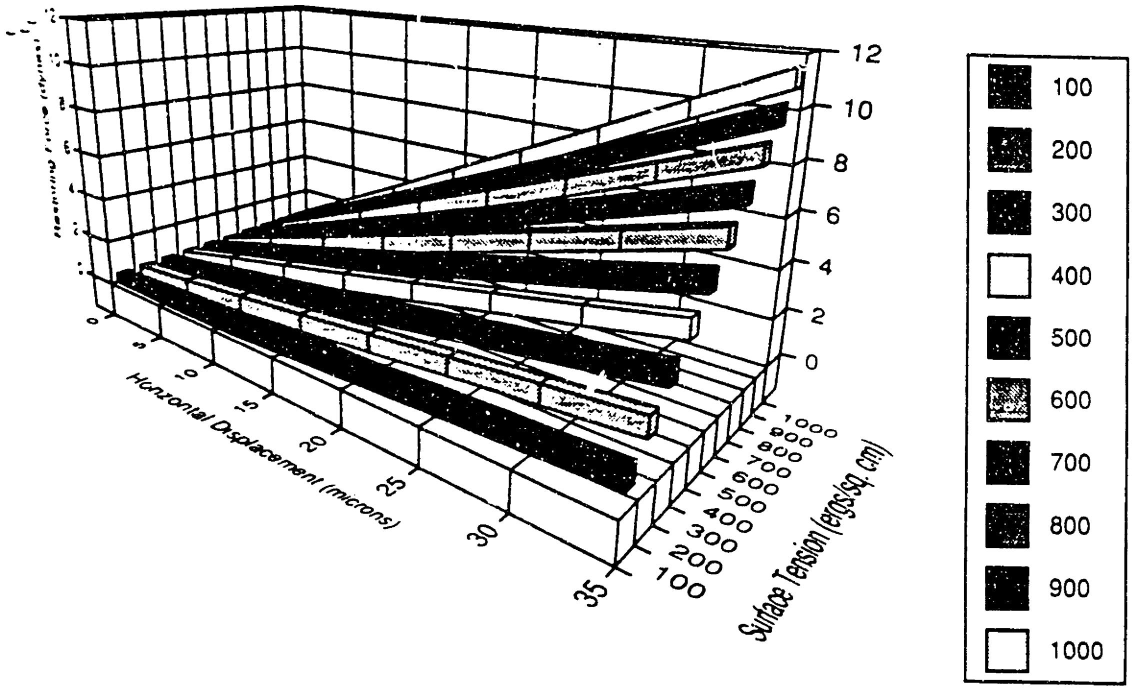

Fig. 4.89: Restoring Force as a function of Horizontal Displacement and Surface Tension for a 70 micron radius circular pad (60 micron separation, Volume = 9e5 cubic microns).

Fig. 4.90 Surface Morphology of a solder joint with a 60 micron vertical height, radius of 55 microns, and solder volume of 6 e^5 cubic microns (0 micron displacement)

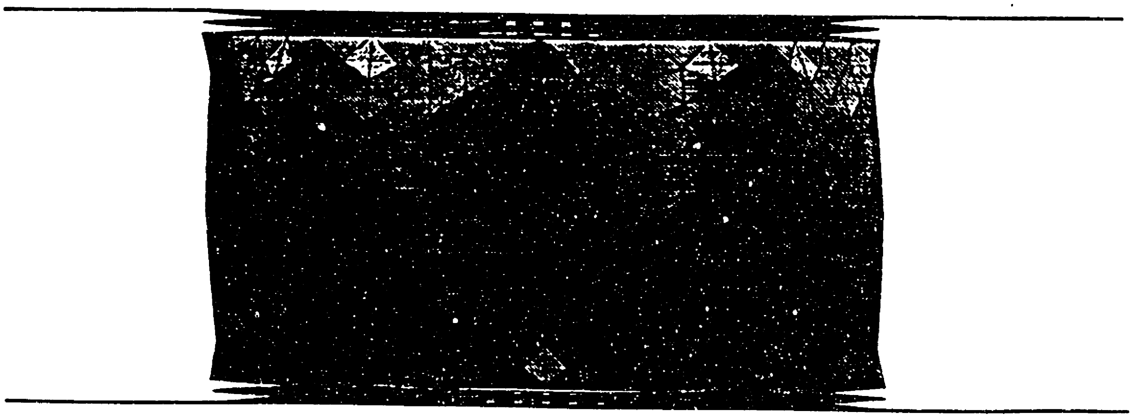

Fig. 4.91 Surface Morphology of a solder joint with a 60 micron vertical height, radius of 55 microns, and solder volume of 6 e^5 cubic microns (35 micron displacement)

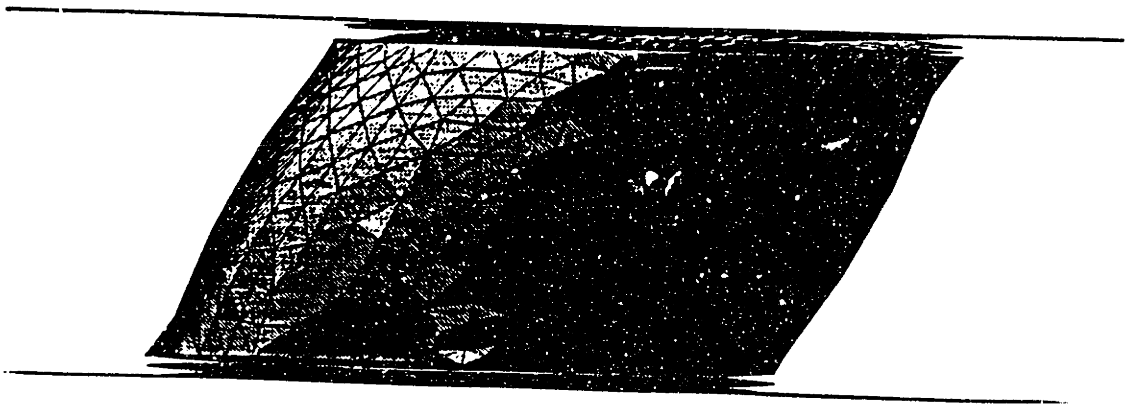

Fig. 4.92 Surface Morphology of a solder joint with a 60 micron vertical height, radius of 70 microns, and solder volume of 9 e^5 cubic microns (0 micron displacement)

Fig. 4.93 Surface Morphology of a solder joint with a 60 micron vertical height, radius of 70 microns, and solder volume of 9 e^5 cubic microns (35 micron displacement)

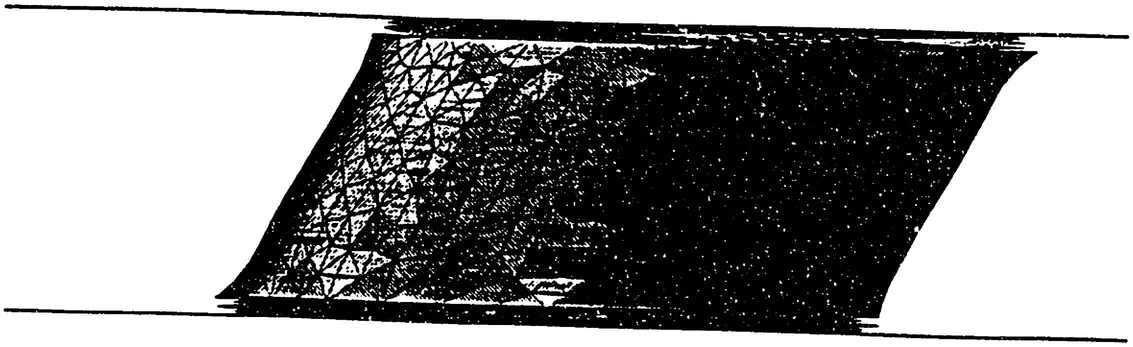

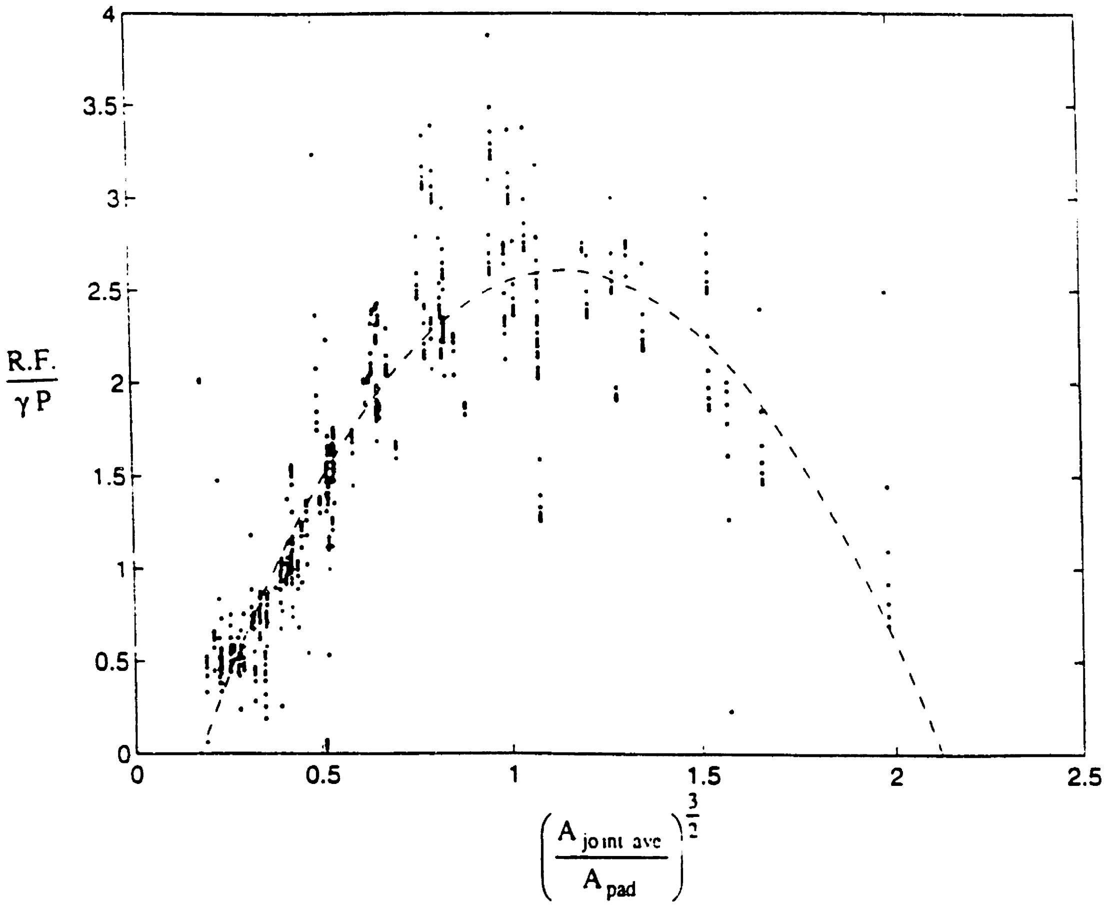

Fig. 4.94 Dimensionless Number plot of all process parameters and model data.

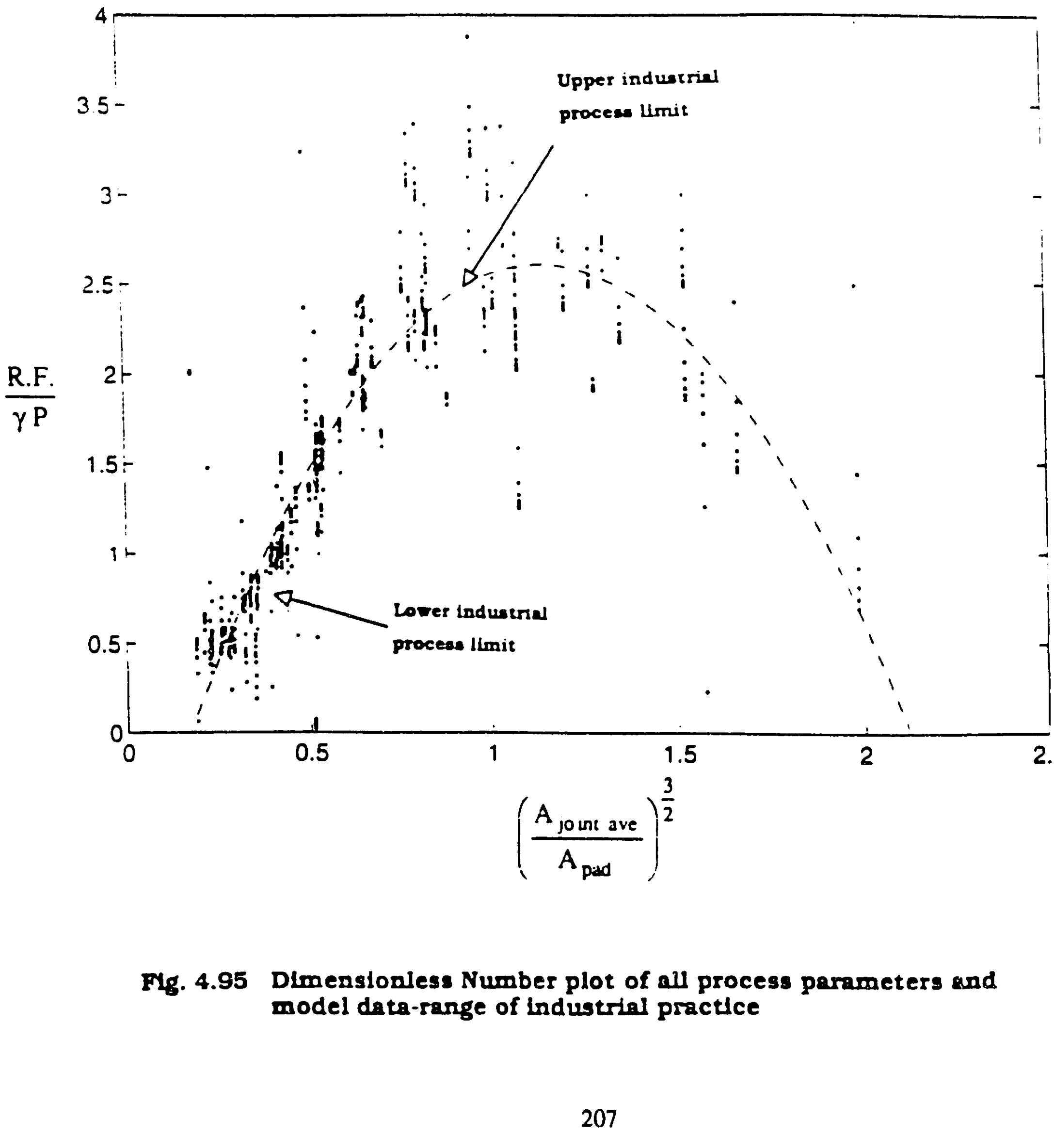

Fig. 4.95 Dimensionless Number plot of all process parameters and model data-range of industrial practice

CHAPTER 5

ALTERNATIVE PAD GEOMETRY MODELS

5.1 Introduction

Current use of flip-chip solder bumping has focused on the use of circular pads to provide the alignment forces needed in opto-electronics. As discussed in earlier chapters, there has been little research into a broad range of factors that have an impact on the level of positioning forces needed to position chips. With the growing needs of opto-electronics applications for low cost positioning methods, there is subsequently a need for information to optimize this process for a variety of chip sizes and alignment tolerances. In order to fully study all of the influences on restoring forces, the effects of different pad geometries need to considered. The four main types of pads modeled is shown in (Fig. 5.1). The use of pad shapes with long arms and sharp edges is of special use. They aid in reducing the cost of flip-chip driven alignment, particularly in the initial tacking stage where assembly is based on the use of visual matching systems. These types of pad geometries are being considered as an alternative to circular pads due to their lower alignment tolerances in the initial tacking stage. A number of studies have been performed which show that as long as solder joints are initially in contact after the rough tack, they will align [1]. The wetting action of the solder will align the chip as long as part of each bump and pad is wetted and in contact. This is useful in terms of the ease of initial registration, which results in lower placement tolerances and less expensive placement equipment [2]. For pad geometries with long arms and edges, it is relatively easier and faster to align chips, than for the standard circular case (fig. 5.2).

While this is an area of great potential for increasing alignment capability, there has been little quantitative research studying the influence of pad shape. There have been a number of qualitative studies on different aspects of solder joint shape and ease of placement [1], but no quantitative measures of the restoring forces generated has been done. In terms of studies of circular pad geometries, Goldmann [4] performed one of the first two-dimensional studies of solder joint shape for C-4 applications followed by the work of Patra [4], McGroarty [5], Yost [6] and who focused on standard solder shapes in flip-chip processes. While these studies focused on relating solder shape to reflow solder joint parameters, they addressed only two-dimensional formulations and standard circular pads. The influence of different types of shape factors have not be studied previously. By explicitly calculating the restoring forces generated by these joint types, we could examine the effect of system geometry and specifically examine the role played by the pad shape in affecting alignment.

Calculation of the surface area and surface energies for these types of joint systems, in particular a fully three dimensional solution, is very difficult and has never been attempted due to the complexity of the individual energy equations and surfaces. Developing solutions for non-classical systems of this type requires numerical methods that can handle increasingly complex surfaces and detailed solid-liquid wetting interactions to solve them. In order to study the influence of pad geometry shape on alignment forces, a series of models were developed using a rigorous mathematical code with different pad geometries which used sharp edges, long arms and 90 degree corners. These models were designed to cover a number of joint geometries. They were also studied for a series of horizontal displacements. Surface energy gradients were determined as a function of process parameters and the restoring forces were then calculated.

The mathematical modeling effort that we used to study self-alignment behavior for these alternative pad geometries addressed the following issues:

1) calculation of the horizontal restoring forces generated in self-alignment for alternative geometries from first principles.

2) calculation of the free surface shapes developed for alternative pad geometries during reflow when an external displacement is applied.

3) calculation of the influence of alternative pad geometries on restoring forces relative to the standard pad shape.

4) calculation of the dependency of restoring forces on joint parameters including pad radius, solder height, solder volume, and surface tension.

5.2 Theory

Calculations of the horizontal and vertical restoring forces generated by the alternative pad shapes were performed in a similar manner to the studies in Chapter 4 for circular pads. Using the Surface Evolver to calculate the surface energy and area of each pad type, the gradient of surface energy as a function of displacement was then calculated. Using this data and the equations in Chapter 3 restoring forces could be related to displacements as a function of solder volume, surface energy, and other joint parameters.

5.3 Mathematical Modeling

5.3.1 Constraints

The standard set of constraints used for each of these models were similar to the set used for the circular pad cases in Chapter 4. Volumes were constrained to values between $4e^5$ microns^3 and $1.28e^6$

microns^3 to cover a wide range of values used in industry. Surface constraints were imposed to insure that the solder remained confined between the metallization pads without penetration and without movement. Solder density was set at 9 g/cm^3, to be applied to the volume during surface evolution. In addition, edge constraints were used to insure that the solder wetted the metallization pads for each series of vertical and horizontal displacements.

5.3.2 Model Parameters

The initial surface of the alternative and standard solder joints examined including relevant dimensions, materials properties and constraints were obtained through a collaborative effort with AT&T Bell Laboratories similar to the one described in Chapter 4. The information gained there was used to form a series of datafiles to study the minimal surfaces developed for four individual alternative joint parameters and for combinations of joint parameters. Constraints on solder density, volume and liquid-vapor interfacial energy were defined as RHO, VOLUME, GAMMLV, using the traditional evolver syntax. Motion constraints were defined to limit the solder to the edges and corners of the metallization pad, as per our assumptions, using a FIXED vertices constraint for vertices as the pad edges.

Units in all the datafiles were defined in the cgs system for convenience and kept consistent throughout the datafile through the use of a constant conversion factor for ease of surface definition. Energies were defined in terms of both surfaces and contact angles, though the fixed constraints on the edges, were applied preferentially before the angle constraint. Joint variables were varied to cover a wide range of relevant factors. Solder volume was set using volume constraints of values from 4.0e^5 cubic microns to 1.28e^6 cubic microns. Surface tension values were set to cover a range from 100 ergs/cm^2. to 1000 ergs/sq. cm, covering both the values for PbSn, as well as for other materials a well. Horizontal displacements ranged from 0 to 35 microns, pad radii were set at 75 microns, and joint heights varied between 60 and 80 microns.

5.3.3 Model Arrangement

The method used to compare restoring forces in standard and non-standard solder bumps involved the use of several models of each joint type (Fig. 5.1). The four major systems studied included:

1) A standard circular metallization pad-based joint
2) A four-pointed star shaped pad
3) An eight pointed star shaped pad
4) A cross-shaped pad.

Datafiles for each of these four metallization pad geometries are shown in Fig. [5.3], [5.4], [5.5], and [5.6].

An important consideration when comparing alternative geometries to standard pad shapes is whether it will be a comparison of joints with the same length and diameter or a comparison of pads with the same pad area. Both factors are important in the design of interconnects due to the high cost of substrate area in modern integrated circuits. This limited surface area should be optimized. The level of design efficacy needed to do this is made possible only by an understanding of the relationship between joint length, joint area and the alignment forces needed. In interconnect applications, where a certain level of restoring force is needed, substitute joint geometries of smaller area or length can be used. These smaller joints must be able to produce the required level of alignment force or a force comparable to a standard joint of much larger size. An important goal of this section was to determine which scale of comparison and what combination of solder parameters is more important.

As a result, two separate cases were studied to examine the relationship between joint geometry and restoring force. Models were compared on the basis of a common base pad area (Case 1) and a common base pad length scale (Case 2). This was to determine which factor (pad area or pad length/diameter) has the largest effect on alignment force. The standard circular joint was used as a control set of data for comparison. The restoring force was calculated for both model cases. Details of the computational method used to determine area and energy will be discussed in the next section.

5.3.4 Computational Methodology

The methodology used to determine the surface area, energy, and shape of a alternative flip-chip solder joint will be defined in this section. In most ways, it was very similar to the method used in Chapter 4 to study circular pads. Initial surfaces were defined for each joint for a series of vertical plate separations and horizontal displacements of the solder column. In terms of accuracy, the surface was refined through the use of two levels of the refinement function to increase the number of facets being studied. The surface was then averaged over the vertices twice and facets were changed from triangular geometries to equiangular facets to improve accuracy. The constraints and parameter values were then checked and the surface allowed to move toward its equilibrium surface for 1000 iterations. This was the number of iterations determined to provide the highest level of accuracy, while maximizing computer time. At the end of the iterations, surface energy and area were recorded for each combination of joint parameter. Fig. 5.7 shows an example of Surface Evolver output after 1000 iterations for an tetra-star pad. Using the surface areas and energies for a number of uniform displacements, surface energy gradients were calculated and the restoring force was determined using the equations outlined in Chapter 3.

5.3.5 Assumptions

Many of the same assumptions made in the circular pad model series were made in the alternative series as well. Gravity effects were assumed to be negligible due to the small scale of the system and surface tension effects were assumed to dominate. Internal temperature gradient driven flow was considered negligible due to the small system length scale as well and the body of the solder was assumed to be homogeneous in terms of compositional changes for all joint types.

A final set of assumptions made involves the interaction of the solder interconnect with the environment and the wettable surfaces. The body of the solder is assumed to be homogeneous to simplify the problem, since calculating the exact composition of the alloy during and after reflow with a number of chemical interactions occurring with the base metals is extremely difficult. It was assumed, furthermore, that the solder fully wets the base metal and is covering all of the designated area on the metallization pad in order to simplify the problem.

5.4 Results

The following series of results illustrate the usefulness of this modeling scheme for both standard and non-standard solder joint geometries. Complex free surface shapes, developed by alternative metallization pads during reflow, were calculated. The restoring forces associated with them were also calculated for a limited initial case using an average bump system and average parameters. In addition, the influence of alternative pad geometries on restoring forces relative to the standard pad shape were compared in terms of a number of joint parameters including solder height, solder volume, and surface tension for a secondary expanded case..

5.4.1 Initial Case

Free surface shapes for each of the solder joints for a 0 micron displacement and a 25 micron displacement were calculated. The major process parameters used in designing the models include 150 μm diameter pads, a solder volume of 1.28 e^6 micron^3 and a liquid-vapor surface tension coefficient of 325 erg/cm^3. Surface free energy for each model is plotted against horizontal displacement in Fig. 5.8 . The final surface morphology for the circular base pad for a 25 μm displacement and at its zero position can be seen in Fig. 5.9 and Fig. 5.10. Similar equilibrium surfaces for the tetra-star, octa-star, and cross-shaped pad, can be seen in Fig. 5.11-5.16. For the length-normalized model case, the horizontal restoring forces for each of the four model types were calculated based on the surface area produced by the surface morphologies. Alignment forces for each of the pad shapes are displayed in Fig. 5.17 which shows the restoring forces for joints that have the same pad diameter, vertical separation, and solder volume. The vertical separation for all the joints was determined by calculating the equilibrium height for each joint. The solder joint volume (1.28×10^6 cubic microns) for this series of studies was calculated for an average solder pad diameter (150 microns) and measured average pre-tack bump heights (60 microns). Restoring forces for an area array of 100 solder bumps are shown in Fig. 5.19. Positioning forces for individual solder joints with the same pad area, vertical separation, and solder volume were compared in Fig. 5.18 and for an area array of 100 bumps for each joint type in Fig. 5.20. Each of these joints were optimized as in the previous case, with a calculation of the equilibrium height for each type of solder connection.

5.4.2 Expanded Case

Restoring forces were also calculated for circular and alternative pads displaced horizontally as a function of the design factors mentioned above for an expanded series of models. This series was designed to examine many of the factors addressed for the circular pad system in Chapter 4, including parameter variation effects and interactions. These results are summarized in the next several sections, addressing the effects of each of these factors individually. Results for all cases represent length-scale normalized joints. The implications of these results will be discussed in the Discussion section and their impact in terms of potential additions to solder joint design rules will be outlined in the Conclusion section.

5.4.2.1 Volume Dependence

Studies to determine the influence of solder volume on length-normalized circular and alternative pads focused on volume variations from $4e^5$ micron^3 to $9e^5$ micron^3 and vertical separation variations from 60 microns to 80 microns. Pad size and surface tension values were kept constant at 75 microns and 100 ergs/cm^2 , respectively. Volume dependency results included free surface shapes and horizontal restoring forces for a both circular pads and alternative pads. Fig. 5.21 shows the restoring force generated by all four joint types for a 75 micron radius pad, 60 micron separation, and volume of $6e^5$ micron^3. For these joint factors, the joint producing the highest restoring force was the octa-star pad, followed by the cross-shaped pad, the tetra-star pad, and the circular pad. Fig. 5.22 shows the restoring force for the same joint parameters, with a solder volume of $8e^5$ micron^3 with the strongest realignment joint being the cross-shaped pad based system. This was followed by the circular pad, the octa-star pad and the tetra-star pad. Fig. 5.23 displays the results for a solder volume of $9e^5$ micron^3 where a circular pad generated the highest amount of restoring force, followed by the cross-shaped pad, octa-star pad, and tetra-star pad.

The restoring force for individual length-normalized solder joint pads was studied for volume ranging from 4-9 e^5 micron^3 and for vertical separations of 60, 70 and 80 microns. In Fig. 5.24 and 5.25 the optimum volume for a tstar-shaped pad is $6e^5$ micron^3 for both a 60 and 70 micron separation with a maximum restoring force for the lower separation. Fig. 5.26 shows that the optimum volume for an octa-star pad is $9e^5$ micron^3 for a joint height of 80 microns. The cross-shaped pad, Fig. 5.27-5.29 displays the effects of volume variation on restoring force. The optimum volume of the cross joint geometry for all 3 joint heights is $9e^5$ micron^3 with a maximum force for the 60 micron height.

5.4.2.2 Height Dependence

Solder joint height dependency was studied for all solder geometries for a fixed pad radius, volume and surface tension range. Results for the cross-shaped joint for 60, 70, and 80 micron heights are shown in Fig. 5.30, 5.31, and 5.32. The tetra-star model results are shown in

Fig. 5.33, 5.34, and 5.35, while octa-star results are shown in Fig. 5.36. Results for a circular pad for 60 and 70 micron heights are shown in Fig. 5.37-5.38.

5.4.2.3 Surface Tension Dependence

Comparisons of the pad geometries in terms of surface tension dependency were performed for a 60 micron separation and results for each pad are shown in Fig 5.39-5.42. The highest levels of restoring force in the horizontal direction are seen in the circular pad geometry (Fig. 5.42) for a 35 micron displacement. The next highest level is produced by the cross-shaped pad, followed by the tetra-star pad, and the octa-star pad. As seen for the circular pads in Chapter 5, surface tension effects are linear for each surface tension variation as expected, with an increase in restoring force for increased surface tension values.

5.5 Discussion

5.5.1 Initial Case

As expected, for each model the total energy of the system and the surface area reduce to minimum values as the surface approaches its final equilibrium position. The restoring force is seen to vary almost linearly with the displacement. This compares well with similar systems on the macro scale like springs where the force is linear for small displacements. It is at its highest value for the largest displacement away from this position and goes to zero when the joint has fully aligned the chip above the substrate. This behavior matches empirical results[]. We note that the forces are very small (on the order of 1×10^{-2} dynes). While these forces are extremely small, they are consistent with physical reasoning, given the small size of the solder droplets and the small size of the chip (approximately 1 mm^2). The forces needed to move a chip of this size in the 0.5 to 1 second interval in which self-alignment takes places is in the range of 1×10^{-5} dynes, assuming constant acceleration.

In examining the results, a number of trends of self-alignment for each type of pad geometry become evident. The first trend seen in the Surface Evolver results is that while each of the alternative geometry surfaces has a higher surface area and energy than the circular pad surface (Fig. 5.8), it is the circular pad which generates the highest level of restoring forces for this set of parameters (Fig. 5.17 and Fig. 5.18). This contradicts a somewhat common perception that the way to increase restoring force in flip-chip joints is to simply increase the total surface area. It is based on the concept that since the classical minimal energy surface is a spherical droplet, then through the use of higher energy surfaces, higher restoring forces can be achieved. In terms of the physics of self-alignment, the *real* key factor for generating restoring force is not the total surface energy, but the gradient of the surface energy as a function of a displacement from the normal equilibrium position. Therefore, increasing the surface area or even changing the surface properties would not necessarily produce a increase in restoring forces. This information is useful for guiding new pad design because it becomes clear that efforts to generate higher restoring forces need to focus more on *how* the solder surface is changing and *what type* of surface shapes it is forming, instead of focusing on its overall properties or geometry. In order to increase the restoring force generated by the joint, changes have to be made not only to the pad shape, but also to the difference between the initial surface and the final equilibrium surface. Increasing the difference between these surfaces would produce an increase in the restoring force.

This result is explained by the interaction between the solder and the base pad during the formation of the equilibrium surface morphology of the non-standard bumps, where the solder is constrained to a number of protruding edges. In contrast to the circular pad where there are no edges to hinder the total surface area from changing shape, the alternative pads have sections of free surfaces which are not being fully deformed during reflow. As the computed data shows, while most of the surface is minimized, the surface around the protruding edges -- particularly for the star-shaped bumps -- is constrained from moving freely. In the circular pad, the entire free surface is being changed and minimized without any sharp edges, so that there is a large difference between the amount of surface area of a misaligned circular joint compared to the surface area of a fully aligned circular joint. Since restoring force is directly related to the gradient in surface free energy, the circular pad is able to generate higher restoring forces than the other shapes since more of its total surface area is able to change from its initial, higher energy value. This is assuming the presence of the volume conditions that are present in this case; changing the volume, or other parameters would obviously change the way each pad shape is behaving in its liquid state.

Another trend that became evident from the results was the difference between a series of solder bumps with the same characteristic length (diameter for the circular pad) and bumps with the same base surface area. Each of the four model types which shared the same surface area were very similar in restoring force particularly for very small displacements, while those models with the same pad length showed a wider range difference in restoring forces. This is useful information for solder optimization studies and future joint designs where different designs need to be used and evaluated. For a system where available substrate surface area is limited and a circular bump could not be used, the next best replacement pad geometry for the standard circular pad would be a cross-shaped pad with the same base surface area and other parameters. The four- and eight- pointed star designs showed the lowest level of restoring force in both series of models, but if the process has only small misalignments, these types of bumps can be used as well, again with the same surface area. In terms of future designs to increase restoring forces, on the other hand, geometries with pointed edges are not a good feature to have since these edges prevent part of the surface from generating the restoring force.

We can develop further insights into the solder reflow process by examining data about those factors that have the greatest effect on self-alignment restoring forces. One of these factors is the dependence of self-alignment restoring forces on the length scale of the metallization pad as compared to the pad surface area. In analyzing the joint geometries in terms of length scale on the base pad, the difference in restoring force is more significant than for pads of similar surface area. In other words, restoring force is influenced far more by changes in the length scale for non-standard joint designs than by changes in the surface area. Both factors are obviously important given the value of substrate surface area; but understanding this relationship between restoring force and pad length can point toward useful directions in future exploration of joint designs and those avenues to avoid. In addition these results also show that in order to increase the restoring force, changes in more than just the joint geometry would have to be undertaken. Areas of change to be further explored include changes in the solder volume, pad length, and the wetting behavior and constraints affecting how the solder interacts with the metallization layer. This research project shows that best way to increase the restoring force is to generate the largest difference between the initial and final solder surface morphology, as opposed to simply increasing the surface area and energy of the solder surface relative to a standard joint.

Some of the obvious differences, between standard circular pads and alternative pad designs, are seen in the pad level interactions for this specific case where the solder comes into contact and is constrained by the metallizatiion layer edges. For the circular pad, the solder is constrained by edges on partially, and its contact angle is dependent mainly on the volume of solder and the height of the joint. The octa-star shaped bump has the largest number of limitations on the solder at the pad base level due the presence of several sharp corners and short straight edges to which the solder is constrained. The tetra-star shaped bump is similar to the octa-star bump, with sharp corners and longer straight edges. The final surface studied, for a cross shaped bump, has 90 degree corners and the longest straight edges of the four model types.

5.5.2 Expanded Case

5.5.2.1 Volume Dependence

Volume variations for a fixed separation and surface tension have a pronounced effect on restoring force generation among the alternative cases studied. For low volumes ($6e^5$ micron3), pointed edge geometries, like the octa-star and tetra-star pads, were favored. This was followed by the next set of pads with less pointed edges, the cross-shaped pad, and the pad with no sharp corners, the circle. As solder volume increases with all other parameters being held constant, the cross-shaped joint begins to generate the highest level of alignment force, followed closely by the circular pad and then the two pointed pads. As solder volume increases even more, the circular pad begins to dominate in terms of force generation, followed by the cross pad and then the octa-star and tetra-star geometries. This is explained by the same types of volume dependency effects that were discovered in Chapter 4 and that affect force generation in circular pads, where a certain quantity of volume had large effects on optimizing alignment forces.

For the lower solder volumes, surface area gradients are very large for the pointed pads relative to the less- or non- pointed pads. In this case, the difference between the initial and final surfaces are rather large and restoring force is equally large to match. As solder volume increases, these large gradients across the surface of the pointed pads decrease, as more and more solder is constrained to match the edge of the base and cap pads of the joint. The pads with long unbroken edges, like the cross and circular pads, have less of the solder constrained by a complex shape and more of it is available to change the shape of the surface towards the minimum shape.

5.5.2.2 Height Dependence

In terms of height variations, the tetra-star pad is optimized for smaller solder volumes combined with shorter joint heights and for larger volumes combined with larger joint heights. Restoring force consistently drops off away from this optimum volume with a restoring force maximum reached for a height of 60 microns. The cross-shape joint generated alignment force is maximized for large solder volumes for all separations and is decreased for smaller quantities of solder. The octa-star pad is optimized in a similar way as the tetra-star pad for small volumes and separations only. In an overall comparison of the alternative pads, the best pad design to deal with height variations was the cross-shaped geometry joint, which produced the highest levels of force most consistently across the entire height variation range.

5.5.2.3 Surface Tension Dependence

In terms of surface tension trends, increasing surface tension through the use of another type of solder is one of the few methods that involves a truly independent joint parameter. For each combination of joint height, volume, etc., an increase in surface tension would consistently produce an increase in surface tension. As a factor that is able to greatly enhance restoring forces without regard for joint geometry, surface tension ranks as the factor to be changed first in order to increase restoring forces.

5.6 Conclusions

In terms of design rules, a number of trends become apparent when studying individual parameter and parameters interaction effects on restoring force. In a manner comparable to the design methodology discussed in Chapter 4, the use of alternative joints to generate higher levels of alignment force should focus on a few specific areas:

- **Surface tension,** is a shared quality of both systems and should be increased where possible through material substitution or the addition of another type of fluxing agent to remove excess oxide layers.

- **Joint Height,** alignment systems designed around the use of short bumps have a greater potential to general restoring force. The level of this generated force is heavily dependent on **solder volume**, which in a similar way to the circular system studied earlier, plays a large role in determining which combinations of solder height, surface tension and pad radius, produce the highest force possible.

To summarize, for each alternative pad, there existed an optimum volume, for which alignment force was maximized -- a key insight that should play a role in an optimized joint design strategy with a goal of maximizing alignment forces. In addition, for each combination of joint parameters, there existed a specific set which produced the highest level of alignment forces.

In the next to chapters, methods for determining the magnitude of this alignment force will be outline and results from experimental methods will be presented. In addition, important experimental and process-related will be discussed and possible solutions wil be proposed.

5.7 References

[1] Dudderar, D., AT&T Technical Memo, AT&T Bell Laboratories, 1993

[2] Myers, T.R., "Flip-chip Microcircuit Bonding Systems", IIT Research Institute Paper, pp. 131-144.

[3] Goldmann, L.S., "Geometric Optimization of Controlled Collapse Interconnections", IBM Journal of Research and Development, vol. 13, no. 3, May 1969, pp. 251-265.

[4] Patra, S.K., Sritharan, S.S., Lee, Y.C., "Minimum-Energy Surface Profile of Solder Joints for Non-Circular Pads", EEp-Vol./PED-vol. 60, Manufacturing Aspects in Electronic Packaging, ASME, 1992.

[5] McGroarty, J., Borgesen, P., Yost, B., Li, C.Y., "Statistics of Solder Joint Alignment for Opto-electronic Components", IEEE Transactions

on Components, Hybrids, and Manufacturing Technology, vol. 16, no. 5, August 1993, pp. 527-529.

[6] Yost, B., McGroarty J., Borgesen, P., Li, C.Y., "Shape of a Nonaxisymmetric Liquid Solder Drop Constrained by Parallel Plates", IEEE Transactions on Components, Hybrids and Manufacturing Technology, vol. 16, no. 5, August 1993, pp. 523-527.

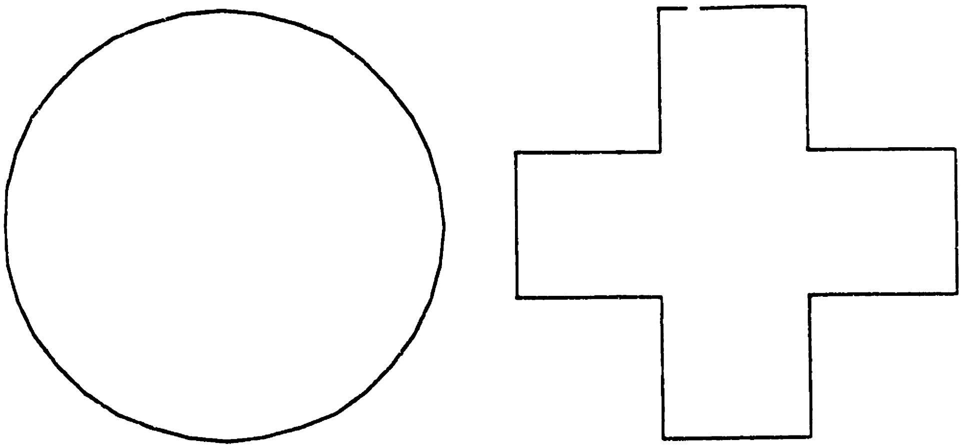

a. Circular pad

b. Cross-shaped Pad

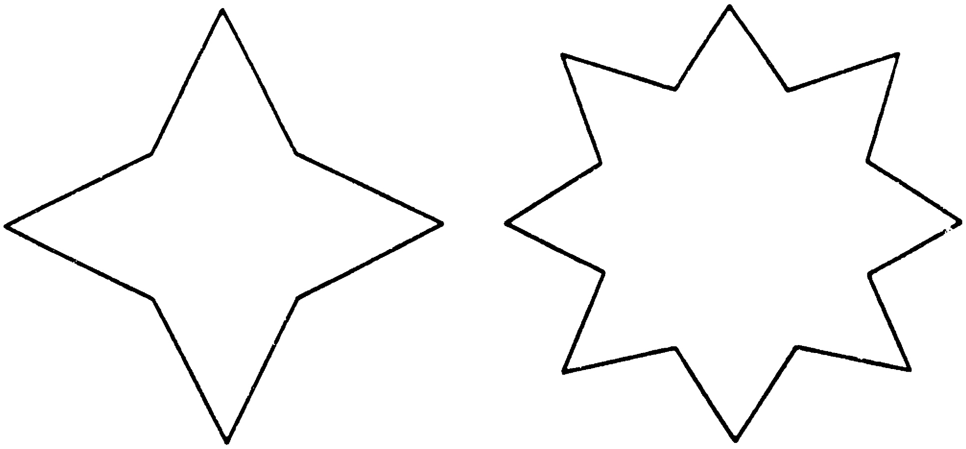

c. Tetra-Star shaped pad

d. Octa-Star shaped pad

Fig. 5.1 The four main types of pad shapes studied

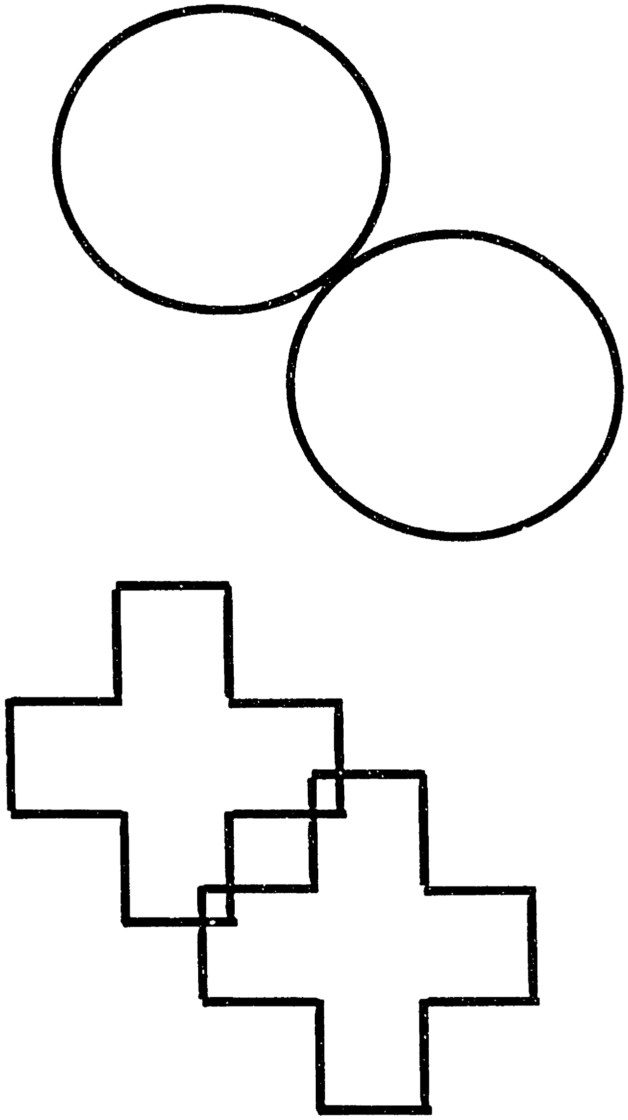

Fig. 5.2 Long Edge Alignment Advantages-cross shaped pads brought into contact

```
//cir.v60 -fixed cgs units in edge files

GRAVITY_CONSTANT 0.0

//Physical parameters
PARAMETER THETAL = 175 //angle between fluid and chip
PARAMETER THETAU = 175 //angle on top plate )
PARAMETER GAMMALV = 325.00 //l-v surface energy (ergs/cm^2)
PARAMETER VS = 0.00000128 //volume of solder in (cm^3)
PARAMETER RHOS = 9.00 //density of solder (g/cm^3)
PARAMETER F = .0001

//Geometric parameters
PARAMETER RMETA = .0075 //radius of lower met. pad constraints
PARAMETER RMETB = .0075 //radius of upper met. pad constraints
PARAMETER RSOLA = .0075 //radius of lower solder column constraints
PARAMETER RSOLB = .0075 //radius of upper solder column constraints
PARAMETER DISP  = 0.00*F  //displacement in x direction

#define DIFFL (GAMMALV*cos(THETAL*pi/180))  //substrate energy on bottom
#define DIFFU (GAMMALV*cos(THETAU*pi/180))  //substrate energy up top

constraint 1
function: z = .0004
energy  //contact angle on lower metallization pad
e1:  -DIFFL*y
e2: 0
e3: 0
// need content for volume
content
c1: 0
c2: -z*x
c3: 0

constraint 2
function: z = .0064
energy  //contact angle on top met. pad
e1: -DIFFU*y
e2: 0
e3: 0
// need content for volume
content
c1: 0
c2: -z*x
c3: 0

constraint 3 // constraint for lower met pad
function:  x^2 + y^2 = RMETA^2

constraint 4 // constraint for lower solder column
function:  x^2 + y^2 = RSOLA^2

constraint 5 // constraints for upper solder column
function:  x^2 + (y - DISP)^2 = RSOLB^2

constraint 6 // constraints for upper met pad
function:  x^2 + (y - DISP)^2 = RMETB^2

//Initial shape of solder column and vertices of subs. and metal. pad
vertices
1  -200.0*F -200.0*F  0.0*F  fixed  /*vertices on ceramic substrate*/
2   200.0*F -200.0*F  0.0*F  fixed
3   200.0*F  200.0*F  0.0*F  fixed
4  -200.0*F  200.0*F  0.0*F  fixed

5  -200.0*F -200.0*F  68.0*F  fixed  /*vertices on silicon chip*/
```

Fig. 5.3 Circular pad datafile sample

```
// ts.n0-.v60-geometry experiment withv star-shaped bump 6.7.93

GRAVITY_CONSTANT 0.0

// Evolver data for star-shaped solder bump

PARAMETER THETAL = 175 //angle between fluid and chip
PARAMETER THETAU = 175 //angle on top plate ?
PARAMETER GAMMALV = 100.00 //l-v surface energy  [ergs/cm^2]
PARAMETER VS = 0.00000128  //volume of solder in [cm^3]
PARAMETER RHOS = 9.00  //density of solder [g/cm^3]
PARAMETER F = .0001

#define//Geometric parameters
PARAMETER DISP  = 0.00*F  //displacement in x direction

#define DIFFL (GAMMALV*cos(THETAL*pi/180))   //substrate energy on bottom
#define DIFFU (GAMMALV*cos(THETAU*pi/180))   //substrate energy up top

constraint 1  /*substrate surface */
formula: z = .0004
energy:   // for lower surface contact angle
e1: -DIFFL*y
e2: 0
e3: 0
// need content for volume
content
c1: 0
c2: -z*x
c3: 0

constraint 2  /* upper chip surface */
formula: z = .0064

energy  //contact angle on top met. pad
e1: -DIFFU*y
e2: 0
e3: 0
// need content for volume
content
c1: 0
c2: -z*x
c3: 0

constraint 3  /*edge-type constraint*/
function: y = -0.5*x - 46.4975*F

constraint 4
function: y = -2*x - 92.9895*F

constraint 5
function: y =  2*x - 92.9895*F

constraint 6
function: y = 0.5*x - 46.4975*F

constraint 7
function: y = -0.5*x + 46.4975*F

constraint 8
function: y = -2*x + 92.9895*F

constraint 9
function: y = 2*x + 92.9895*F

constraint 10
```

Fig. 5.4 **Tetra-star pad datafile sample**

```
  noct.vdl- evolver data fo a octa-star shped bump

GRAVITY_CONSTANT 0.0

// Evolver data for octa-star-shaped solder bump

PARAMETER THETAL = 175 //angle between fluid and chip
PARAMETER THETAU = 175 //angle on top plate ?
PARAMETER GAMMALV = 325.00 // l-v surface energy  [ergs/cm^2]
PARAMETER V0 = 0.00000128   //volume of solder in [cm^3]
PARAMETER RHOS = 9.00   //density of solder [g/cm^3]
PARAMETER F = .0001

#define//Geometric parameters
PARAMETER DISP  = 0.00*F //displacement in x direction

#define DIFFL (GAMMALV*cos(THETAL*pi/180))   //substrate energy on bottom
#define DIFFU (GAMMALV*cos(THETAU*pi/180))   //substrate energy up top
constraint 1  /*substrate surface *
formula: z = .0004
energy:    for lower surface contact angle
e1: -DIFFL*y
e2: 0
e3: 0
// need content for volume
content
c1: 0
c2: -z*x
c3: 0

constraint 2  /* upper chip surface */
formula: z = .0064

energy   //contact angle on top met. pad
e1: -DIFFU*y
e2: 0
e3: 0
// need content for volume
content
c1: 0
c2: -z*x
c3: 0

//Initial shape of solder column and vertices of solder, subs, and met.pad

vertices
1  -200.0*F -200.0*F  0.0*F  fixed  /*vertices on ceramic substrate*/
2   200.0*F -200.0*F  0.0*F  fixed
3   200.0*F  200.0*F  0.0*F  fixed
4  -200.0*F  200.0*F  0.0*F  fixed
5  -200.0*F -200.0*F  68.0*F  fixed  /*vertices on silicon chip*/
6   200.0*F -200.0*F  68.0*F  fixed
7   200.0*F  200.0*F  68.0*F  fixed
8  -200.0*F  200.0*F  68.0*F  fixed

9   -74.99*F    0.00*F  4.0*F fixed /*lower solder vertices */
10  -41.02*F  -16.99*F  4.0*F fixed
11  -53.02*F  -53.02*F  4.0*F fixed
12  -16.99*F  -41.02*F  4.0*F fixed
13    0.00*F  -74.99*F  4.0*F fixed
14   16.99*F  -41.02*F  4.0*F fixed
15   53.02*F  -53.02*F  4.0*F fixed
16   41.02*F  -16.99*F  4.0*F fixed
17   74.99*F    0.00*F  4.0*F fixed
18   41.02*F   16.99*F  4.0*F fixed
```

Fig. 5.5 Octa-star pad datafile sample

```
/ncrs.v60-geometry experiment with cross shaped bump

 / Evolver data for cross-shaped solder bump

PARAMETER THETAL = 10 //angle between fluid and chip
PARAMETER THETAU = 10 //angle on top plate ?
PARAMETER GAMMALV = 325.00 //l-v surface energy  [ergs/cm^2]
PARAMETER VS = 0.00000128    volume of solder in [cm^3]
PARAMETER RHOS = 9.00  //density of solder [g/cm^3]
PARAMETER F = .0001

#define//Geometric parameters
PARAMETER DISP  = 0.00*F //displacement in x direction

#define DIFFL (GAMMALV*cos(THETAL*pi/180)),  //substrate energy on bottom
#define DIFFU (GAMMALV*cos(THETAU*pi/180))  //substrate energy up top

constraint 1  /*substrate surface */
formula: z = .0004
energy:  / for lower surface contact angle
e1: -DIFFL*y
e2: 0
e3: 0
 / need content for volume
content
c1: 0
c2: -z*x
c3: 0

constraint 2  /* upper chip surface */
formula: z = .0064

energy   //contact angle on top met. pad
e1: -DIFFU*y
e2: 0
e3: 0
// need content for volume
content
c1: 0
c2: -z*x
c3: 0

//Initial shape of solder column and vertices of solder, subs, and met.pad

vertices
1  -200.0*F -200.0*F   0.0*F  fixed  /*vertices on ceramic substrate*/
2   200.0*F -200.0*F   0.0*F  fixed
3   200.0*F  200.0*F   0.0*F  fixed
4  -200.0*F  200.0*F   0.0*F  fixed
5  -200.0*F -200.0*F  68.0*F  fixed  /*vertices on silicon chip*/
6   200.0*F -200.0*F  68.0*F  fixed
7   200.0*F  200.0*F  68.0*F  fixed
8  -200.0*F  200.0*F  68.0*F  fixed

9  -25.00*F -75.00*F   4.0*F  fixed  /*solder vertices-low*/
10  25.00*F -75.00*F   4.0*F  fixed
11  25.00*F -25.00*F   4.0*F  fixed
12  75.00*F -25.00*F   4.0*F  fixed
13  75.00*F  25.00*F   4.0*F  fixed
14  25.00*F  25.00*F   4.0*F  fixed
15  25.00*F  75.00*F   4.0*F  fixed
16 -25.00*F  75.00*F   4.0*F  fixed
17 -25.00*F  25.00*F   4.0*F  fixed
18 -75.00*F  25.00*F   4.0*F  fixed
19 -75.00*F -25.00*F   4.0*F  fixed
20 -25.00*F -25.00*F   4.0*F  fixed
```

Fig. 5.6 Cross-shaped pad datafile sample

Fig. 5.7 Sample Evolver Output

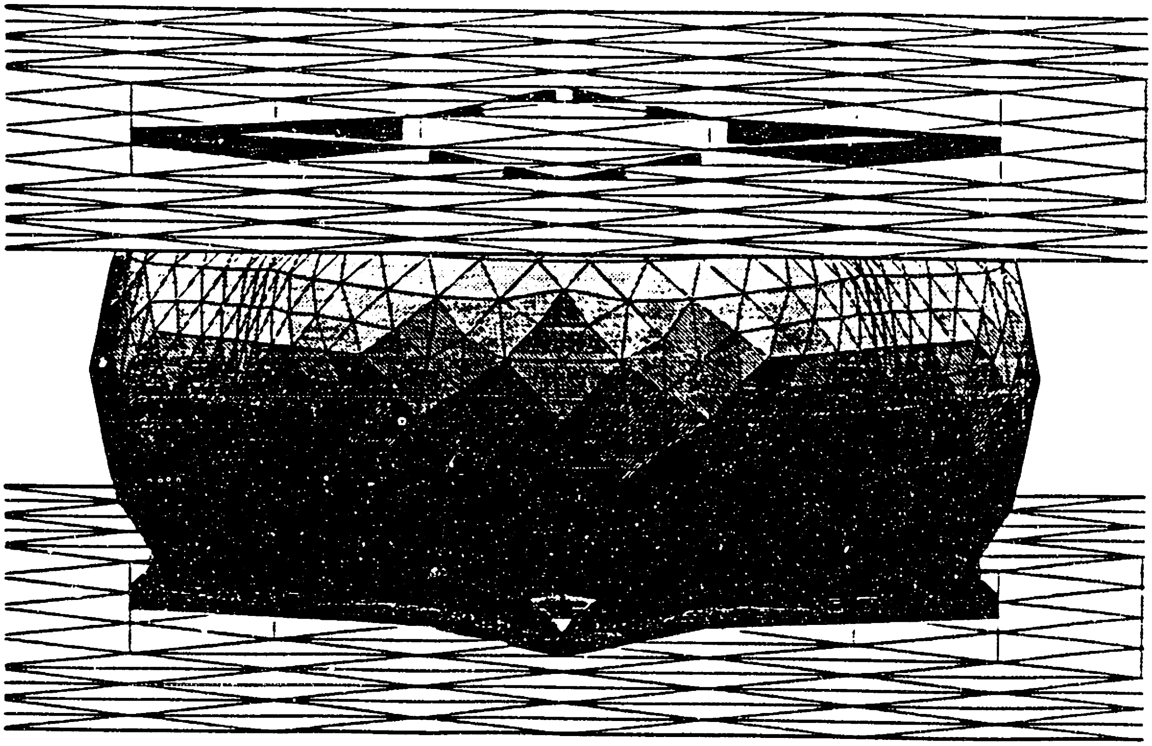

Fig. 5.8 Surface free energy for each model is plotted against horizontal displacement

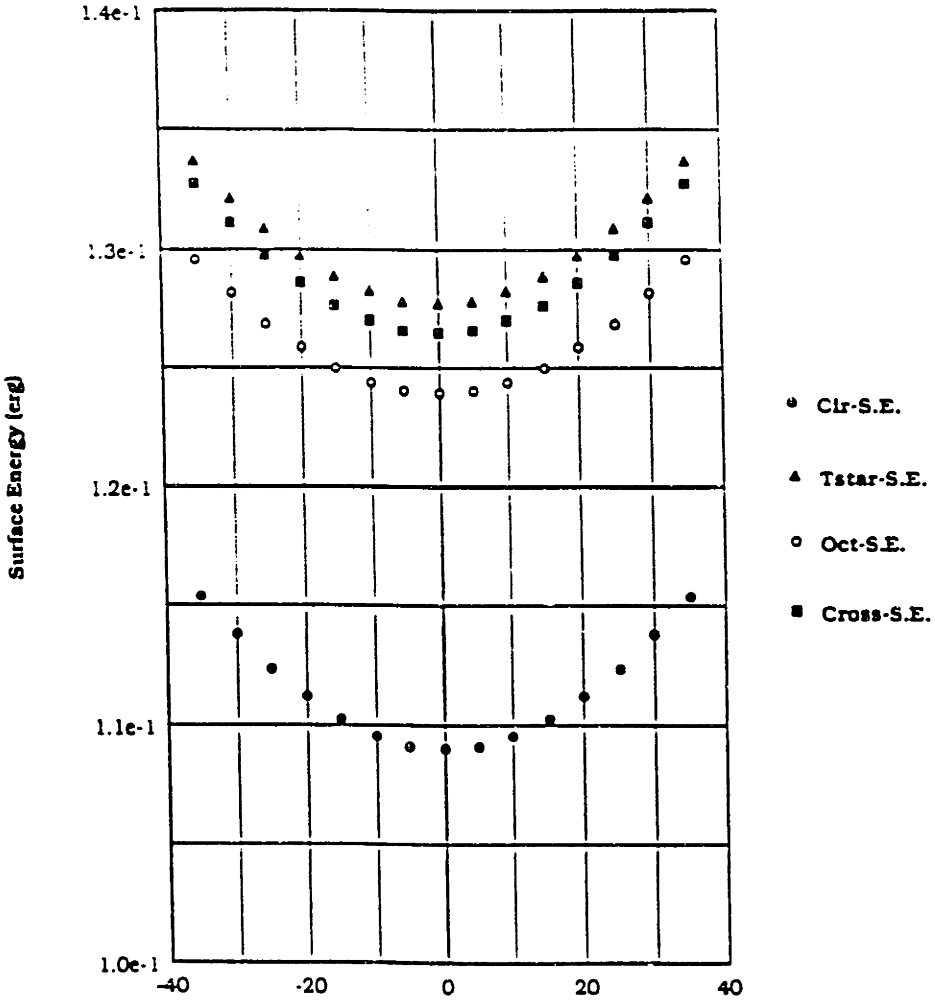

Horizontal Displacement (microns)

Fig. 5.9 The final surface morphology for the circular base pad for a 0 μm displacement.

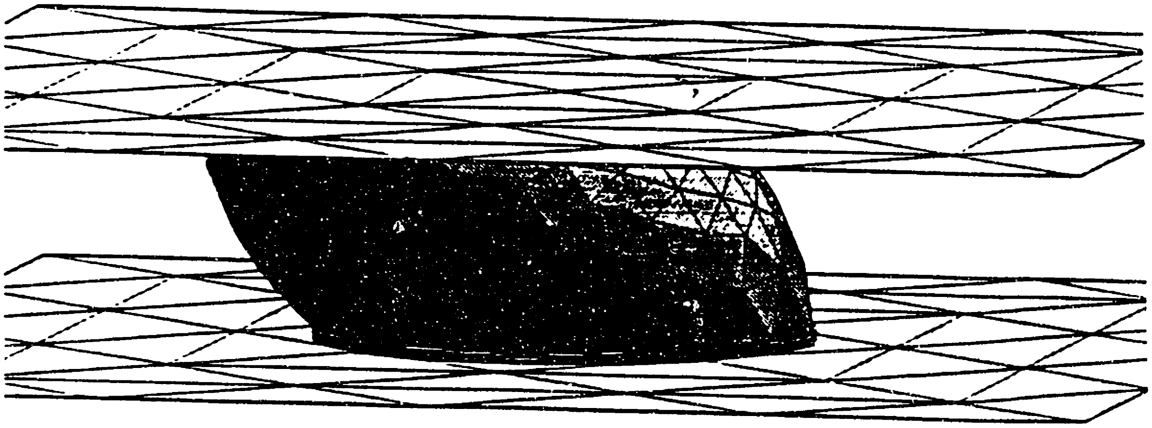

Fig. 5.10 The final surface morphology for the circular base pad for 25 μm displacement.

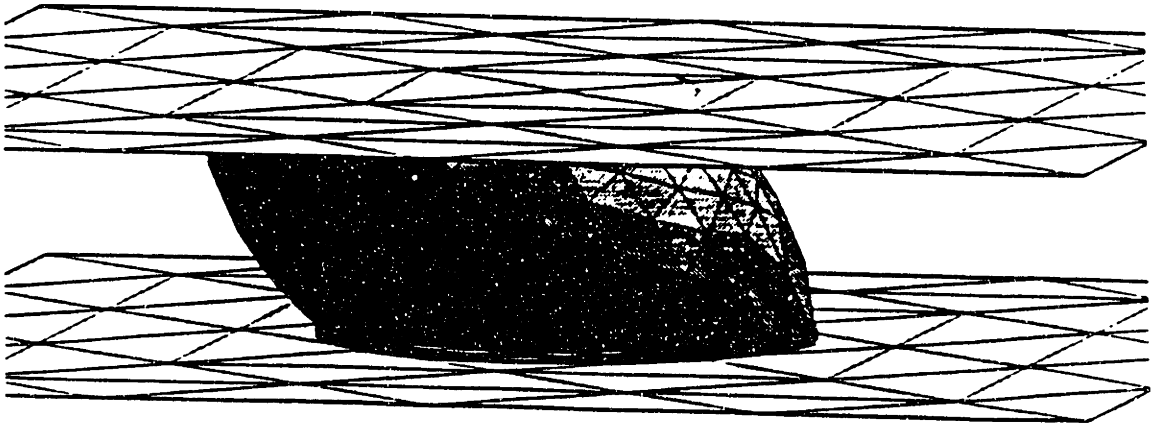

Fig. 5.11 Equilibrium surfaces for the tetra-star pad for a zero displacement.

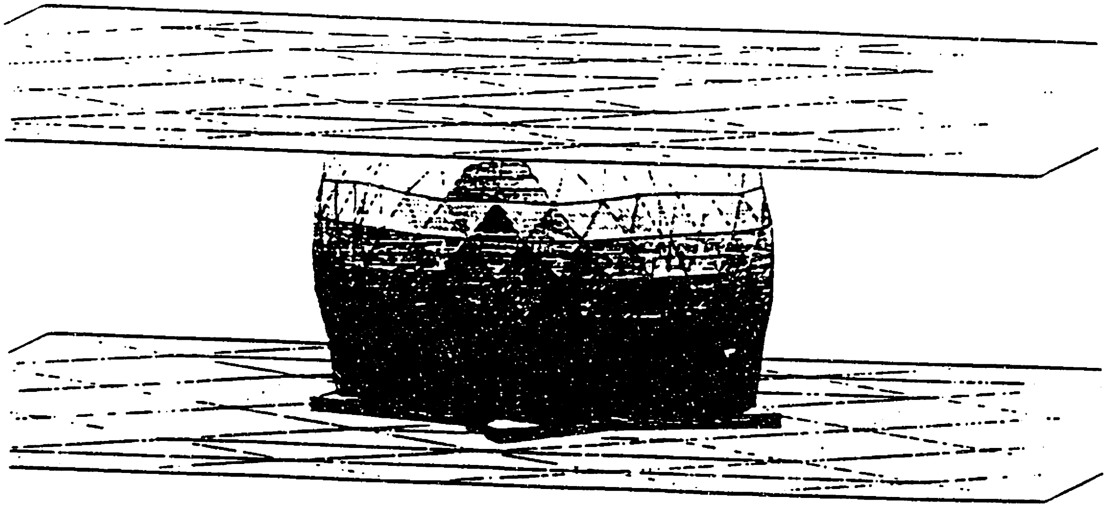

Fig. 5.12 Equilibrium surfaces for the tetra-star pad for a 25 micron displacement.

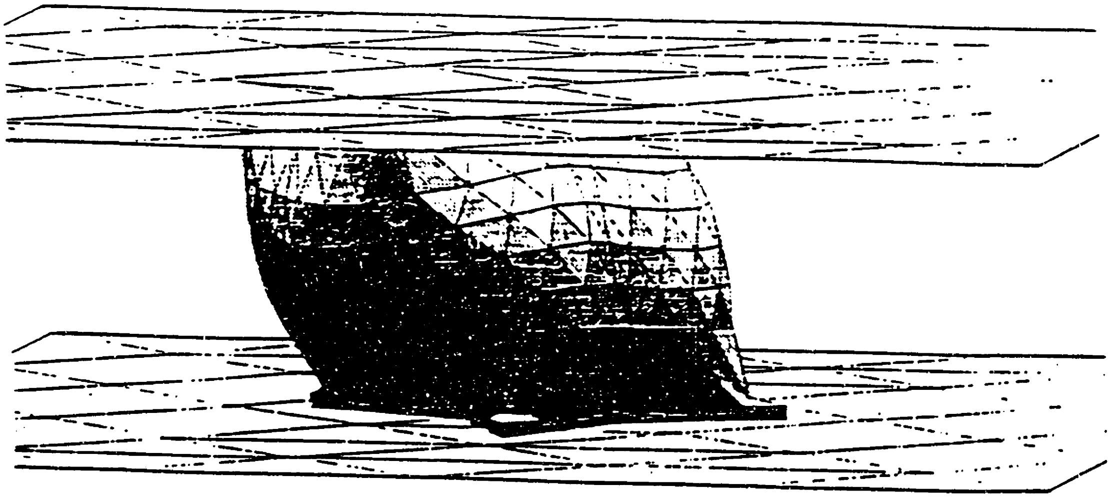

Fig. 5.13 Equilibrium surfaces for the octa-star pad for a zero displacement.

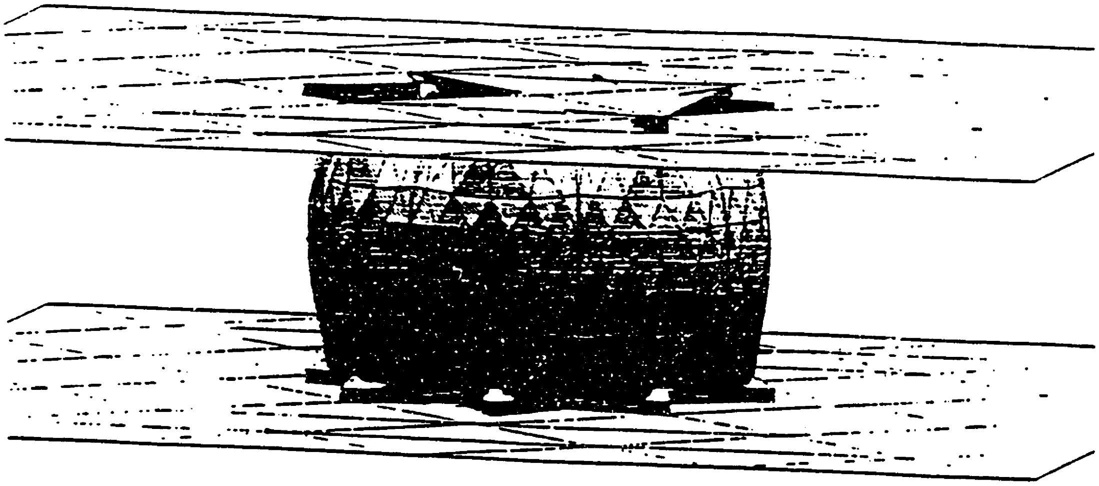

Fig. 5.14 Equilibrium surfaces for the octa-star pad for a 25 micron displacement.

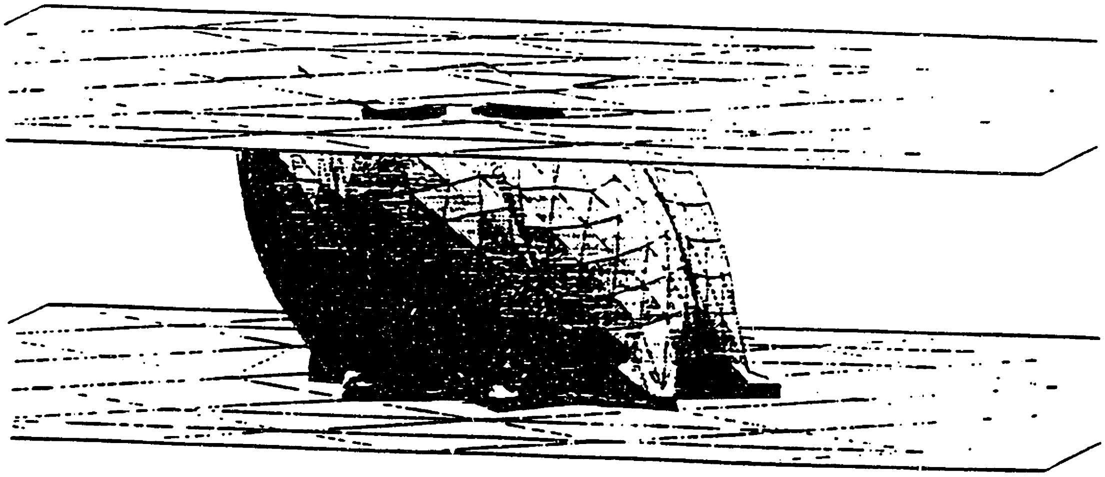

Fig. 5.15 Equilibrium surfaces for the cross-shaped pad for a zero displacement.

Fig. 5.16 Equilibrium surfaces for the cross-shaped pad for a 25 micron displacement.

Fig. 5.17 **Restoring Force vs. Horizontal Displacement for length normalized joints**

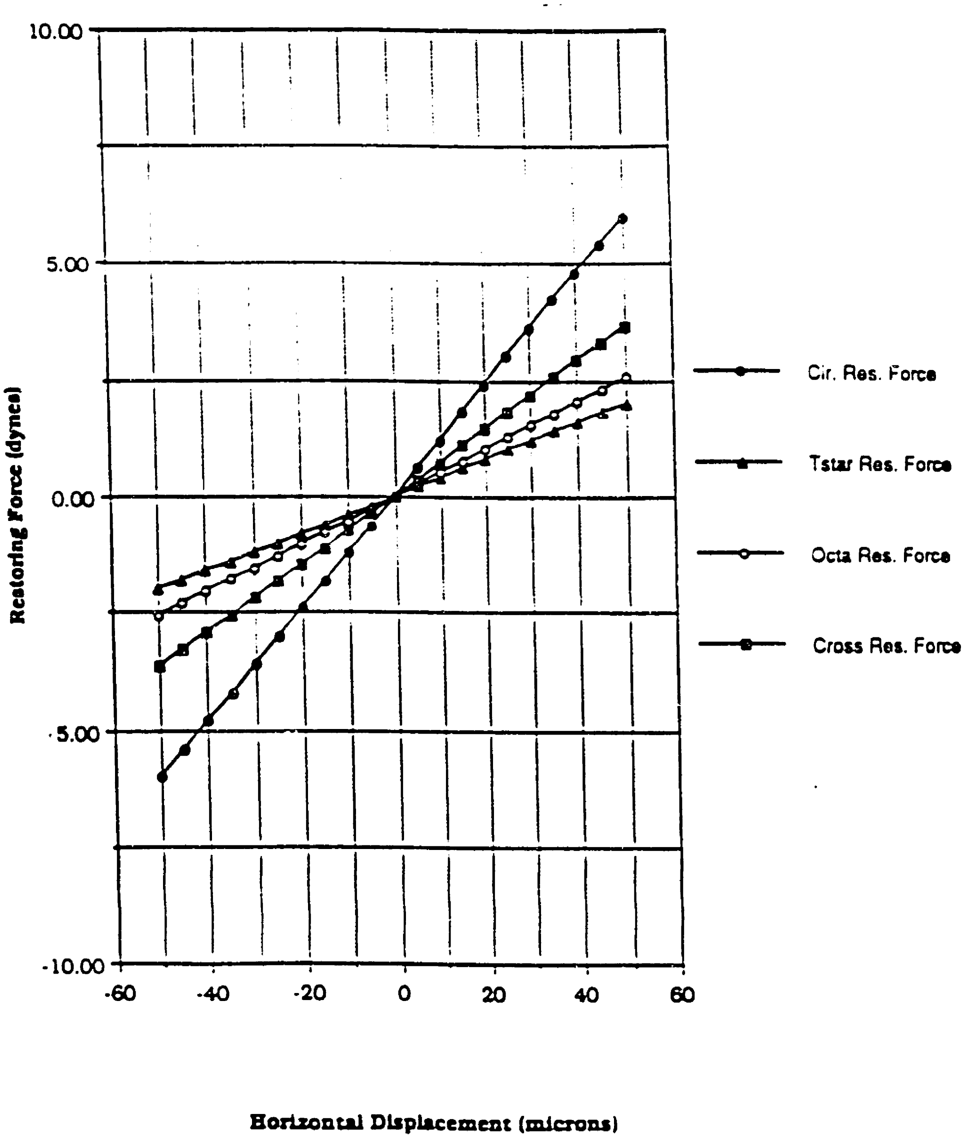

Fig. 5.18 Restoring Force vs. Horizontal Displacement for area normalized joints

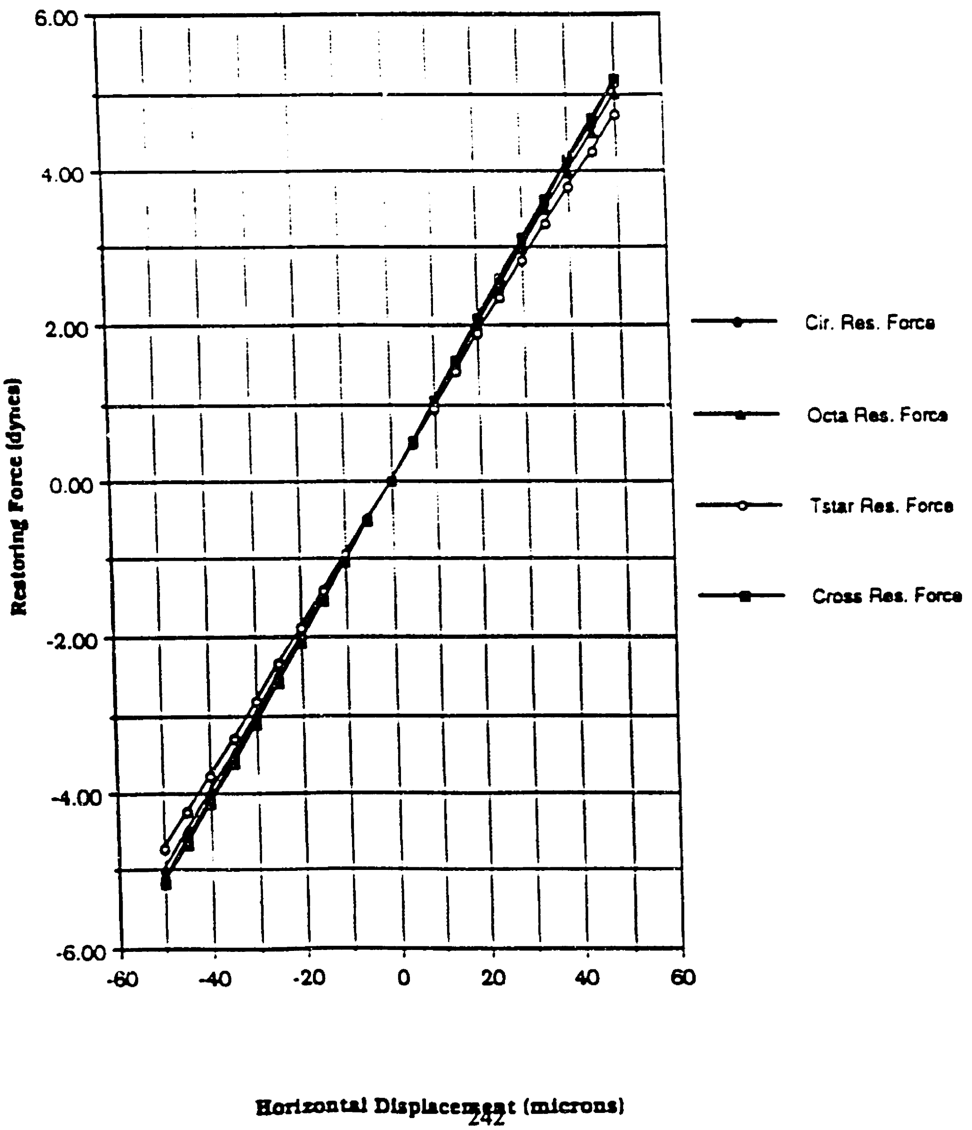

Fig. 5.19 Restoring Force vs. Horizontal Displacement for an area array of 20 length normalized joints

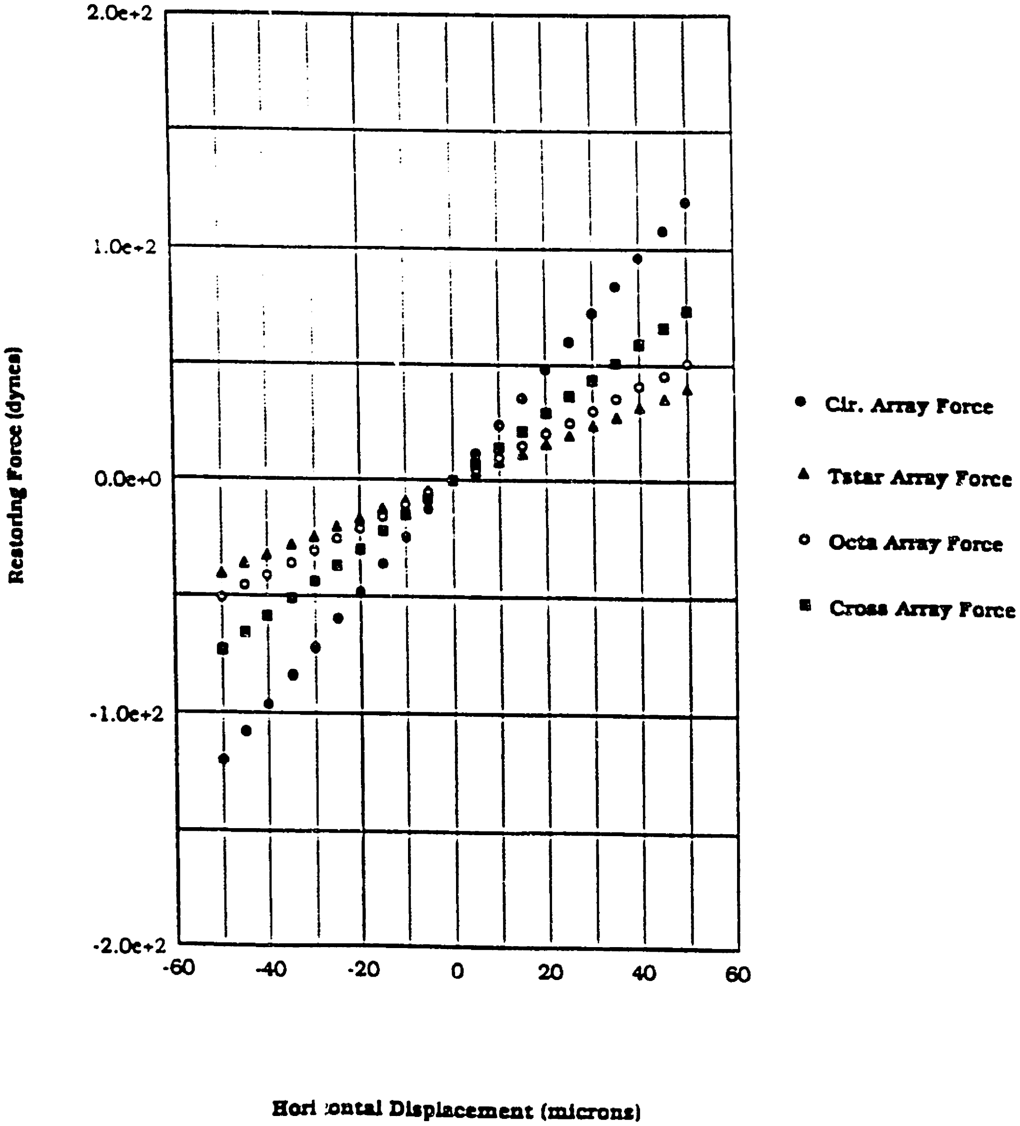

Fig. 5.20 Restoring Force vs. Horizontal Displacement for an area array of 20 area normalized joints

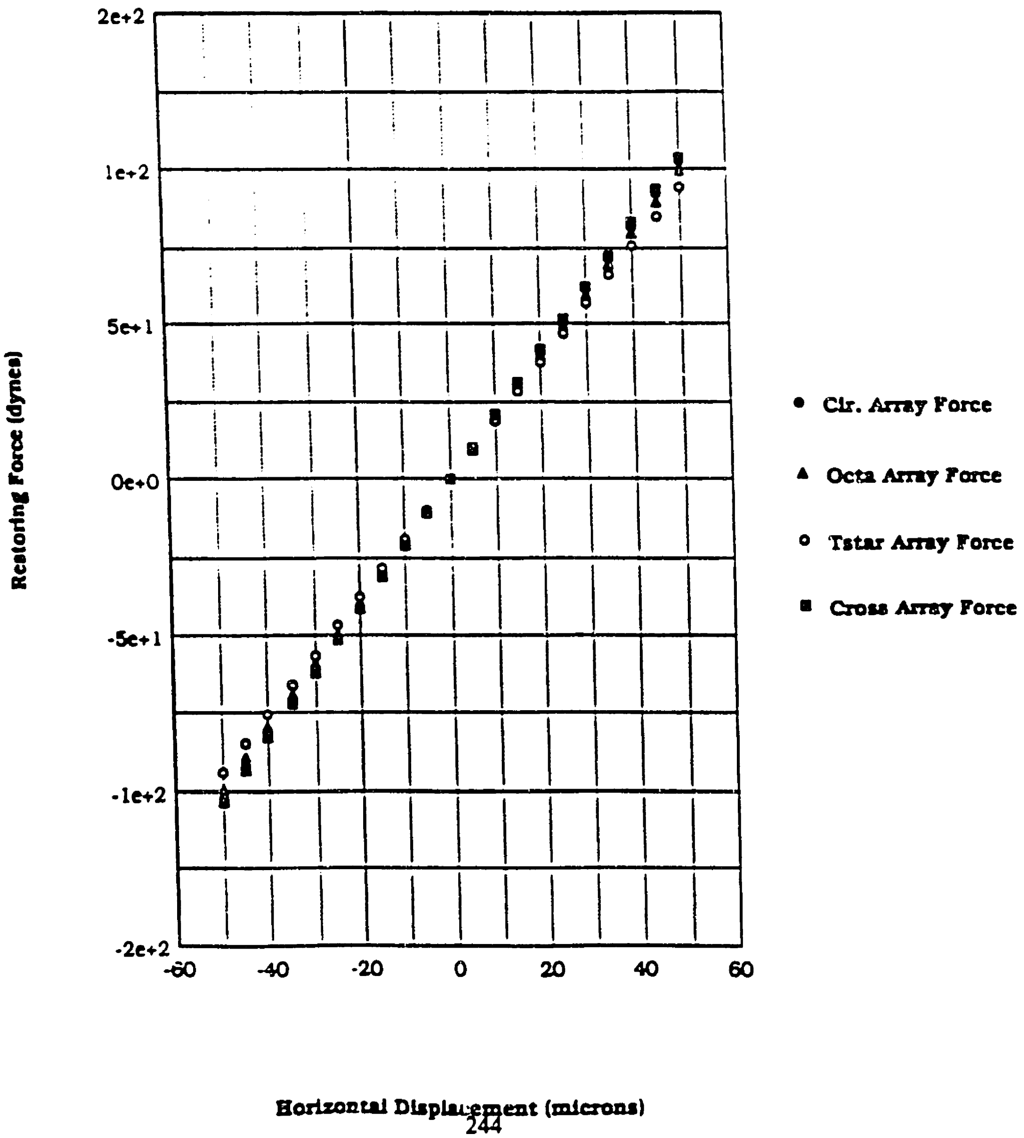

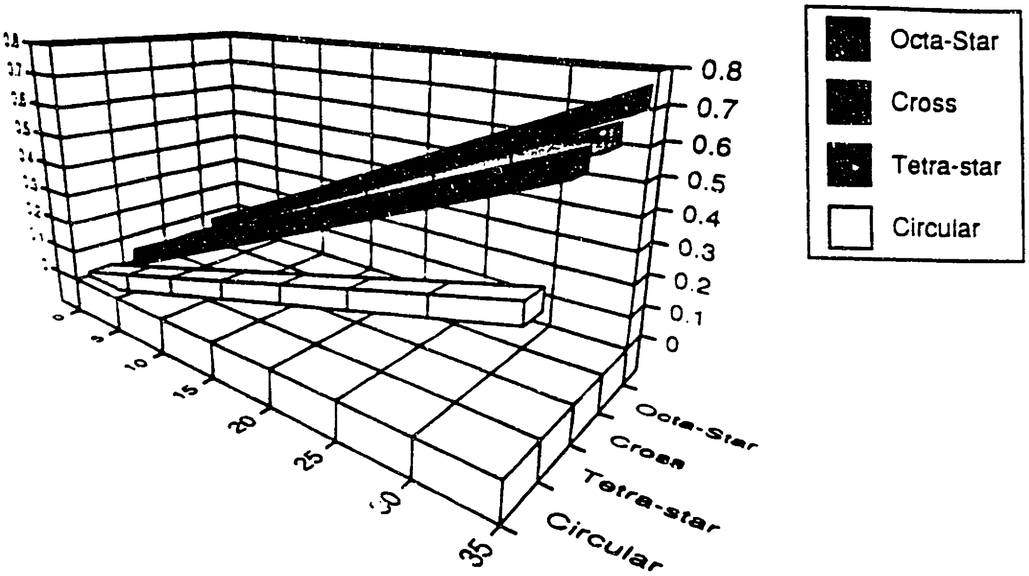

Fig. 5.21: Restoring Force as a function of Horizontal Displacement and 75 micron radius circular pad and alternative geometries for a 60 micron separation.

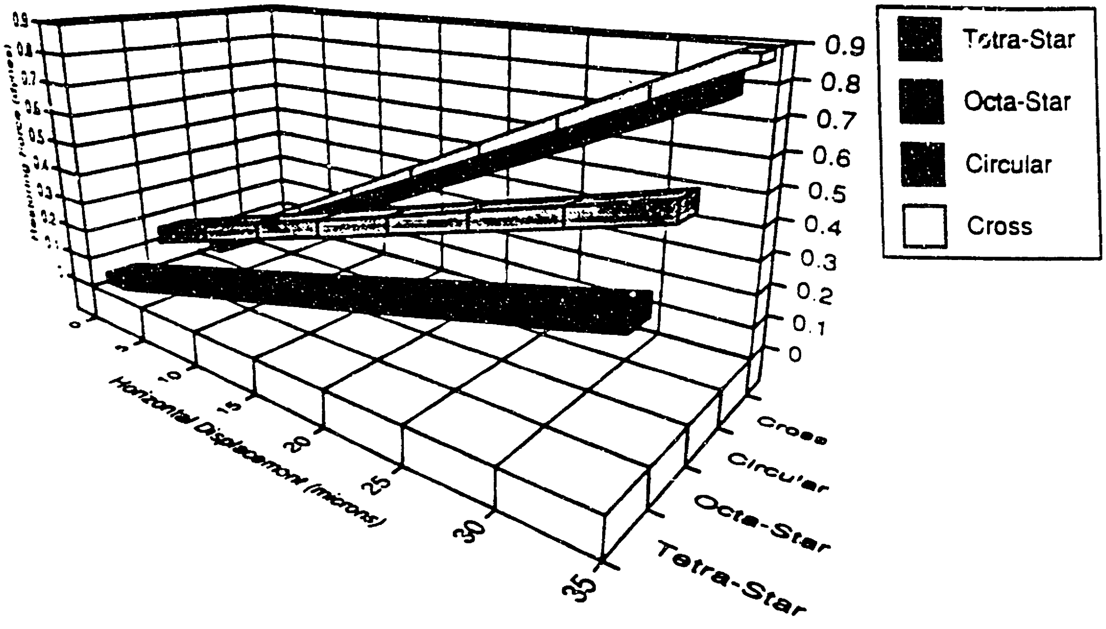

Fig. 5.22:Restoring Force as a function of Horizontal Displacement and 75 micron radius circular pad and alternative geometries for a 60 micron separation.

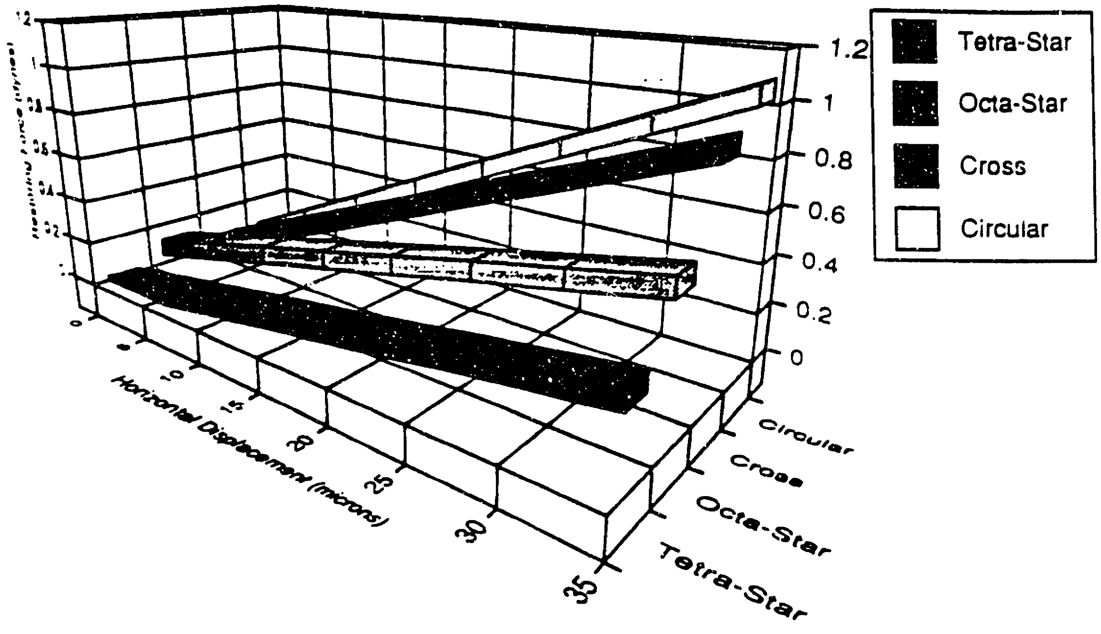

Fig. 5.23: Restoring Force as a function of Horizontal Displacement and 75 micron radius circular pad and alternative geometries for a 60 micron separation.

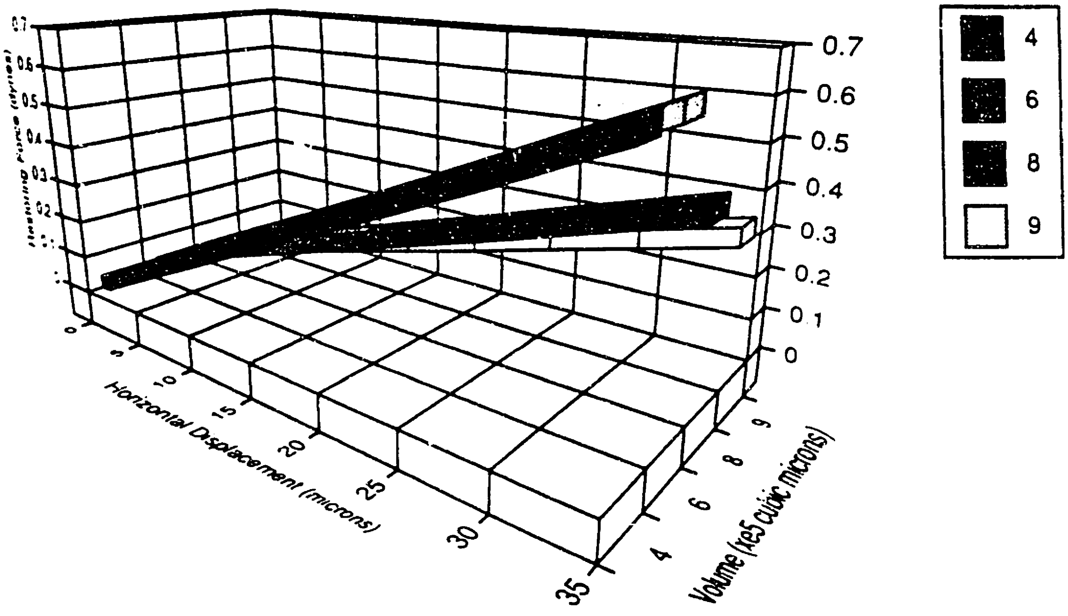

Fig. 5.24: Restoring Force as a function of Horizontal Displacement and Volume of a tetra-star pad for a 60 micron separation.

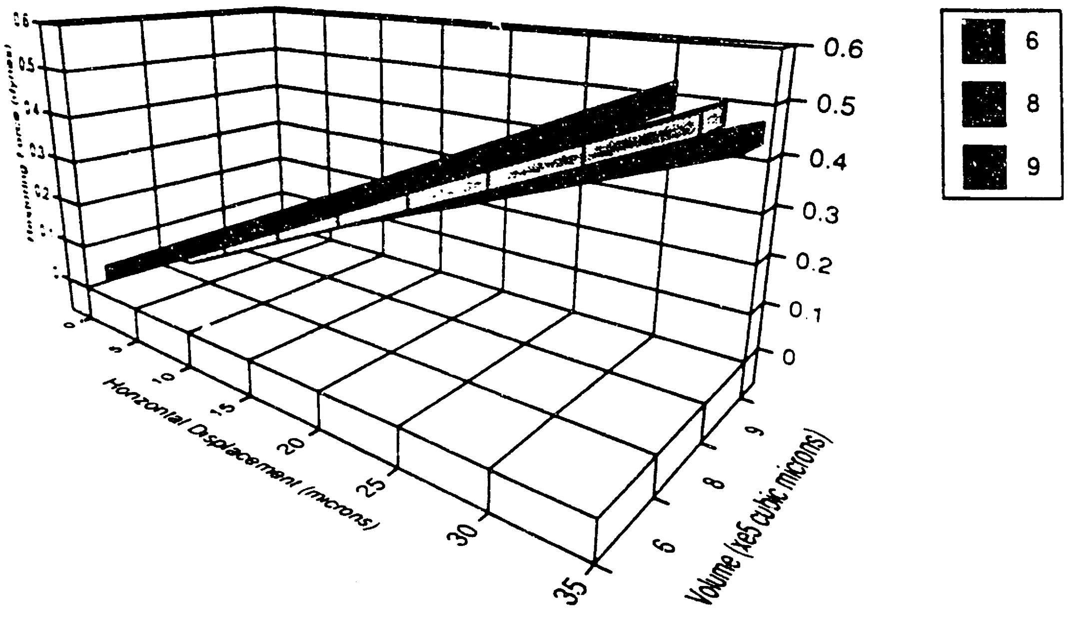

Fig. 5.25 :Restoring Force as a function of Horizontal Displacement and Volume of a tetra-star pad for a 70 micron separation.

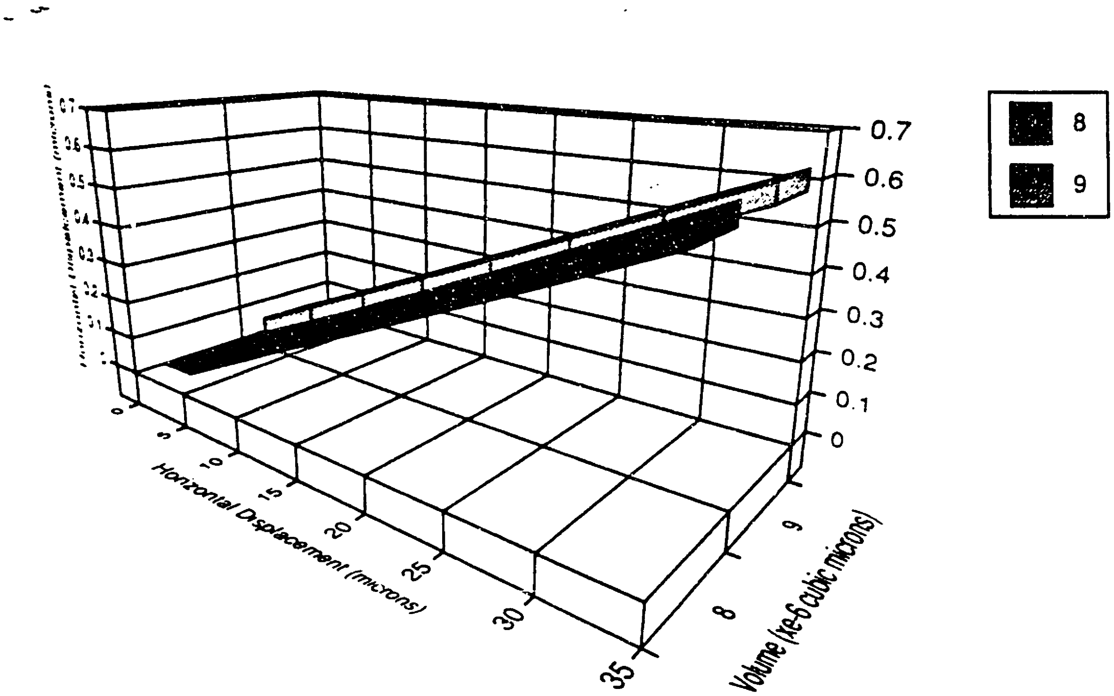

Fig. 5.26:Restoring Force as a function of Horizontal Displacement and Volume of an octa-star pad for a 80 micron separation.

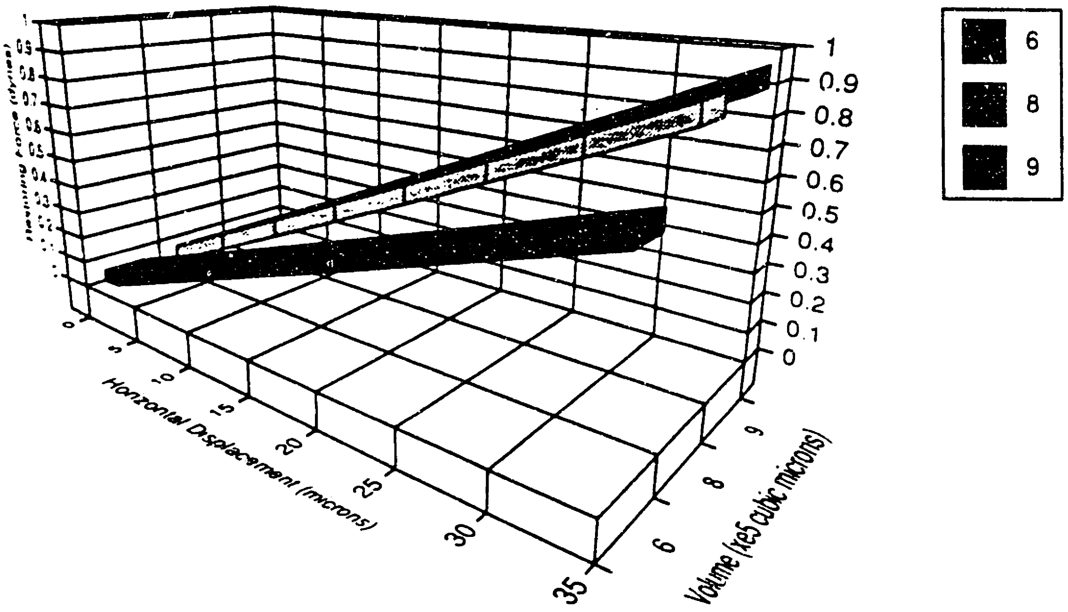

Fig. 5.27: Restoring Force as a function of Horizontal Displacement and Volume of an cross-shaped pad for a 60 micron separation.

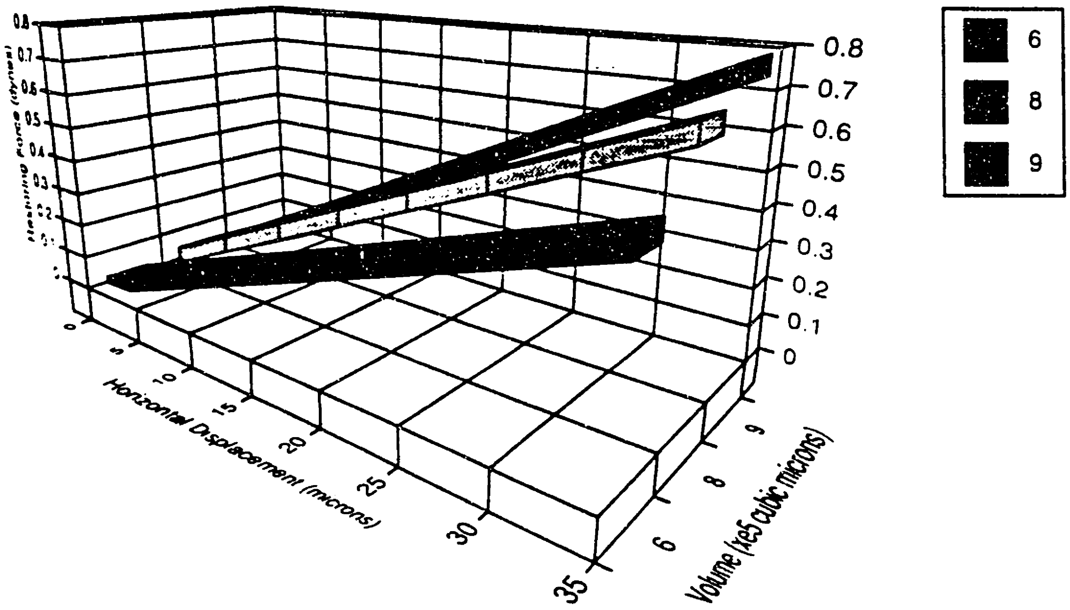

Fig. 5.28: Restoring Force as a function of Horizontal Displacement and Volume of an cross-shaped pad for a 70 micron separation.

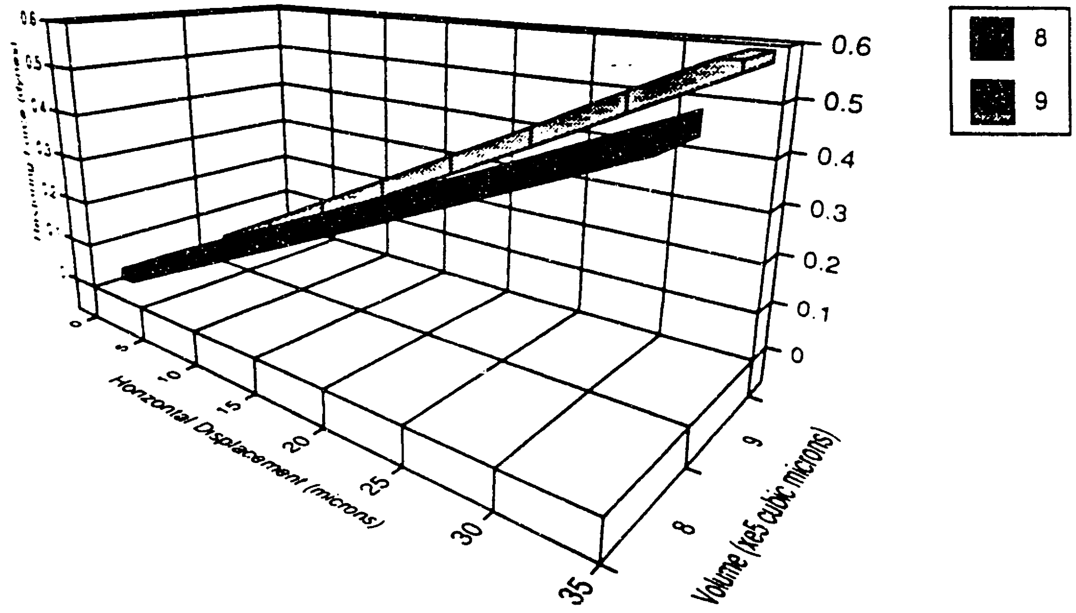

Fig. 5.29: Restoring Force as a function of Horizontal Displacement and Volume of an cross-shaped pad for a 80 micron separation.

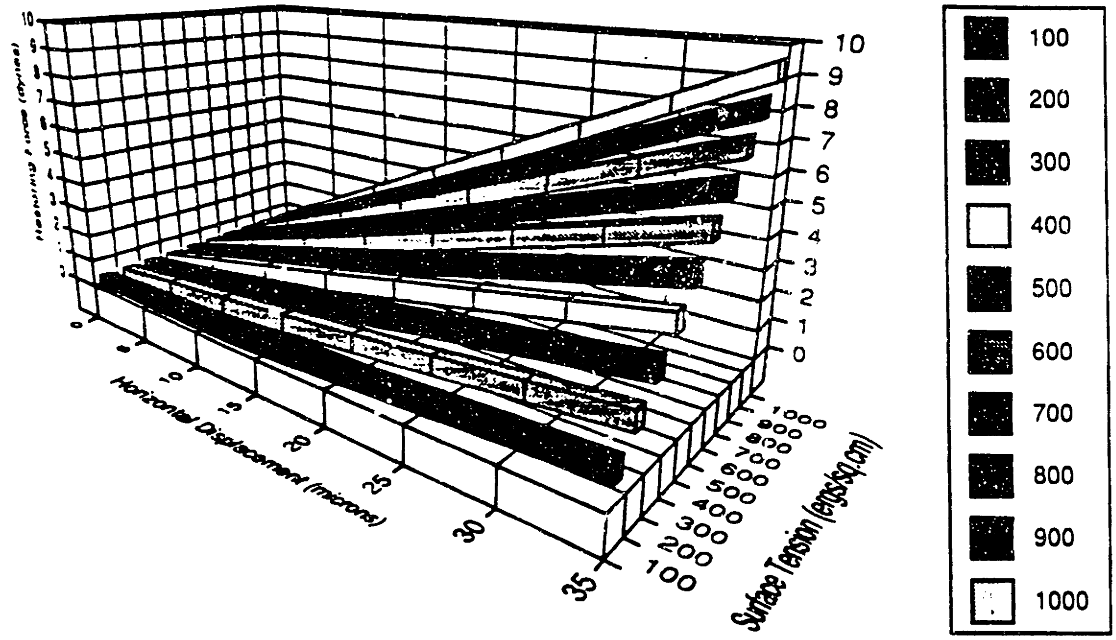

Fig.5.30: Restoring Force as a function of Horizontal Displacement and Surface Tension for a cross-shaped pad for a 60 micron separation.

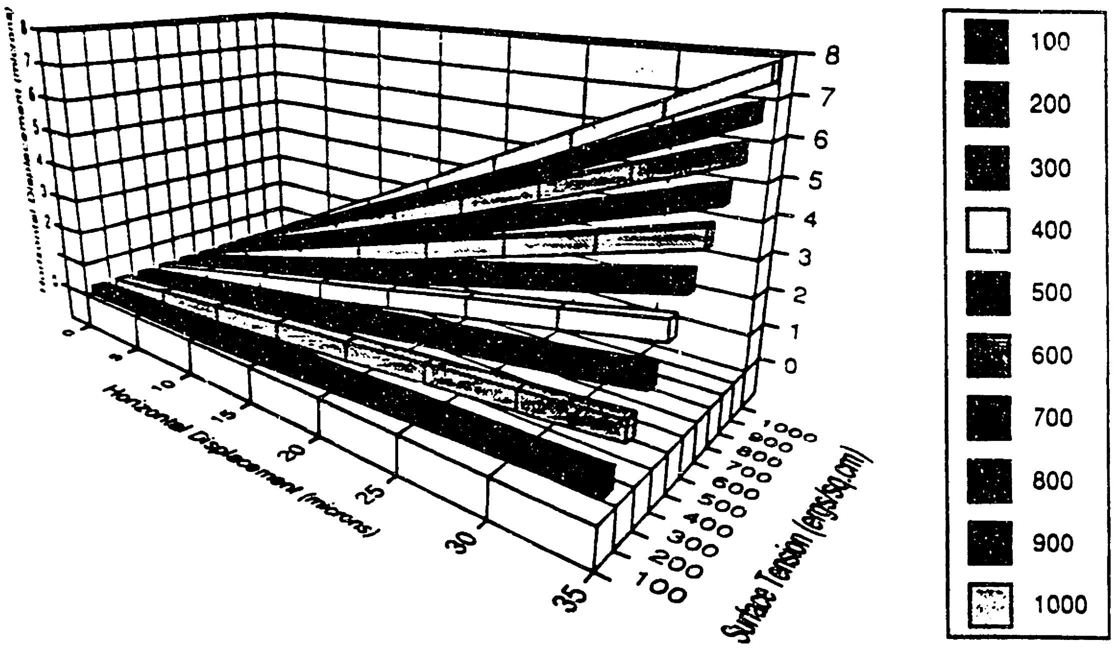

Fig. 5.31: Restoring Force as a function of Horizontal Displacement and Surface Tension for a cross-shaped pad for a 70 micron separation.

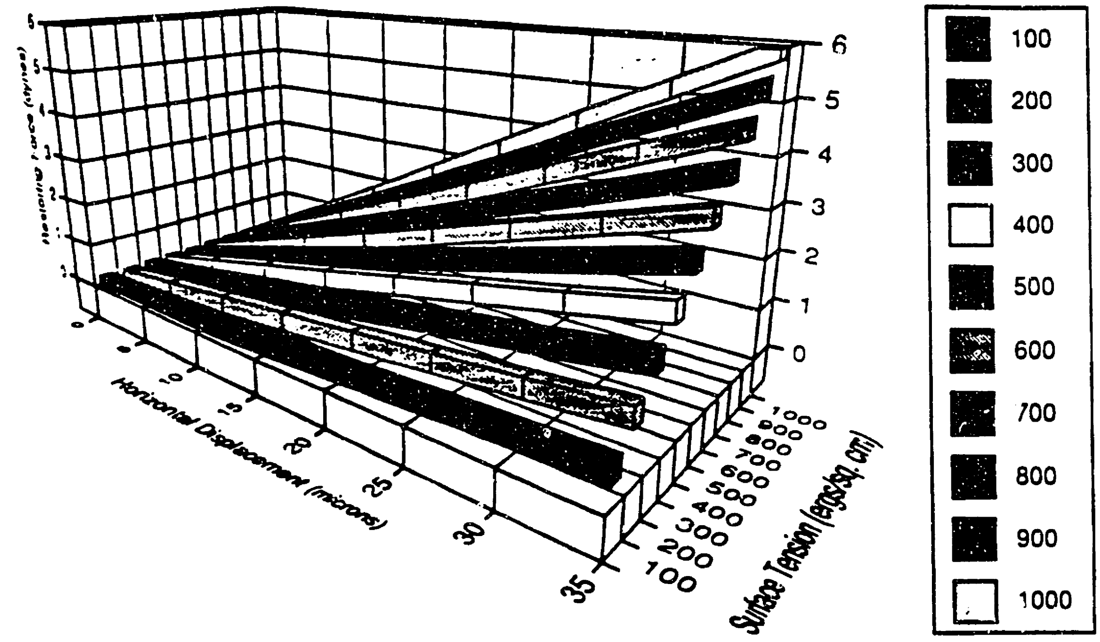

Fig. 5.32: Restoring Force as a function of Horizontal Displacement and Surface Tension for a cross-shaped pad for a 80 micron separation.

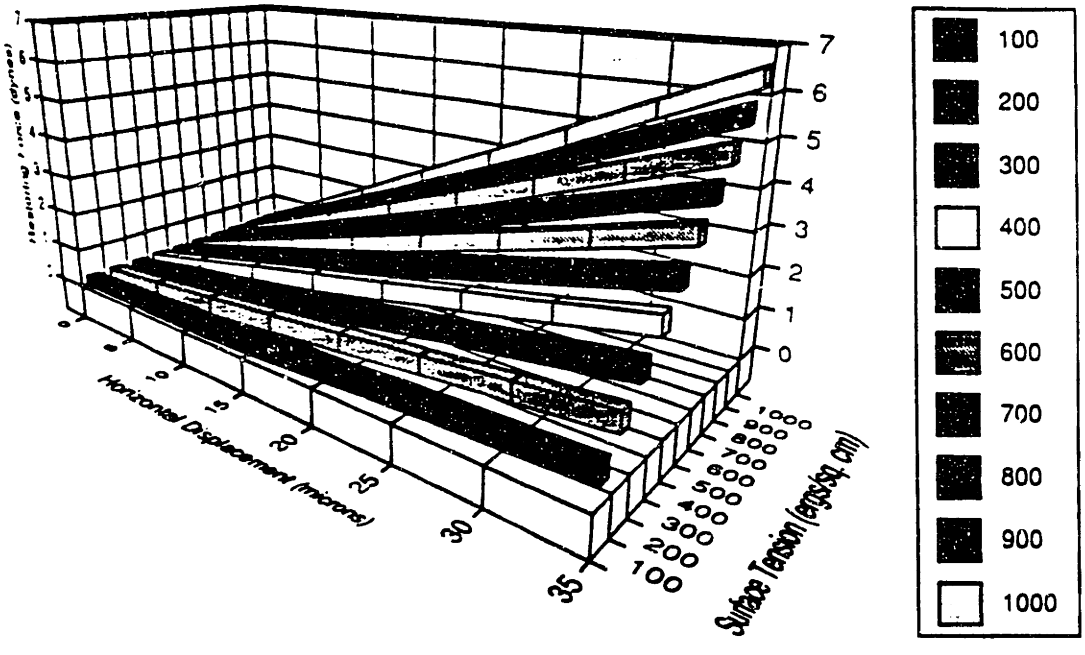

Fig. 5.33: Restoring Force as a function of Horizontal Displacement and Surface Tension for a tetra-star pad for a 60 micron separation.

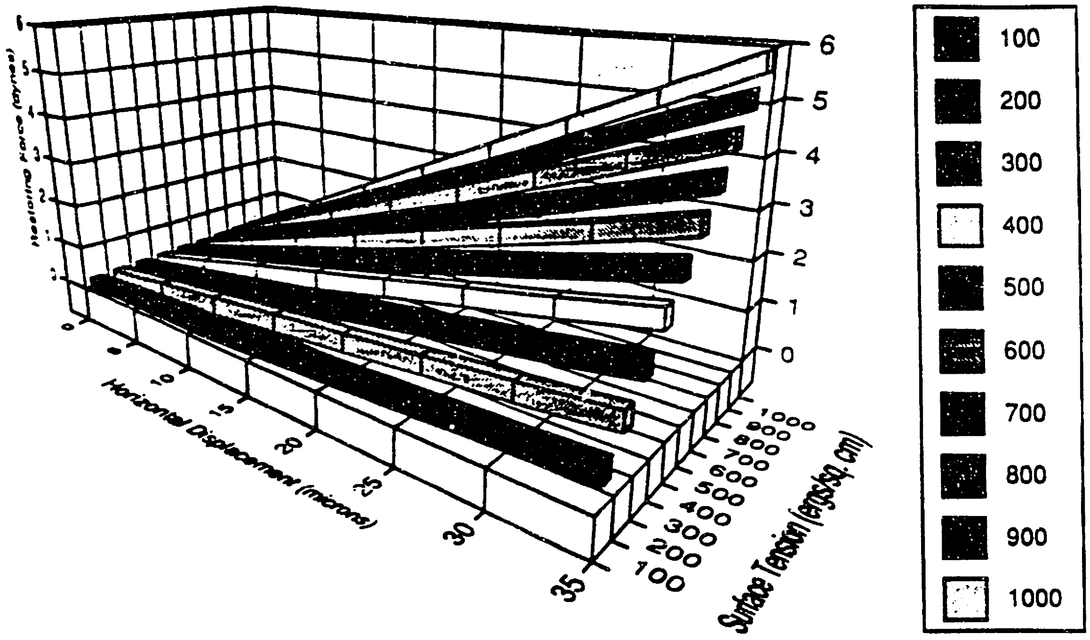

Fig. 5.34: Restoring Force as a function of Horizontal Displacement and Surface Tension for a tetra-star pad for a 70 micron separation.

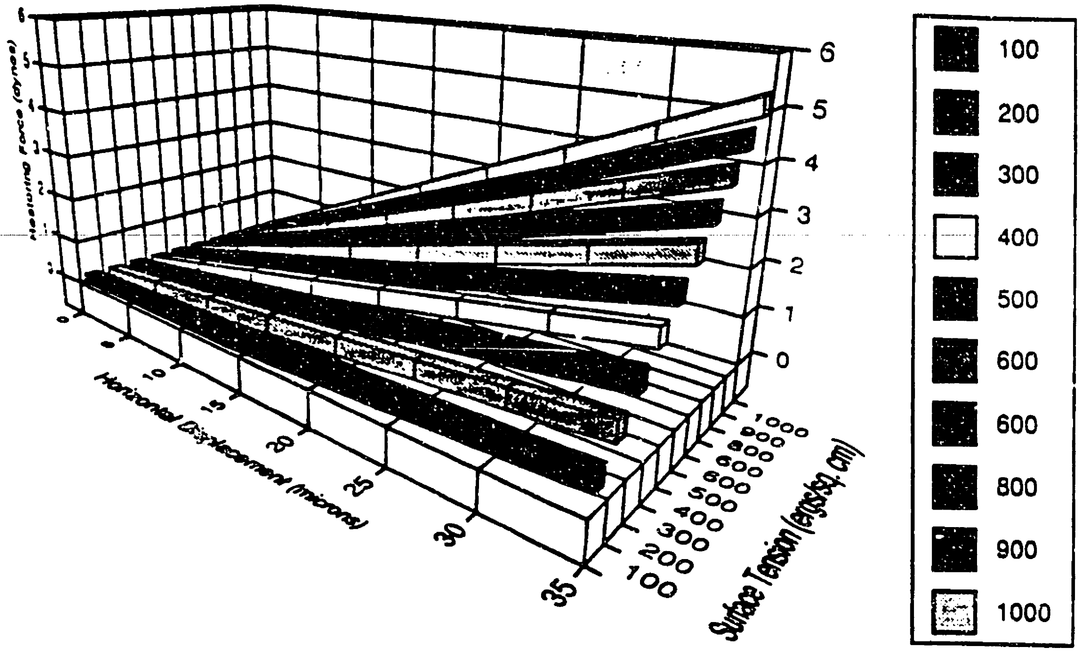

Fig.5.35: Restoring Force as a function of Horizontal Displacement and Surface Tension for a tetra-star pad for a 80 micron separation.

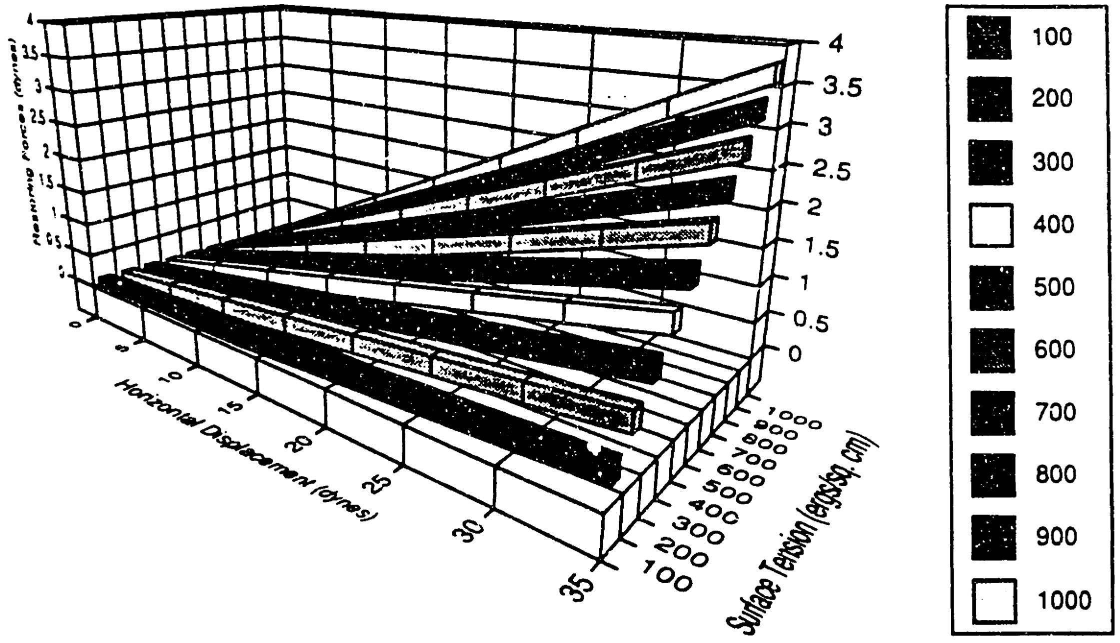

Fig. 5.36: Restoring Force as a function of Horizontal Displacement and Surface Tension for a 75 micron radius circular pad (60 micron separation, Volume = 6e5 cubic microns).

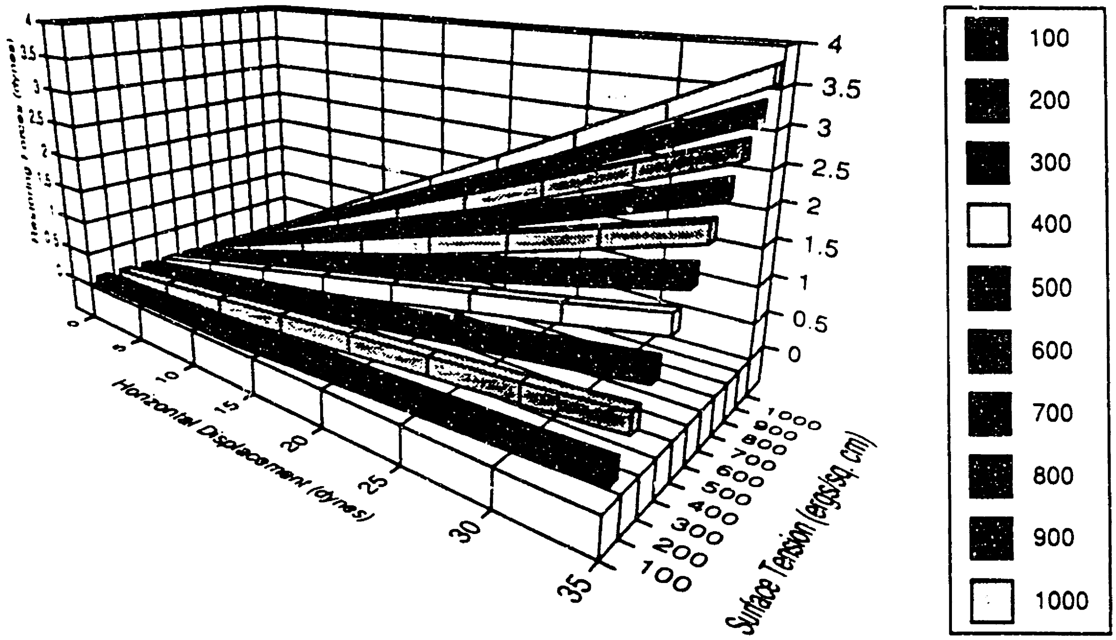

Fig. 5.37: Restoring Force as a function of Horizontal Displacement and Surface Tension for a 75 micron radius circular pad (60 micron separation, Volume = 6e5 cubic microns).

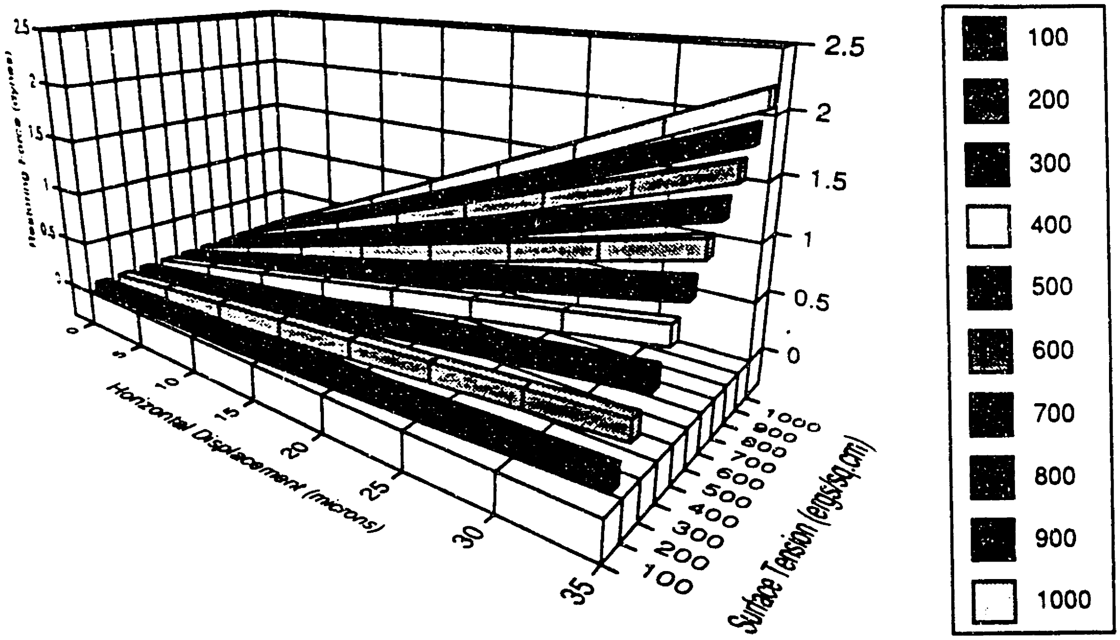

Fig. 5.38: Restoring Force as a function of Horizontal Displacement and Surface Tension for a 75 micron radius circular pad (70 micron separation, Volume = 6e5 cubic microns).

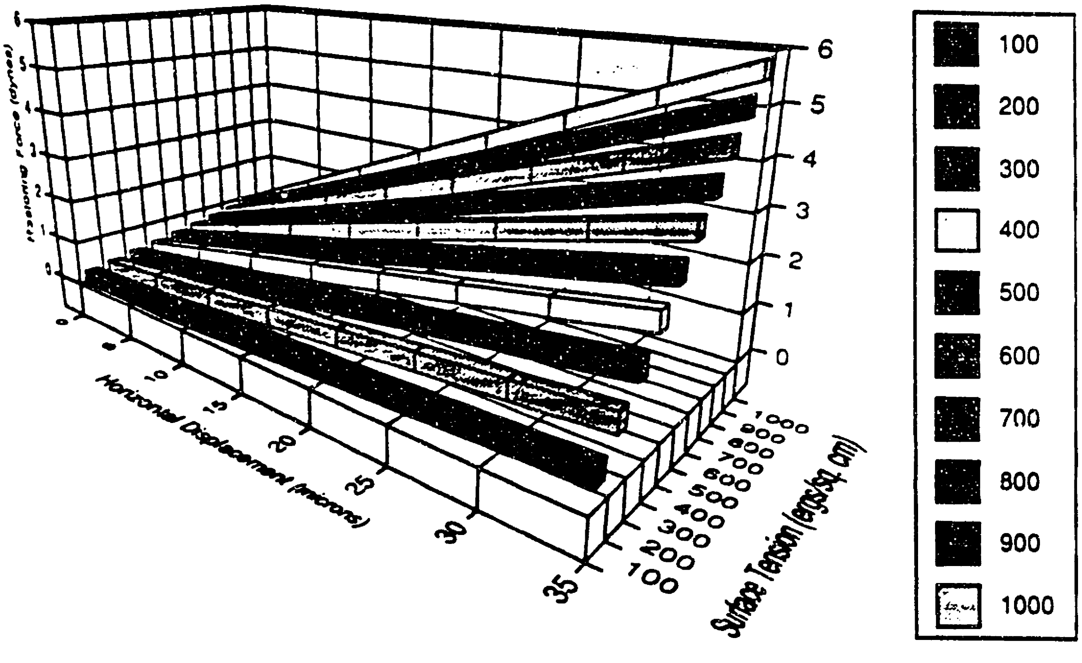

Fig. 5.39: Restoring Force as a function of Horizontal Displacement and Surface Tension for a octa-star pad for a 60 micron separation.

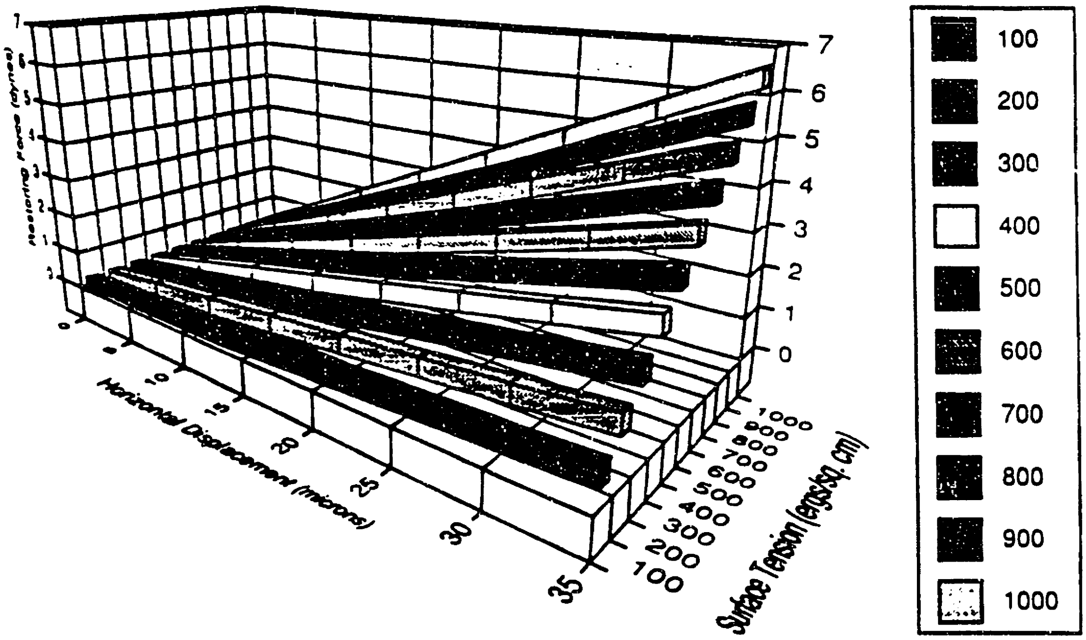

Fig. 5.40: Restoring Force as a function of Horizontal Displacement and Surface Tension for a tetra-star pad for a 60 micron separation.

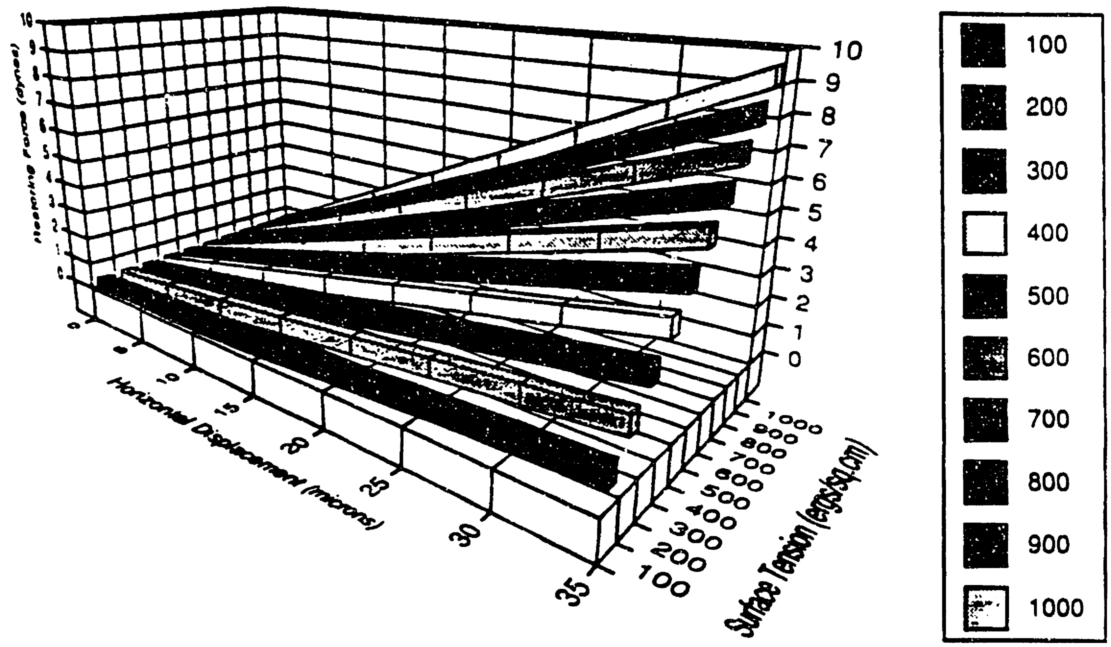

Fig. 5.41: Restoring Force as a function of Horizontal Displacement and Surface Tension for a cross-shaped pad for a 60 micron separation.

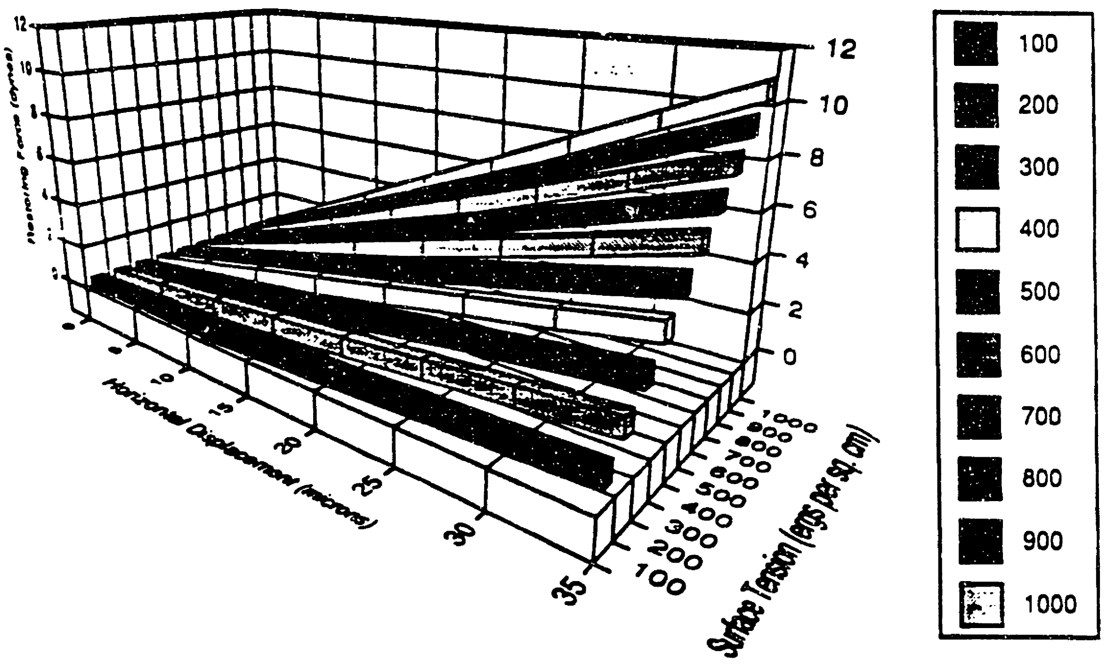

Fig. 5.42: Restoring Force as a function of Horizontal Displacement and Surface Tension for a circular pad for a 60 micron separation.

CHAPTER 6

STATIC HORIZONTAL RESTORING FORCE MEASUREMENTS

6.1 Introduction

The study of horizontal restoring forces in reflow alignment is a growing field, particularly for the high-precision alignment applications. One example of this is in the field of opto-electronics were there is an increasing use of flip-chip solder joints in their liquid state to precisely align fiber optics with terminals and waveguides. Due to the relationship between fiber optic position and signal losses, several studies were performed to numerically calculate the forces necessary to correct mis-aligned components. There has not been a great deal of study on the number of process factors contributing to joint alignment limits. There has also not been any research on developing methods to accurately measure alignment forces during refow; as a result there is no data on the actual magnitude of these forces. As part of the project of developing a good characterization of the system through both models and physical experiments, a series of experiments were performed to relate restoring force to the horizontal misalignment it must correct. An additional goal was the development of experimental methods for measuring capillary system effects.

6.2 Reflow Research-Experimental Measurements

Previous research on horizontal forces has focused on three specific areas. Hayashi [1] studied the accuracy of horizontal alignment and developed a correlation between solder bump diameter and the final position of the chip. Patra [2], developed a series of models of restoring force for a few combinations of solder joint parameters.

McGroarty, Borgesen, Yost, and Li [3], studied the sensitivity of alignment to variations in solder joint volumes. Conway, Borgesen, and Li [4] studied the mechanical stresses and strains associated with solder joints undergoing thermal excursions, while Sarihan [5] developed a temperature dependent viscoplastic simulation of solder joints undergoing thermal cycling.

6.3 Method

6.3.1 Experimental Issues

Three main issues had to be addressed in the experimental arrangement for this method. The first issue was that of controlling and measuring the influence of process environment on alignment force. Normally, reflow soldering is performed in an inert nitrogen atmosphere. This project focused on measuring the magnitude of restoring forces varies for reflow performed in air and comparing this with the results of measurements performed in nitrogen. A second issue that needed to be dealt with in this measurement setup was the influence of vibration on the position and orientation of the sample in their liquid state. Incidental vibration is a possible source of external forces acting upon the fragile joints, so the experimental assembly was isolated with an air table to minimize the influence of external vibration.

An intermediate issue for all the physical experiments was the determination of the in-process position and orientation of the sample. There was a real question as to whether this would be the same as the initial position before the phase transition or equal to an average of the final post-reflow positions of a large statistically valid sample base. Due to the extremely small scale of the system, the high process temperature and the need for an enclosed environment, it was not possible to precisely monitor the exact position of the reflowed chip during the heating and cooling cycles, aside from gross rotations and displacements. A large series of base runs was made with zero external horizontal force in nitrogen atmosphere to determine the equilibrium position of the chip. This was assumed to be the position of the chip during reflow.

The next issue concerned the development of a method of applying a small horizontal displacement force into system in a consistent and smooth fashion so that the sample was not destroyed upon heating. Several attempts were made to develop techniques for applying this type of force in a controlled manner, but each had several limitations in terms of repeatability, consistency and control. The first of two methods used in this research project settled upon using the forces of gravity acting upon the chip and an added known mass to induce a horizontal force of known magnitude. This had the advantages of being easy to implement, avoiding direct contact with the sample and avoiding the need for a large assembly. The last advantage was particularly useful for one component of this series of experiments, which required a sealed nitrogen atmosphere at a controlled temperature.

6.3.2 Experimental Setup

A simplified depiction of the inclined plane heating assembly used in this technique is shown in Fig. 6.1 along with an example of the sample and added mass. The sample carrier shown in Fig. 6.2 was used to load samples in a low flow rate nitrogen oven Fig. 6.3 for the heating stage. This carrier was designed to vary the inclination angle of the samples in the central hot zone of the oven, allowing for variation of the force exerted on the solder joints. It also provided a stable platform for the samples and a way to ensure that the samples were exposed to a constant temperature to guarantee full melting of the solder during heating. The oven was designed to heat the sample evenly over above the melting point and to provide a low nitrogen flow rate to ensure that the environment remained consistently inert.

External forces on the solder joint were produced through the addition of a series of customized weights of varying mass to the approximate center of mass of the upper chip surface.. With the data and the equation described in a later section, it was possible to apply a small, non-destructive horizontal displacement to the solder joints as a function of angle of inclination.

6.3.3 Samples

Samples for the measurement were obtained from manufactured GDX ™ circuits produced by AT&T Bell Laboratories. Fig. 6.4 shows a standard circuit with eight flip-chip mounted devices. Each circuit had previously been fluxed and reflowed on the manufacturing line and discarded later due to bent leads along the edges; otherwise the circuits were undamaged. The circuits were joined with a perimeter array of solder interconnects, seen in Fig. 6.5 with a bump diameter of 160 microns and height of approximately 60 microns. Circuits were diced into eight separate samples around the edges, divided into two separate cases by their specific array pattern, randomized by computer to avoid lot processing linkages and prepared for measurement. The two area patterns differ only by a 180 degree rotation necessary to orient them for placement in the test vehicle. In spite of their similarity in joint volume, height, and pitch, the pattern around the periphery is somewhat different when the sample is rotated. The array pattern for Case A is seen in Fig. 6.6 while the array pattern for Case B is seen in Fig. 6.7

6.3.4 Experimental Methodology

The measurement of in-process displacements began with a measurement of initial positions for each sample. This was performed in terms of the positions of each corner of the chip relative to four permanent fiducials on the substrate in four separate x,y coordinate systems (Fig. 6.8). Measurements were performed using a Nikon Measurescope™, an instrument designed to measure x,y,z coordinates cn integrated circuits. After the initial measurement step, masses were attached directly to the upper surface of the chips using a high temperature rubber cement and the samples were loaded into their carriers. After a 10-minute heating cycle to bring the system up to the solder's liquidus temperature (630+ degrees F), the samples were allowed to plateau at this temperature for up to 5 minutes. They were then cooled slowly far below the melting temperature with the weights still attached. This ensured that the solder joint continued to have constant force applied through the solder phase change from liquid to solid. After the samples had cooled to a temperature with which they could be handled safely, they were examined again to determine their final, post displacement positions using the measurescope.

The measurement process to establish chip position was based on determining the position of each of the four corners of the chips relative to permanent fiducials on the ceramic substrate. The fiducials being used to measure chip position (Fig. 6.9) are used in the reflow manufacturing line to determine chip misalignments. Their layout is standard for all the circuits studied and provided a permanent coordinate system with which to determine the movement of the chip edges.

A key experimental issue that had to be addressed was the determination of actual in-process position of the aligned sample chip. There were two possible measures of this position that had to be evaluated for accuracy. The first measure could be the average of the measured initial positions of a large number of randomly chosen samples. Another measure would be the measured final positions of a large number of pure samples (no added weights) performed for a 0 degree inclination in the nitrogen furnace. Both methods were attempted, and the latter method was deemed the more accurate of the two given the degree of uncertainty in the sample process history. An extra reflow process step under controlled conditions was considered the best way to provide a level measure of the unweighted position of the chips. In both of these methods, the effects of solder consolidation were considered negligible following established experimental procedures for experiments of this type [3]. Several other methods of determining chip displacements were attempted, including x-ray analysis of solder surfaces and metallographic studies of chip cross-sections. Each of these methods had problems, ranging from lack of resolution through device circuit layers (x-ray method) to increasing the number of samples damaged or destroyed after testing (metallographic method). As a result the use of both averaged positions and measured initial chip positions was necessary.

6.3.5 Equations

The main equation used to relate restoring force the experimental setup angle of inclination is shown below:

$$Fres = - Fg \sin \theta \tag{6.1}$$

where:
θ= angle of inclination
F_{res} = restoring force
F_g = force of gravity

Restoring forces were calculated as a function of gravity for a fixed set of added weights. Chip displacements were calculated as the difference between the initial position of the solder (assumed to be the average of a large number of base runs) and the final measured position of the solder. The position of the chip was calculated using the formulas below for the center of mass of the chip:

$$\frac{1}{n} \Sigma \Delta x_i = \Delta x_{cm} \tag{6.2}$$

and

$$\frac{1}{n} \Sigma \Delta y_i = \Delta y_{cm} \tag{6.3}$$

where: $\Delta x_1, \Delta x_2, \Delta x_3, \Delta x_4$ are x coord. of the chip edges
$\Delta y_1, \Delta y_2, \Delta y_3, \Delta y_4$ are y coord. of the chip edges
Δx_{cm} and Δy_{cm} are the x and y positions of the center of mass

In addition to initial and final chip position, chip rotation is measured using the center of mass and the formulas below where:

$$\tan\theta = \frac{1}{4}\left(\frac{\Delta y_1'}{\Delta x_1'} + \frac{\Delta y_2'}{\Delta x_2'} + \frac{\Delta y_3'}{\Delta x_3'} + \frac{\Delta y_4'}{\Delta x_4'}\right) \quad (6.4)$$

where: θ= chip rotation
$\Delta y_1' = \Delta y_1 - \Delta y_{cm}$
$\Delta y_2' = \Delta y_2 - \Delta y_{cm}$
$\Delta y_3' = \Delta y_3 - \Delta y_{cm}$
$\Delta y_4' = \Delta y_4 - \Delta y_{cm}$

where: $\Delta x_1' = \Delta x_1 - \Delta x_{cm}$
$\Delta x_2' = \Delta x_2 - \Delta x_{cm}$
$\Delta x_3' = \Delta x_3 - \Delta x_{cm}$
$\Delta x_4' = \Delta x_4 - \Delta x_{cm}$

In order to measure pure chip displacement only samples with less than a 0.1 degree rotation were included in the analysis.

6.4 Results

Fig. 6.10a shows the results from a set of measurements of displacements performed in nitrogen atmosphere. This series of runs examined the Case A series of samples described previously if the final position was formed by the average of a large number (300) of base samples. The measured restoring force magnitude varied from a low value of approximately 148 dynes for a 4 micron displacement to a maximum of 248 dynes for a 15 micron displacement. Fig. 6.10b shows the results for another run performed with the in-process sample position being the initial position measured before testing. Fig. 6.11a and Fig. 611b show the results from a comparison of Case A and Case B type samples measured under the same processing conditions..

Restoring force behavior is both cases is similar in term of spread, magnitude of force and displacement.

6.5 Discussion

When the measured data is compared with the mathematical model results in Fig. 6.12a and 6.12b, other observations can be made about the accuracy of the measuring system. Fig. 6.12a shows the restoring forces calculated using the average position assumption, while Fig. 16 shows the predicted results reached by assuming that the initial position is approximately the in-process position. The restoring forces predicted by the mathematical models are within an order of magnitude of the measured results (on the order of a few hundred dyne). Restoring forces as measured by both assumptions were several times those predicted by the model and non-linear in their behavior, but still within a reasonable range. As the first attempt at measuring restoring forces, the static measurement results confirm that the restoring forces calculated by the mathematical models developed in Chapters 4 and 5 are realistic.

The high alignment forces measured using this method can be understood by a discussion of the impact the measurement method had on the sample and, by extension, the restoring force. A major limitation of the process is the effect of weight added onto the chip while the solder is in its liquid state, effectively compressing the solder far more in the vertical direction than it would be normally. In this system, the measured post-reflow bump height averaged 35 microns, but there were definite 1-5 micron differences in height from one end of the chip to the other. If these two effects were of course occurring during the heating stage the solder height exposed to this extra weight was probably significantly shorter than the final height measured. Fig. 6.13 shows the predicted influence of solder height on restoring force for a model of the experimental joint system, with higher levels of force being generated for shorter joint heights. Fig. 6.14 shows a predicted solder shape for a 40 micron separation, the limit of the Surface Evolver to resolve without significant contact between the solder and the chip and substrate. A surface formed by an extremely small vertical separation for a fixed volume would have an extremely distorted surface far from the metallization pads, a condition for which the Surface Evolver solution tends to blow up. The measured data is consistent with a data set for a separation within this distorted regime, with increased restoring force for smaller displacements (i.e., a higher slope on the graph) or for a condition where one half of the bumps were seeing a totally different force than the other bumps.

An evaluation of the results of measurements performed using this method yield several insights into both self-alignment behavior and experimental issues that need to be addressed. As the first attempt of its type to measure restoring forces, several other insights into experimental issues were be developed.

One of the first observations of the measured data is its magnitude; restoring force is of the order of magnitude of 100-200 dynes for the range tested. It should be noted that one of the limitations of this process is its inability to measure restoring forces for small displacements from the equilibrium position. Due to the lower limit of force imposed by the weight of the bare chip acting upon the solder joints, the lower range of forces could not be studied. Another observation the can be made about the measured data for both sets of arrays is that they each have the same degree of spread. This spread covers a range of 4-14 microns within each of the randomized cells and increases for increased applied vertical and horizontal force. This error is attributed to the measuring method used, a method based on the accurately determining the positions of each of the four chip edges. During the heating process, some of the chip edges were broken or shattered to varying degree introducing a measurement uncertainty of up to 5 microns. When comparing the two cases of postional assumptions, there seemed to be little difference in either the force level or the displacement of the chip. Both Fig. 10a and 10b displayed a certain amount of spread, but the plots were very consistent. Therefore is appears that each method produces about the same degree of accuracy in calculating the displacement of a system as a function of measured positions after reflow.

Another observation that can be made is that the difference between Case A and B samples is very small in terms of magnitude of force, displacement, and spread of data. This can be attributed to two factors, the first of which is the direction and orientation chosen for this system. Given that the main direction of application of the external force is along an axis perpendicular to the largest differences between the arrays, this data fits nicely with expected behavior. Another factor contributing to this similarity is that the differences between the two arrays are at mostly in the positions of two or three bumps, which when compared to the alignment influence of the other seventeen is still rather small.

In the next Chapter, another experimental method for measuring restoring force is described and it's advantages in addressing the issues mention above will be outlined along with results for a number of samples.

6.7 References

[1] Hayashi, T., "An Innovative Bonding Technique for Optical Chips Using Solder Bumps That Eliminate Chip Positioning Adjustments", IEEE Transactions on Components, Hybrids, and Manufacturing Technology, vol. 15, no. 2, April 1992, pp. 225-231.

[2] Patra, S.K., Lee, Y.C., "Quasi-Static Modeling of the Self-Alignment Mechanism in Flip-Chip Soldering-Part 1: Single Solder Joint", Journal of Electronic Packaging, vol. 113, December 1991, pp. 337-342.

[3] McGroarty, J., Borgesen, P., Yost, B., Li, C-Y., "Statistics of Solder Joint Alignment for Optoelectronic Components", IEEE Transactions on Components, Hybrids, and Manufacturing Technology, vol. 16, no. 5, August 1993, pp. 527-529.

[4] Conway, H.D., Borgesen, P., Li, C-Y., "Elastic Analysis of Flip-Chip Solder Joints Undergoing Thermal Excursions", Journal of Electronic Packaging, Transactions of the ASME, vol. 116, June 1994, pp. 110-115.

[5] Sarihan, V., "Temperature Dependent Viscoplastic Simulation of Controlled Collapse Solder Joint Under Thermal Cycling", Journal of Electronic Packaging, Transactions of ASME, vol. 115, March 1993, pp. 16-21.

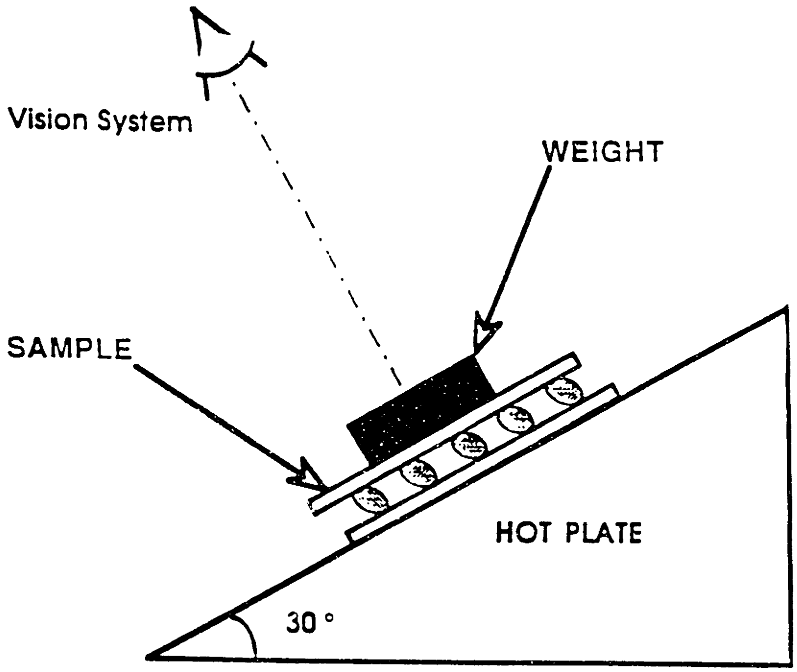

Fig. 6.1 **Inclined plane heating assembly**

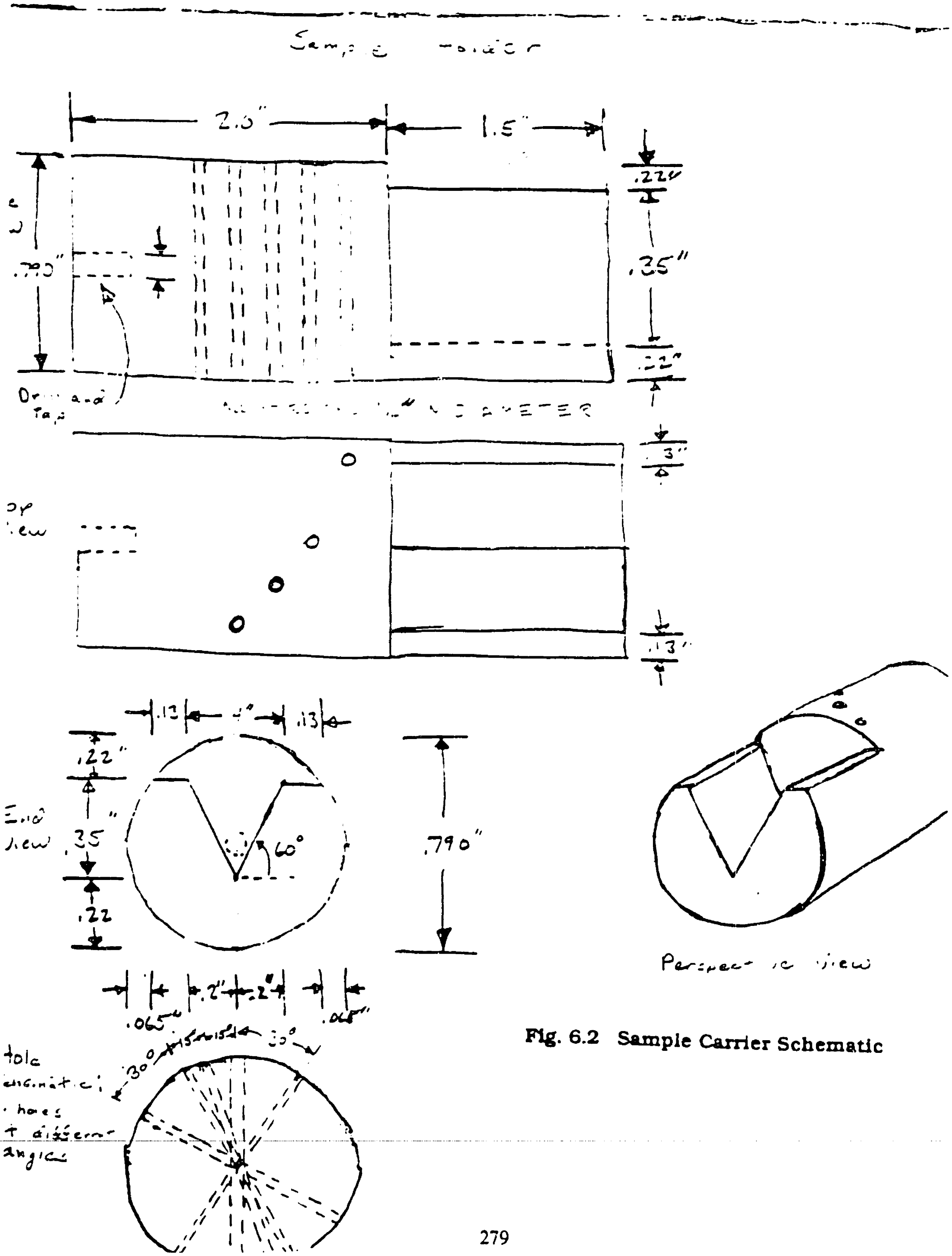

Fig. 6.2 Sample Carrier Schematic

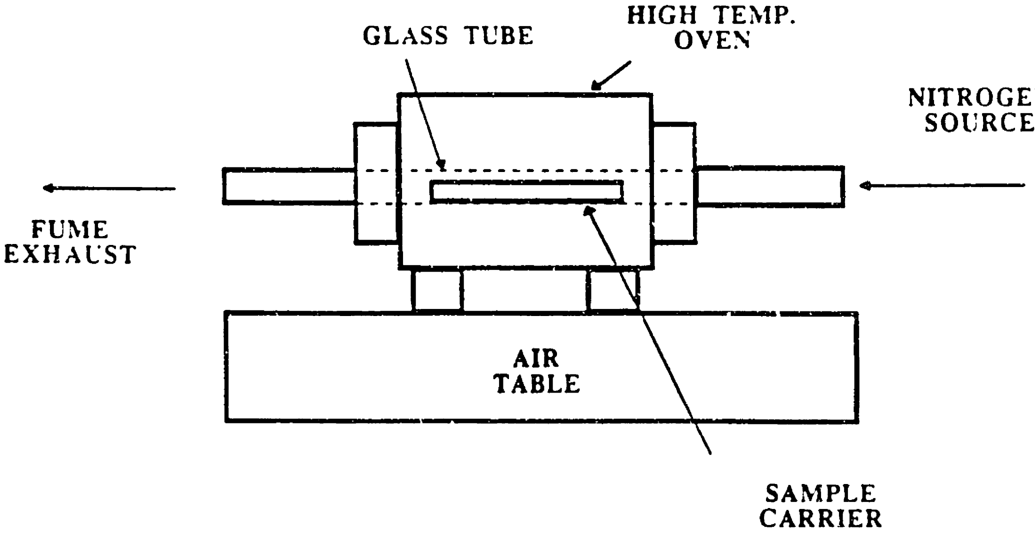

Fig. 6.3: NITROGEN OVEN

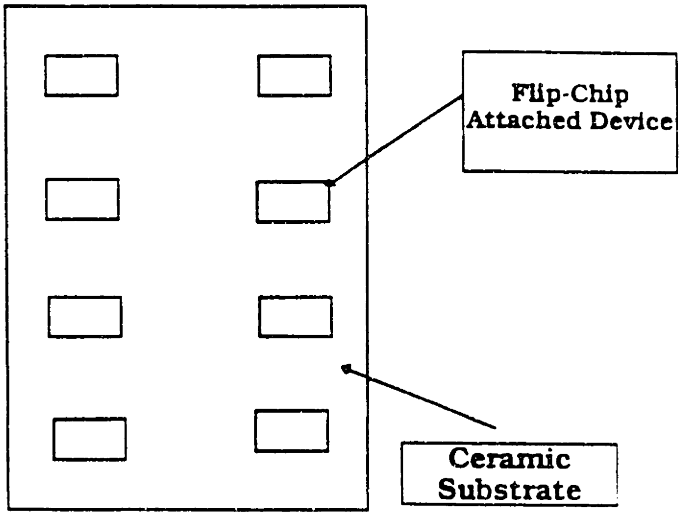

Fig. 6.4: GDX Circuit

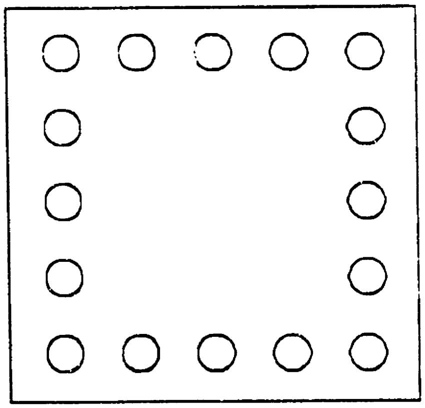

Fig. 6.5: **Standard Perimeter Array**

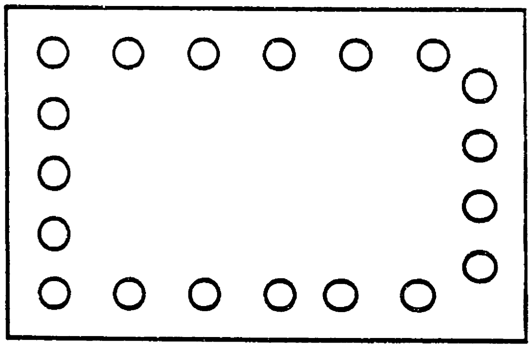

Fig 6.6: Case A Sample Pattern

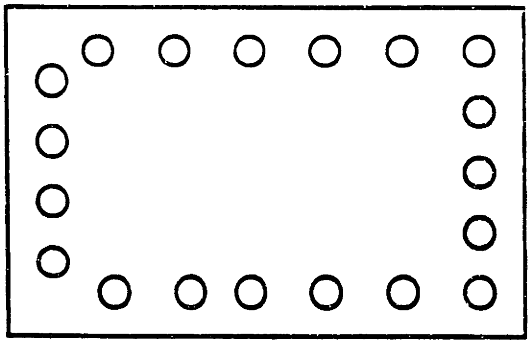

Fig 6.7: Case B Sample Pattern

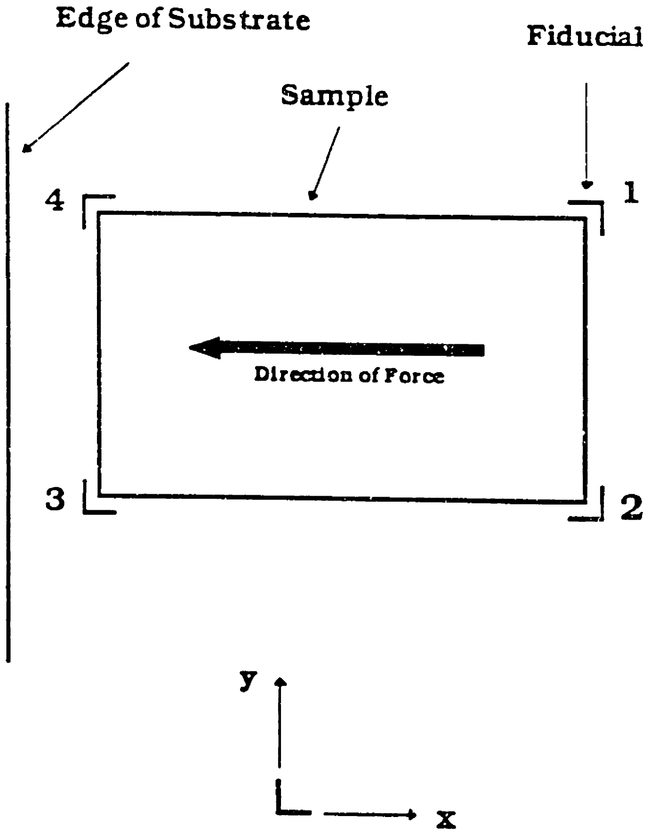

Fig. 6.8: Experimental Coordinate Systems

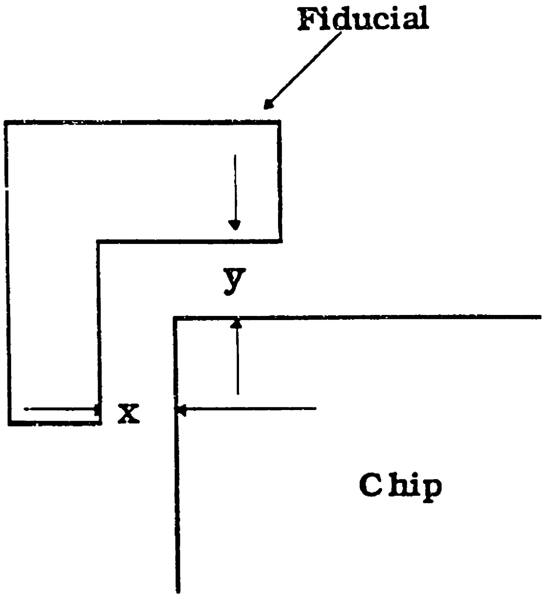

Fig. 6.9: Fiducial and chip edge

Fig. 6.10a: Restoring Force vs. Horizontal Displacement based on an average chip postion.

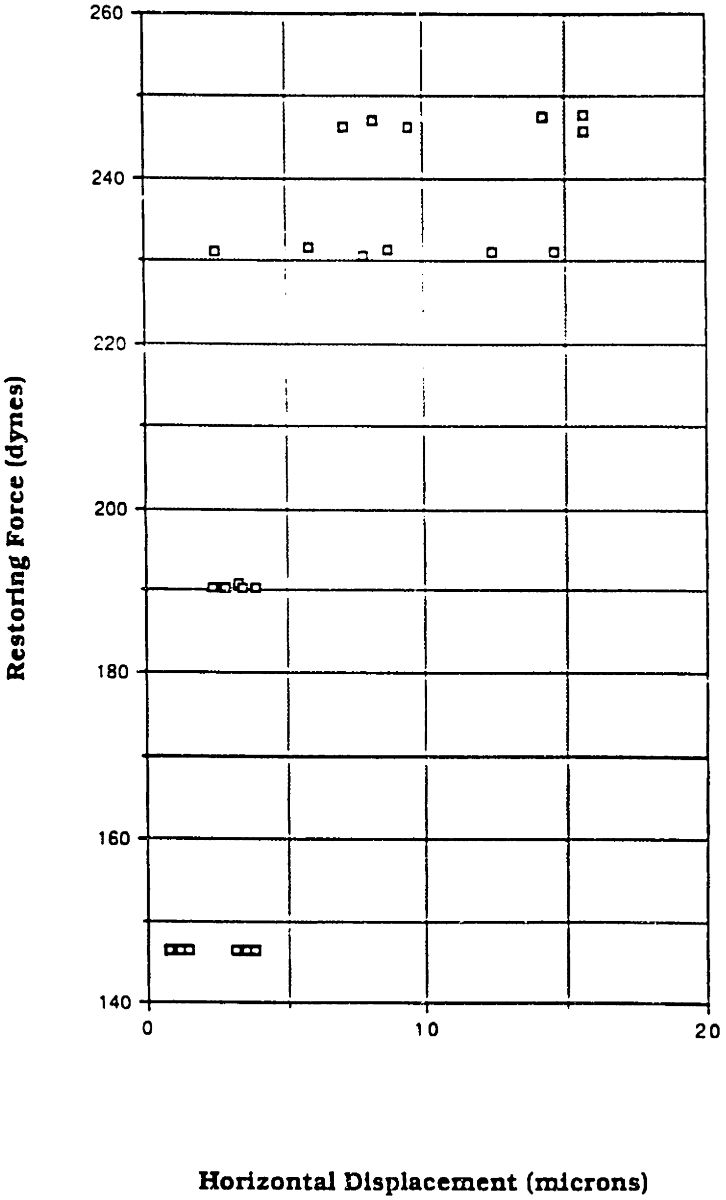

Fig. 6.10b: Restoring Force vs. Horizontal Displacement based on an initial positon measurement.

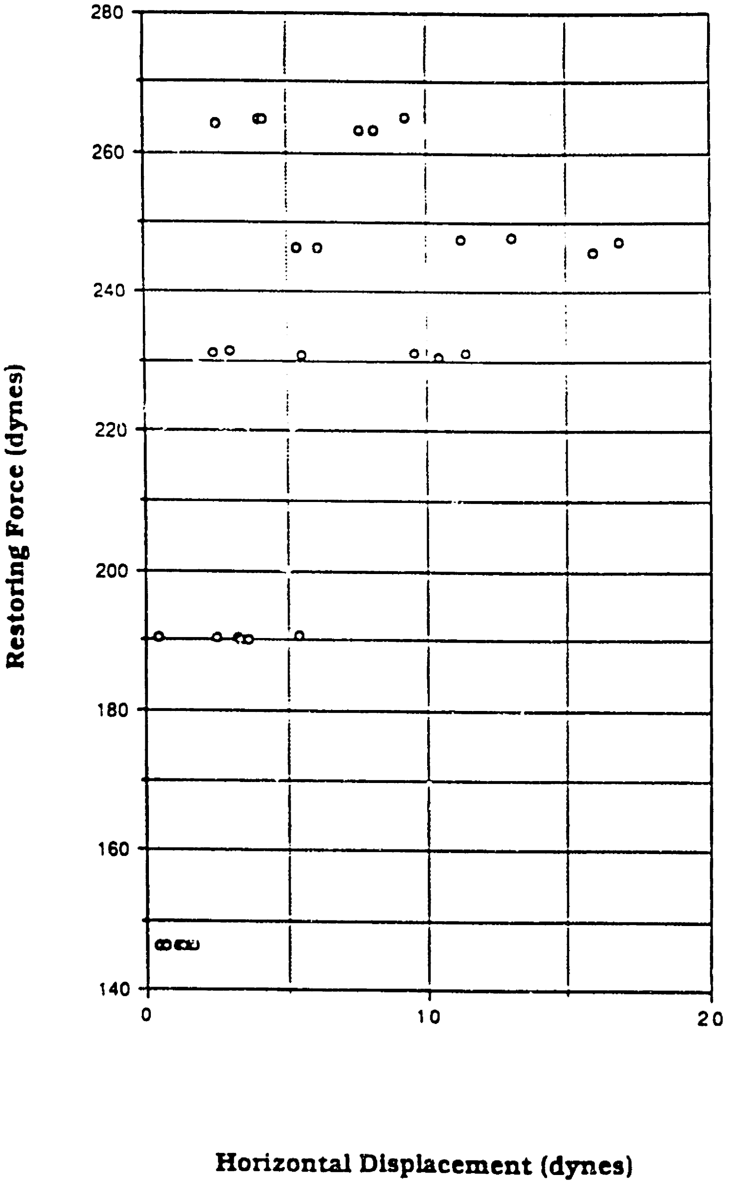

Fig. 6.11a: Restoring Force vs. Horizontal Displacement for Case A samples

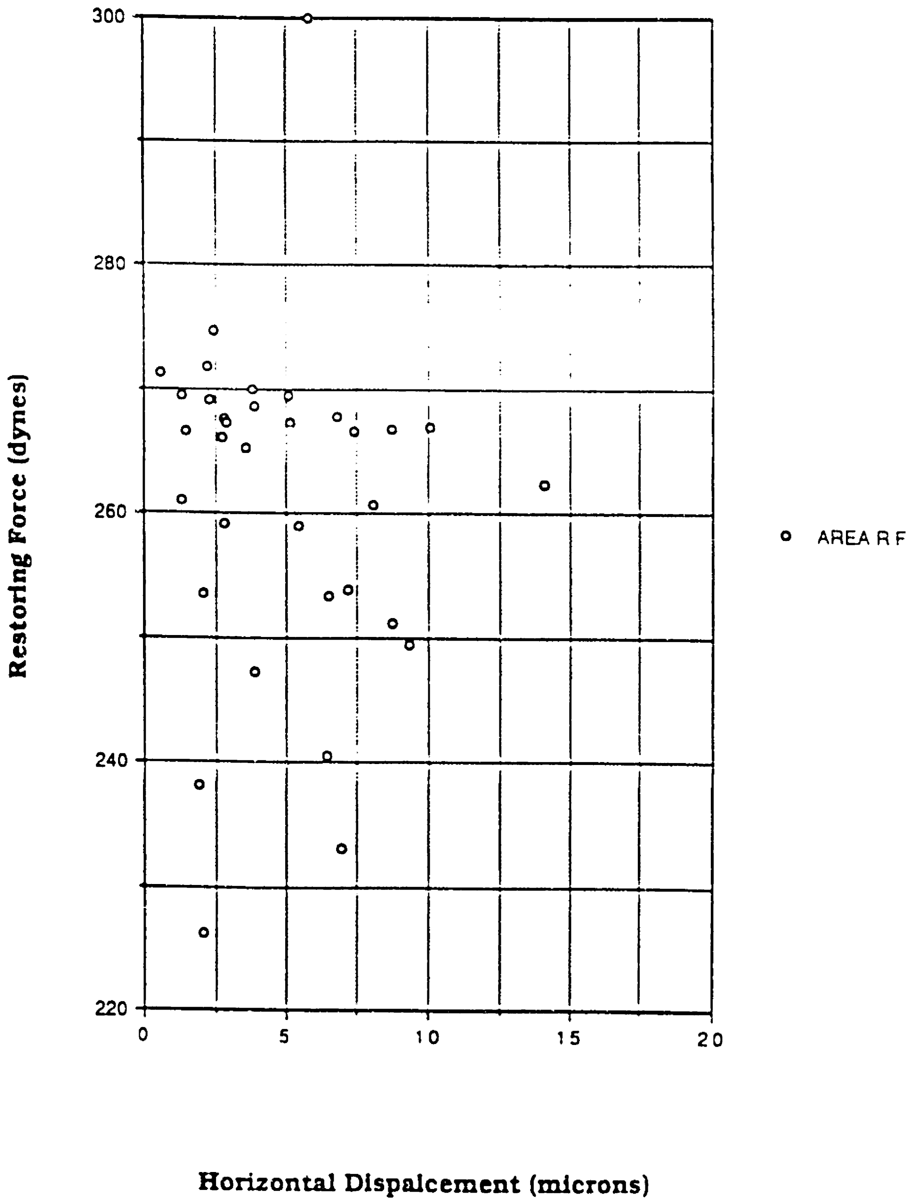

Fig. 6.11b: Restoring Force vs. Horizontal Displacement for Case B samples

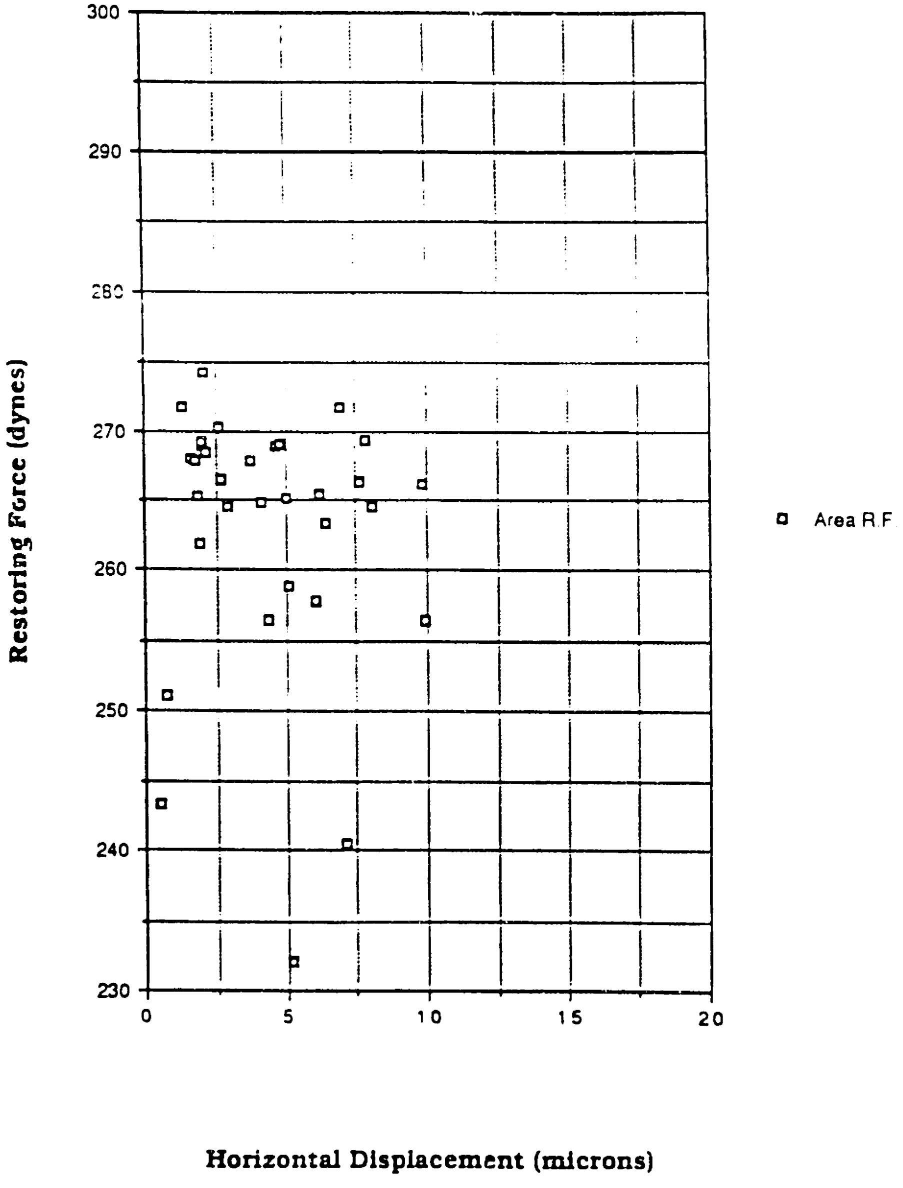

Fig. 6.12a: Static Measurement Results vs. Mathematical Model Results (ave. case)

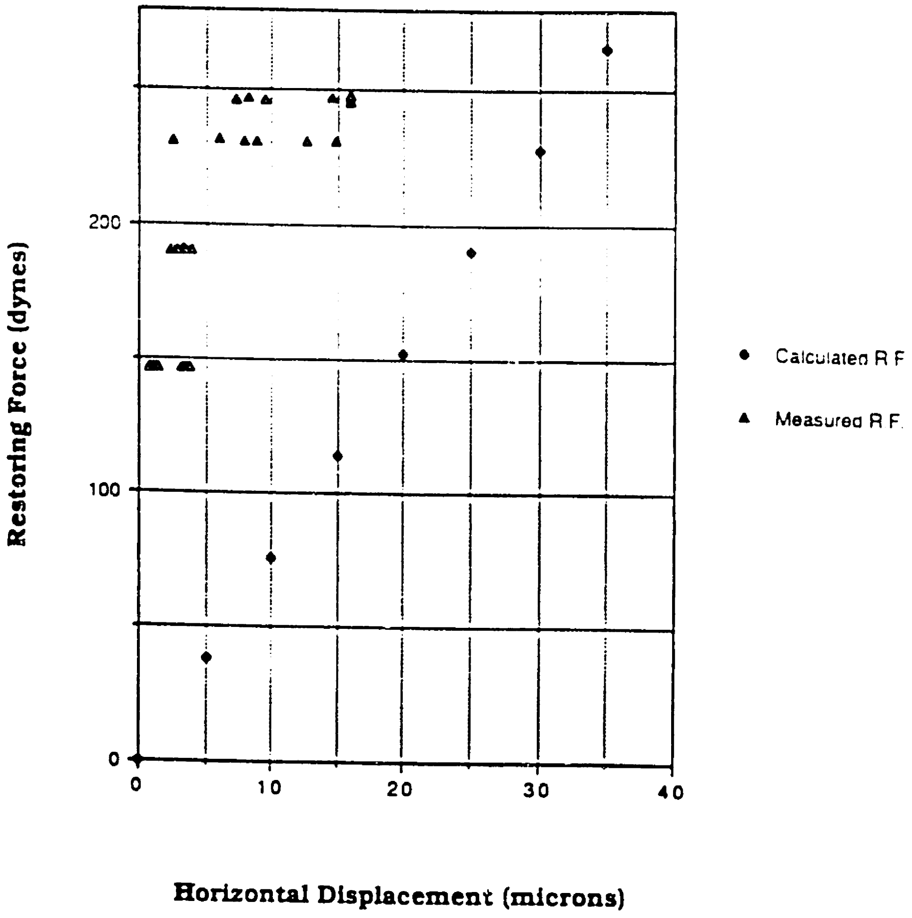

Fig. 6.12b: Static Measurement Results vs. Mathematical Model Results (initial case)

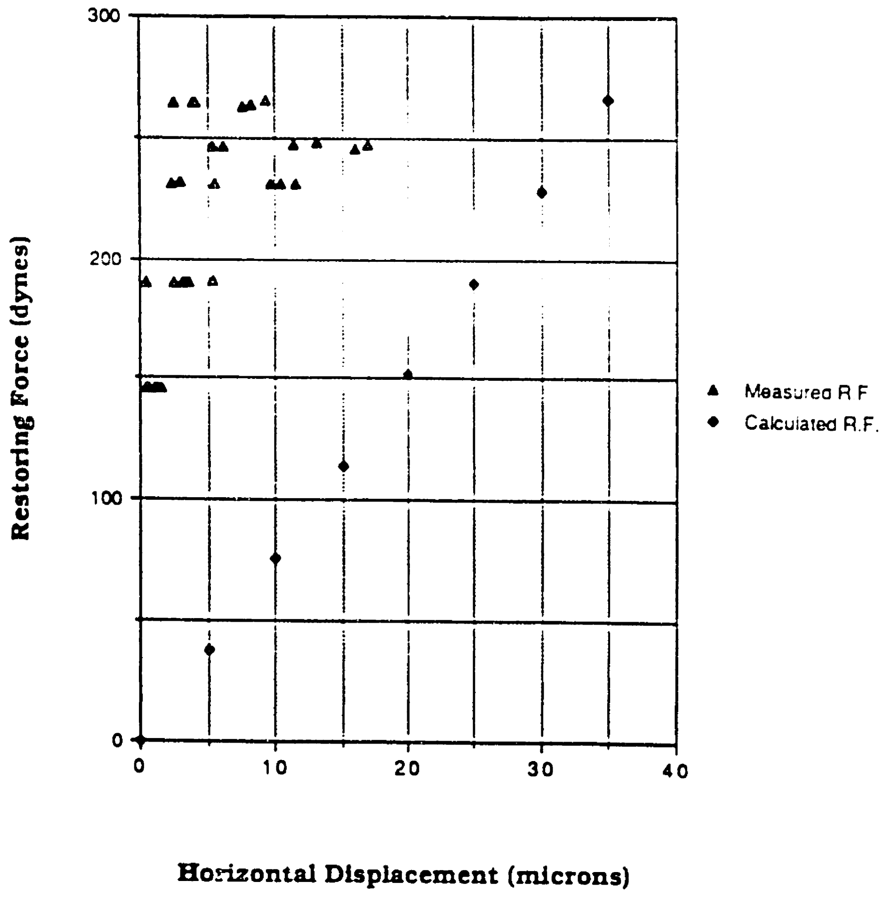

Fig. 6.13: Calculated (Expected) Horizontal Restoring Force as a function of joint height.

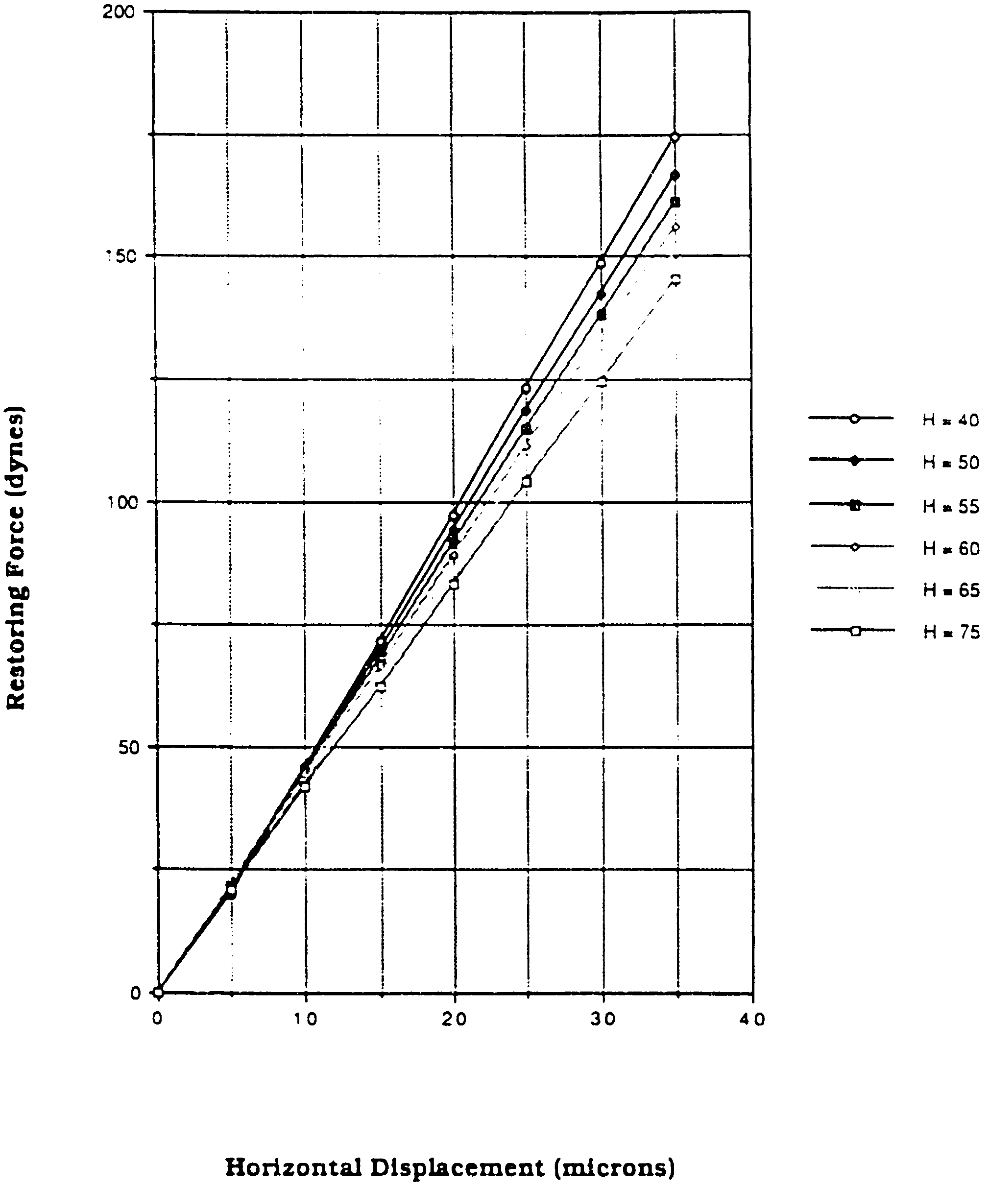

Fig. 6.14 Surface Morphology of crushed joint at limit of Evolver accuracy

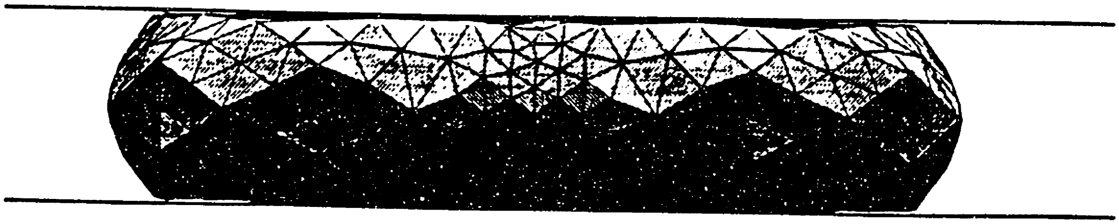

CHAPTER 7

DYNAMIC HORIZONTAL RESTORING FORCE MEASUREMENTS

7.1 Introduction

The second method developed to study horizontal restoring forces was based on inputing a variable external force through direct contact with the reflowed chip. This dynamic measurement method was achieved through the use of a series of thin beams of known characteristics which are use to apply a variable force to displace the reflowed chip at high temperature. In this Chapter, the experimental approach will be described and compared with previous work. In addition results will be presented and experimental issues addressed by this method will be outlined. Finally, recommendations for future types of experimental approaches will be made.

7.2 Dynamic Measurement Research

There have been few physical research projects in the area of dynamic solder restoring force measurement in the past few years as a result of the traditional need for more post-reflow type research. This research has focused on solder joint reliability, thermal fatigue behavior, etc. Literature in area of general dynamic research projects includes the work of Ellis and Masada [1], Heimann [1], and Borgesen [3]. Ellis and Masada focused on developing a dynamic module of tombstoning effects for surface mount capacitors followed by limited data. Heimann developed an optical technique for measuring standoff heights in flip-chip solder bonding in its solid state, while Borgesen studied area array alignment interactions in a statistical manner.

Aside from the work outlined in Chapter 6 of this thesis and the method outlined in this chapter, there are no other methods available for measuring the magnitude of alignment restoring forces.

7.3 Method

The basic approach of this method will be discussed in this section including important experimental issues to be address, experimental setup and equipment, major equations and calculations and experimental methodology.

7.3.1 Experimental Issues

Some of the important issues in this measurement method were based on the need to apply a small, variable displacement force to the interconnects in an accurate and repeatable manner without destroying the sample. These issues ranged from the development of a method of applying a force on the magnitude of dynes to control of the atmosphere throughout an extended heating cycle. The first major issue was the development of a method of applying the a small force directly to the sample without causing many of the secondary external force effects seen in the method in Chapter 6. The system had to be able to apply an external force to the chip surface in one direction consistently for a large number of samples.

A number of methods were attempted, from buoyancy-based systems using a heated flux bath to highly elaborate force generation schemes using small-scale capacitors and sensors. The major limiting factors to force application was of course the small scale of the system (the chip itself is 1 mm2) and the high temperature to which it would be exposed to on a continual basis. Both of the alternative methods above failed due to accuracy and control limitations or due to an inability to apply a force of this magnitude in a dynamic fashion. The method used to apply a force had to be in contact with the chip at the reflow temperature (600 degrees F) without damaging itself or losing sensitivity. As a result of these limitations, the beam approach was used due to its advantages in three practical areas:

1) Controlled application of a dynamic force;

2] Ease of use and it's ability to be controlled easily;

3)Temperature resistance of the stage;

Control of the force is a major issue, as seen in Chapter 6, even extra external forces in the vertical direction can have a large role in determining the level of measured restoring force. In order to address this, the measurement assembly was designed to have limited contact with the sample and to be able to generate a variable force to be exerted primarily in the x-direction of the sample. Given the small size of the size of the samples and the displacements being applied to them, ease of use and the ability to control the force was an important practical factor in terms of consistency and accuracy. As the rough data in Chapter 6 shows, the sample are very fragile at high temperatures and the measurement method as designed to be able to deal with the need for handling these types of samples easily. The final issue, temperature resistance was rather important given the open design of the measurement assembly. Unlike the method described in Chapter 6, this system was not self-contained and required a number of moving parts and assemblies that needed to be able to continue to provide an accurate measure of the applied force and displacement throughout a number of temperature cycles.

In addition to the issue of force application, another major issue was that of the environment of the sample. The issue of environment can be divided in three specific areas;

1) Oxidation effects in the liquid solder

2) Sample cleanliness and handling

3) The Influence of external vibration

Oxidation of the solder in the absence of a non-reducing or inert atmosphere was an issue that several attempts were made to address. One of the limitations of this experimental setup is that it was not possible to do the experiments in an inert nitrogen atmosphere to prevent surface oxidation as in the previous method in Chapter 6. The large size of the lens, vision system, hot plate, and beam movement system assembly as well as the need for manual manipulation of the beam contact with the assembly precluded the use of a closed chamber with a constant atmosphere. In addition, the need for being able to load and manipulate samples during the measurements would have made a lock system difficult to operate efficiently. This necessitated the experiment being done in an ambient atmosphere and as a result, some consideration must be given to this factor in analysis of the data. In order to address this, a number of attempts were made to introduce a series of high molecular- weight rosin fluxes into the sample to prevent oxidation, but these produced a large number of problems including introduction of a large amount of nucleate boiling around the sample and the need for extra ventilation to handle the large clouds of noxious gaseous flux produced.

The introduction of a flux produced an additional sample cleanliness problem because of a charred residue left over from the exhausted flux which obscured the solder/chip interface. This residue could not be easily removed without disturbing the sample and in many cases destroyed samples before the final measuring stage. Additionally, the flux would form a sticky residue that would bond the chip to the beam assembly, resulting in even more destroyed samples. This developed into a serious chip handling and measurement accuracy problem. The best solution to this issue was to heat the sample quickly and apply the force as soon as the chip/substrate/joint system temperature was above the reflow temperature. This introduced some spread in the data due to oxidation and changing solder composition [4], but this error could not be eliminated from the setup; it could only by minimized through careful chip handling and measurement technique.

The final environmental issue to addressed involved the presence and possible influence of external vibration on the sample during the reflow heating stage. Vibration in this system was damped using an air table assembly and an experimental requiring as little in-process manipulation as possible. The beam assembly was effectively isolated from the heating stage and vision system to reduce the influence of vibration. Vibration-associated errors in measurement step were reduced greatly through the use of these isolated assemblies and damping of devices where possible.

7.3.2 Experimental Setup

The experimental setup is shown in Fig. 7.1 and is composed of a heating element, beam assembly, Cognex Vision System, and air table. The heating stage is designed to provide temperatures above the melting point of the solder and secure the samples during displacement. The heating element for the experiments was a hot plate rated to temperatures up to 650 degrees F, monitored by a thermocouple system. The temperature cycle for the experimental measurements included three major stages: a *heating stage*; an *intermediate plateau stage*, where force is applied; and a *cool down cycle* to reform the solder into solid joints. The temperature cycle during the measurements began with an initial 10 minute heating stage from room temperature to above the melting point of the 95Pb/5Sn solder, approximately 630 degrees F. At this point the sample was introduced to the heating system. During the intermediate stage, the temperature was maintained above the melting point for up to 2 minutes while the beam was brought into contact to displace the chip. Immediately after this the final cooling cycle began to bring the system temperature down well below the melting temperature. This stage lasted about 20 minutes.

The Cognex Vision system is an industrial tool for monitoring chip motion through the use of a video camera and monitor, as well as a pattern-recognition system. For each series of measurements, the vision system recognition program is calibrated to provide a monitoring device with a length scale. This allowed for precise in process displacement measurements and observation of the sample to avoid excessive chip displacement. One of the limitations of the system was the high temperature the samples were exposed to during the measurements. The vision system had to be carefully designed, positioned and calibrated to monitor the sample accurately without being damaged during heating. A series of zoom lenses and a specially designed stage were used to view the system in the horizontal plane with good resolution. This allowed the sample to be seen from the side during the displacement step and observed as the beam made contact.

In order to produce a variable force covering a wide range of displacement forces, several different beams of varying length and thickness were used. The beam assembly (Fig. 7.1) was designed to allow movement and manipulation of the beam during the measurement step through the use of a micrometer. Details of the beam assembly including the dimensions and material properties of all deflected beams are discussed below. A sample beam and its deflection range is shown in Fig. 7.2. Dimensional data on each of the beams used is shown in the table below. Each beam was made of Aluminum with a elastic modulus of $2.068e^{-11}$ N/m^2 and was carefully monitored to prevent the presence of bends or curves. The four types of beams were used in order to cover a wide range of restoring forces were:

Beam #	Length (in)	Width(in)	Thickness(in)
1	3.65	.5	.006
2	3.33	.5	.006
3	3.20	.5	.006
4	1.8	.5	.008

7.3.3 Samples

Samples were obtained from the same source as for the experiments in Chapter 6 and prepared in a similar manner. This included an initial measurement of each chip position, a dicing stage and a randomization step (accomplished through the use of a customized computer code). Each individual GDX circuit was divided into randomized cells of six samples each for measurement to insure that the influence of previous processing steps was evenly distributed for all cells. The organizational scheme of two separate cases for each type of perimeter array was used as well. While sample orientation was less of an issue for this experimental method, the previous scheme was continued in order to keep track of each sample type. In order to determine the in process position of the chip, an average of the positions of a number of randomized samples which have not been displaced is used. This provides a good estimate of the in-process position of the chip when the force is applied.

7.3.4 Experimental Methodology

The method used to determine restoring forces and related displacements use a combination of a carefully applied force in the dyne range and a careful measurement of the in-process movement and final position of the chip. The measurement process begins with an initial heating of the sample stage to the melting point of Pb/Sn solder (approximately 630 degrees F). This stage lasts approximately 10-20 min. and at its completion the sample is placed on the heating assembly. While the solder is melting, the vision system is calibrated and the beam produced displacement force is then applied while being monitored through the video camera. The displacement of the chip and molten solder joints is accomplished through the use of the deflected beam brought into contact with the upper sample surface. This stage was accomplished usually in about 2 minutes. While the sample and beam edge are monitored, the upper part of the beam is displaced via micrometer until the sample is moved a small increment. This stage is performed relatively slowly to avoid jerks or excessive bending of the beam, or destruction of the sample. All displacements are displaced in the range of zero to 70 microns to avoid overstretching of the liquid solder. After the chip is displaced, the system is cooled to 300 degrees F to insure that the solder has transformed fully to a solid. To prevent movement of the chip, the beam is kept in contact with the chip until cooling is completed. This cooling stage lasts approximately 20 minutes. The sample is then removed from the heating stage for a final position measurement using the measurescope.

In order to use the beam assembly to apply the forces at different levels, the entire chip assembly had to be monitored in process using a sophisticated vision/positioning system. Careful measurement during the process was a key factor in the experiment due to the need to cover a wide range of possible displacements and to insure that the sample was not displaced too far or destroyed. As a result, the procedure for handling the vision system played a large role in the overall experimental methodology. One of the important parts of the method was maintaining the calibration of the vision system [5] for each sample. Calibration of the Cognex Vision System is performed for each run and is based on a comparison of the measured height of the chip, and the know chip height. This provided a conversion factor for on-screen displacements relating X_{real} to X_{image} for each sample that was guaranteed to be accurate.

7.3.5 Equations

In order to apply a small force to the interconnects in an even, variable manner a thin, narrow beam of known qualities was brought into contact with the chip at the solder melting temperature. The governing equation for the force exerted by the beam is the classic beam deflection equation shown below:

$$P = \frac{3EI\delta}{L^3}$$

where:

P = load at beam end
I = moment of inertia
δ = deflection of beam
L = beam length

where:

$$I = \frac{bh^3}{12}$$

with b = beam width
and h = beam thickness

This equation relates beam deflection to applied load, which for this experiment is the opposite of the restoring force. The beam deflection is calculated by comparing the overall movement of the beam assembly to the monitored movement of the beam tip using a high precision vision system.

The position and determination of the angle of rotation of the chip were calculated using the equations and relationships developed in Chapter 6.

7.4 Results

Fig. 7.3 shows the restoring force for a series of displacements of a number of samples from the Case A type. Fig. 7.4 shows similar data for measurements of the Case B samples while Fig. 7.5 and 7.6 show a comparison of each case with mathematical data for a model of the area array. The model was designed with the same pad radius, an estimated joint height and an estimated surface energy of 900 ergs/sq.

cm.

7.5 Discussion

7.51 Observations

One of the first observations that we can make about our measured data is that in comparison to the mathematical model data, our data is of the same order of magnitude which is from 0-150 dynes per sample. This method avoids the extra vertical force applied in the previous method and the data reflects this change. As a result, we can see a lot of the restoring forces are very similar in magnitude to the values that we calculated. Another major difference in this method is that this method allows for calculation of the lower regions of restoring force and displacement. The measured data for this technique covers the entire range of interest. The mathematical model data for the parameters we estimated the joint to have during reflow are shown in Fig. 7.5 and Fig. 7.6. The linear curve represents data for an array of soldered joints with heights of approximately 40 microns, pad radii of 75 microns and the same volume as the solder originally deposited.

One obvious trend that is made clear by these figures is that there is a difference between the calculated data and measured restoring forces. The measured data shows no real trend toward a linear value and a large amount of spread can also be seen in the data for each level of restoring force. The non-linearity of the data and the spread is most likely caused by variations in the solder joints, an error source that will be discussed below. As a first attempt at measuring the restoring forces, this method provided the first measure of the actual level of the alignment forces, a value that has only been estimated with little confirmation in previous research projects. In this capacity it worked quite well, providing both valuable empirical data and several insights into potential causes of force variation. Another observation that we can make from the data is that the influence of the different pad array positions is not very pronounced. Samples from the Type A batch were similar to the Type B batch in most respects. This points to a lack of dependence of the restoring force on the pitch and arrangement of the soldered joints, but more research should be performed to confirm this.

In comparison to the limited experiments of Patra [4] and others, this experimental data compares fairly well in terms of magnitude of force measured. As a first attempt at developing a measurement method for forces on the dyne level it works well, after manufacturing and environmental error is taken into account. Fig. 7.10 shows a comparison of the physical experiment data to the dimensionless correlations developed in Chapter 4. Fig. 7.11 shows a comparison of the experimental data, the range of current industrial practice, and the mathematical correlation. In both graphs, the measured restoring forces and other process parameters are within the range of values currently used in industry, as well as those predicted by the mathematical models. In terms of industrial practice, the samples used in the experiments represented the upper levels of joint parameters and as a result demonstrated somewhat high levels of force. When compared to the mathematical model data, these joints produced forces somewhat under the maximum force level predicted for solder joints. The shaded region in Fig. 7.10 and Fig. 7.11 represents the spread of the experimental values caused by a number of experimental and manufacturing process factors. These factors, as well as their sources will be discussed in the next section which addresses sources of variation.

7.5.2 Sources of Variation

Some of the spread can be explained partially by measurement errors after the process due to broken chip edges. This sources of error had a variability of ± 5 microns in terms of individual position coordinates. Calculated error for the beam method in terms of vision system resolution was approximately 3-5 microns. Another source of error is variation among the solder joints in terms of solder pad radius, solder joint height, and solder volume. A final source of error is due in large part by the influence of oxidation on the solder joints during the experiment. In this section we will discuss the last two sources in detail, since these seem to be the major sources of experimental error.

Non-uniformity among the solder joints produced a large part of the spread and difference in the experimental when compared to the mathematical model predictions. A basic assumption in the mathematical models was that the bumps were similar across the array, and the experimental results show that this is not the case. It has been shown in Chapters 4 and 5 that variations in joint height, volume, and surface tension can have a large influence on final restoring forces. In the experimental data, we are mainly seeing the results of these types of variations, applied across the array of bumps during the process. Analysis of the process uniformity in terms of radius, surface chemistry and initial bump height showed variations in each of these quantities [5]. Solder pad radius variations of ± 10 microns are common for this particular solder system due to limits of the wet chemistry and etching process. In performing studies of height variations of several non-reflowed initial solder bumps we discovered height variations of ± 10 microns as well, which matched numbers encountered in industrial practice [5], [6]. This would account for some of the data spread, as seen in Fig. 7.4 which shows a calculation of the restoring force variation as a function of radius variation and compares it to the physical experiment data. A variation in restoring force can be seen for radius variations of 10 microns in either direction. Another source of manufacturing variation was the result of different solder joint heights across the array. Measured non-planarity from one end of the samples to the other showed height variations in the outer bumps of ± 10 microns [5]. Fig. 7.5 shows the calculated variation in restoring force for a vertical height variation in this range.

A final source of manufacturing error was produced by variations in surface composition a result of surface oxidation and corrosion of the solder during previous reflow processing steps. and is causing a large variation in restoring force for a particular displacement in the sample joints. There is currently no data on what the exact difference among the area arrays of bumps in chemical composition and surface chemistry and this lack of information remains one of the limiting factors of all the modeling work to date. Empirical evidence [5], [6], [7] does point to a number of chemical factors at work in the solder joints during reflow, including changes in the Sn composition at the surface and the formation of voids within the solder. One analysis showed that Sn compositions at the surface of the solder were essentially zero, due to preferential chemical reactions between the Tin and Au metallization layers. A change in the Sn composition would have affect the chemical interactions at the surface and possibly change the surface tension. At best, only an approximation of the functional relationship between restoring force and displacement in these joints systems can be developed. Fig. 7.9 shows the projected effects of a surface tension variation on restoring force for a modeled joint. Surface tension values for this system have been calculated at 900 ergs/sq. cm [5] under ideal conditions, but changes in surface composition would change this value significantly [8]. A comparison to the physical data shows that a great deal of the spread is covered within this type of variation. Without the presence of a protective flux layer or inert atmosphere, oxidation of some of the solder surfaces is taking place, possibly causing the large variation among the joints in chemical properties. As a result, the measured restoring force is varying as the force varies across the array. The data presented in Chapter 6 shows a smaller spread of displacements and restoring force values for samples displaced in an N_2 environment. This points to the importance of environment and controlled surface chemistry.

An area of future research that would be very useful for continued modeling work in self-alignment would focus on chemical changes among area arrays of solder joints under a number of chemical conditions, including fluxing. This would provide a great deal of useful information into the exact chemical interactions influencing self-alignment. There is currently no experimental data on the influence of oxidation on solder self-alignment, though there is research on solder oxidation in general [8], [9], [10], [11], [12]. This is an area that should be explored more fully in future , particularly in terms of compositional and chemical changes on the solder surface. While this experimental method was designed to quickly heat and cool the samples as soon as possible to avoid extensive oxidation, the results clearly show that there was still a fair amount of oxidation taking place. One key limitation to modeling this type of joint system is the lack of exact information about the actual parameters during processing. With the high temperature and special environment requirements of this system, it is very difficult to develop a system that can monitor joint height, solder volume and surface chemistry during the heating cycle. In addition, the position of the chip during the heating stage had to be estimated as well. As a result, our model data is based on an estimated joint height across the array, an estimated surface chemistry and an assumed solder volume. As the mathematical model data shows, any variation in the properties during reflow can lead to a large difference in measured restoring force. The largest cause of measured data seems to be the difference in surface condition and chemistry among the solder joints during the process, followed by the influence of radius variation and finally height variation. Within the limited information that we have of this systems parameters, the models match fairly well, but there is definitely ample areas for future research.

A number of insights into measurement methods were developed from this experiment. One of the first insights is that dynamic method for measuring restoring force can produce reasonable results when process issues are properly addressed and assumptions are made concerning the chemical effects. This type of method is particularly useful for examining the range of restoring forces as a function of initial misalignments. A second insight is that the model data is within the range of measured forces for a series of displacements. The model results are calculating the correct range of restoring forces given the limitations of our assumptions about the joint geometry. A final insight is the importance of the surface chemistry and it's influence on restoring force.

7.5.3 Recommendations for Future Research

Several recommendations for future research can made concerning directions, methods and experimental setups that should be explored to improve the accuracy of the measurement process. These recommendations include tight control of the sample source, control of experimental environment, a new design for the testing setup and the use of other types of force application methods. Research in each of these areas could provide a great deal of information about the flip-chip process that is currently unknown. It would also greatly improve the accuracy of the measured alignment force results.

The first area of improvement, sample source control, is very important and a great deal of effort needs to be focused on the design and testing of samples and sample processes to insure that variations across the arrays are reduced greatly or eliminated. As the above experiments show, variations in bump radius, bump height and surface chemistry have a large effect on measured restoring forces. There is currently no experimental data on the measured restoring forces for solder joints with different radii or height. There is also a need for investigations into the wet chemistry process and etching technique improvements in order to produce bumps with high dimensional tolerances [5]. For the majority of flip-chip operations using solder joints as mainly mechanical and electrical connections, the tolerances in joint geometry are rather low. With the high tolerance requirements of optical placement applications, there is a great need for higher tolerances on the size and shape of deposited solder bumps. The uniformity of pad radius and bump height for large numbers of bumps in particular should especially be studied due to the combined variation that both of these factors can produce and the influence of non-planarity across the array. Another useful endeavor would be the development of solder bump test vehicles with simplified array patterns similar to the one shown in Fig. 2.9 and Fig. 2.10. A useful application of this would be an series of experiments using 1, 2, 4 and 8 solder bumps in both area and perimeter arrays. This would allow for the measurement of individual restoring forces as well as limiting the potential effect of non-uniform joint interactions. These bumps should have tightly controlled radius, volume and surface conditions and have a detailed process history performed. Another method to increase process control is the use of glass substrates with etched optical markings to increase the measurement accuracy.

The second major area for future research development involves control of the experimental environment. For studies of this type the major environmental factors to be controlled include sample stage vibration, reflow atmosphere or fluxing agent use, and chamber temperature. Sample stage vibration should be controlled through the use of air table setups and isolation or damping of potential sources of vibration like heating elements, etc. from the samples. Chamber temperature control is best achieved with the use of small chambers filled with inert gas and a cooling/heating cooling system designed to raise or lower the temperature quickly. The design of a very small sample stand would also reduce the amount of area and volume to be heated and improve the heating and cooling rate. The use of IR. heating coils within the chamber and a series of cooling vanes or coils on the outer chamber surface would provide an excellent way of controlling the temperature without adding extra external forces to the joint system. Atmosphere control for this system is best achieved in a small chamber as described above with a controlled quantity of inert gas protecting the sample during the reflow process. Due to the need to remove surface oxides from the sample surface, fluxes should still be used to clean off oxide layers prior to measurement. These fluxes should then be cleaned from the samples and the samples stored for processing within an inert environment to prevent the formation of new oxides. Fluxes should not be allowed to remain on the sample surface during the heating and displacement step due to the extra effects of nucleate boiling and the problem of flux residue interfering with the measurement system. Another problem of heated fluxes is the resultant cleaning issues prior to the analysis stage.

The third major area of measurement technique improvement is in the redesign of the experimental setup. Several practical considerations in measuring alignment level forces can easily be addressed through a number of chamber design changes. As mentioned above, the use of a small closed chamber with controlled temperature and atmosphere is necessary for accurate measurements. A closed system with a good heating and cooling system would allow for faster cycling of samples, reducing the time needed to raise and lower the joint temperature above the melting point. The average time for a current experimental cycle is approximately 40 minutes per sample including the heating and cooling cycles, resulting is a slow sample throughput. From another practical standpoint, future experimental stages should include a vision system or microscopy component in order to observe sample movement and position first hand. This type of system combined with the use of etched optical markings would work well for the dynamic beam type of method developed in this project or any other system where observation of the sample during the process is possible. Another practical issue to be addressed is the movement and positioning of the sample on the heating stage. A major design factor advance for future measurement chambers would involve the use of automated or motorized sample positioning and placement. This would make experimental sample displacement more precise and repeatable. Sample handling would be easier, avoiding samples being broken or damaged. It would also insure that the sample is in the same position in terms of linear axes, rotation, and stage level.

Several alternative methods of force application were surveyed for use in this research project. A large number of them were rejected to cost limitations, but at least a few can be attempted with a good probability of success. The main issues in force application described including a smooth method of force generation, the need for limited contact between a probe or displacement rod and the sample, and high precision at high temperature. In terms of producing a force on the levels required to effectively study self-alignment, a dynamic setup similar to the one described in this chapter is preferable to a static setup; this provides a means to apply a specific level of force for a specific displacement. The two method described below were evaluated for their ability to produce this type of force in addition to a precise measurement of chip movement.

The first type of force application method studied involved the use of a capacitance sensor to both measure and apply the restoring force [13]. This method involves not contact with the sample and is able to be used for a wide range of material types. Capacitance sensors can operate in liquid or inert atmosphere environments and offer a resolution of 1 μm. This is currently the best resolution possible of any sensor system. One of the limitations of this type of system is it lack of high temperature tolerance. Capacitance sensors can only operate in the 0-50 deg. C temperature range, far below the reflow temperature need to form liquid joints. One possible way to still use this type of sensor is to isolate it from the inert atmosphere chamber through the use of tightly sealed locks that would allow a probe to be near the sample without interference.

Another possible method of applying and measuring forces would be through the use of a Linear Variable Differential Transformer [13]. This uses electromagnetic induction to sense linear motion. Contact with the sample would be direct via a spring system or the use of a loaded sensor tip. The resolution for this method is virtually infinite; measurements of displacements on the order of nanometers are possible. This type of setup is able to handle temperature ranges from the low cryogenic range to high radiative levels without a loss in accuracy. LVDT is normally used to measure relative motion between objects whose surfaces only move small distances relative to each other. Of the two force application methods mentioned, the latter has the best potential for use in a high temperature, high precision experimental apparatus.

7.7 References

[1] Ellis, J.R., Masada, G.Y., "Dynamic Behavior of SMT Chip Capacitors During Solder Reflow", IEEE Transactions on Components, Hybrids, and Manufacturing Technology, vol. 13, no. 3, September

1990, pp. 545-552.

[2] Heimann, P.A., "Measurement of the Standoff Height, Between a Flip-Mounted IC Chip and Its Substrate", IEEE Transactions on Components, Hybrids, and Manufacturing Technology, vol. 14, no. 1, March 1991, pp. 187-191.

[3] McGroarty, J., Borgesen, P., Yost, B., Li, C., "Statistics of Solder Joint Alignment for Optoelectronics Components", IEEE Transactions on Components, Hybrids, and Manufacturing Technology, vol. 16. no. 5, August 1993, pp. 527-529.

[4] Patra, S.K., Lee, Y.C., "Modeling of self-alignment mechanism in flip-chip soldering--Part II: Multichip solder joints." Proceedings-Electronic Components Conference, 1991, pp. 783-788.

[5] Marinis, T., AT&T Bell Laboratories, personal communication, 1992-1995.

[6] Dudderar, D., Wong, C.C.., AT&T Bell Laboratories, personal communication, 1991.

[7] Ophila, R., S. Deering, unpublished paper on influence of flux residue and solder dewetting in void formation, 1994.

[8] Shipley, J.F., "Influence of Flux, Subsrate and Solder Composition and Solder Wetting", Welding Journal , 1975, 54, (10), pp. 357s.

[9] Deshmukh, R.D., Brady, M.F., Roll, R.A., Shmulovich, J., Zolnowski, D.R., King, L.A., "Active Atmosphere solder self-alignment and bonding of optical components", International Journal of Microcircuits and Electronic Packaging, vol. 16, No. 2, 1993, pp. 97-108.

[10] Pickering, K., Southworth P., Wort, C., Parsons, A., Pedder, D.J., "Hydrogen Plasmas for Flux Free Flip-Chip Solder Bonding", Journal of Vacuum Science Technology, vol. 8, No. 3, May/June 1990, pp. 1503-1508.

[11] Di Giacomo, Giulio, "Oxidation of Pb-Sn Eutectic Solder and Degradation of Thermal Contact Resistance", Proceedings of the 1986 International Symposium on Microelectronics, International Society for Hybrid Microelectronics, 1985. pp. 322-327.

[12] Miller, R.G., Bowles, C.Q., "Oxidation of 63Sn/37Pb at typical soldering temperatures", Oxidation of Metals, vol. 33, no. 1-2, Feb. 1990, pp. 95-101.

[13] Trumper, D.L., M.I.T., Mechanical Engineering Department, personal communication, 1994.

Fig. 7.1 Beam Assembly

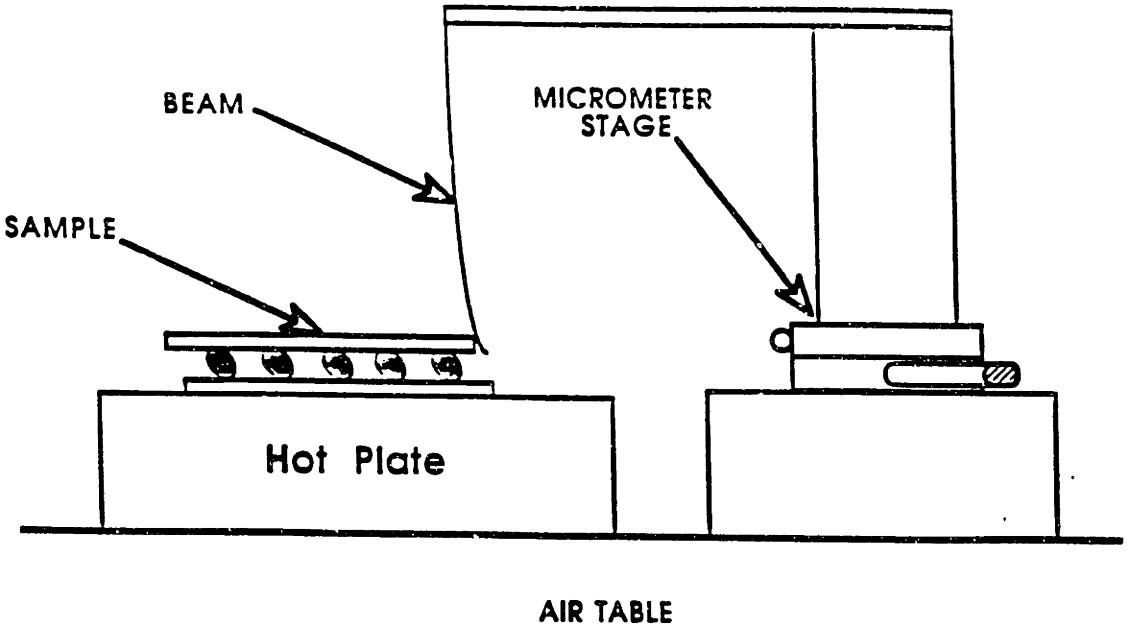

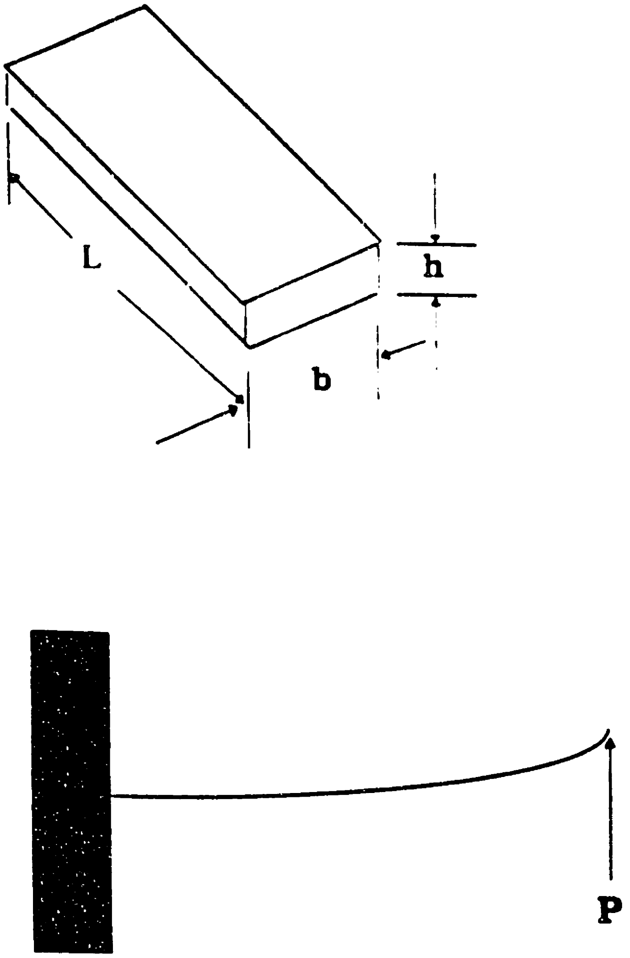

Fig. 7.2 Sample Beam Dimensions and Deflections

Fig. 7.3: Restoring Force vs. Horizontal Displacement (Case A)

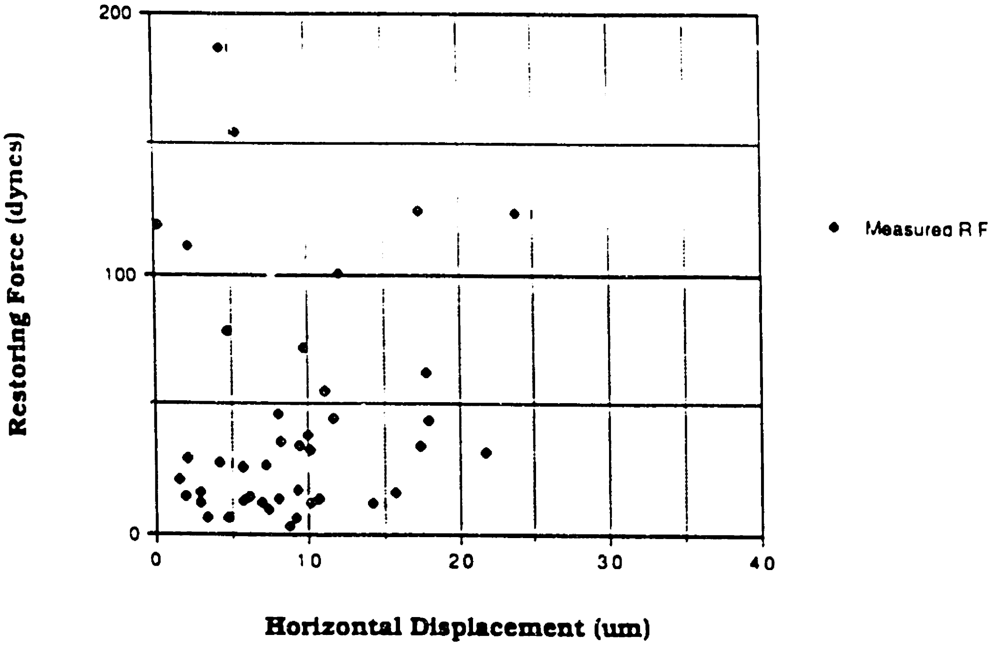

Fig. 7.4: Restoring Force vs. Horizontal Displacement (Case B)

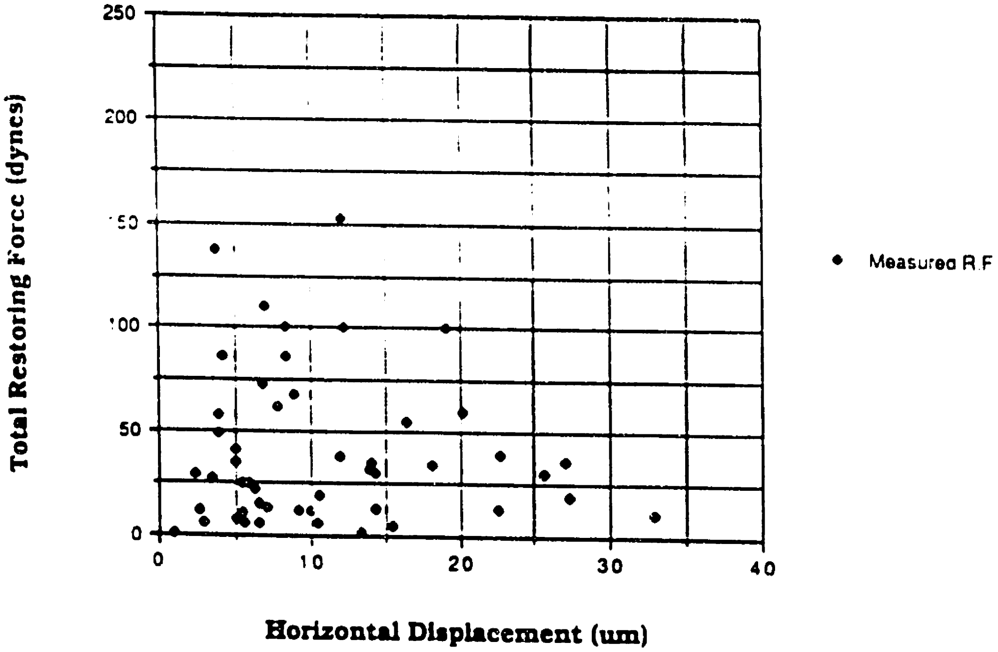

Fig. 7.5: Physical Measurements vs Mathematical Calculation results (Case A)

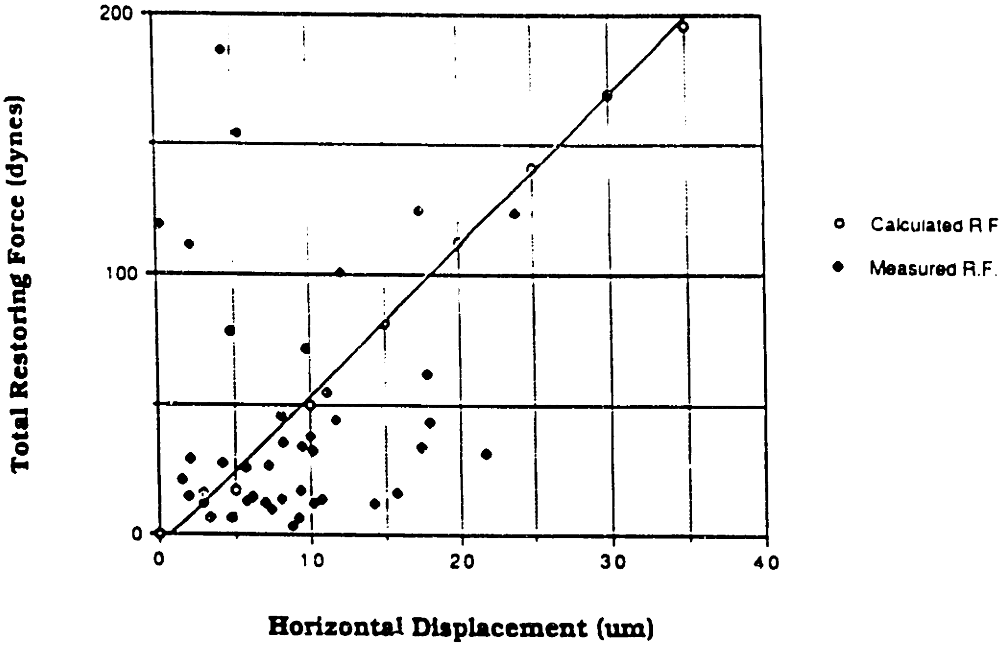

Fig. 7.6: Physical Measurements vs Model Calculation Results (Case B)

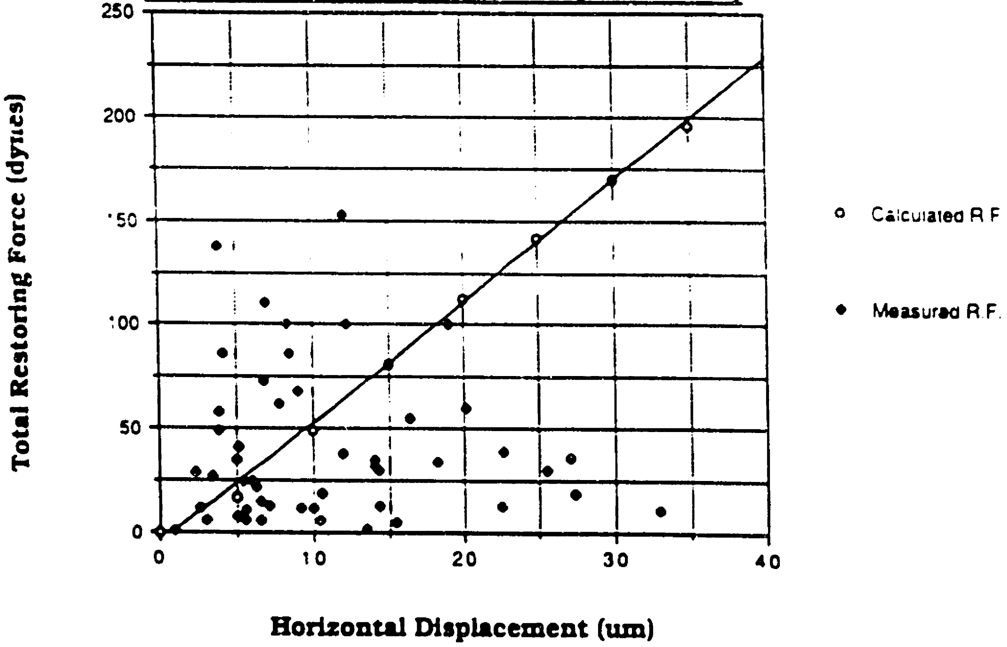

Fig. 7.7: Calculated influence of radius variation

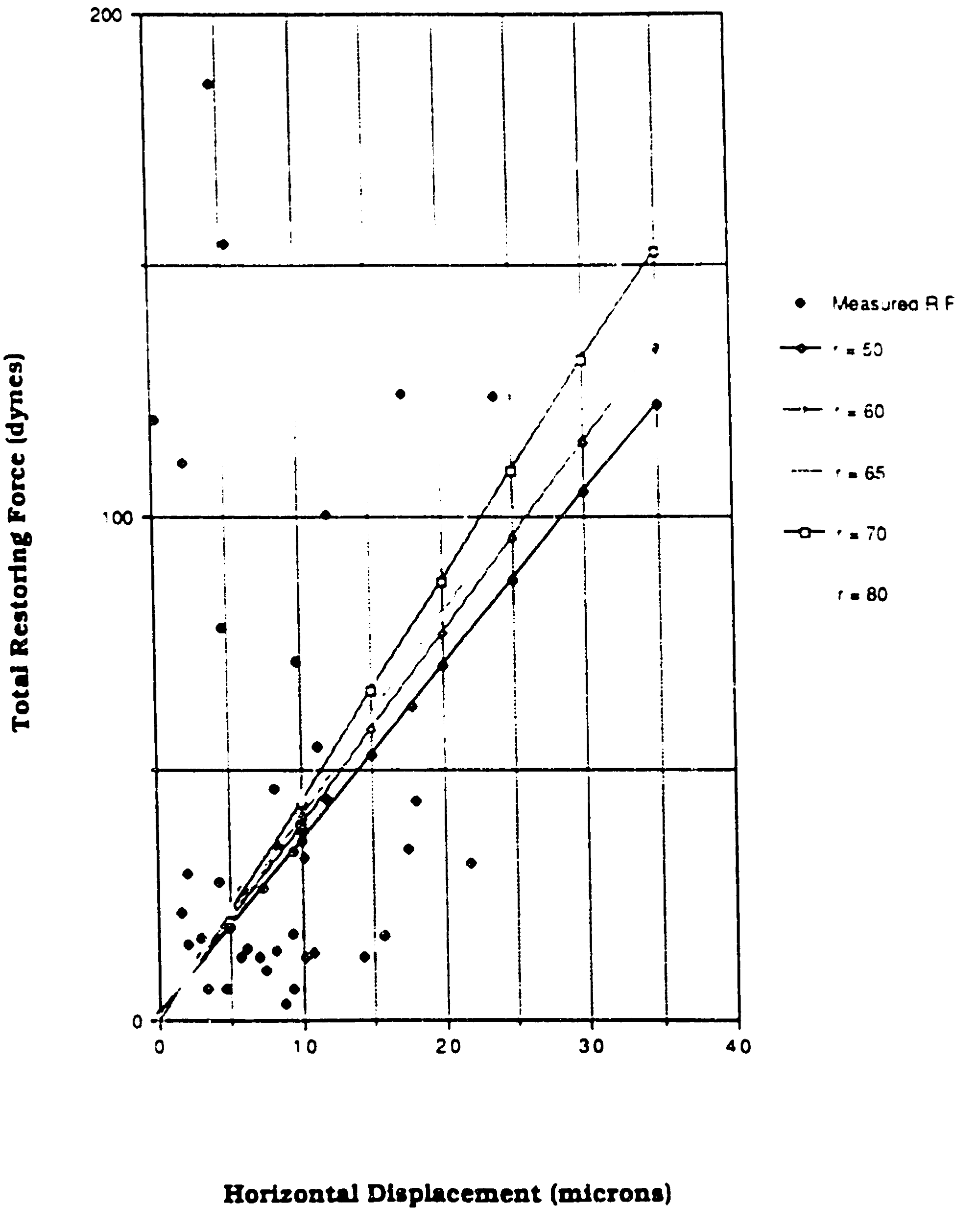

Fig. 7.8: Influence of joint height variation

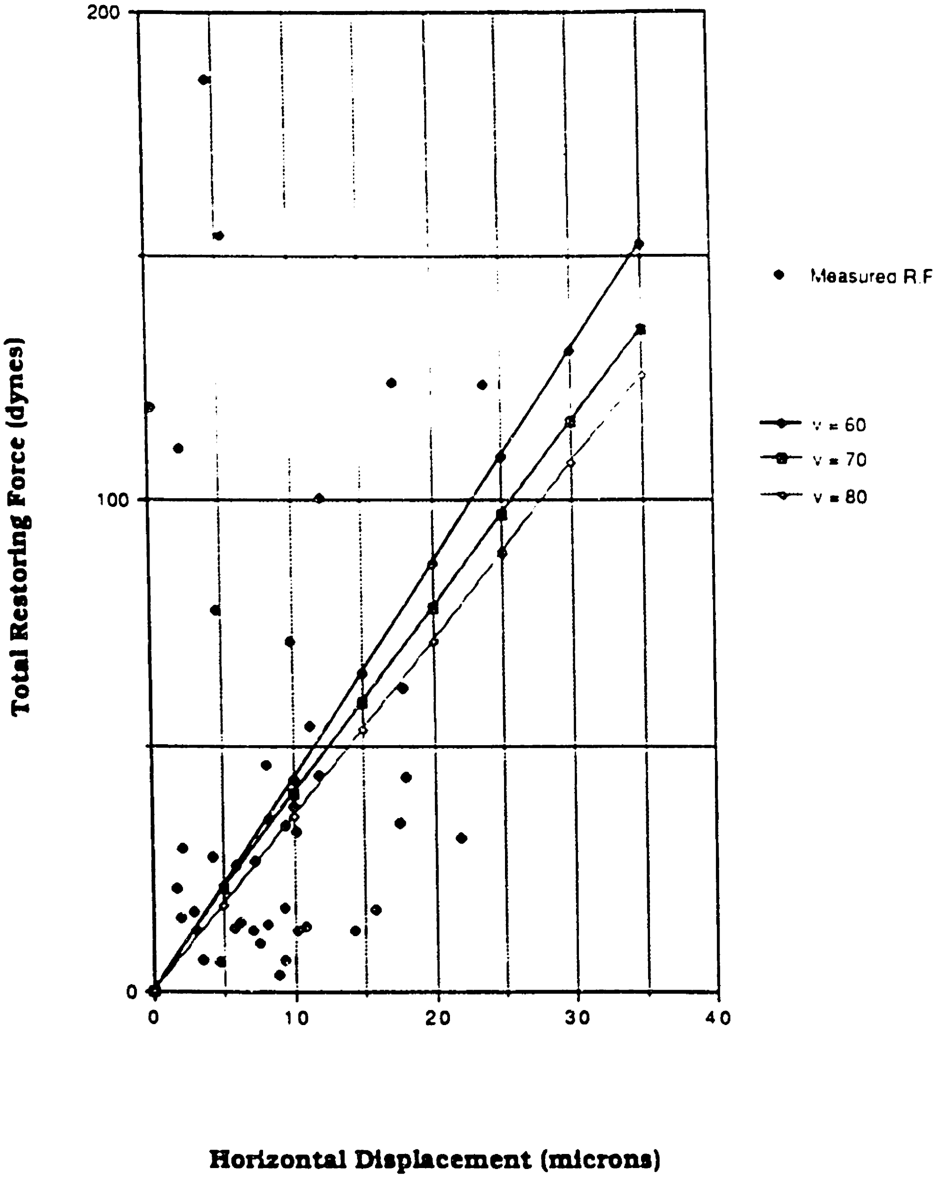

Fig. 7.9: Calculated influence of gamma variation

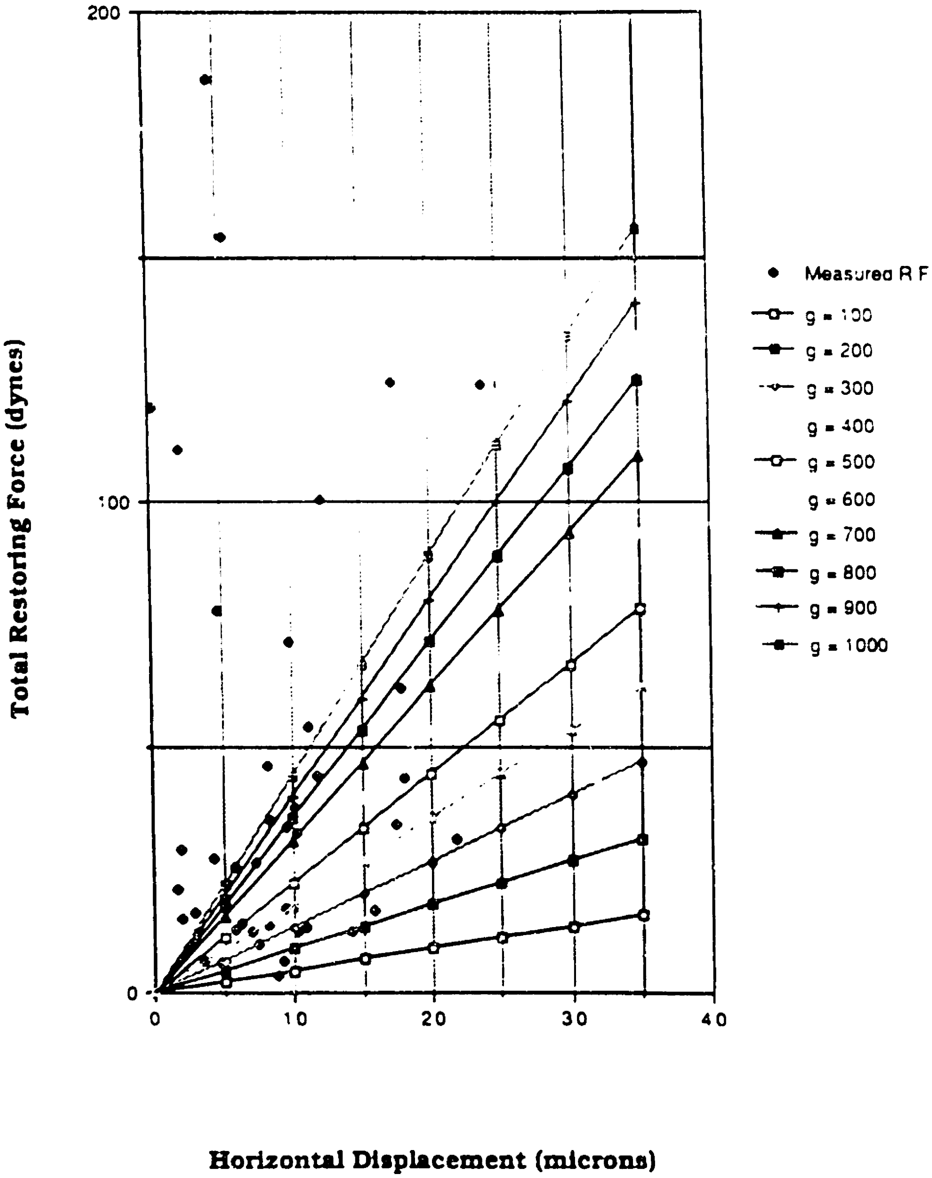

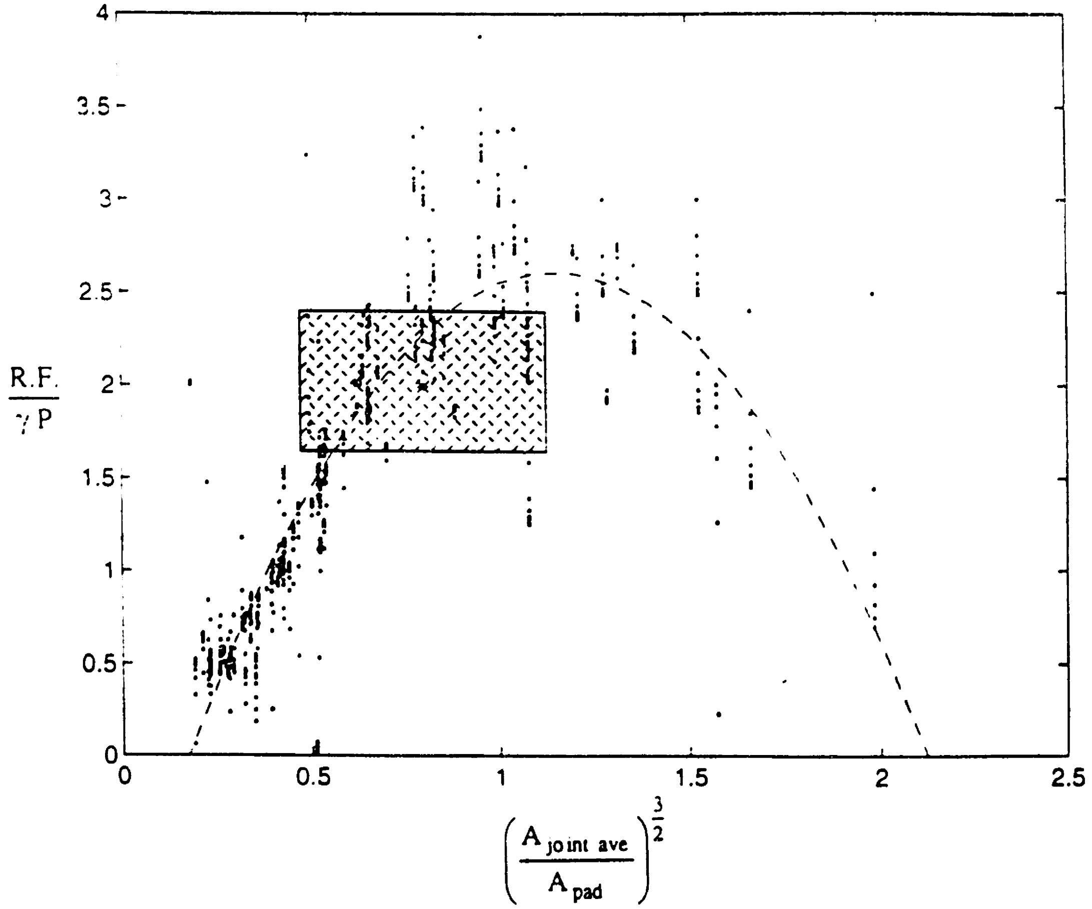

Fig. 7.10 Comparison of physical experiment parameters to dimensionless correlation.

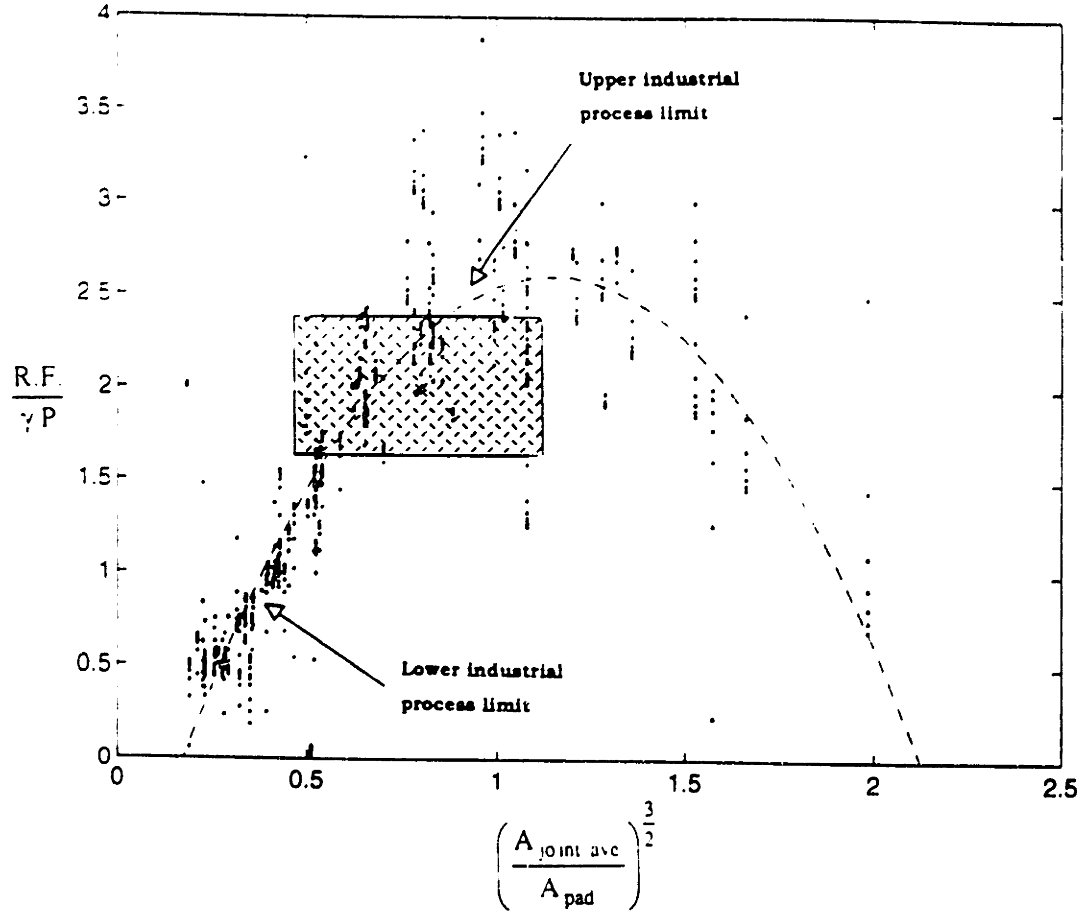

Fig. 7.11 Comparison of range of industrial practice and range of physical experiments to dimensionless correlation.

Chapter 8

CONCLUDING REMARKS

The most important achievements of this work was the development of computational and experimental methods that were used to develop a series of design guidelines for flip-chip based alignment operations. Specifically the individual influences of the following factors on self-alignment behavior have been modeled successfully:

- Influence of solder volume
- Influence of solder pad radius
- Influence of solder joint height
- Influence of surface tension
- Influence of solder pad shape
- Influence of parameters interactions

A number of dimensionless groups were developed to correlate the interacting of several process variables and their influence on restoring force. This is the first dimensionless correlation developed for systems of this type and it shed a great deal of light on the dynamics of the process. In addition two experimental methods were devleloped to measure restoring forces during the reflow process. These results were compared to the mathematical model results and confirmed them to within an order of magnitude. In the following sections, the influence of indivdual joint parameters as well as the influence of combinations of factors will be discussed.

Influence of Solder Volume

Calculation of the influence of varying solder volume in a 3 Dimensional model of both standard circular pads and alternative pad shapes made it possible to calculate its overall effect on alignment forces. All of the cases studies showed a strong relationship between solder volume and restoring force. It was discovered that there exists an optimum solder volume for each combination of joint geometry and shape, that results in a maximum in horizontal restoring forces. This volume is directly related to a solder surface shape that approximates the equilibrium shape of the liquid system. This relationship was true for a large number of parameter interactions. For non-optimum solder volumes, the solder shape occupied one of two extremes, either a convex shape for low volumes of a bulging high volume shape.

Influence of Solder Joint Height

Solder joint height was shown to have a moderate effect on horizontal restoring forces. Given a constant volume, surface tension, and pad radius, shorter solder joints were shown to produce the high levels of horizontal restoring force. The smaller vertical separations made it easier for the free surface to form a shapes that lead to high restoring forces. Deviations away from this shape lead to wide differences in restoring force.

Influence of Solder Pad Radius

Solder pad radius had an large influence on restoring forces that consistently pointed to larger pad sizes as a means of increasing positioning forces. For a broad range of volumes, heights and surface tension values, the highest levels of restoring force were generated for larger pads sizes. This produced solder shapes close to the equilibrium solder shapes, the deformation of which produced large surface energy gradients and as a result, large restoring forces. There is a limit to the trend of increasing to restoring force and this limit ssearch when the pad area is approximately equal to the corss-sectional area of the.

Influence of Surface Tension

The influence of surface tension was predicted as a result of our formulation of the governing equations for self-alignment force generation. Our mathematical model results confirmed that increases in surface tension, either through a change in material or the influence of a material on surface chemistry, lead to increases in restoring force for all combinations or joint parameters. This is a key factor for alteration due to the large correlation between surface tension and the restoring force.

Design Rules as a Result of Parameter Interactions

The influence of a number of process parameters on restoring forces can be summarized in the following series of design rules. Horizontal alignment restoring forces are optimized by a combination of shorter interconnect lengths, broader bonding pad areas and increases in surface tension values when all other process variables are kept constant. Additionally, parameters can be linked to an optimum solder volume that will lead to the generation of the highest levels of positioning forces to overcome a misalignment. This is explained by the need for the system to minimize free surface area and energy through a deformation of the surface away from configurations imposed upon it by the joint parameters. The optimum configuration is a function of all the process parameters and produces a slightly concave shape that is close to the equilibrium shape of the solder. In all cases the highest levels of restoring force are generated when the correct solder volume is matched to the correct height, pad radius, and surface tension value. Fig. 4.95 shows the current range of industrial practice and the calculated restoring force value for a number of parameters combinations. One of the major conclusions of this calculation is that there is room for improvement of the current joint designs, either by a change in the pad radius or the matching of the right solder volume with the right joint geometry. By choosing the right joint parameters, it is possible to improve and even optimize restoring force for a given configuration.

Confirmation by physical experiments

The accuracy of the mathematical models was confirmed by a comparison with experimental results, which also yielded many insights into the measurement of self-alignment forces and the influence of certain joint parameters such as joint height. Restoring forces were measured using two methods; a static force measurement and a dynamic measurement method. The results in each case were of the same order of magnitude as calculated using the mathematical models. Differences between the ideal behavior of the model and the measured results were explained by the influence of external forces and a number of issues described in detail below. Calculated restoring forces were also confirmed by the modeling efforts of other research groups studying similar problems.

Physical Experiment Issues

Some of the issues addressed the physical experiments included the influence of process variables including vibration, environment, external forces, and temperature. A great deal of effort was used to physically isolate the system from vibrational effects during the heating stage, a major source of error in earlier attempts. Another important issue in physical measurements of this type was the influence of the environment. The main component of this effect was caused by oxidation of the solder during heating which accounted for a some of the data spread when compared to the static results performed in an inert environment. Oxide formation on the molten solder surface is known to impede the free motion of surface tension forces in terms of bump formation in the early phase of the reflow process (i.e. dewetting from substrate surface). A third major issue was the method of external force application to the chips during measurement. Several different methods were attempted to apply a force to the system in a non-intrusive manner, the best of which seemed to be the dynamic beam method. The use of gravity and a series of added weights to study the system produced errors due to the large component of force in the vertical force influencing the joint height. The dynamic method avoided this type of effect and covered a much broader range of restoring force and displacement values.

Future Research Needs and Issues

The most glaring need in study of self-alignment effects is in the area of experimental methods of measuring restoring forces. The physical experiments performed in this project were the first of their kind in developing ways of applying a discrete force for a measurable displacement of the joint system. Many of the problems associated with the physical experiments were caused by the lack of equipment to precisely measure forces on the dynes scale in a high temperature environment without destroying the sample. Approaches similar to the dynamic approach used in this project need to be developed that will be able to be operated repeatedly in the process environment without adding to the effects being studied (i.e. non-intrusive). This type of approach shows the greatest potential for generating a large amount of data on restoring force effects in a reliable manner.

A number of recommendations can be made with regard to designing new test structures to measure restoring forces. Many of the same issues mentioned above will remain in any assembly. These include environmental control, vibrational damping, controlled force application. Several suggestions were formulated for the best directions future research should take as well as potential solutions to some of the current problems. The key areas for future research include improved force application methods, research into the influence of experimental environment and the continued study of joint parameter variation by experimental means.

BIOGRAPHICAL NOTE

Scott E. Deering was born of February 20, 1967, in Plainfield, New Jersey to Nathan and Niataja Deering. He attended elementary school at Evergreen Elementary School in Plainfield, N.J., and middle school at Maxson Middle School. He graduated from Plainfield High School, New Jersey as salutatorian of the class of 1985 and entered MIT on a Bell Communications Research Engineering Scholarship.

He graduated in 1989 from MIT with a Bachelors of Science degree in Materials Science with a concentration in polymer science and a minor in visual arts and design.

With the financial support of a AT&T Bell Laboratories Cooperative Research Fellowship, he began his graduate studies in the Department of Materials Science and Engineering at MIT in the fall semester of 1989 under the supervision of Professor Julian Szekely. His doctoral work was supplemented by summer and in-term work at Bell Laboratories.

As a graduate student, he also served as a graduate resident tutor at 500 Memorial Drive (Next House), an undergraduate dormitory at MIT. He was founder and president of Agrographics, a computer graphics and support company for local small businesses including Bridge Builders, an educational services and consulting firm. In addition, he was a 1993 grant recipient for the MIT Council of the Arts for his work in computer generated art and photography and art work on display in the Boston area.

After completing his studies at MIT, he will work as a Member of Technical Staff for Allied Signal in Morristown, N.J.